Microfluidic Devices for Neural and Behavioral Screening of *C. elegans* Using Electric Field

Khaled Youssef Mohamed Youssef

A DISSERTATION SUBMITTED TO
THE FACULTY OF GRADUATE STUDIES
IN PARTIAL FULFILLMENT OF THE REQUIREMENTS
FOR THE DEGREE OF
DOCTOR OF PHILOSOPHY

GRADUATE PROGRAM IN MECHANICAL
ENGINEERING
YORK UNIVERSITY
TORONTO, ONTARIO
January 2021

Abstract

C. elegans is an invaluable model for studying human diseases, from understanding disease pathology to screening for chemicals toxicity and therapeutic effects. However, technological deficiencies in achieving automated, fast, simple, and low-cost *C. elegans*-based screening assays have hindered the widespread use of this organism in the gene screening, toxicology and chemical screening areas. Various microfluidics and lab-on-a-chip systems have been reported for precise control and quantification of different sensory-motor processes of *C. elegans* such as electrotaxis, i.e., response to the electric field (EF) by swimming towards the negative electrode in a polarized system like a microchannel. The current electrotaxis microfluidic devices have a large footprint, low-throughput, and are slow due to their dependency on gait behaviours in terms of speed, body bend frequency, and reorientation. On-chip neuronal imaging has not been incorporated for the correlation of electrotaxis deficiency with neurodegeneration. Moreover, up until now, most of the electrotaxis assays have been conducted by exposing the entire worm to EF and were limited to gait behaviours, giving less attention to understanding *C. elegans* electrosensation and behaviours other than electrotaxis. Therefore, this thesis aimed to enhance our understanding of *C. elegans* electrosensation and the effects of EF on different phenotypes using microfluidic devices with enhanced behavioral throughputs. In Objective 1 of the thesis, we increased the number of worms that could be electrotactically tested and fluorescently imaged simultaneously, achieving a behavioral throughput of at least 9 worms every 5 minutes, which has not been achieved previously for electrically induced

behavioral assays even with automated systems. In Objective 2, the electrotaxis response of semi-mobile worms was introduced to provide an assay inside a more confined area and study whether selective exposure of the worm's head or tail to EF results in a directional electrotaxis. Interestingly, the results indicated the involvement of the vulva neurons in electrotaxis, which implied that the head neurons are not solely responsible for electrotaxis. Since vulva neurons showed involvement in *C. elegans* electrosensation, in Objective 3, we introduced, for the first time, a novel on-demand EF-evoked behaviour, termed electric egg-laying, in a simple to use microfluidic device that enabled trapping and exposure of individual worms to controlled EF conditions. Interestingly, we found that egg-laying is EF polarity dependent with a significant increase in the egg-count for anode-facing worms. Lastly, in Objective 4, we enhanced the behavioral throughput of our electric egg-laying assay while allowing on-chip fluorescent imaging and showed the technique's effectiveness for toxicity assessment. As a proof of concept, we used genetically and chemically induced models of Parkinson's disease as well as microplastics toxicity for showing the applicability of our techniques for behavioural and neuronal screening. A significant advantage offered by our devices was their ability to keep the identity of a worm known throughout an assay, which enabled correlating the chemical uptake heterogeneity with neuron degeneration and behavioral outputs at a single-worm resolution. It is anticipated that these microfluidic devices will play a major role in facilitating a fundamental understanding of *C. elegans* electrosensation, disease investigations, and chemical screening and toxicity assays.

Acknowledgements

A PhD is a long journey that would not have been made possible without the support from my supervisors, committee members, colleagues, family, and friends. I would like to take this opportunity to express my genuine gratitude to all of them for their continuous support. This thesis is for all of them.

First, I would like to express my sincere appreciation to my PhD supervisors, Professor Pouya Rezai and Professor Anurag Tandon, for their support and guidance throughout these past four years. No words can describe Prof. Rezai's support and help in cranking out this dissertation. He is my primary resource for getting helpful insights and for answering my research questions. His willingness for discussion, as well as his open-door policy, have made the journey much more comfortable. I have learned from Prof. Rezai how to be well-organized and work hard, efficient, and smart. I have been fortunate and honored to be his first PhD student at York University. I hope that I could one day be as enthusiastic, energetic, insightful, knowledgeable, and supportive as Prof. Rezai. I would like to thank Prof. Rezai for his support through the birth of my daughter, Lareen. I would also like to thank Prof. Tandon for his continuous availability and support, and for giving me the privilege to work in his laboratory.

I would also like to thank my committee members, Professor Terrance Kubiseski and Professor Derek Wilson, for their advice during my annual committee meetings and comprehensive exam. *Caenorhabditis elegans* maintenance, the fundamental basis of my thesis, would not have been possible without Prof. Kubiseski's who gave me the privilege to work in his laboratory. Personally, I would like to thank Professor Hossam Sadek for his continuous presence and help throughout my stay at York University, without whom I would not have come to York University in the first place.

The work of this thesis would not have been possible without the help of my colleague and friend, Daphne Archonta. I have known Daphne since her high-school, and she has shown a great dedication to work during her undergraduate studies at York. Her contribution to data analysis, worm maintenance, and experimentation has helped to get the research faster. I am grateful to my colleagues in the ACUTE lab, Amin Shams and Pouriya

Bayat, who have given me a lab tour and taught me the soft lithography technique. All respect and appreciation to ACUTE lab members especially, Arsalan Nikidoost, Alireza Zabihi, and Arezoo Khalili, for their continuous support and help throughout my PhD.

I would also like to thank all students in the mechanical engineering department at York University for making the office an enjoyable place to work and for all the fun moments that we enjoyed together. Too many to mention, but I would like to thank Ahmed Elkholy, Yehia Ezzat, Mohamed Abdelhamid, Omar Khaled, Nima Talebzadeh, Milad Shakeri, Hossein, Menna Elsayed, and Aya Elsayed.

I would also like to acknowledge all funding received throughout my PhD from Ontario Government for offering me the Ontario Trillium Scholarship for four consecutive years, Natural Sciences and Engineering Research Council (NSERC) of Canada for grants awarded to Prof. Rezai, York University for offering me the Susan Mann Dissertation Scholarship, and Mitacs for offering me the Mitacs Research Training Award.

Being an international student, the first few days in Toronto would have been more intimidating without my friends who provided me with great companionship. I would like to thank Ahmed Alsayed, Islam Heleza, Nader El-Taweel, Mohamed Abdelhamid, Mohamed Salem, Moomen Soliman, Ahmed Fergala, Mohamed Zaki, Ahmed Elkholy, and Hassan El-Komy. Thanks to all of you for your continued presence and support, and thanks for being there whenever is needed. I would also like to thank my friends back in Egypt, Khaled Marzook and Basem Farghly, who have been supportive regardless of the long-distance.

I would also like to acknowledge that I would have never been close to this dissertation without the help and selfless support of my whole family, mom, dad's spirit, and brothers. I am also grateful for the birth of my daughters Lareen and Leen. I would never forget Lareen saying, "Daddy, go working, or Daddy, stop working and play with me."

Lastly, it is impossible to understand the role and contribution of my wife, Haneen Khalaf, as well as her wonderful family to this thesis. This thesis is not only a culmination of hard work, but it is also an assortment of lots of ups and downs during which my wife has been by my side, showing selfless support. No words can convey how much I love her and how deeply I appreciate her support. She is always there to enlighten my path and adding joy to the family. During the times that I, myself, did not have faith in myself, her faith in me has empowered and motivated me to hold my thoughts and finish this long journey. I would not have been where I am now without her being by my side.

Dedication

بسم الله والحمد والشكر لله الذي بنعمته تتم الصالحات ..

الحمدلله الذي وفقني إلى ان اصل لهذه اللحظة بإكمال مسيرتي العلمية والحصول على درجة الدكتوراة..

إلى أمي الحبيبة وروح أبي الطيبة .. إلى من كان لهم الفضل بعد الله تعالى في وجودي ..

إلى زوجتي وصديقتي .. إلى غاليتي وحبيبتي ورفيقة دربي .. إلى من شاركتني لحظات السعادة والحزن ..

إلى إخوتي .. سندي عند الشدائد في هذه الدنيا ..

إلى أصدقائي .. عائلتي الثانية ..

In the name of God, praise and thanks be to God, by whose grace all good works are fulfilled.

Praise be to God, who helped me reach this moment by completing my scientific career and obtaining a PhD.

To my beloved mother and my father's kind spirit. To those who have the credit after God Almighty in my presence.

To my wife, my sweetheart, and my companion, who shared the moments of happiness and sadness during this long journey.

To my brothers, who support me in the hardships of this world.

To my friends, my second family.

Table of Contents

List of Tables

List of Figures

Abbreviations

2D	Two-Dimensional
6-OHDA	6-Hydroxydopamine
AC	Alternating Current
AD	Alzheimer's Disease
ADE	Anterior Deirid
ALS	Amyotrophic Lateral Sclerosis
BBF	Body Bend Frequency
BiFC	Bimolecular Fluorescence Complementation
BSR	Basal Slowing Response
BWBU	Body Wall-Butanol
BWEA	Body Wall-Ethyl Acetate
C. elegans	*Caenorhabditis elegans*
CAD	Computer-Aided Design
CEP	Cephalic
CGC	*Caenorhabditis* Genetics Center
COPAS	Complex Object Parametric Analyzer and Sorter
Cr	Chromium
CTL	Catalases
DC	Direct Current
DLD	Deterministic Lateral Displacement
DNs	Dopaminergic Neurons
DTT	Dithiothreitol
E. coli	*Escherichia Coli*
EF	Electric Field
ERK	Signal-Regulated Kinase
ETI	Electrotaxis Time Index
ETT	Electrotaxis Turning Time
FACS	Fluorescence Activated Cell Sorting
GFP	Green Fluorescent Protein
HD	Huntington's Disease

HSN	Hermaphrodite Specific Neuron
HTS	High-Throughput Screening
IPA	Isopropyl alcohol
LB	Luria Broth
LBs	Lewy Bodies
L-DOPA	Levodopa
LEAD	Line Excitation Array Detection
MESA	Methanol Extracts of Sorbus Alnifolia
MFI	Mean Fluorescent Intensity
MPTP	1-Methyl-4- Phenyl-1,2,3,6-Tetrahydropyridine
NAC	Non-Amyloid Component
NDs	Neurodegenerative Diseases
NGM	Nematode-Growth Medium
PD	Parkinson's Disease
PDE	Posterior Deirid
PDMS	Polydimethylsiloxane
PF127	Pluronic F127
PMMA	Polymethyl Methacrylate
qPCR	Quantitative Polymerase Chain Reaction
ROI	Region of Interest
SDS	Sodium Dodecyl Sulfate
SEM	Standard Error of The Mean
Si	Silicon
SN	Substantia Nigra
SOD	Superoxide Dismutase
VC	Ventral Cord
VCN	Ventral Cord Neuron
VIBU	Viscera-Butanol
VIEA	Viscera-Ethyl Acetate
VMs	Vulva Muscles
WBBU	Whole Body Butanol
WBEA	Whole Body-Ethyl Acetate
WT	Wild Type
YFP	Yellow Fluorescent Protein
α-syn	α-Synuclein

Glossary of terms

1-methyl-4-phenyl-1,2,3,6-tetrahydropyridine (MPTP)
A substance that is found as a contaminant in some drugs, and is converted in the body to MPP+, causing Parkinson's disease.[1]

6-hydroxydopamine (6-OHDA)
A neurotoxin that is closely related to dopamine and is taken into dopaminergic and noradrenergic neurons via their normal reuptake mechanism, whereupon it destroys the neuron terminals, causing the organism to lose the ability to perform simple actions to obtain rewards.[1]

Ablation
A technique for the removal of a tissue or a particular cell type during development.[2]

Alzheimer's disease (AD)
A degenerative brain disease with insidious onset beginning before 65 years of age, followed by slow development over several years, characterized by dementia called dementia of the Alzheimer type (DAT), loss of memory, and emotional instability, accompanied by postmortem evidence of amyloid plaques and other brain pathology, usually leading to death between four and twelve years after the onset of the disease.[1]

Amino acid
Any of a group of water-soluble organic compounds that possess both a carboxyl (–COOH) and an amino (–NH2) group attached to the same carbon atom, called the α-carbon atom. Amino acids can be represented by the general formula R-CH(NH2)COOH. R may be hydrogen or an organic group, which may be nonpolar, basic, acidic, or polar; the nature of the R group determines the properties of any particular amino acid. Proteins are composed of various proportions of about 20 commonly occurring amino acids. The sequence of these amino acids in the protein polypeptides determines the shape, properties, and hence biological role of the protein.[3]

Basal ganglia
Structures containing clusters of neuron cell bodies in and around the thalamus near the base of the brain.[1]

Bradykinesia
Abnormal slowing of bodily movements, notably as a feature of Parkinson's disease.[1]

Collagen
An insoluble fibrous protein found extensively in the connective tissue of skin, tendons, and bone.[3]

Dopamine
A biogenic amine and catecholamine that is one of the neurotransmitter substances involved in central nervous system functioning while also functions as a hormone.[1]

Dopaminergic neuron (DA)
One type of a class of neurons all of which use biogenic amines as neurotransmitters.[1]

Electrophoresis
The migration of suspended particles usually through a gel or colloid under the influence of an applied electrical field, the lightest particles tending to move furthest. Also called gel electrophoresis.[1]

Electrophysiology
The branch of physiology that deals with the electrical phenomena associated with nervous and other bodily activity.[4]

Endocytosis
The uptake by a cell of particles, fluids, or specific macromolecules by phagocytosis, pinocytosis, or receptor-mediated endocytosis, respectively. The functions in which endocytosis plays a role include antigen presentation, nutrient acquisition, clearance of apoptotic cells, pathogen entry, receptor regulation, and synaptic transmission.[5]

Escherichia coli
A rod-shaped Gram-negative *bacillus* (0.5 × 3–5 μm) abundant in the large intestine (colon) of mammals.[6]

Exocytosis
The discharge by a cell of intracellular materials to the exterior.[2]

Fluorescence-activated cell sorter
A type of flow sorter in which cells are characterized and sorted by the intensity of the fluorescence they emit when passing through an exciting laser beam.[2]

Fluorescent protein
A protein isolated from the jellyfish, *Aequorea victoria*, that fluoresces when exposed to excitation light (there are several spectral variants, including yellow, cyan, blue, and red). GFP has important applications in research: the gene can be expressed in other living organisms, making it possible to create gene fusions and hence to visualize the localization of specific gene products inside living cells.[2]

Gene
In the classical literature it is defined as a hereditary unit that occupies a specific position (locus) within the genome or chromosome; a unit that has one or more specific effects upon the phenotype of the organism; a unit that can mutate to various allelic forms; and a unit that recombines with other such units.[5]

Genotype
The genetic constitution of a cell or an organism, as distinguished from its physical and behavioral characteristics.[5]

Glutamine
The trivial name for the γ-amide of glutamic acid; glutamic 5-amide; α-aminoglutaramic acid; 2-amino-4-carbamoylbutanoic acid; H2N–CO–[CH2]2–CH(NH2)–COOH; a chiral α-amino acid.[2]

Hermaphrodite
An organism having both male and female reproductive organs. A simultaneous hermaphrodite has both types of sex organs throughout life. A sequential hermaphrodite may have the ovary first (protogyny), to be replaced by a testis later, or may develop the testis first (protandry), to be replaced later by an ovary.[5]

Homologue
Homologs are characteristics that are similar in different species because they have been inherited from a common ancestor.[5]

Huntington's disease (HD)
A rare hereditary disorder (affecting about 1 in 20,000 people) transmitted by a single dominant gene on the tip of chromosome 4, with damage to the basal ganglia, characterized by widespread degeneration of the brain, with onset after the age of 40 and slow progression leading to death usually within 10–15 years.[1]

In-vitro
Of or relating to biological processes or experiments that occur outside the organism in artificial environments.[1]

In-vivo
Of or relating to biological processes or experiments that occur in living organisms.[1]

Knock-in
A transgenic animal to which a new gene has been added rather than eliminated.[6]

Knock-out
An informal term for an organism in which the function of a particular gene has been completely eliminated.[6]

L-DOPA
Laevo-dihydroxyphenylalanine, a substance that is synthesized in the body from tyrosine

and is an immediate precursor of dopamine. Dopamine cannot cross the blood-brain barrier, but L-dopa can, therefore a synthetic form of L-dopa is used in the treatment of Parkinson's disease, which arises from a failure of dopamine production in the brain. Also called levodopa.[1]

Lewy bodies
An aggregate of fibrillar ubiquitinated α-synuclein occurring in the substantia nigra in Parkinson's disease.[2]

Methylphenylpyridine (MPP+)
A substance that is produced in the body from MPTP and that selectively destroys neurons in the substantia nigra, causing Parkinson's disease.[1]

Mutation
A change in the genes or chromosomes of a cell, capable of being transmitted to offspring as a heritable alteration of the organism.[1]

Neurotoxin
Any substance such as 6-hydroxydopamine that is poisonous to neurons or that interferes with their electrochemical functioning.[1]

Neurotransmitter
Any of about 50 chemical substances, usually a small amine or a peptide but also a substance such as the gas nitric oxide, by which a neuron communicates with another neuron or with a muscle or gland via a synapse.[1]

Orthologs
A gene, protein, or biopolymeric sequence that is evolutionarily related to another by descent from a common ancestor, having diverged as a result of a speciation event.[2]

Parkin
A ubiquitin-protein ligase whose substrate is a glycosylated form of α-synuclein. The substrate accumulates in parkin-deficient brain. Mutations in the gene are associated with an autosomal recessive form of Parkinson's disease.[2]

Parkinson's disease (PD)
A progressive, degenerative neurological disorder affecting 2 percent of people over 65 in the developed world, associated with malfunction to neurons that produce dopamine in the substantia nigra.[1]

Phenotype
The totality of the observable functional and structural characteristics of an organism as determined by interaction of the genotype of the organism with the environment in which it exists.[1]

Polyglutamine
A stretch of amino acids in a protein that is entirely composed of glutamine.[2]

Polymerase Chain Reaction (PCR)
A method whereby a specific sequence of nucleotides within a double-stranded DNA is amplified.[2]

Rotenone
An inhibitor of the electron transport chain found naturally in the roots of the South American barbasco shrub Lonchocarpus nicou (formerly Robinia nicou). A very potent poison for fish and causes Parkinson's disease-like symptoms in rats.[6]

Substantia Nigra
One of the basal ganglia, implicated in motor control. It is a dark, pigmented area in the midbrain, just below the thalamus, containing neurons that synthesize and release dopamine and project primarily to the striatum. Lesions in this area are associated with Parkinson's disease.[1]

Transgenic
Animals into which cloned genetic material has been experimentally transferred. In the case of laboratory mice, one-celled embryos have been injected with plasmid solutions, and some of the transferred sequences were retained throughout embryonic development. Some sequences became integrated into the host genome and were transmitted through the germ line to succeeding generations. A subset of these foreign genes expressed themselves in the offspring.[2]

Vulva
The orifice of the vagina, constituting the external genitalia of a human female.[1]

Wild-type
The phenotype that is characteristic of most of the members of a species occurring naturally and contrasting with the phenotype of a mutant.[2]

α-synuclein (α-syn)
A brain presynaptic protein that is expressed also in other tissues, but at very low levels. It is highly conserved, rodent and zebrafish α synucleins being 95% and 86% identical to human. Some mutations are linked to familial Parkinson's disease.[2]

β-amyloid (Aβ)
A glycoprotein associated with Alzheimer's disease, and derived from a precursor capable of several forms through alternative splicing.[2]

Contributions

Journal papers

1. Youssef, Khaled, Daphne Archonta, Terrance J. Kubiseski, Anurag Tandon, and Pouya Rezai. "Microplastic Toxicity at the Neuronal, Behavioural and Physiological Levels Investigated on *C. elegans* in a Multi-Nematode Lab-on-a-Chip Device with Population and Single-Worm Screening Capability." Science of the Total Environment (2021)"Under review".

2. Youssef, Khaled, Daphne Archonta, Terrance J. Kubiseski, Anurag Tandon, and Pouya Rezai. "Electric Egg-laying: a New Approach for Regulating *C. elegans* Egg-laying Behaviour in a Microchannel Using Electric Field." Lab on a Chip (2021), In Press, DOI: 10.1039/D0LC00964D.

3. Youssef, Khaled, Daphne Archonta, Terrance Kubiseski, Anurag Tandon, and Pouya Rezai. "Parallel-Channel Electrotaxis and Neuron Screening of *Caenorhabditis elegans*." Micromachines 11, no. 8 (2020): 756.

4. Youssef, Khaled, Daphne Archonta, Terrance J. Kubiseski, Anurag Tandon, and Pouya Rezai. "Semi-mobile *C. elegans* Electrotaxis Assay for Movement Screening and Neural Monitoring of Parkinson's Disease Models." Sensors and Actuators B: Chemical 316 (2020): 128064.

5. Youssef, Khaled, Anurag Tandon, and Pouya Rezai. "Studying Parkinson's Disease Using *Caenorhabditis elegans* Models in Microfluidic Devices." Integrative Biology 11, no. 5 (2019): 186-207.

Book chapters

1. Youssef, Khaled, Daphne Archonta, and Pouya Rezai. "Microfluidic Devices to Study the Effect of Electric Field on *Caenorhabditis elegans* and *Danio rerio*." ElSeiver, 2020 "Under review".

2. Youssef, Khaled, Pouriya Bayat, Amir Reza Peimani, Sina Dibaji, and Pouya Rezai. "Miniaturized Sensors and Actuators for Biological Studies on Small Model Organisms of Disease." In Environmental, Chemical and Medical Sensors, pp. 199-225. Springer, Singapore, 2018.

Conference publications

1. Youssef, Khaled, Daphne Archonta, Terrance J. Kubiseski, Anurag Tandon, and Pouya Rezai. "Electric Field Induced *C. elegans* Egg Laying is Neuronmediated and Dependent on Field Polarity." μTAS, USA (2020).

2. Youssef, Khaled, Daphne Archonta, Terrance J. Kubiseski, Anurag Tandon, and Pouya Rezai. "Egg Laying Neuron Mediates Electrosensation in *Caenorhabditis elegans*." μTAS, USA (2020).

3. Youssef, Khaled, Daphne Archonta, Terrance J. Kubiseski, Anurag Tandon, and Pouya Rezai. "On-demand Direct Current Electric Field Immobilization Enables High-resolution Imaging of *C. elegans*." μTAS, USA (2020).

4. Youssef, Khaled, Daphne Archonta, Terrance J. Kubiseski, Anurag Tandon, and Pouya Rezai. "A Microfluidic Device to Enhance the Throughput of Electrotaxis Screening with *Caenorhabditis elegans* Models of Parkinson's Disease." μTAS, Basel, Switzerland (2019).

5. Youssef, Khaled, Daphne Archonta, Terrance J. Kubiseski, Anurag Tandon, and Pouya Rezai. "On-demand Electric Field Induced Egg Laying of *Caenorhabditis elegans*." μTAS, Basel, Switzerland (2019).

6. Youssef, Khaled, Daphne Archonta, Terrance J. Kubiseski, Anurag Tandon, and Pouya Rezai. "Neuronal and Behavioral Effects of Alpha-synuclein Protein and 6-OHDA Neurotoxin in Parkinson's Disease Investigated with a *C. elegans* Electrotaxis Microfluidic Assay." μTAS, Kaohsiung, Taiwan (2018).

List of additional publications

1. Khalili, Arezoo, Amir Reza Peimani, Nickie Safarian, Khaled Youssef, Georg Zoidl, and Pouya Rezai. "Phenotypic chemical and mutant screening of zebrafish larvae using an on-demand response to electric stimulation." Integrative Biology 11, no. 10 (2019): 373-383.

2. Rashtchian, Sadaf, Khaled Youssef, Pouya Rezai, and Nima Tabatabaei. " Imaging of *Caenorhabditis elegans* by spectrally encoded confocal microscopy." IEEE Photonics Conference, (2020).

3. Khalili, Arezoo, Ellen van Wijngaarden, Khaled Youssef, Georg Zoidl, and Pouya Rezai. "Microfluidic Device to Screen the Electric Induced Behavioral Response of Multiple Zebrafish Larvae." μTAS, USA (2020).

4. Khalili, Arezoo, Khaled Youssef, Georg Zoidl, and Pouya Rezai. "Neurotoxin-induced Impairment and Neuroprotective-based Recovery of Electrotactic Locomotion in Zebrafish Larvae As a Model for Neurobehavioral Studies in Parkinson's Disease." μTAS, Kaohsiung, Taiwan (2018).

Chapter 1

Introduction

1.1 Background Information and Research Direction

Disease studies, toxicity screening, and gene screening processes involve High-Throughput Screening (HTS) of large chemical compound libraries on specific biological targets* which must be done in a sensitive, fast, and cost-effective manner.[7] In drug discovery, preliminary hits (potential therapeutic compounds) are achieved by using *in-vitro* cell-based HTS assays. The positive hits are then tested using expensive and laborious assays on whole-animal mammalian models to find out the chemical potency and toxicity before the preliminary clinical trials are commenced.[8] Very commonly, the optimized lead chemicals that are developed during preclinical *in-vitro* assays in drug discovery fail at *in-vivo* stages of screening, mainly due to toxicity effects.[8] Small organisms such as *Caenorhabditis elegans* (*C. elegans*)[7,9], *Drosophila melanogaster*[10] and *Danio rerio*[11] have shown promising characteristics as simple biological models for toxicology and chemical screening to fill the gap between *in-vitro* cell-based and *in-vivo* whole animal studies. This research focuses on

*Biological entities, usually proteins or genes, that interact with, and whose activity is modulated by a particular compound.

the use of microfluidics technology to enhance phenotypic assays on *C. elegans* as a model for gene screening, toxicology, and chemical screening.

C. elegans or the roundworm is a versatile model organism which offers many experimental advantages such as small size (<1 mm length), rapid growth, and body transparency which enhance its amenability to HTS and cellular and molecular visualization using fluorescent imaging.[7,9] In contrast to mammalian animals, *C. elegans* reproduces in a short life cycle of approximately 3 days that starts with the embryonic stage followed by four larval stages (L1-L4) and adulthood (Figure 1.1 A-B), and it is easier to be maintained in the laboratory conditions. This makes the worm one of the most cost-effective whole model organisms for system biology and disease studies. Moreover, the worm's genome has been fully sequenced showing a high degree (60-80%)[12] of genetic similarity to humans.[7,9] For instance, *C. elegans* share various gene orthologues for many of the neurological disorders.[13] Therefore, they have been exploited extensively as models for neurodegenerative diseases (NDs) such as Parkinson's disease (PD), Alzheimer's disease (AD), and Huntington's disease (HD).[14] *C. elegans* behavioural phenotypes such as mobility, body morphology, pharyngeal pumping, brood size, and development, along with *in-vivo* fluorescent cell expression (Figure 1.1 C) have been quantified for chemical efficacy testing.[12,15–17] Moreover, some behaviours, including movement, egg-laying, and food intake can be regulated through a wide range of stimuli such as chemicals, light, temperature, electric field (EF), and touch. They can be modulated accurately for on-demand stimulation of responses in *C. elegans* and studying their biological basis. Indeed, it has been shown that *C. elegans* is a powerful tool for understanding the neuronal pathways underlying various sensory-motor mechanisms such as chemotaxis, thermotaxis, phototaxis, mechanosensation and electrotaxis.[18–22]

Electrotaxis is one of several behaviors preserved across many species, which is the ability of an organism to sense and move towards a desired direction in the presence of an external electric field (EF).[22] EF can be defined as the applied voltage between two elec-

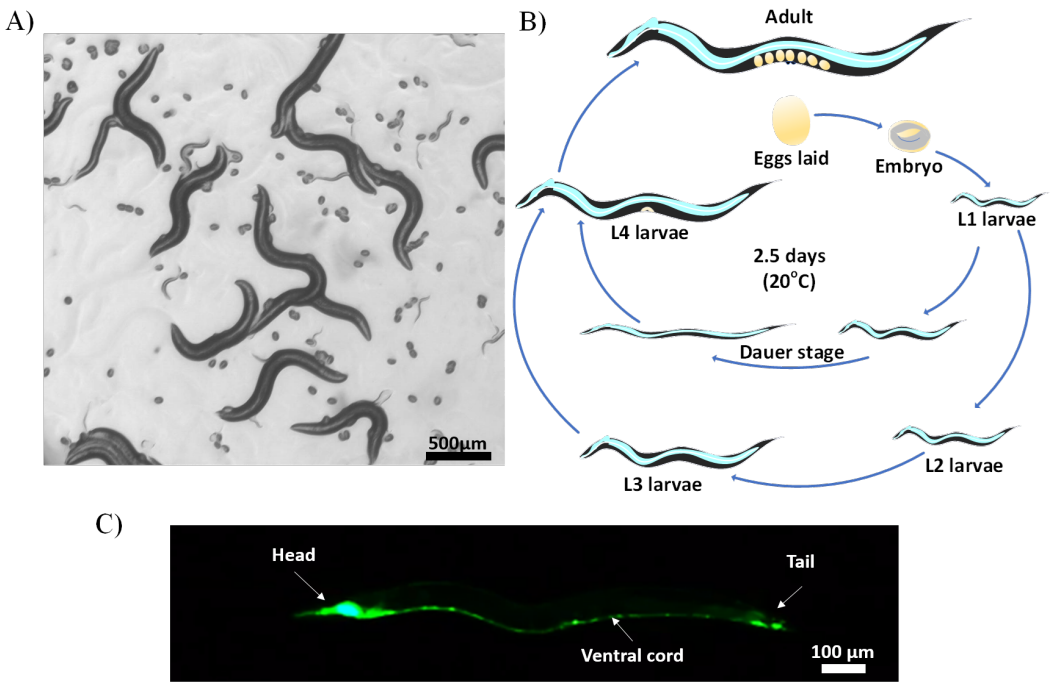

Figure 1.1: *C. elegans* worm and its life cycle. (A) A normal culture on an agar plate showing different worm stages; (B) *C. elegans* life cycle at 20°C, which is approximately three weeks including embryogenesis, four larval stages and adulthood; (C) Green fluorescent protein (GFP) expression in pan-neurons of transgenic *C. elegans* strain NW1229, showing the neurons in the head and tail, connected through the ventral cord.

trodes divided by the distance between them. Electrotaxis has been found to be utilized for navigation and food search across many species like aquatic animals, amphibians, cockroaches, bees, and *C. elegans*[22]. Researchers have developed various experimental setups to study electrotaxis in petri dishes due to their widespread use in culturing small organisms in laboratories (Figure 1.2A). In 1978, Sukul and Croll[23] studied the electrotaxis of *C. elegans* on agar plates and found that cathodal movement (locomotion towards the negative pole of the EF) was substantial in the range of 3 to 4 volts. Klein et al.[22] studied the electrotaxis behaviour of L1 to young adult *C. elegans* on agar plates at low and high EFs. At 0.7 V/cm, they showed that the worms moved randomly towards the cathode, while, at 4 V/cm, the worms robustly moved towards the cathode in a specific angle, which formed

a V-shaped movement pattern (Figure 1.2B). The behavioral response diminished in L1 and increased with age until it reached the most robust response for L4 and adult worms. Next, Gabel et al.[24] attempted to explore the involvement of genetic and neuronal bases in electrotaxis using the step-wise rotation EF method. Mutation or laser ablation in some genes and sensory neurons showed that genes such as *che-2*, *che-13*, *eat-4*, *osm-3*, *osm-5*, *osm-6*, *osm-10* and *tax-6* are involved in electrotaxis, and different neurons such as ASJ, ASH, AWC, ASK, and AWB are essential for the electrotactic motor decision making[24]. Recently, Chrisman et al.[25] elucidated the role of the AWC neuron pairs (AWC^{OFF} and AWC^{ON}) on electrotaxis and showed that genetic ablation of the neurons is less disruptive than the loss of function asymmetry.

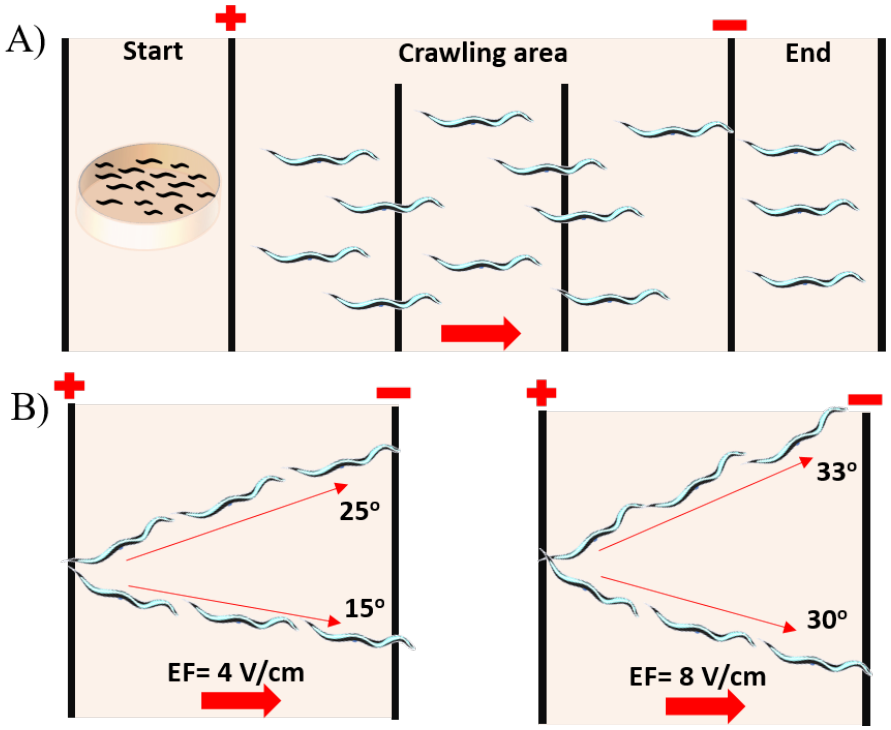

Figure 1.2: Off-chip electrotaxis in *C. elegans*. (A) Experimental configuration for electrotactic speed calculation on agar substrate. (B) EF effect on *C. elegans*' angle of movement.

Despite many advantages offered by the abovementioned assays, they possess vari-

ous drawbacks such as EF non-uniformity, susceptibility to media evaporation, and low throughput, all because of the open substrate nature of the experimental setups. Due to the small size of *C. elegans*, in the range of tens of micrometers to a millimeter, microfluidics was first adopted in 2010 for studying electrotaxis while providing well-controlled microenvironments for precise phenotypic assays.[26] Microfluidics is the science and technology of handling fluids at the micrometer to millimeter scale using microfabricated and micromachined components such as channels, chambers, valves, and pumps[27]. It has successfully led to the introduction of major scientific and technological breakthroughs in studying various molecular, cellular, and behavioral processes in *C. elegans*[13]. Some of the advantages provided by microfluidic devices are precise control on handling the organisms and chemicals, automation of assays, enhancement of throughput, lowering the consumption of biochemicals, and making complex biological experiments simple, and convenient for the end users. By the integration of various actuation and sensing mechanisms on these microfluidic devices, researchers have been able to perform laboratory-based manual assays automatically on a chip with enhanced precision and accuracy in quantifying complex behaviors or cellular processes in model organisms.

Microfluidic devices have aided in precisely controlling the microenvironment for understanding the effect of EF on *C. elegans*[26,28]. Rezai et al.[26,28] were the first to exploit microfluidics to examine the swimming behaviour of *C. elegans* using direct current[26] (DC) or alternate current[28] (AC) EFs while maintaining controlled test conditions in terms of EF uniformity and strength as well as worms' movement direction (Figure 1.3). Different developmental stages of *C. elegans* were tested at a wide range of EFs. It was found that the sensitivity in electrosensation increases with age in microfluidic environments, just like the observation reported by Klein et al[22] on open chamber substrates.

Ever since 2011, electrotaxis has been used to sort worms based on their age or to demonstrate that electrotaxis impairment is an indicator of *C. elegans* neuron degeneration[29–34]. Many neurological disorders result in sensory-motor system malfunctions and

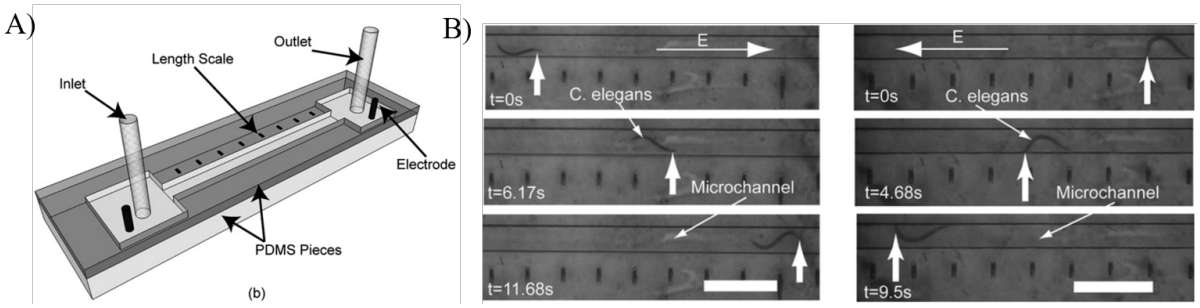

Figure 1.3: (A) The first microfluidics device developed to study *C. elegans* electrotaxis using DC, Pulsed DC, and AC Signals. (B) Time-lapse images of *C. elegans* electrotactic movement in an EF= 3 V/cm (scale bar= 1mm)[26].

behavioural deficiencies such as uncoordinated movement. As an example, PD is a progressive neurodegenerative disease known for the loss of dopaminergic neurons (DNs) in the brain[14]. DNs degeneration in *C. elegans* has been mimicked using different neurotoxins [e.g., 6-hydroxydopamine (6-OHDA)] that induce several symptoms of PD, such as tremor and slow crawling[14]. By developing a microchip to immobilize individual mutant worms in parallel channels using controlled microvalves, Ma et al.[35] demonstrated that neurotoxins, such as Methylphenylpyridine (MPP+), could induce neuron degeneration and mobility defects, for instance slow and coiled movements, in *C. elegans*. Shi et al.[36] developed a droplet-based device to study the effect of MPP+ and 6-OHDA on mutant worms by encapsulating them within droplets. Their findings supported the results of Ma et al.[35] on MPP+ and concluded that 6-OHDA was also able to degenerate DNs due to increased oxidative stress. In the above papers, *C. elegans* movement was not induced on-demand by any controlled external stimulus and was completely random and voluntary. In addition to the natural behaviors of the worm investigated in the papers above, induced responses by different stimuli such as EF have also attracted attention. For instance, Salam et al.[37] utilized electrotactic screening to investigate the movement behavior of worms under exposure to neurotoxins. Their studies revealed that PD-like movement disorder symptoms could be induced using neurotoxin chemical compounds and could be suppressed using known

neuroprotective chemicals such as acetaminophen. To enhance the speed of this technique, Liu et al.[29] developed an automated system to achieve a throughput of 20 worms/hour in a single-channel device and validated the system using a worm model of PD.

1.2 Scientific and Technological Gaps

As mentioned above and in our amended review paper[14] and book chapter[38], previous studies have solely focused on the electric-induced *C. elegans* movement and its use for chemical and genetic screening. In this thesis, we identified several scientific and technological gaps for further understanding of the electro-sensory response of *C. elegans* and its use to enhance the efficiency and the behavioral throughput of various assays.

In terms of the scientific gaps, **previous electrotaxis assays have been conducted by exposing the entire worm to EF, limiting the possibility of investigating the involvement of neurons or muscles in certain body parts in electrotaxis** via exposing desired segments of the worm to the EF. This limitation brought into question whether the head, tail and mid-body neurons play independent roles in *C. elegans* electrosensation. Therefore, a technique in which different body segments could be exposed to EF while allowing the worms to respond to the EF and quantify their electrotactic behaviours is still needed. Next, **most of the electrotaxis studies on *C. elegans* have investigated the effect of EF on the larval and young adult stages, giving less attention to the response at later ages,** which is essential in studying age-dependent diseases like HD, PD and AD. Moreover, **investigations were limited to gait behavior in terms of speed, body bend frequency, and reorientation.** Thus, we questioned whether EF exposure and aging can lead to any other behaviour than electrotaxis. In a pursuit to answer that question, we found that at later developmental stages, *C. elegans* exhibit an egg-laying behaviour in response to a DC EF rather than only swimming towards the cathode. Therefore, studying the *C. elegans*' electrically induced egg-laying is

in question and worthy of further investigation.

In terms of the technological gaps, **the current electrotaxis microfluidic devices have large footprints, and the assays are slow** due to the need for the worm to swim for a few centimeters along a channel, especially when multiple worms are required to be monitored. Moreover, **on-chip neuronal imaging of the same population of the worms that have been electrotactically screened has not been demonstrated**, which is preferred for determining the **correlation of electrotaxis deficiency with neurodegeneration (this is also a scientific gap in this field)**. Therefore, simple and easy to use microfluidic electrotaxis-based chips are needed for, firstly, testing of multiple worms to enhance the behavioral throughput of electrotaxis screening and simultaneous neuron imaging to correlate movement malfunctions with neuron and muscle degeneration, preferably at single animal resolution. Secondly, they are needed for decreasing the assay footprint, providing an electrotaxis assay inside a more confined area. Next, *C. elegans* egg-laying is a behavior of interest in neurobehavioral studies, governed by a sensorimotor circuit regulated by different neuronal and muscle cells[39,40]. **Optogenetics** is the primary method used to stimulate neurons to study the sensorimotor pathways involved in egg-laying[39]. However, it is **restricted to genetically-modified worms with light-sensitive ion channels, calling for a simple, on-demand, and more comprehensive egg-laying stimulation technique applicable to wild-type and non-optogenetic worms**. Therefore, a simple and easy to use microfluidic device is needed to characterize the electric egg-laying phenomena while studying multiple worms in parallel. Lastly, egg-laying has been reported as a quick technique for antidiabetic drug screening[41]. Therefore, our technique can be an asset to shorten the egg-laying rate assay time and provide a fast quantification technique for determining the toxicological effects of glucose and other contaminants like microplastics on *C. elegans*.

1.3 Thesis Goals and Objectives

Given the abovementioned scientific and technological gaps, this thesis aimed to enhance our understanding about *C. elegans* electrosensation and the effects of EF on different phenotypes using novel neurobehavioral screening microfluidic devices with enhanced behavioral throughputs. We aimed at exploiting these devices as tools for chemical and pollutant screening with quantitative cellular and behavioral readouts. In this thesis, the word "throughput" is called upon the behavioral assays, which are currently in the range of tens of worms per hour. We acknowledge that the throughput of cellular and molecular screening of *C. elegans* has reached the range of thousands of worms per minute.

In terms of addressing scientific gaps in this thesis, we developed a novel microfluidic technique in which the worm was captured from one end while the rest of the body was exposed to EF. Important advantages such as fluorescent imaging of the worm and spatial control on EF exposure were achieved. This technique helped us understand whether tail and mid-body neurons are involved in electrosensation independently. Moreover, we developed a microfluidic platform to study the effect of EF on other *C. elegans* behaviors at the adult stage, such as egg-laying which is a phenomenon that has not been exploited to date. This device helped us characterize the electric induced egg-laying phenomena and study the effect of aging on the egg-laying behavior.

For addressing technological gaps, we aimed at enhancing the throughput of the electrotactic behavioral assays (electrotaxis and electric egg-laying) and using them as tools for chemical and genetic screening based on on-demand behavioral readouts. As an application, the worms' electrotaxis and electric egg-laying phenomena were used to detect the worms' defective response and the associated neuronal dysfunctions due to exposure to 6-OHDA, glucose and microplastics. A significant advantage offered by our devices was their ability to keep the identity of a worm known throughout an assay, which enabled correlating the chemical uptake heterogeneity with neuron degeneration and behavioral outputs

at a single-worm resolution. Considering the limitations associated with the integrability of microfluidic devices in biological laboratories, the proposed devices were designed with cost-efficiency and operational simplicity in mind. To achieve our goals, the following objectives were pursued.

1. Enhance our understanding of *C. elegans* electrotaxis by improving the throughput of the conventional freely moving electrotaxis assays (Figure 1.3) and providing on-chip cellular imaging of the worms.

2. Investigate the effect of EF on partially-exposed worms to study whether EF is sensed by neurons in certain body segments such as the head, tail, and mid-body.

3. Study the effect of EF on gravid adult *C. elegans* and determine the presence of non-electrotactic behavior(s) such as egg-laying.

4. Enhance the throughput of non-electrotactic assays, with single-animal resolution neurobehavioral readouts, and provide proof of concepts for chemical and pollutant screening applications.

1.4 Publication Contributions

This thesis has been written in a sandwich format based on the papers co-authored by the PhD candidate (See Contributions section). Thus, the articles constituting Chapters 2-4 are appended in Appendices A and B. The following describes my contribution to these articles. Chapter 2 has been extracted from a review paper[14] and a book chapter[38]. The review paper was originally drafted by me and revised by my supervisors, Prof. Pouya Rezai and Prof. Anurag Tandon. The book chapter was written by me, with the help of Daphne Archonta (undergraduate student) who wrote the zebrafish section of the chapter, while it was revised by Prof. Pouya Rezai. The contents of chapters 3-4 have been extracted from

four journal articles[42–44] (Two under review). For all papers, I designed and performed the experiments, from device design and implementation to data analysis in collaboration with Daphne Archonta. I wrote the original drafts and the initial responses to reviewers and they were revised by Prof. Pouya Rezai. Prof. Pouya Rezai and Prof. Anurag Tandon helped with idea development and device design enhancement and provided constructive feedback to guide my research. Prof. Terrance Kubiseski provided the required *C. elegans* strains and training for *C. elegans* maintenance. He also helped with reviewing final drafts of the journal and conference papers. I was financially supported by the Ontario Trillium Scholarship in years 1-4 and by NSERC and MITACS grants to Prof. Pouya Rezai for my research costs in years 1-5 and stipend in year 5.

1.5 Thesis Outline

In this thesis, various *C. elegans* microfluidic platforms were developed to improve the EF-based assays and further understand the electrosensation of *C. elegans*. This thesis consists of 5 chapters presented in a "sandwich thesis" format. It contains an introductory Chapter 1, a literature survey in Chapter 2, a brief description of the common materials and methods in Chapter 3, a summary of published or under review papers in Chapter 4, and finally a conclusion Chapter 5 with recommendations for future works. Chapters 2-4 have been extracted from the published book chapter[38], review paper[14] and technical journal papers[42–44] as described before.

- **Chapter 1: Introduction**

  Chapter 1 provides the motivation behind the work, the scientific and technological gaps, the thesis goal and objectives, and the thesis outline.

- **Chapter 2: Literature survey**

  This chapter is divided into two main sections. Section 2.1 provides a review of *C.*

elegans based conventional and microfluidic approaches to study PD and other diseases. As a focal point, we provide a brief introduction about PD and its genetic and environmental causes. Then, the applicability of *C. elegans* as a model for PD is discussed in order to give an insight into the neurotoxicity and neurodegenerative disease pathologies, pathogenesis, mechanisms, and pathways. Moreover, a complete list of the commonly used *C. elegans* strains for studying PD and multiple compounds that show PD therapeutic effects in *C. elegans* is provided. Next, we show that using microfluidics, conventional laboratory-based assays on *C. elegans* have been automated by incorporating various actuation and sensing mechanisms to enhance the assay precision and sensitivity. The common worm manipulation techniques such as worm immobilization, synchronization, body orientation, and stimulus exposure are reviewed while focusing on the methodologies that can be utilized for *C. elegans* PD studies in the future. Finally, the worm-based microfluidic technologies for studying NDs that aided in HTS of drugs were reviewed.

In the second section of the chapter (Section 2.2), an up-to-date review is provided on the developed techniques to interrogate and use electrosensation of *C. elegans* for the development of various manipulation and chemical and genetic screening tools. Several on-plate and on-chip techniques are reviewed to investigate the worms' response to DC and AC EF.

- **Chapter 3: Experimental methodology and common procedures**

  In this chapter, a brief summary of the common experimental procedures, used throughout the thesis, is presented. The common fabrication techniques for the development of microfluidic devices presented in this research are discussed in detail. Followed by that, *C. elegans* preparation techniques, and the common experimental setup are reviewed. These techniques are extracted from the publications listed in Chapter 4 while providing more details about the animal handling procedures. The data analysis methods are discussed separately in each paper.

- **Chapter 4: Summary of published papers**

  In this chapter, the published papers and submitted manuscripts resulting from this research are summarized. In chapter 2, the potential application of *C. elegans* electrotaxis to chemical and gene screening will be shown. However, most of the developed techniques were based on testing single animals with no on-chip imaging and a maximum throughput of 20 worms per hour[29], hindering the possibility of using electrotaxis for large scale chemical and gene screening. Therefore, to increase the electrotaxis assay's throughput and incorporate on-chip imaging, two methods were developed to either increase the number of worms tested simultaneously or shorten the assay time by performing the electrotaxis test in a more confined environment. The first paper[43], addressing Objective 1, focuses on enhancing the throughput of the electrotaxis assay by proposing a parallel-channel device that allowed electrotaxis testing and neuronal imaging of up to 16 worms simultaneously. The second paper[42] which is related to Objective 2 introduces a complementary microfluidic device and method to the free movement-based electrotaxis assay. The T-shaped channel in this device incorporated an electrotaxis channel and a tapered channel for worm capturing and imaging. It allowed immobilizing the worm partially from one side while letting the other side respond to EF, achieving a faster assay in a more confined space. The device also allowed correlating the electrotaxis behaviors with the neuronal processes in worm models of PD exposed to neurotoxins and neuroprotective compounds. It also helped in answering fundamental questions related to the involvement of neurons in specific body regions to the EF in Objective 2. The results suggested that the mid-body neurons around the vulva are involved in electrosensation. Building upon that, the third paper[44] (Objective 3) investigates the effect of EF on the *C. elegans* egg-laying circuit in a discovered phenomenon termed "electric egg-laying". We showed that egg-laying circuit could be activated on-demand using DC EF. The paper offers a thorough understanding of the effect of EF on physiological and neu-

ronal responses of *C. elegans* leading to egg deposition. Next, the fourth paper[45] (Objective 4) shows the development of a microfluidic device to parallelize and perform the electric egg-laying assay in a faster manner, while using it as a technique for glucose and microplastic toxicity screening. This paper offers various phenotypic readouts in worm population and individual worm formats, demonstrating the importance of neurobehavioral screening at single-worm resolution to investigate the effect of microplastics uptake heterogeneity on neuron degeneration and egg-laying deficiency.

- **Chapter 5: Conclusions and recommendations for future work**

  This chapter provides the reader with an overview of the conclusions presented in this thesis and recommendations for the future work.

- **Appendices**

  The published or under review versions of the papers and chapters used to develop this sandwich thesis are amended in Appendices A and B.

Chapter 2

Literature Survey

The goal of this thesis was to enhance our understanding of *C. elegans* electrosensation, at neuron to behavior level, using microfluidic devices with controlled EF stimulations and enhanced behavioral throughputs. We applied these devices to study PD worm models and to screen the effect of various chemicals (e.g., 6-OHDA and glucose) and pollutants (e.g., microplastics) on worms. Therefore, we divided this chapter into two stand-alone literature survey sections, which have been published as a review paper[14] (Appendix A.1) and a book chapter[38] (Appendix A.2), with abstracts included below.

In the first paper, we briefly introduced PD and its environmental and genetic causes, highlighting that, to date, the exact roots of PD are yet to be known. Then, we showed that *C. elegans* is an invaluable model organism for neurological and behavioral research, especially in neurodegenerative disease investigations and chemical screening, by summarizing all identified compounds that show PD therapeutic effects in *C. elegans*. Followed by that, we showed that despite many advantages offered by this organism, technological deficiencies in achieving automated, sensitive, high-throughput, simple and low-cost screening have hindered the widespread use of this model in chemical screening, toxicology and gene screening. Thus, microfluidic techniques developed to phase out tedious laboratory-

based manipulation techniques for achieving automated assays with accurate quantitative analyses of the neurobehavioral responses of *C. elegans* to various external stimulations were reviewed. Moreover, we comprehensively reviewed the conventional and microfluidic approaches developed to study the effect of different neurotoxins and neuroprotective compounds on the aggregation or misfolding of a protein of interest in *C. elegans*. With this review paper[14], we aimed to provide the readers with the recent trends and advancements on the use of microfluidics and *C. elegans* for studying PD and other NDs at large.

In the review paper[14], we found that most of the developed microfluidic techniques for chemical screening focus on correlating the neurotoxins effects on the neurons by using fluorescently labeled cells while paying less attention to the sensory-motor behavioral responses. For instance, the use of active methods such as electrotaxis to evoke movement is beneficial in controlling and assessing the locomotion of worms in NDs. Therefore, in our recent book chapter[38], we presented the history of studying the electrosensation of *C. elegans* conventionally and using microfluidics. We have elaborated on the recent findings on the neuronal basis of electrosensation in *C. elegans* and shed light on the promising applications of the electrotaxis assay in disease pathology and chemical and gene screening. We hope that the knowledge acquired through reading this chapter will aid scientists and researchers in implementing microfluidic platforms for various biological applications involving *C. elegans* as a model.

2.1 Studying Parkinson's Disease using *Caenorhabditis elegans* Models in Microfluidic Devices

Youssef K, Tandon A, Rezai P., Integrative biology: quantitative biosciences from nano to macro, 2019, 11(5):186-207, doi:10.1093/intbio/zyz017. See Appendix A.1 for the full paper.

Review Paper Abstract- Parkinson's disease (PD) is a progressive neurological disorder associated with the loss of dopaminergic neurons (DNs) in the substantia nigra and the widespread accumulation of α-synuclein (α-syn) protein, leading to motor impairments and eventual cognitive dysfunction. *In-vitro* cell cultures and *in-vivo* animal models have provided the opportunity to investigate the PD pathological hallmarks and identify different therapeutic compounds. However, PD pathogenesis and causes are still not well understood, and effective inhibitory drugs for PD are yet to be discovered. Biologically simple but pathologically relevant disease models and advanced screening technologies are needed to reveal the mechanisms underpinning protein aggregation and PD progression. For instance, *Caenorhabditis elegans* (*C. elegans*) offers many advantages for fundamental PD neurobehavioral studies including a simple, well-mapped, and accessible neuronal system, genetic homology to humans, body transparency and amenability to genetic manipulation. Several transgenic worm strains that exhibit multiple PD-related phenotypes have been developed to perform neuronal and behavioral assays and drug screening. However, in conventional worm-based assays, the commonly used techniques are equipment-intensive, slow and low in throughput. Over the past two decades, microfluidics technology has contributed significantly to automation and control of *C. elegans* assays. In this review, we focus on *C. elegans* PD models and the recent advancements in microfluidic platforms used for manipulation, handling and neurobehavioral screening of these models. Moreover, we highlight the potential of *C. elegans* to elucidate the *in-vivo* mechanisms of neuron-to-neuron protein transfer that may underlie spreading Lewy pathology in PD, and its suitability for *in-vitro* studies. Given the advantages of *C. elegans* and microfluidics technology, their integration has the potential to facilitate the investigation of disease pathology and discovery of potential chemical leads for PD.

2.2 Microfluidic Devices to Study the Effect of Electric Field on *Caenorhabditis elegans* and *Danio rerio*

Youssef K, Archonta D, Rezai P., In: Micro and Nano Systems for Biophysical Studies of Cells and Small Organisms, Elsevier; 2021 (under review). See Appendix A.2 for the full book chapter.

Book Chapter Abstract- The central nervous system allows organisms to perceive the world by integrating and processing sensory information into motor outputs. The neuronal processes that guide a particular behavior like navigation are not well understood in humans and higher animal models due to their complexities. Model organisms such as *C. elegans* and *D. rerio* have made these investigations feasible due to their simple sensory and motor systems. Different stimuli such as heat, light, sound, mechanical force, and electrical signals have been used to probe the organism's sensing and movement mechanisms and processes. Electrical stimulation is of interest due to its suitability to stimulate nerves and muscles precisely and controllably. However, due to the small size and continuous stochastic movement of these model organisms, and the complexity of their environment, electrical stimulation has been limited in the existing experimental assays. Microfluidics has offered various platforms to interrogate the effect of electric stimulation on small model organisms in an automated, high-throughput, and accurate manner. In this chapter, we reviewed the majority of the conventional and microfluidic techniques developed to date to investigate the neuronal circuits involved in electrosensation of *C. elegans* and *D. rerio*. Moreover, we reviewed the promising electric-based applications for on-demand manipulation and screening of these organisms. Our assessment of the field reveals that despite the noteworthy research on electrosensation and electrotaxis, many fundamental and applied questions and gaps are yet to be addressed. The major ones are the underlying pathways of

electrotaxis, the limitations of electric sensorimotor screening, enhancing the throughput of electrotactic technologies and developing phenotypic assays that are specific towards organisms' identity.

Chapter 3

Experimental Methodology and Common Procedures

In this chapter, we cover all standard experimental procedures employed in the research conducted for this thesis. In particular, the first section (Section 3.1 consists of the design and fabrication of the photolithography masks and silicon (Si)-based molds to develop Polydimethylsiloxane (PDMS)-based microfluidic devices used in this research. In the second section, common chemicals and materials used, *C. elegans* maintenance and culture, and the standard experimental equipment are provided. By reading this chapter, one should be able to gain a more comprehensive and organized knowledge of the methodologies common between testing of different devices in this thesis and skip through the experimental sections of the attached papers.

3.1 Microfabrication

3.1.1 Mask Design and Fabrication

In this thesis, various microfluidic chips were developed to investigate different responses of *C. elegans* to electric signals, and each chip required a different design through fabrication of a dedicated photolithography mask. Therefore, each design was sketched by the computer-aided design (CAD) software SOLIDWORKS® (USA), and adjusted for printing on the mask using DRAFTSIGHT® software. There are various techniques to develop a mask. For example, the patterns can either be printed as a 5"×5" photomask on a 25,000 DPI transparency (CAD/Art Services Inc., USA) or imprinted on a 5"×5" Chromium mask using photolithography patterning and Chromium etching or lift off[46,47]. Photolithography is used to transfer a pattern onto a substrate by exposing a layer of photosensitive compounds (photoresist) to ultraviolet (UV) light to modify the solubility properties of the photoresist. Two types of photoresist, i.e., positive, or negative, could be used based on the design and the required final dimensions. Generally, a positive photoresist is used when the UV is used to make the exposed areas soluble to the etchant solution while the exposed areas of a negative photoresist will become insoluble in the etchant solution. In this thesis, all Si-molds were prepared using 5"×5" photomasks printed at CAD/Art Services. Briefly, the CAD files were laser imprinted using a laser photoplotter (LP9008M-UR, Orbotech) onto a polystyrene mylar mask (HPR-7s, Fujifilm, Tokyo, Japan). Then, the mylar mask is processed with a solution developer (QR-D1, Fujifilm, Tokyo, Japan) and a fixer (UR-F1, Fujifilm, Tokyo, Japan). Finally, the photomask is heat dried before usage.

3.1.2 Microfluidic Chip Fabrication

Si wafers with 4 in diameter and 500-550 μm thickness were procured from Wafer World Incorporation, USA. Negative photoresist SU-8 2075 and SU-8 developer were ordered from

MicroChem Corporation, USA. PDMS was purchased from Dow Corning Corporation, USA. A 4 in Si wafer was cleaned using acetone for 30 s, isopropyl alcohol (IPA) for 30 s, and deionized water for two minutes, followed by heating the wafer at 110°C for 5 minutes to evaporate the molecular water layer. Then, Si wafer surface cleaning was performed for enhancing the photoresist adhesion by exposing it to oxygen plasma (PDC-001-HP Harrick Plasma, USA) for 30 seconds. Different devices used in this thesis had different channel heights, but for better understanding, the process of fabricating 65 μm channels is described here. Four milliliters of SU-8 2075 was deposited on the Si substrate and pre-spun at 500 rpm for 5 s, then ramped to 3500 rpm for 30 s to achieve a 65 μm-thick layer (Figure 3.1A-I). Soft baking was performed at 65°C for 3 minutes and 95°C for 6 minutes prior to UV exposure at 365 nm with 11.1 mW/cm2 (UV-KUB 2, KLOE, France) for 14s, as shown in Figure 3.1A-II. Post bake was performed at 65°C for 1 minute and 95°C for 6 minutes, followed by rinsing the baked wafer in SU-8 developer for 5 minutes, then drying with an air gun (Figure 3.1A-III). Finally, the mold was hard-baked for 25 minutes at 150°C to obtain the final master mold. Features thicknesses were measured with a Bruker optical profiler (Bruker Optics, USA).

The negative replicas of the master molds were fabricated using the standard soft lithography process[48]. Masterflex tubes (L/S 14 size, Gelsenkirchen, Germany) were placed over the inlet and outlet reservoirs on the master molds (Figure 3.1B-I). Then, PDMS mixture in the ratio of 10 grams of elastomer base to 1 gram of curing agent was poured over the master molds and cured for 2 hours at 80°C (Figure 3.1B-I). The peeled PDMS layers were then irreversibly bonded to a glass substrate or other PDMS layers, as needed as per device design, using oxygen plasma (PDC-001-HP Harrick Plasma, USA) at 870 mTorr pressure and 30W for 30s (Figure 3.1B-I). The bonded devices were kept for 10 minutes at 65°C to enhance bonding. For EF application to the devices, two copper electrodes were inserted into the inlet and outlet reservoirs of the screening channels by punching through the PDMS, and then the surrounding areas were sealed by liquid PDMS

pre-polymer (Figure 3.1B-II). Finally, the devices were cured using a hotplate at 120°C for 15 minutes.

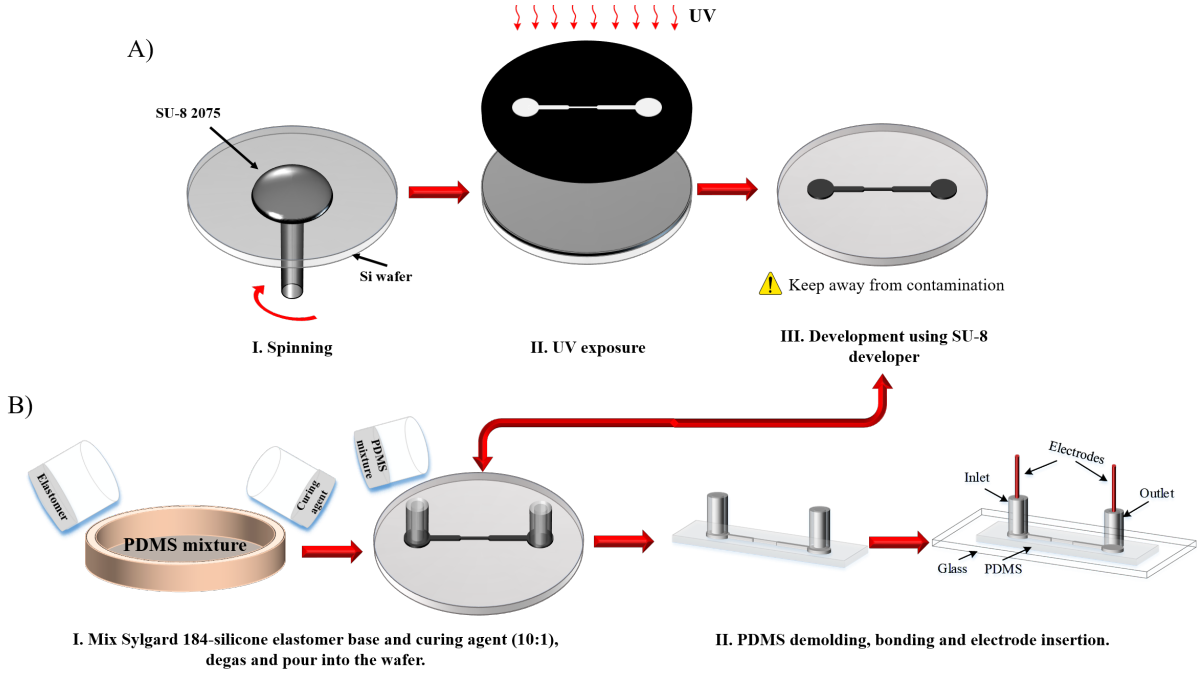

Figure 3.1: Microfabrication process for the development of single-layer Si-SU8 molds and PDMS-based microfluidic devices. (A) The photolithography process utilized to fabricate a SU8 layer on top of a Si wafer with a desired thickness corresponding to microfluidic channel depth. (B) Soft lithography process used to cast PDMS onto the Si master mold, followed by PDMS curing, bonding to a glass slide using oxygen plasma, and installation of electrodes at the inlet and outlet reservoirs.

3.2 Governing Physics for the Design of Our Microfluidic Devices

This section is divided into two subsections for discussing the basics of fluid flow and EF generation in microchannels.

3.2.1 Fluid Flow in Microchannels

The following three fundamental principles govern the physical aspects of any fluid flow: mass, momentum, and energy conservation, which form the well-known Navier-Stokes equations and can be reviewed in literature[49]. Fundamentally, to distinguish between the inertial and viscous flow regimes, Reynolds number (Re) which is the ratio between inertial ($F_I = ma = m\frac{du}{dt}$) and viscous ($F_v = \mu A\frac{du}{dy}$) forces is used as defined in Eq. 3.1.

$$Re = \frac{\text{Inertial forces}}{\text{Viscous forces}} = \frac{\rho U L}{\mu} \tag{3.1}$$

where ρ (Kg/m^3) is the density of the fluid, U (m/s) is the average fluid velocity, L (m) is the characteristics length of the channel, and μ (Pa.s) is the fluid dynamic viscosity. Most microfluidic channels are non-circular conduit-like channels. Therefore, the channel characteristic length equals the hydraulic diameter (D_h), which is defined as $((4A_c)/p)$. A_c (m^2) is the channel cross-sectional area, and p (m) is the wetted perimeter of the channel. For micro-swimmers like *C. elegans*, with very small size and slow swimming speed, and using microchannels in the range of 10s to 100s of micrometers, Re in M9 buffer would be in the range of 0.05-1.[50] At such low Re numbers, laminar flow is dominant due to the dominance of the viscous forces over inertial forces. Therefore, *C. elegans* can be manipulated inside the microchannel using pressure-driven flows generated with manual syringes, hydrostatic pressures, or syringe pumps. When no fluid flow is needed during an experiment, a zero-pressure difference across the channel should be maintained by manipulating the hydrostatic pressures at the inlet and outlet of the channel. The pressure drop across any channel can be estimated using Hagen Poiseuille's law (Eq. 3.2).

$$\Delta P = R_f Q, \qquad R_f = \frac{128\mu l}{\pi D_h^4} \tag{3.2}$$

where Q is the flow rate, R_f is the fluid flow resistance, and l is the channel length.

3.2.2 Electric Field in Microchannels

In addition to flow interactions with *C. elegans*, we would like to introduce the working principles of EF inside a microchannel. Microchannels are mostly fabricated in Si, glass, or polymers with rectangular cross-sections and specific lengths, widths, and heights depicted by l, W, and H, respectively.[51] Metal electrodes are either microfabricated or wire-connected from a power supplier to the inlet and outlet reservoirs for EF application. In the latter simpler case used in this thesis, the distance between the two electrodes is equal to the channel length (l). In the case of uniform electric charge density, Eq. 3.3 can be used to estimate the electrical potential difference, V , between the two electrodes.

$$V = -\int_1^2 E.dl \tag{3.3}$$

where E is the EF intensity at any point along the path l. According to Equation 3.3 and for a microchannel with a constant cross-section, E will be dependent on the applied external electric potential V and the distance l between the electrodes.

$$E = \frac{V}{l} \tag{3.4}$$

In addition to E and V, it is often required to know the electric current and the power dissipation in the channel. The channel electric resistance, R, can be used for this purpose; R is dependent on the channel dimensions (l, W, and H) and the electrical resistivity of the buffer (ρ_e). For a rectangular microchannel, R can be expressed as:

$$R = \frac{\rho_e l}{A_c} \tag{3.5}$$

The current flowing through the microchannel and the power dissipated to the media can be calculated based on Eq. 3.6 and Eq. 3.7, respectively.

$$I = \frac{V}{R} \tag{3.6}$$

$$P = \frac{V^2}{R} = \frac{E^2\, Vol}{\rho_e} \tag{3.7}$$

where Vol $(= l \times H \times W)$ is approximated as the microchannel volume.

The above principles were used to design all microfluidic devices used in this research. However, in the case of a complicated channel network, EF distribution was obtained using two-dimensional (2D) numerical simulation. In order to simulate the system, the steady-state DC electric module of the commercial software COMSOL Multiphysics® was used to solve the EF within a conductive media using Ohm's law (Eq. 3.6). The 2D geometry of the computational domain was generated using SOLIDWORKS® and imported into COMSOL for grid generation and application of boundary conditions. Generally, the models consisted of an assortment of channels connected through inlet and outlet reservoirs, where the electrodes were inserted. Electric conductivity of M9 media was determined experimentally using a 300μm-wide straight microchannel and found to be approximately 1.6 siemens/meter. This value was manually inserted into our model. Electric insulation boundary condition was set at all boundaries except the two end-reservoirs; one was defined with an electric potential, and the other was defined as ground. For grid generation, the built-in mesh module of COMSOL was used to generate triangular mesh elements. A grid independency study was conducted, and the optimum number of elements obtained was reported for each design.

3.3 *C. elegans* Maintenance

The *C. elegans* strains used in this study are listed in Table 3.1 and were obtained by the lab of Prof. Terrance Kubiseski at York University from the *Caenorhabditis* Genetics Center (University of Minnesota, USA). *C. elegans* were grown on standard nematode-growth medium (NGM) agar plates (6 cm in diameter Petri dishes) and maintained at room temperature (approximately 22°C) inside a biological safety cabinet. The cabinet was pre-sterilized with UV light and was daily cleaned with a mixture of 70% ethanol in water to eliminate any possible contamination. All chemicals were purchased from Sigma-Aldrich, USA. The detailed maintenance procedures are discussed in this section.

Table 3.1: *C. elegans* strains used in this study.

Strain	Genotype	Description	Ref
N2	WT Bristol	Wild type	
NW1229	evIs111 [F25B3.3GFP + dpy-20(+)]	Pan-neuronal GFP expression	[52]
BZ555	egIs1 [dat-1p::GFP]	GFP expression in DNs	[53]
NL5901	pkIs2386 [unc-54p:: α-syn::YFP + unc-119(+)]	α-syn YFP expression in muscle cells	[54]
LX1918	lite-1(ce314) vsIs164 lin-15(n765ts) X	VMs GCaMP5, mCherry	[39]
LX1960	vsIs172; lite-1(ce314) lin-15(n765ts) X	VC GCaMP5, mCherry	[39]
LX2004	lite-1(ce314), vsIs183 lin-15(n765ts) X	HSN GCaMP5, mCherry	[39]
MT1082	egl-1 (n487)	Egg-laying defective. Retains late stage eggs.	[40]

3.3.1 Nematode-growth Media and Bacterial Culture Preparation

The worm plates were prepared according to the Wormbook standard procedures.[55] Briefly, the NGM-plates were seeded with a "lawn" of *Escherichia coli* (*E. coli*) strain OP50 as a food source at room temperature. The food source was prepared by inoculating L-Broth media using a single colony of *E. coli* from the streak plate and culturing overnight at 37°C

on a shaker-incubator. L-Broth medium was prepared by autoclaving a mixture of 10 g Bacto-tryptone, 5 g Bacto-yeast, and 5 g NaCl in 1 L distilled water. Then, the inoculated enriched media was centrifuged to concentrate the bacterial culture, and the plates were seeded with 100 µl of the food source then left to dry overnight. All experiments were conducted using freshly prepared plates and bacterial culture.

3.3.2 Worm Chunking

To maintain the worms' viability, they were transferred to new NGM plates in a process termed 'Chunking', done due to the disappearance of the bacterial lawn and the formation of worm aggregates. The chunking process was performed close to a Bunsen burner or an alcohol burner to prevent contaminating the new NGM plates. A scalpel was sterilized by dipping it into ethanol and passing it across the alcohol burner. It was then used to cut and transfer a 0.5 cm^2 piece of the agar containing old or starving worms to a freshly prepared bacterial-seeded plate. The new plate was moved back to the biosafety cabinet and left to reproduce for worm synchronization. In case of any mold or fungus contamination, the chunking process was done twice in 5 minutes. A small piece of agar from the contaminated plate was cut and transferred to the sides of the new plates and far away from the bacterial lawn. Within 5 minutes, many worms were able to crawl towards the bacterial lawn. A new cut was then transferred to another bacterial-seeded plate to maintain a viable patch without any contamination. The same procedures were done every 2-3 days for all strains.

3.3.3 M9 Buffer Preparation

All *C. elegans* experiments presented in this thesis were conducted in microchannels filled with M9 buffer. M9 buffer contains various salts and is commonly used by the *C. elegans* research community because the worms can live in M9 for a week without any alteration

in their behaviors.[56] M9 buffer was obtained by adding 3 g KH_2PO_4, 6 g Na_2HPO_4, and 5 g NaCl in 1 L distilled water. The mixture was sterilized by autoclaving at 120°C for 30 minutes and left to cool down before adding 1 ml of pre-prepared and autoclaved 1 M $MgSO_4$. The buffer was renewed every month or when depleted.

3.3.4 Worm Synchronization

In all experiments, age synchronized, well-fed young adult worms were obtained using the popular Alkaline hypochlorite treatment.[56] Three days before the experiment, two plates from the required strain were chunked and left until most of the worms reached the gravid adult stage. Then, the plates were washed using M9 buffer and collected in a 15 ml Eppendorf tube (Figure 3.2A). The tubes contained a mixture of larvae, eggs, and bacteria. The mixture was centrifuged (Thermo Scientific™ Sorvall™ ST 40R, USA) three times at 1500 rpm for 2 minutes, and the supernatant was discarded and replaced with a new M9 buffer each time to eliminate the bacteria presence in the mixture. The collected worm pellet during the last centrifugation was then treated for 10 minutes with a solution of 3.875 mL double-distilled water, 125 µL NaOH, and 1 mL commercial bleach (Figure 3.2A). Following the treatment, the eggs were obtained by centrifuging the sample three times at 1500 rpm for 1 minute and incubated at room temperature overnight in 1 mL of M9 buffer using a RotoFlex™ tube rotator (Cole-Parmer, RK-04397-40, Canada). On the following day, the hatched larvae concentration was adjusted by counting the number of worms in a 10 µL suspension using Hemocytometer. Then, 1000-2000 L1 larvae were plated on freshly prepared NGM plates to allow for normal growth. Figure 3.2B shows the exact time to obtain a certain *C. elegans* age to be used in our experiments at room temperature.

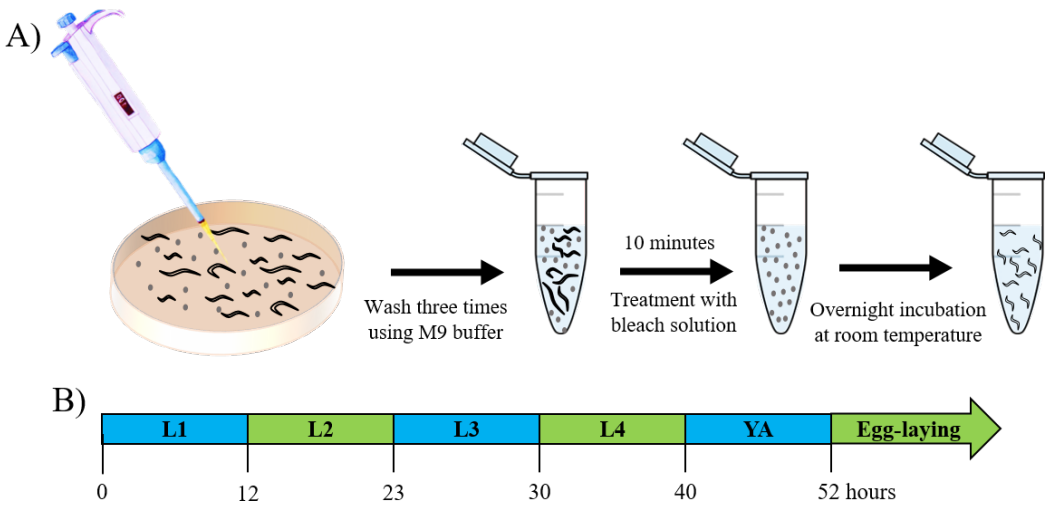

Figure 3.2: (A) Synchronization protocol using 5 ml bleach solution (3.875 mL of double-distilled water, 125 µL of NaOH, and 1 mL of commercial bleach). (B) Culture time needed to obtain specific larvae stage from L1 larvae population.

3.3.5 Worm Loading to the Microfluidic Device

Worms were either picked individually or washed off the plates for loading into the devices, based on the nature of the experiment. The picking was done using a worm picking tool with a platinum wire, acquired from the Wormstaff (USA). Before picking a worm, the tool was sterilized by dipping it in ethanol and burning it off using a Bunsen burner. It was then used to gently scrub the edge of the bacterial lawn from a pre-seeded NGM plate to make the tip sticky for simplifying the picking process. Moreover, it was also designed with a flat tip platinum wire to allow for gently lifting the worm of interest without injuring or killing it. Finally, the worm was loaded into the microfluidic device inlet.

For washing the worms off the plates, 3 mL of M9 buffer were used to collect the worms in a 15 ml Eppendorf tube. Then, the tube was left upwards on the bench for 15 minutes to allow for all adult worms to sediment while the smaller worms were floating in the supernatant. 2.5 mL of the supernatant were removed, keeping approximately 0.5 mL of M9 with adult worms.

3.4 Statistical Analysis

In this thesis, the data were presented in two formats, either as the mean ± standard error of the mean (SEM) or using box plots with medians, 25% and 75% percentiles, and maximum and minimum data points. The exact sample size used for each experiment is presented in the figure captions. We used the Mann-Whitney test to determine the statistical significance between two groups, while the statistical differences among multiple data points were determined using one-way ANOVA analysis. The significance levels were identified by stars, i.e., * for p-value<0.05, ** for p-value<0.01, *** for p-value<0.001, and **** for p-value<0.0001.

3.5 Experimental Setup

Figure 3.3 depicts the schematic diagram of the used experimental setup to investigate the response of *C. elegans* to EFs in microchannels. The setup consisted of one of the microfluidic devices designed in this research, a worm manipulation system, and an image acquisition system. The worm manipulation system consisted of a DC sourcemeter (KEITHLEY 2410, Keithley Instruments Inc., USA) and a vacuum pressure regulator (41585K43, McMaster-Carr, USA) connected to a vacuum pump (KNF™ Neuberger UN86KTP115 V, USA). The sourcemeter was controlled using a custom-developed MATLAB code to regulate the applied voltage, stimulation time, and EF direction. The EF polarity was easily reversed using the sourcemeter. The vacuum pump was regulated by a manual controllable vacuum pressure regulator. The image acquisition system consisted of an inverted microscope (DMIL LED Inverted Routine Fluorescence Microscope, Leica, Germany) coupled with a color camera (MC170 HD, Leica, Germany). It was used for capturing fluorescent images and movie clips for neuronal and behavioral analyses, respectively. In some assays needing a large field of view, imaging of worms inside the device was done by an upright

microscope (Leica MZ10F fluorescence microscope, Leica, Wetzlar, Germany).

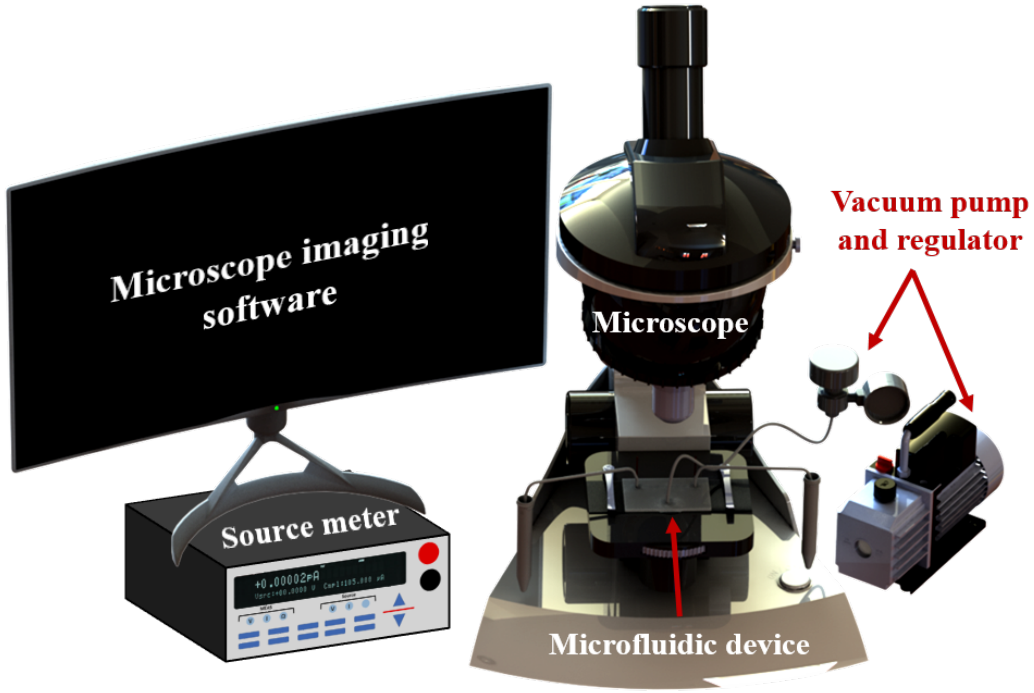

Figure 3.3: Schematic diagram of the experimental setup used to investigate *C. elegans* electric movement and egg-laying behaviors inside microfluidic devices. The experimental setup consisted of a microfluidic device, a worm manipulation system (manual syringes, electric sourcemeter, vacuum pressure regulator and vacuum pump), and an image acquisition system (a computer and an upright or inverted fluorescent microscope with a camera).

Chapter 4

Summary of Papers Presented in Full in Appendices

In this chapter, the published or under review papers and manuscripts of our research [42–45,57] as listed below, are summarized. In addition to the summary of the papers, this chapter will provide connectivity between the papers and how they are related to the research gaps and thesis objectives described in Chapter 1. The full papers are provided in Appendix B and are recommended for gaining a detailed understanding of our findings.

I. K. Youssef, D. Archonta, T. Kubiseski, A. Tandon, and P. Rezai, "Parallel-Channel Electrotaxis and Neuron Screening of *Caenorhabditis elegans*," Micromachines, 2020, 11, 8, p. 756.(Appendix B.1)

II. K. Youssef, D. Archonta, T. J. Kubiseski, A. Tandon, and P. Rezai, "Semi-mobile *C. elegans* electrotaxis assay for movement screening and neural monitoring of Parkinson's disease models," Sensors and Actuators, B: Chemical, 2020, 316, p. 128064.(Appendix B.2)

III. K. Youssef, D. Archonta, T. J. Kubiseski, A. Tandon, and P. Rezai, "Electric egg-laying: a new approach for regulating *C. elegans* egg-laying behaviour in a microchannel using electric field," Lab on a chip, 2021, In press, DOI: 10.1039/D0LC00964D.(Appendix B.3)

IV. Youssef, D. Archonta, T. J. Kubiseski, A. Tandon, and P. Rezai, "Microplastic Toxicity at the Neuronal, Behavioural and Physiological Levels Investigated on *C. elegans* in a Multi-Nematode Lab-on-a-Chip Device with Population and Single-Worm Screening Capability," Science of the Total Environment, 2021 "Under review".(Appendix B.4)

The focus of this research can be divided into three main directions, i.e., enhancing the behavioral throughput of the freely moving *C. elegans* electrotaxis assay while providing on-chip imaging for the tested worms (Objective 1)[43], investigating the involvement of neurons at specific body segments of *C. elegans* in electrotaxis response and using it as a confined assay for chemical and gene screening (Objective 2)[42,57], and investigating whether EF can induce other behaviours than electrotaxis (Objective 3)[44] with an intention to develop a single-worm resolution assay with enhanced behavioral throughput[45] (Objective 4).

In the introduction chapter, we showed the effectiveness of electrotaxis in controlling and assessing the voluntary locomotion of *C. elegans* for phenotypic behavioral studies and on-demand sensory-motor screening. However, the developed assays were based on testing single animals with no on-chip imaging and a maximum throughput of 20 worms per hour[29], hindering the possibility of using electrotaxis for large scale chemical screening. Therefore, in Paper I[43] and II[42], we developed two methods to either increase the number of worms tested simultaneously (Paper I) or shorten the assay time by performing the electrotaxis test in a more confined environment (Paper II).

In Paper I[43], addressing Objective 1 of the thesis, we report a simple and easy-to-use microfluidic method to conduct *C. elegans* electrotaxis movement assay and neuronal

imaging on up to 16 worms in parallel. Our device consisted of four channel sections, each 60μm-thick, as shown in Figure 4.1A; (1) tree-like branching channels for worm loading and distribution, (2) 16 parallel 300μm-wide channels for electrotaxis screening, (3) tapering channels, from 40 to 20 μm, for worm immobilization and fluorescent imaging of neurons, and (4) tree-like branching channels for unloading the worms. Constant channel dimensions at each bifurcation were used to maintain the same pressure and voltage drop up to the electrotaxis screening channels to smoothly load the worms and provide a constant EF throughout all the 16 screening channels for electrotaxis studies (Figure 4.1B). In the absence of EF stimulation, the worms were haphazardly swimming inside the microchannels. During the EF stimulation period, several phenotypes including swimming speed, body bend frequency (BBF), electrotaxis turning time (ETT)[37], electrotaxis time index (ETI)[37], and neuronal fluorescence intensity were analysed. ETT is the time at which the worm successfully performed a complete turn after an EF reversal and started to swim towards the cathode. ETI is the ratio between the actual swimming time towards the cathode to the total time of the experiment. It was defined to account for the intermittent stops and reversals happening during the movement towards the cathode. The performance of the device was confirmed by investigating the electrotaxis responses of wild type worms and validated against established single-worm electrotaxis[26,37] phenotypes, highlighting the applicability of our method for multi-worm screening. Then, mutant screening was demonstrated using the NL5901 strain[14], carrying human α-synuclein in the muscle cells, by showing the associated electrotaxis defects in average speed (Figure 4.1C), BBF and ETI. Moreover, chemical screening of a PD worm model was shown by exposing the BZ555 strain, expressing GFP in the DNs, to 6-OHDA neurotoxin. The neurotoxin-treated worms exhibited a reduction in electrotaxis swimming speed, BBF, and ETI as well as DNs fluorescence intensity (Figure 4.1C). Our technique increased the number of worms that could be tested simultaneously, achieving at least 9 worms every 5 minutes, which has not been achieved previously for electrically induced behavioral assays even with automated

systems[29]. We envision our technique to be used widely in *C. elegans* based movement disorder assays to accelerate behavioral and cellular phenotypic investigations.

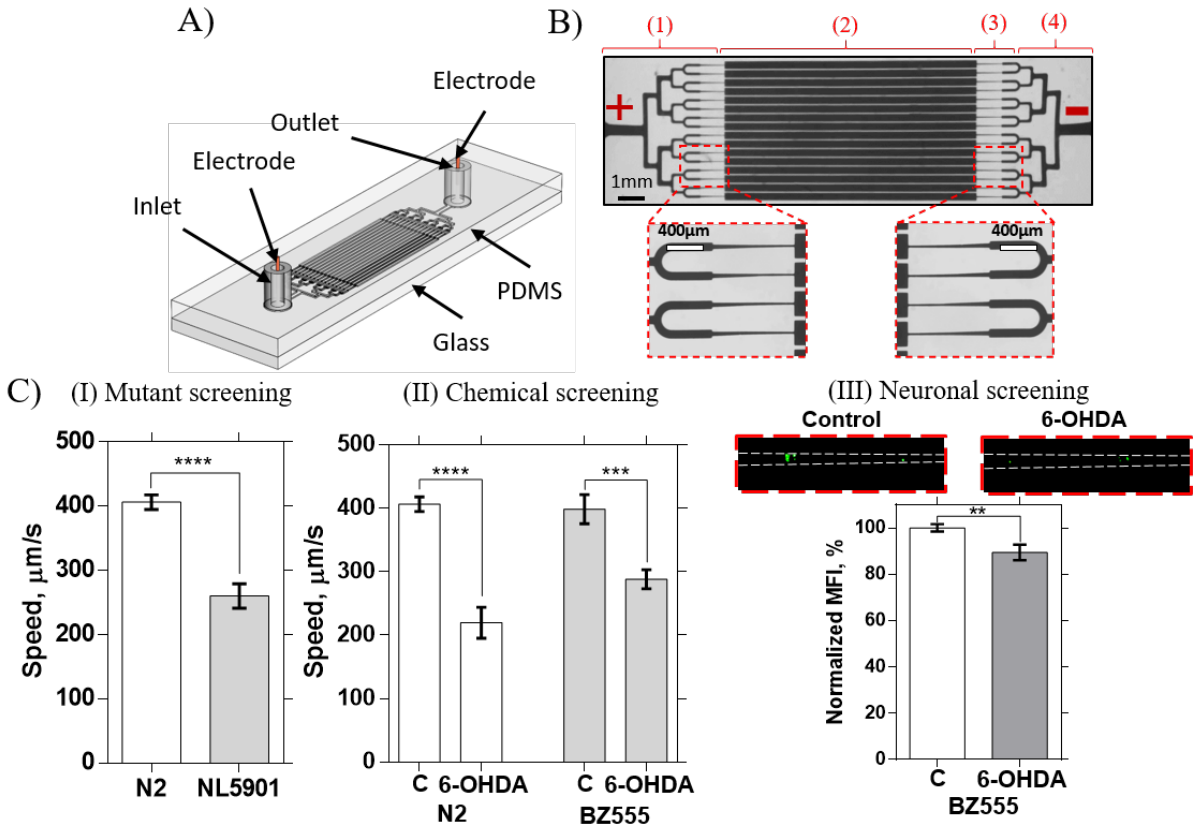

Figure 4.1: (A) Schematic of the parallel electrotaxis microfluidic chip (3 cm × 1.5 cm) consisting of one inlet and one outlet that are connected by four modules shown in (B): (1) worm loading and distribution channels, (2) 16 parallel electrotaxis screening channels, (3) tapered channels for worm immobilization and imaging, and (4) unloading channels. (C) Application of the microfluidic device at EF = 3.7 V/cm to (I) mutant screening using NL5901 strain expressing α-syn (N=19/21 responders), (II) chemical and (III) neural screening using N2 (N = 16/17 responders for control and N = 27/29 responders for exposed worms) and BZ555 strain (N = 19/20 responders for control and N = 24/29 responders for exposed worms) exposed to 250 µM 6-OHDA (controls are shown by "C").

Next, we noticed that all previously developed electrotaxis techniques including our parallel technique are based on the free movement of *C. elegans* and exposing the entire

worm to EF, limiting the ability of investigating the neuronal basis of electrotaxis using non-mutant worms[24,26,29,30,33,37,43]. Moreover, although our developed technique in Paper I[43] increased the behavioral throughput of the electrotaxis assay, it had a large footprint, requiring the use of a stereomicroscope with low magnification. Each round of experiments required at least 5 minutes due to the need for the worm to swim for a few centimeters along the electrotaxis channel. Therefore, we sought to address these limitations by investigating the electrotaxis of semi-mobile worms, which could help in further understanding the electrosensation of *C. elegans* and making the assay faster. In this investigation (Paper II[42]), **addressing Objective 2 of the thesis**, we first studied the effect of selective exposure of the worm's head or tail to electricity to explore whether partial exposure results in a directional electrotaxis. We investigated the involvement of neurons or muscles in certain body parts in electrotaxis. To do so, we introduced a novel microfluidic device to test the electrotaxis of semi-mobile *C. elegans* and image them immediately after the behavioral assay. The device, shown in Figure 4.2A-B, consisted of an electrotaxis screening channel integrated with a mid-region perpendicular tapered microchannel that was used for (1) worm tail or head trapping for electrotaxis screening and (2) full-body immobilization for neuron imaging (Figure 4.2C). A young adult worm could be trapped from its tail or head using a negative pressure inside the tapered channel, leaving the rest of the worm's body free to move inside the electrotaxis channel (Figure 4.2D). In the absence of electric field, erratic flapping behavior was observed, and the worms were not able to sustain a specific direction. Semi-mobile *C. elegans* with trapped tails demonstrated electrotaxis orientation towards the cathode, which implies that the tail neurons are not heavily involved in electrosensation. Interestingly, the response of head-trapped worms was also with the tail towards the cathode but with significantly lower ETI and slower ETT compared to the tail-trapped worms, implying the involvement of the mid-body neurons in electrotaxis (Figure 4.2D). For biological application to PD studies, we showed that human α-synuclein protein accumulation or exposure to neurotoxin 6-OHDA affected the electrotaxis phenotypes of

semi-mobile worms (Figure 4.2E). Moreover, L-DOPA rescued the electrotaxis of 6-OHDA exposed worms. The above behavioral effects of 6-OHDA and L-DOPA corresponded well with the degeneration of DNs and rescue of dopamine transmission, confirmed by on-chip fluorescent imaging. The semi-mobile *C. elegans* electrotaxis assay time is 3-folds shorter and 20-folds less space-consuming, compared to the freely moving assay. This makes the technique amenable to parallelization for the design of multi-worm electrotaxis and neuronal screening devices. This multi-worm semi-mobile assay was also attempted in our investigations with preliminary results reported in Chapter 5.

Using the semi-mobile technique, we indicated that the head neurons are contributing to electrotaxis but are not exclusively responsible for it, highlighting an interesting question of whether the mid-body neurons are involved in electrotaxis. *C. elegans* neuronal system is predominantly located at the head and the tail, connected through the ventral cord which runs through the entire length of the worm[58]. In the mid-body, some ventral cord neurons as well as the vulva neurons are located[40]. Therefore, as a proof of concept, the MT1082 strain[40] lacking hermaphrodite-specific neurons (HSN) in mid-body, responsible for initiating egg-laying in *C. elegans*, was tested by trapping their tail in the device in a follow up conference paper[57]. The results showed that MT1082 worms were able to sense the EF and orient towards the cathode but again with significantly lower ETI and slower ETT. Accordingly, we concluded that the loss of HSN motor neuron significantly decreases the electrosensory behaviour, which supports its involvement in electrotaxis. Since vulva neurons showed involvement in *C. elegans* electrosensation, we asked whether the egg-laying and electrotaxis behaviors may partially share pathways. Therefore, we fabricated a 4cm-long and 300µm-wide microfluidic electrotaxis channel[26] and tested the effect of EF on gravid adult worms. In these preliminary assays, worms were first facing towards the cathode, however when the EF was reversed, they showed a tendency to turn slowly towards the cathode and while doing so, they also deposited eggs, a phenomenon that was

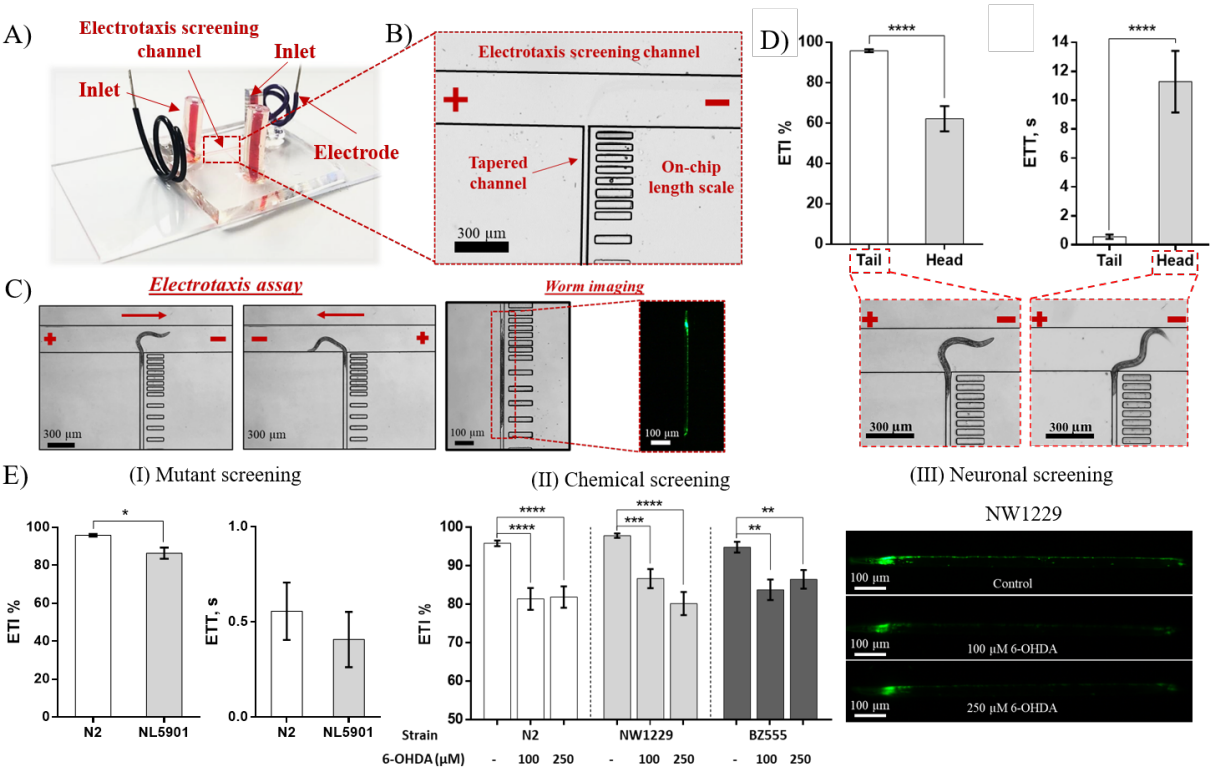

Figure 4.2: (A) 3D schematic of the microfluidic chip for investigating the electrotaxis response of semi-mobile *C. elegans* which consists of the electrotaxis screening channel with end electrodes and a perpendicular tapered channel for worm partial and full trapping as well as imaging. (B) The T-junction region of the device shown under 5x microscope magnification. (C) Electrotaxis response of a semi-mobile tail-trapped worm under exposure to a 4V/cm DC EF (head towards cathode) and an immobilized NW1229 worm fluorescently imaged inside the microfluidic device. (D) Electrotaxis response of semi-mobile head and tail trapped N2 *C. elegans* in the microfluidic device. (E) Application of the microfluidic device to (I) mutant screening using NL5901 strain expressing α-syn and (II) chemical and (III) neuronal screening using N2, NW1229, and BZ555 strains exposed to 100 and 250 µM 6-OHDA.

not shown before.

C. elegans egg-laying is an established rhythmic behavior of interest to the neuroscience community. It is controlled by a simple neural circuit that can be excited to produce a consistent behavioral output[39,40]. *C. elegans* egg-laying involves interactions between vulva muscles (vms), two HSNs, and six ventral cord (VC) neurons[39]. Worms lay eggs in a

temporal stochastic manner that fluctuates between active state, during which the worm lay eggs, and inactive state, during which no egg-laying occurs[39]. Several environmental factors can stimulate or halt egg-laying[59]. For instance, optogenetics is the primary method used to stimulate neurons to study the sensorimotor pathways involved in egg-laying[39]. However, it is restricted to genetically modified worms with light-sensitive ion channels, calling for a simple, on-demand, and inclusive egg-laying stimulation technique applicable to wild-type worms. In this endeavor, we demonstrated for the first time that DC EF evokes the *C. elegans* egg-laying neural circuit (Paper II). Therefore, in Paper III[44], a simple mono-layer microfluidic device was developed with end-electrodes for electric stimulation and an electrical trap to confine the worm in the field of view of a microscope, while allowing regular egg release (Figure 4.3A-B). At first, the novel effect of EF on adult *C. elegans* egg-laying in a microchannel was discovered and correlated with neural and muscular activities, **addressing Objective 3 of the thesis**. The quantitative effects of worm aging and EF strength, direction, and exposure duration on egg-laying was studied phenotypically using egg-count, body length, head movement, and transient neuronal activity readouts (Figure 4.3C-D). The worms' muscle activity was quantified through the rate of contraction and relaxation under the influence of EF, and we showed that it was independent of the EF direction. Transgenic lines expressing the fluorescent Ca^{2+} reporter GCaMP5 in HSNs, vms, and VCs neurons and a HSN mutant line were used to investigate the electric egg-laying behavior (Figure 4.3E-F). This study has provided exciting insights about egg-laying due to exposure to EF, but the reason behind cell excitation towards the anode, not the cathode, needs further investigation. Next, we aimed at investigating whether the loss of HSNs will reduce the electric egg-laying rate to show the application of our technique in mutant screening. Our microfluidic chip has aided, for the first time, in studying the role of HSNs in electrosensation and egg-laying, and we showed that loss of HSNs does not fully stop the electrical egg deposition, but it decreases the egg-laying rate significantly. This highlights the applicability of this technique for cellular screening and mapping of the

neural basis of electrosensation in *C. elegans*.

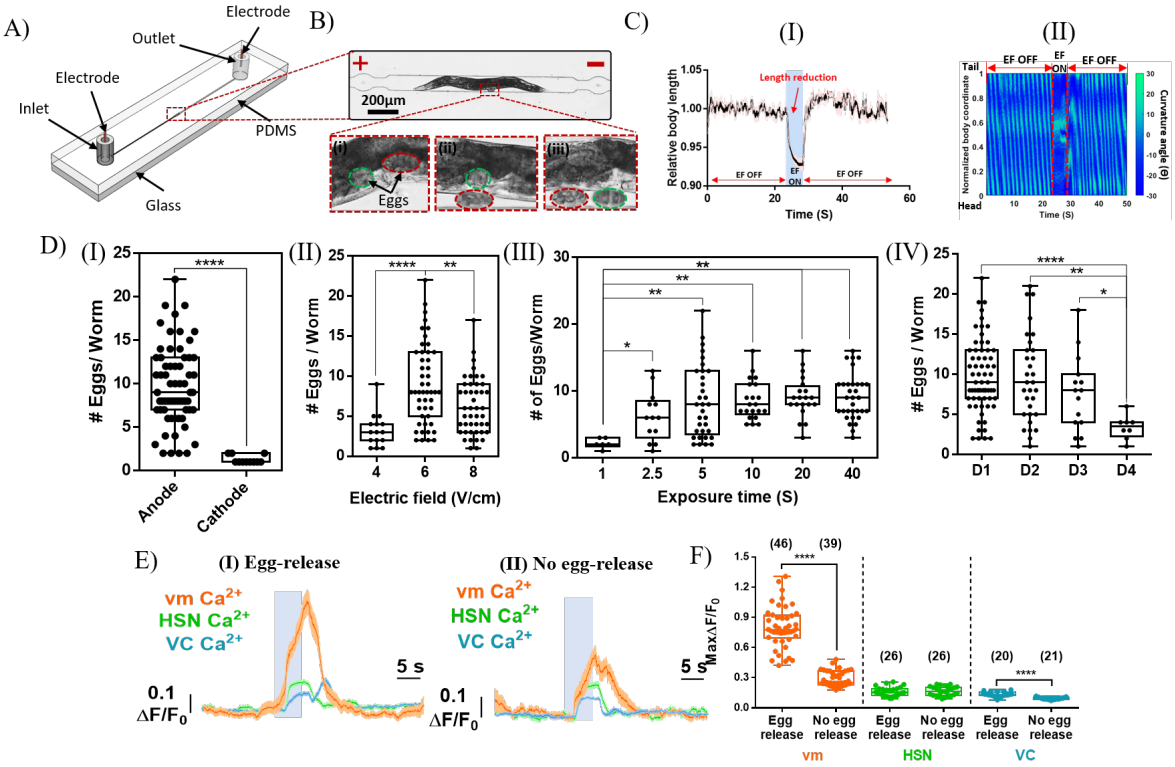

Figure 4.3: (A) Microfluidic device (2.5cm×1cm) consisting of an inlet, an outlet, and a symmetrical microchannel with a mid-trap for worm testing and two end electrodes for EF stimulation. (B) worm trap. A worm was trapped, and eggs were released with various EFs. (C) (I) Normalized body length, and (III) body curvature plot. (D) (I) EF direction, (II) EF strength, (III) EF pulse duration, and (IV) worm age effects on the total number of eggs laid over 10 minutes. (E) Overlapped Ca^{2+} transients of the vms, HSN, and VC neurons during (I) egg-release and (II) no egg-release states. (F) Peak normalized fluorescent activities of vms, HSNs and VC neurons during egg release and no egg release states under anodal stimulation of 6 V/cm EF pulses with 5s on and 25s off.

Lastly, we aimed at parallelizing and performing the electric egg-laying technique in a faster manner for toxicological studies to **address Objective 4 of the thesis**. Therefore, in Paper IV[45], we reported a novel microfluidic electric egg-laying assay for phenotypical assessment of multiple worms in parallel (Figure 4.4A-B). The device contained 8 paral-

lel worm-dwelling microchannels called electric traps, with equivalent electrical fields, in which the worms were electrically stimulated for egg deposition and fluorescently imaged for assessment of neuronal expression (Figure 4.4A-B). Exploiting the concept of hydrodynamic resistance, tree-like branching channels were used for worm loading, distribution and unloading in this device (Figure 4.4C). Moreover, a new bidirectional stimulation technique was developed, and the device design was optimized to achieve a testing efficiency of 91.25%. We achieved an assay time of 10 min and a behavioral throughput of up to 40 worms/hr, which was mainly limited by our microscopic field of view. Our method is significantly faster than conventional egg-laying assays with 4 hr assay time and 5 worms/hr throughput. The established effect of glucose on natural reproduction[60] was used as a proof-of-principle experiment to test the suitability of our assay. Exposure of worms to 100mM glucose resulted in a significant reduction in their egg-laying and size. Next, we noticed that environmental pollutants like microplastics are posing health concerns on aquatic animals and the ecosystem[61,62]. Microplastic toxicity studies using *C. elegans* as a model are evolving[63–69], but methodologically hindered from obtaining statistically strong data sets and detecting toxicity effects based on microplastics uptake and correlating physiological and behavioral effects, at an individual-worm level. Therefore, the effects of 1μm polystyrene microparticles at concentrations of 100 and 1000 mg/L on the electric egg-laying behavior, size, and neurodegeneration of N2 and NW1229 (expressing GFP pan-neuronally) worms were also studied (Figure 4.4D-E). Of the two concentrations, 1000 mg/L caused severe egg-laying deficiency and growth retardation as well as neurodegeneration (Figure 4.4D-E). Additionally, using single-worm level phenotyping, we noticed intra-population variability in microplastics uptake and correlation with the above physiological and behavioral phenotypes which was hidden in the population-averaged results. Taken together, these results suggest the appropriateness of our microfluidic assay for toxicological studies and for assessing the phenotypical heterogeneity in response to microplastics.

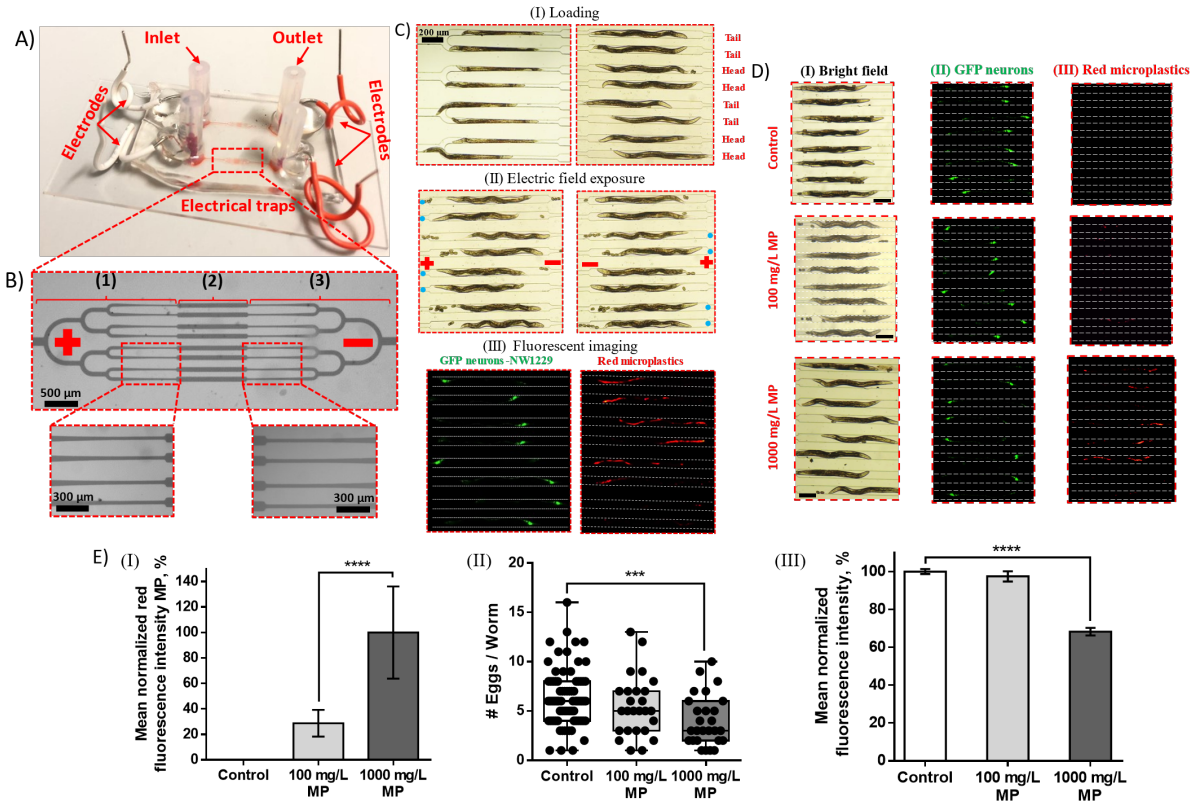

Figure 4.4: Microfluidic device for studying the electric egg-laying of 8 worms in parallel. (A) An image of the actual chip, housing two devices in parallel, each consisting of one inlet and one outlet interconnected with three channel sections shown in (B): (1) Tree-like worm loading and distribution channels with end-tapered channels (left inset), (2) 8 parallel electrical traps for worm housing and imaging during the experiment, and (3) worm unloading channels with tapered connections to the electric traps (right inset). (C) Capturing and investigating the electric egg-laying behavior and microplastic accumulation in 8 worms in parallel. (I) Loading procedure through the branching channels. (II) Egg-laying response of worms when the anode was at their head or tail. (III) fluorescent images at the traps showing (left) GFP neurons of NW1229 worms and (right) red fluorescent microplastics ingested by the same worms. (D) GFP expression of NW1229 *C. elegans* fed with 100 (N =30) and 1000 (N= 45) mg/L 1µm polystyrene microplastics. (I) Bright field (Scale bar = 200 µm) and fluorescent images for neuronal system (II) and microplastics (III) at 0 (control), 100, and 1000 mg/L microplastics. (E) The effect of microplastics at 100 mg/L and 1000 mg/L concentrations on adult NW1229 *C. elegans* expressing GFP pan-neuronally. (I) Microplastic intake rate determined by calculating the mean red fluorescent intensity of the ingested microplastics and normalizing with the signal at 1000 mg/L. (II) Number of electrically deposited eggs per worm counted over 10 min. (III) Neurodegeneration determined by calculating the normalized mean green fluorescent intensity of the neurons.

Chapter 5

Conclusions and Future Work

5.1 Summary of the Thesis

The process of discovering a drug is extremely time consuming and expensive. The optimized lead chemicals that are developed during preclinical *in-vitro* assays in drug discovery usually fail at *in-vivo* stages of screening, mainly due to the toxicity effects[8]. So far, the search for *in-vitro* and *in-vivo* models for toxicology and chemical screening has resulted in the introduction of small-scale whole biological organisms that have a great potential to fill the gap in between conventional 2D cell cultures and complex animal models[13]. One of the most widely used small-scale model organisms for toxicology and chemical screening is *C. elegans*. This organism offers several advantages such as cellular and neuronal simplicity, genetic homology to humans, rapid and low-cost growth and maintenance in labs, body transparency for microscopy, and amenability to genetic manipulation for the investigation of various neurobehavioral processes in a whole biological organism[14]. Models of *C. elegans* for studying human diseases have already been developed and helped not only to expand the fundamental understanding of disease pathology, but also to screen for potential genes

and chemicals as well as their relation to behavioral phenotypes[14]. Nonetheless, despite many advantages offered by these organisms, technological deficiencies in achieving automated, fast, simple, and low-cost screening assays have hindered the widespread use of these models in the chemical screening, toxicology, and gene screening arenas. Therefore, interests in *C. elegans* research and its small size have aroused the development of various lab-on-a-chip systems to provide precise control and quantification of the nematode different sensory motor behaviors, such as electrotaxis, for chemical and gene screening.

Like many model organisms, *C. elegans* respond to electric field (EF) in a robust, concise, and persistent manner, by crawling towards the negative electrode of a polarized system in a phenomenon termed electrotaxis. Previous studies have solely focused on the electrotactic-induced *C. elegans*' movement and its use for chemical and genetic screening within microfluidic devices. Less attention has been paid to enhancing the throughput of this technique, understanding the involvement of different body parts in electrosensation, and investigating electrically-induced behaviours other than movement. Therefore, in this thesis, we developed microfluidic devices for enhancing the electrotaxis assay throughput and further investigating the electrosensation of *C. elegans*. Then, as a proof of concept for our developed assays, we used genetically and chemically induced models of PD as well as microplastics toxicity for showing the applicability of our techniques for behavioural and neuronal screening.

To cover the literature, a review paper[14] was published to comprehensively review the available *C. elegans*-based research, focusing on determining the effect of various neurotoxins and α-syn aggregation on neuron dysfunction and movement impairment of worms using conventional and microfluidic-based approaches. Then, we developed a book chapter[38] to review the majority of the conventional and microfluidic techniques used to date to investigate the neuronal circuits involved in electrosensation of *C. elegans*. Moreover, we reviewed the promising electric-based applications for on-demand manipulation and screening of *C. elegans* while showing how our work has contributed to the literature. Our

assessment of the field reveals that despite the noteworthy research on electrosensation and electrotaxis, many fundamental and applied questions and gaps are yet to be addressed. The major ones are enhancing the behavioral throughput of electrotactic technologies, developing phenotypic assays that are specific towards organisms' identity, and the underlying pathways of electrotaxis. In this thesis, we aimed to provide microfluidic technologies to fill some of these scientific and technological gaps.

In Paper I[43] (Objective 1), an easy to operate, simple to fabricate, and reusable microfluidic device where up to 12 worms could be smoothly loaded and electrotactically tested and imaged simultaneously was developed. Our assay took on average six minutes for all worms which significantly reduced the electrotaxis test time for each worm from 3-4 min[26] to about 30s in our parallel-channel device[43]. We showed that this device can be used in a wide range of *C. elegans* assays wherein movement and cellular phenotypes need to be investigated such as neurodegenerative disease studies using genetic and chemically induced models of PD. For instance, genetic screening was conducted using a worm model of PD expressing α-syn in muscle cells, and we proved that α-syn overexpression induced significant reduction in the worms' average speed, BBF, and ETI, whereas no effect on the ETT was observed. These findings implied that α-syn aggregation in muscles affect the worms' response to the EF, causing a decrease in worm motility and difficulty for the worm to maintain continuous swimming towards the cathode. In the future, it would be interesting to test a strain with α-syn overexpression in DNs to interrogate the behavioral effect of protein aggregation inside the neurons. Moreover, worms' electrotaxis response after exposure to 6-OHDA was studied to demonstrate the application of our device in chemical screening. Worms exposed to 6-OHDA demonstrated a noticeable decrease in electrotaxis and neuron fluorescent expression, contrary to the untreated worms, which showed intact neurons with strong GFP expression.

Most of the developed microfluidic techniques, including our parallel device[43], for exploiting *C. elegans* electrotactic activities for behavioral and genetic screening have large

footprints which necessitated the use of a microscope with large field of view. Moreover, the worms' continuous movement hinders the ability of exposing certain body segments to EF to further understand *C. elegans* electrosensation. Therefore, we, in Paper II[42] (Objective 2), proposed a technique in which the worm was captured from one end while the rest of the body was exposed to electric current with the advantages of fluorescently imaging the worm and spatially controlling the electrical signal exposure. Our results demonstrated that the tail-trapped worms show a robust response towards the cathode, just like the freely swimming worms, but at a 3-fold faster rate within a 20-fold smaller assay area. Moreover, contrary to what was expected when head-trapped worms are exposed to EF, we found that they also orient their tails towards the cathode, potentially indicating that the mid-body sensory-motor neurons are contributing to electrotaxis. Further investigation of this hypothesis requires designing devices to control the electrical exposure of worms with higher spatial resolution while applying less mechanical force to the head. Moreover, we showed that trapping the worms up to 30% of their length did not significantly affect their electrotaxis response rate, while the response was diminished when the worms were trapped at or beyond their vulva. This result further confirmed our hypothesis of mid-body neurons being involved in electrotaxis. Thus, in a follow up conference paper[57], we investigated whether neurons in the midbody region are contributing to the *C. elegans* electrosensation through testing MT1082 strain (lacking HSN in mid-body, responsible for initiating egg-laying in *C. elegans*). Our results showed that *C. elegans* electrosensation is not solely executed by the head neurons via testing a strain lacking a mid-body specific neuron.

The capability of our technique for gene and chemical screening was phenotypically tested using *C. elegans* models of PD. The results showed that both ETI and ETT alter by α-syn overexpression in *C. elegans* muscles and worms' exposure to 100-250μM 6-OHDA. Moreover, implementing imaging within an electrotaxis screening chip was not achieved before, which adds an advantage to our device. At each condition, the worms were flu-

orescently imaged and assayed to relate neural degeneration to electrotaxis impairment. Pre- and post-exposure of 6-OHDA treated worms to 100 μM L-DOPA, a commonly prescribed drug for PD, rescued dopamine transmission and revitalized electrotaxis response in worms. In the future, we aim to determine the pathway of action behind electrotaxis and its relationship with different PD-related genes.

In Paper III[44] (Objective 3), we further investigated *C. elegans* electrosensation and introduced, for the first time, a novel EF-evoked behaviour, termed electric egg-laying in a simple to use microfluidic device that enabled trapping and exposure of individual worms to controlled EF conditions. We investigated the effect of worm aging, EF strength and direction, and pulse duration on the egg-laying behaviour, and showed that on-demand egg-deposition could be electrically stimulated in our microfluidic device. Briefly, we characterized the electric egg-laying behaviour in a worm-fitting microchannel and determined the limiting worm age and EF strength, direction, and pulse duration within which maximum egg-deposition is observed. Egg-count was quantified along with several other phenotypes, including body length, head movement, and transient neuronal activities as measures of electrosensation at a single animal resolution. Interestingly and similar to stimulation of electrotaxis behaviour, electric egg-laying was maximized for the anode-facing worms with a significant increase in the egg-count and reduction in the body length and head motion. The EF stimulation was found to be associated with shortening in the body length and a decrease in the head movement frequency. Moreover, the worms appeared significantly more sensitive at the EF strength of 6V/cm, while all worms exhibited significantly lower response at low EF strengths. The egg-count was found to be independent of pulse duration, whereas the egg-laying response rate and duration were indirectly proportional to pulse duration. Due to the reduction in response duration at longer pulses, our technique has the potential to provide the pathway for developing a high-throughput egg synchronization method without involvement of chemicals (e.g., bleach[55]) or harming the organism.

This is the first time a connection between the egg-laying circuit and electrosensation

is reported, unraveling a pathway for further investigation and mapping of the neural basis governing these phenomena in *C. elegans*. Various strains, expressing intracellular calcium ion dynamics among the egg-laying neural circuit, including HSNs, VC neurons, and vms were imaged during the EF stimulation. The results exhibited EF directional-dependency of the HSNs, VCs, and vms, which might elucidate the innate cathode-driven orientation of *C. elegans* as a safety mechanism to lower the excitation of its cells. We further tested a mutated strain lacking the HSNs and demonstrated that EF still induces egg-laying but with a defective phenotype, which shows the applicability of our technique for mutant screening. Altogether, we reported novel electrically induced physiological and behavioural phenotypes discovered in *C. elegans* aiming to drive new hypotheses on the biological mechanisms governing electrosensation. Additionally, we established that EF stimulation of *C. elegans* within our microfluidic device has no adverse effects on the physiology of the nematodes.

Lastly, we envisioned that with small modifications to the existing design, several nematodes can be tested simultaneously under identical conditions, accommodating the needs to develop higher throughput electric egg-laying screening devices. Thus, in Paper IV (Objective 4), we showed that *C. elegans* electric egg-laying is an effective technique for toxicity studies using a mono-layer microfluidic device that enables trapping and exposing up to 8 individual worms in parallel to EF while allowing for on-chip fluorescent imaging. We optimized our microfluidic device and adopted a new bidirectional stimulation technique to achieve a behavioral throughput of 40 worms/hr, which could be further enhanced in the future with a larger microscope field of view. Using our microfluidic device, a large data set of multiple parameters such as electric egg-laying, worm length, worm diameter, and length reduction as well as neuronal and microplastics mean fluorescent intensities was obtained and analyzed in a population-averaged and individual responses manner. Glucose effect was investigated as a proof of concept for toxicity assays. Our findings implied that 100 mM of glucose induced abnormal electric egg-laying behaviour and resulted in

a smaller body size. Thus, in the future, we aim to use the technique for anti-diabetic drug screening. Moreover, we employed our device with two *C. elegans* strains (N2 and NW1229) to investigate the toxicity effects of 1 μm polystyrene microparticles, for the first-time using microfluidics, at concentrations of 100 and 1000 mg/L. Electric egg-laying, worm size, and neurodegeneration were analyzed in a fast manner using single-worm phenotyping. Our results showed that exposing worms to 1000 mg/L affected both neurons and their electric egg-laying behavior as well as their body size significantly. Using hierarchical clustering analysis and principal component analysis, we showed that single-worm phenotyping can reveal heterogeneity in microplastics uptake which was correlated to the deficiency in egg-laying.

5.2 Recommendations for Future Works

5.2.1 Challenges and Future Improvements of the Proposed Microfluidic Devices

Despite many of the experimental advantages offered by the developed microfluidic devices and methods in this thesis, we acknowledge that they may not be completely ready for adoption by the end user scientists to supplement or even replace their time-consuming and labor-intensive techniques. Here, we share our perspectives on how the microfluidic community needs to address the gap in technology implementation by communicating and collaborating with scientists. Moreover, we discuss some challenges and limitations of our devices that need to be tackled to make them more affordable and available for end-users with no engineering background.

For a microfluidic device to be fully adopted, it must provide appealing criteria from the economic and technical points of view. From an economic perspective, issues related

to cost-effectiveness, integrability, and adaptability are needed to be addressed in microfluidic devices. While the cost of microfluidic devices can be relatively low, the technology integrability within the biologists' laboratories and adaptability with existing facilities in the lab are significantly important. For instance, and as shown by a few recent papers[70,71], microfluidic devices need to be compatible with the existing pipetting-based fluid handling and multiwell plate-based screening techniques in biology laboratories. However, it will add a high cost to integrate the supporting equipment and to provide the required personnel training to use microfluidic devices under these settings. From a technical perspective, most of the current microfluidic technologies are sophisticated yet not stand-alone or fully automated to be used by minimally trained personnel. Standardization and robustness of device operation are other barriers to microfluidics implementation in end-user labs. It appears that technology adoption by small laboratories can be achieved easier with less complicated devices. While smaller labs may require devices that can assay a few worms at a time, many of the larger-scale end-users demand technologies with high-throughput and high-content screening capabilities, which are yet to be fully achieved with microfluidics in many of the *C. elegans* assays.

In terms of the proposed devices in this thesis, they were designed with cost-efficiency and operational simplicity in mind. However, for the devices to be efficiently working, more robust fabrication techniques need to be used to enhance the working cycles of these devices without breaking down. For instance, most of the devices in this thesis cannot be used over hundreds of cycles due to the degradation of the copper electrodes over time and leakage because of failure in the bonding of PDMS to glass or sealed surrounding areas of the electrodes. These issues can be tackled by using metal-deposition for gold electrode fabrication within the chips. To eliminate any leakage possibility, better fluidic interconnections should be used to seal the ports of the system while allowing the Plug'n'Play functionality without affecting the fluid flow. Moreover, during the experiments, maintaining a zero-pressure difference across the channels was problematic. Although integrating

on-chip microvalves will eventually stabilize the flow, it will add remarkable complexity to the devices. Another challenge was obtaining high-resolution images with objectives higher than 40× due to the use of standard microscope slides for sealing the PDMS devices. To overcome this issue, thin coverslips can be used to seal the devices; however, the devices will be prone to breaking, which will require the development of a custom-made holder for limiting the user access to the device.

Another challenge with all devices was with image processing of the recorded videos that took a tremendous amount of time to be analyzed. A dedicated custom-written image processing software is needed for each device, similar to what we have developed in Paper III.[44] For instance, for Paper I[43], we tried to develop software for determining the average speed, ETI, and ETT of the worms tested in parallel by following similar approaches for worm tracking using MATLAB. We were able to determine the worms' speed efficiently; however, the code is still under-developed to calculate the rest of the parameters such as ETI, ETT, and BBF. For Paper II[42], a custom-written MATLAB software can be developed to help determine the ETI and ETT of the worms by setting two threshold lines at the right- and left-hand sides of the worm in the electrotaxis screening channel. Using the times when the worm crosses the threshold lines, the two parameters can successfully be obtained. While the code developed in Paper III[44] has helped identify multiple phenotypes, we could not include the number of eggs as a parameter due to the proximity of the eggs to the worms' body that makes the software sometimes consider them as one object. However, we anticipate that by using machine-learning techniques to train our software on identifying the differences between eggs and worms, we can add the egg-laying parameter to the software. The development of this software will help automate the data analysis process and decrease human error probability.

The following steps were taken to develop a more automated setup control system for worm loading and imaging in microfluidic devices, in an attempt to increase the throughput of our experiments. In this pursuit, we developed a semi-automated system using our

parallel-electrotaxis device (Paper I[43]) for worm loading, electrotaxis testing, worm imaging, and worm unloading. The system, depicted in Figure 5.1, consisted of the microfluidic device, a worm manipulation system, and an image acquisition system. The worm manipulation system consisted of a DC sourcemeter (KEITHLEY 2410, Keithley Instruments Inc., USA), a pressure regulator (P#PR4021-200, Ingersoll Rand, Canada), a solenoid valve (P01540-11, Cole-Parmer, Canada), a power supply (SN B900655, Good Will Instrument Co., LTD. Taiwan), and a function generator (SN AFG3022C, Tektronix, USA). The function generator with a maximum voltage output of 5V and a custom-made signal amplification circuit were used to control the solenoid valve by generating a step function with variable duty cycles. The DC sourcemeter was used to supply an electric voltage of 50 V (equivalent to 4 V/cm electric field) for testing the electrotaxis response of the worms. The function generator and the DC sourcemeter were controlled using a custom-written MATLAB code for automating the process. Unfortunately, the air-pressure was regulated by a manual controllable pressure regulator; however, for automating the process, a MATLAB-controlled pressure regulator must be integrated within the system. The image acquisition system consisted of an inverted microscope (BIM-500FLD, Bio-imager Inc., Canada) and a camera (SN 14120187, Point Gray Research Inc. Canada) which was used for capturing movie clips of different experiments. The microfluidic device was connected through the inlet to a T-valve that connects the inlet to two separate Erlenmeyer flasks; one was containing the worms in an M9 solution; and the other was containing clean M9 buffer for device washing. The solenoid valve was connected to the T-valve for applying a pulsating pressure with different pressure values and duty cycles for investigating the loading process. The outlet of the device was connected to another Erlenmeyer flask for collecting the worms. A missing component that would have added great potential to the system is a motorized stage. Our preliminary investigations show the potential of automating the system for enhancing the behavioral throughput of our microfluidic devices. However, further investigations are needed to optimize the process and develop the system.

The fully-automated system will offer versatility in terms of applications (as detailed in the next section), worm control and image acquisition.

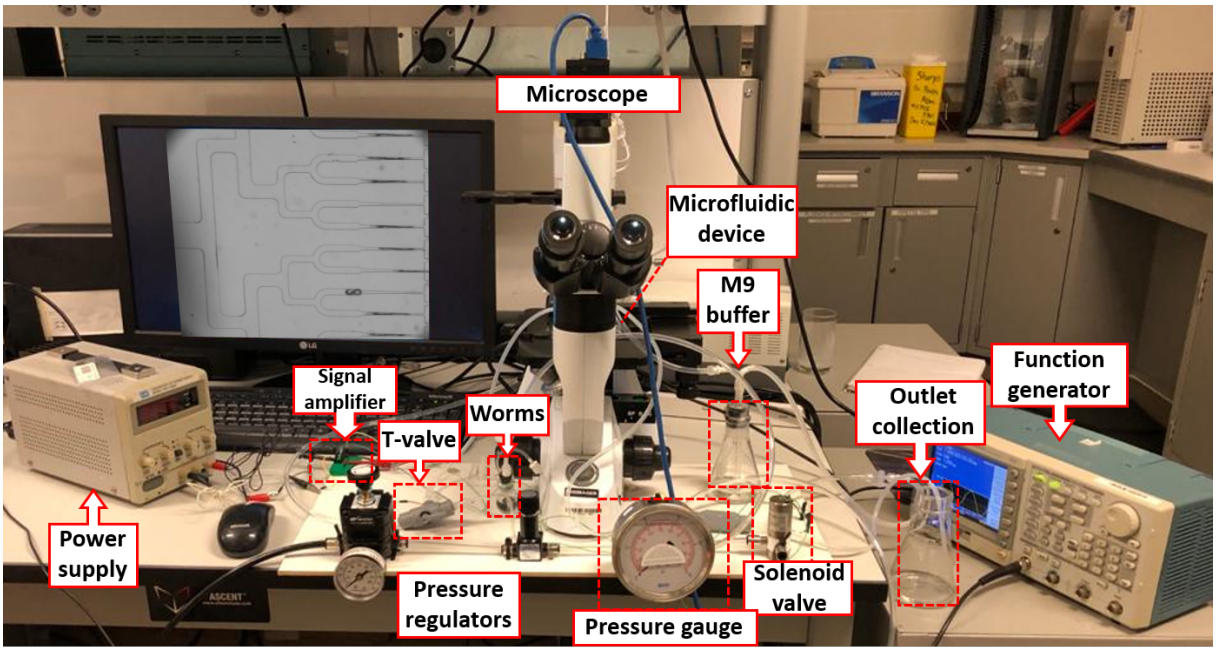

Figure 5.1: Experimental setup consisting of different components for automating the parallel electrotaxis device. The power supply, solenoid valve, pressure regulator, function regulator and signal amplification chip were used to supply pressure pulses for loading the worms into the microfluidic chip. The inverted microscope equipped with a camera was used for capturing videos for post-processing.

Lastly, throughout the thesis, we enhanced the behavioral throughput of the free-moving worm electrotaxis (Figure 4.1) and the electric egg-laying (Figure 4.4) assays by testing multiple worms in parallel. To enhance the behavioral throughput of the semi-mobile electrotaxis chip (Figure 4.2), we developed a proof of concept microfluidic device based on replicating the worm trap along the electrotaxis channel (Figure 5.2). The modifications do not meet the demands for high throughput screening yet, but this is the first step towards increasing the throughput of our technique in the future.

Figure 5.2A and B show the developed 60µm-thick single layer chip, which consisted of an electrotaxis screening channel and eight perpendicular trapping channels separated by

1.2 mm. All trapping channels were connected via tree-like branches to a single reservoir for applying a vacuum pressure. The electrotaxis channel length was increased from 2 cm to 3 cm to accommodate for the increased number of worms, and therefore, the applied voltage was increased from 8V to 12V to obtain a suitable range of EF. The same modeling approach reported in Chapter 3 was applied to determine the EF distribution in the microfluidic device with multiple trapping channels (Figure 5.2C). EF along the centerline A-A of the channel was plotted in Figure 5.2D where it is shown that the EF varies symmetrically from 3.5 V/cm at the two center traps to 4.2 V/cm in the two outer traps and the main channel. The reason behind this variation is the electric paths provided by the U-shape channels connecting the traps to each other. The effect of this EF variation on the electrotaxis response of young adult worms was neglected because the worms respond similarly to a range of 2-4V/cm EFs as reported earlier by Rezai et. al.[26].

Upon testing the device, most of the channels were filled with worms within 30s of activating the suction pressure (Figure 5.2B). From the 8 traps, N=6 were occupied with tail-trapped worms, N=1 with head-trapped worm and one trap was left open. However, the loading orientation and the trapped length of the worms were random with no consistent pattern between trials, which made testing the device and getting consistent results difficult. We focused on the tail-trapped worms and applied a DC EF on the worms while recording their responses. Unfortunately, although the worms were responding normally to EF when they were freely swimming in the electrotaxis screening channel, they were barely responding when trapped with their tails. We attributed the loss in response, potentially, to the fact that each worm was experiencing two different EF values due to the stepwise decrease in the EF (Figure 5.2C).

Next, we attempted to investigate different designs to control the trapped length of the worms, and to maintain constant EF across the electrotaxis screening channel. Figure 5.3 shows two different designs with two to four traps in parallel for characterization purposes.

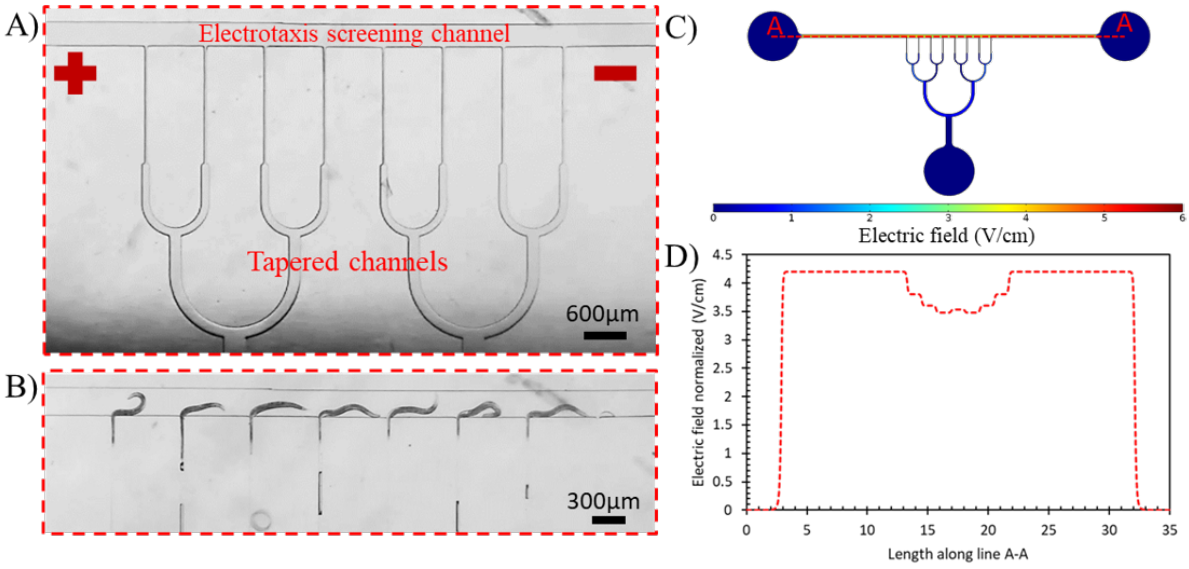

Figure 5.2: Proof of concept microfluidic chip design for parallel semi-mobile worm electrotaxis and COMSOL simulation of EF distribution in the multi-trap device when a 12V stimulus was applied along the electrotaxis channel. (A) A microscopic view of the chip showing the electrotaxis screening channel with end electrodes and branches of tapered channels. (B) Eight worms trapped in the chip for testing. (C) EF distribution in the chip. (D) EF along line A-A, showing that the EF along the electrotaxis channel is in the optimal range for young adult worms according to Rezai et al.[26].

In both designs, we decided to get rid of the tree-like branches that were the main reason for EF loss in the previous design. Therefore, each trap was connected directly to the suction chamber, far away from the electrotaxis screening channel.

In design I (Figure 5.3A), we used an S shaped trap to hinder the worms from being sucked completely into the tapered channels without the use of high-suction pressure. While we successfully trapped certain lengths inside the trap and worms were responding to EF (4V/cm), they were also randomly loaded with no tail or head preference. Pulling the worm inside the tapered channel for fluorescent imaging was also not easily achievable even with high-pressures. Moreover, the S-shaped channel prevented the smooth turning of the worm during the electrotaxis experiments.

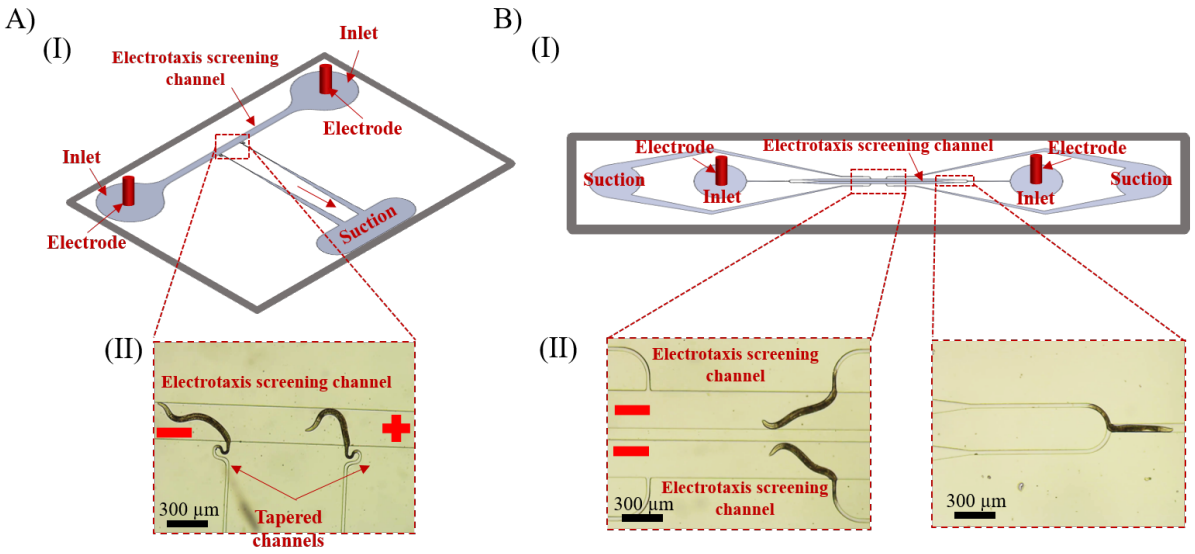

Figure 5.3: Microfluidic devices for enhancing the throughput of the semi-mobile worm electrotaxis assay. (A) (I)3D schematic of the microfluidic chip consisting of the electrotaxis screening channel with end electrodes and two perpendicular tapered channel with S-shaped entrance for worm partial and full trapping as well as imaging. (II) The perpendicular channels showing two worms captured with tail and responding towards the cathode at EF of 4 V/cm. (B) (I) 3D schematic of the microfluidic chip consisting of two parallel electrotaxis channels with four perpendicular traps for worm partial and full trapping as well as imaging. (II) A closer look at the worm loading through the U-channel connecting the two parallel electrotaxis channels (right) and at the four perpendicular traps with two worms captured with tail and responding towards the cathode at EF of 4 V/cm (left).

In design II (Figure 5.3B), We tried to tackle multiple issues in the previous designs. The microfluidic device consisted of two parallel electrotaxis channels connected via one inlet and outlet channel through a U-shaped channel (Figure 5.3B-II). The worm traps were installed perpendicular to the electrotaxis screening channel while each two facing traps were connected to the same suction outlet. worms were manually picked from a synchronized population and loaded into the device already filled with M9 buffer. With the aid of negative pressure at the trapping channels, the loaded worms evenly distributed through the U-channel and guided towards the tapered channels (Figure 5.3B-II). Once the worms were trapped and acclimated to the environment, DC electric field of 4 V/cm

was applied for 30 s using the sourcemeter, and the worms showed promising responses. Although our proof-of-concept tests provided a promising perspective for increasing the test throughput, more experiments are needed to control the loading process and the trapped length of the worms, and to ensure that most of the worms are loaded with tail-first.

5.2.2 Potential Applications of the Proposed Microfluidic Devices

By combining *C. elegans* and microfluidics, several platforms have been proposed and made significant contributions from modeling disease pathology to chemical and genetic screening by understanding various molecular, cellular, and behavioral processes in *C. elegans*. These platforms have facilitated analyzing the worms' sensory-motor responses to various environmental cues, including chemicals, EF, mechanical forces, thermal actuation, optical stimulations, and acoustic waves. Many have also shown the potential for studying multiple worms in parallel, aiming to enhance the behavioral throughput of the screening assays for identifying chemicals and gene targets. None of the above devices has enhanced the throughput of the electrotaxis assays or provided new electrically evoked behaviours. The work of this thesis has demonstrated the great potential of the EF-based assays to understand *C. elegans* electrosensation further; to evoke movement on-demand for assessing the locomotion of multiple worms in parallel; to induce other non-locomotory electrically induced behaviours such as the electric egg-laying phenomenon; to facilitate the genetic and chemical screening of movement-related disorders such as PD; to correlate neuron degeneration with the electrically-induced phenotypes at a population and a single worm resolution; and to provide a tool for phenotypical assessment of multiple worms in parallel in toxicity screening. While the developed devices have added value to the scientific knowledge in this field, not all possible applications were tested in the thesis, and the devices possess some challenges that need to be addressed for perfecting their usage. This section provides

the potential applications for our devices.

Using the proposed microfluidic platforms in this thesis and transgenic lines, key insights on neurodegenerative diseases pathogenesis can be revealed, and chemical and gene screening can be performed. Most of the neurodegenerative diseases have common disease pathogenesis; however, we will focus on PD while the same applications can be performed for AD, HD, and amyotrophic lateral sclerosis. In the case of PD, we have shown that α-syn aggregation in muscles did not affect the ability of the worms to sense and turn quickly towards the cathode but slightly affected their ability to maintain a directional preference for an extended period. An interesting line of research that can be pursued in the future is on worms overexpressing α-syn in DNs, which are also known to be affected in PD. Moreover, in our review paper[14], we provided a list of multiple natural antiparkinsonian compounds that show PD therapeutic effects in *C. elegans*. However, no information has been provided on the ability of these compounds to revitalize the electrically-induced responses, which reflect on the neuronal system integrity. Thus, our techniques can be useful in testing and determining the sublethal toxic doses of these compounds. Moreover, the pathway of action behind electrotaxis and its relationship with different PD-related genes can be determined. This can be achieved by silencing different PD-related genes, including *ATP13A2*, *dj-1*, *lrk-1* and *pdr-1*, using RNAi. Moreover, to further establish a connection between the electrotaxis and dopaminergic pathways, worms exposed to different dopamine agonists and antagonists can be tested using our proposed devices with better behavioral throughput.

Another exciting research line is performing precise *in-vivo* imaging of protein cell-to-cell transfer and associating it with behavioural deficiencies. For instance, misfolding α-syn cell-to-cell transfer has been suggested to contribute to the pathogenesis of PD. However, the *in-vivo* mechanisms involved in this progression are yet to be explained in detail. Two groups have recently used the bimolecular fluorescence complementation (BiFC) technique to develop worm models for studying protein cell-to-cell transfer in PD

and HD.[72–74] In the BiFC technique, the two halves of a fluorescent protein (e.g., GFP or YFP) are fused to the protein of interest (e.g., α-syn). The hybrid proteins will only emit fluorescence when the two complementary GFP halves are brought together by α-syn self-assembly, thereby reconstituting their function as a single protein to emit fluorescence. Hence, this technique has contributed to developing *C. elegans* models to study cell-to-cell interaction. By combining the BiFC technique and our microfluidic devices, we envision that the correlation between protein cell-to-cell progression and sensory-motor behavioural deficiencies at different neurotoxins and antiparkinsonian compounds can be attained. As stated earlier, the same approaches can be followed for other NDs by investigating models of PolyQ aggregation for HD and amyloid-beta for AD.

This thesis also showed some preliminary results, demonstrating that the egg-laying pathway is being shared with the electrosensation pathway. Earlier in 2007, Gabel et al.[24] attempted to explore the genetic and neuronal bases of *C. elegans* electrosensation using mutation or laser ablation in some genes and sensory neurons. We envision using laser ablation of other egg-laying related muscles and neurons; we can build a clear connection between the egg-laying and electrosensation pathways in *C. elegans*. Although the electrosensation and egg-laying pathways are distinct, their functions are overlapping. Therefore, it would be interesting to test the effect of various neurotoxins and neuroprotective compounds on the electric egg-laying of *C. elegans*. It is worth emphasizing that we performed some preliminary experiments by exposing the N2 strain to 5mM of 6-OHDA (for 1 hr at L1 stage) and tested their electric egg-laying phenomenon using our single-channel device (reported in Paper III). Our results showed a significant reduction in the egg-laying count, as shown in Figure 5.4A. Therefore, we envision that our technique might help screen for different neurotoxins and neuroprotective compounds in the future. Moreover, it would be interesting to test the effect of α-syn accumulation in muscles and neurons on the egg-laying behaviour of *C. elegans*. We also investigated the electric egg-laying behaviour of the NL5901 strain, expressing α-syn in muscle cells, and found no associated deficiency

in the egg-laying behaviour on-chip (Figure 5.4B). Further investigations are needed upon exposure to neurotoxins to increase the protein aggregation.

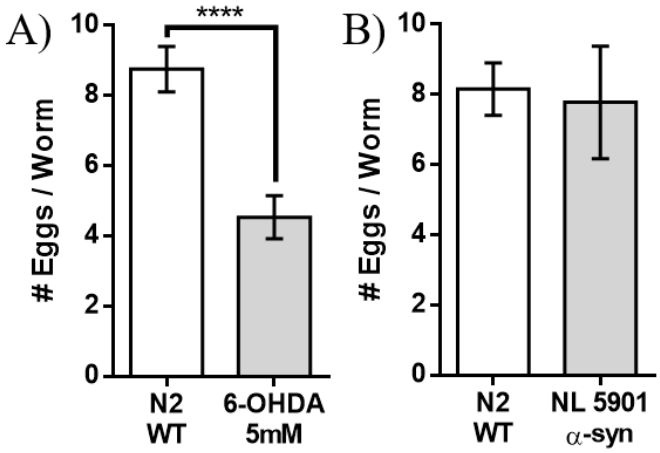

Figure 5.4: (A) Electric egg-laying response of N2 strain treated with 5 mM 6-OHDA (N = 15). (B) α-syn aggregation in muscles did not affect the electric egg-laying behaviour of *C. elegans* (N= 11).

While we showed that our technique could be used for PD pathology studies and potentially for other neurobehavioral disorders modeled in *C. elegans*, we also showed that the electric egg-laying technique could be used for glucose and microplastics toxicity screening. Moreover, egg-laying has been reported as a technique for antidiabetic drug screening.[41] Therefore, our technique can be an asset to shortening the egg-laying assay time and provide a fast quantification technique for antidiabetic drug screening. Also, our findings implied that electric egg-laying decreases with worm aging, following the natural off-chip behaviour. Previous studies have shown that egg-laying can be used as a quantitative and user-independent indicator for physiological aging. However, aging and life-span studies utilize Fluorodeoxyuridine (FUdR), an inhibitor of DNA synthesis, in a *C. elegans* population to block progeny production and assist the maintenance of synchronous nematode populations for longer times.[75] FUdR has shown complex effects on aging in *C. elegans*, which opposes its use in aging studies. Therefore, in the future, this gap in experimen-

tal procedures could be bridged through the use of EF-induced egg-release to deplete the uterus allowing for an extended period without progeny production. Moreover, due to the reduction in response duration at longer pulses, our technique has the potential to provide the pathway for developing a high-throughput egg synchronization method without the involvement of chemicals (e.g., bleach[56]) or harming the organism.

In terms of microplastics toxicity, several potential applications can be pursued using our multi-worm assay (presented in Paper IV[45]). In Paper IV[45], we used the commonly available microplastics (polystyrene); however, different types of plastic such as polypropylene, polyethylene, and polyvinyl chloride can also be tested. Moreover, microplastics are produced during the fragmentation process of plastics with heterogeneous morphology and sizes. Therefore, it would be interesting to test microplastics with irregular shapes and different chemical compositions. Next, microplastics toxicity has been correlated to elevated oxidative stresses, which can be certainly investigated using our technique using transgenic strains to assay the level of oxidative stress by fluorescent microscopy and correlate it to the egg-laying deficiency. Lastly, *C. elegans* has the potential to study the toxicity of different heavy metals. Thus, using our microfluidic assays, we can test the effect of heavy metals such as zinc, cadmium, and iron on the electrically-induced behaviours, and it can be used to determine the sublethal end-points for ecotoxicity screening.

References

[1] Colman, A. M. A Dictionary of Psychology (Oxford University Press, 2009).

[2] Cammack, R. et al. Oxford Dictionary of Biochemistry and Molecular Biology (Oxford University Press, 2008).

[3] Martin, E. & Hine, R. A Dictionary of Biology (Oxford University Press, 2008).

[4] Stevenson, A. Oxford Dictionary of English (Oxford University Press, 2010).

[5] King, R. C., Stansfield, W. D. & Mulligan, P. K. A Dictionary of Genetics (Oxford University Press, 2007).

[6] Lackie, J. A Dictionary of Biomedicine (Oxford University Press, 2010).

[7] Kinser, H. E. & Pincus, Z. High-throughput Screening in the *C. elegans* Nervous System. Molecular and Cellular Neuroscience **80**, 192–197, DOI: 10.1016/j.mcn.2016.06.001 (2017).

[8] Leung, C. K. et al. An Ultra High-Throughput, Whole-Animal Screen for Small Molecule Modulators of a Specific Genetic Pathway in *Caenorhabditis elegans*. PLoS ONE **8**, e62166, DOI: 10.1371/journal.pone.0062166 (2013).

[9] O'Reilly, L. P., Luke, C. J., Perlmutter, D. H., Silverman, G. A. & Pak, S. C. *C. elegans* in High-throughput Drug Discovery. Advanced Drug Delivery Reviews **69-70**, 247–253, DOI: 10.1016/j.addr.2013.12.001 (2014).

[10] Wu, Q., Kumar, N., Velagala, V. & Zartman, J. J. Tools to Reverse-engineer Multicellular Systems: Case Studies Using the Fruit Fly. Journal of Biological Engineering **13**, 33, DOI: 10.1186/s13036-019-0161-8 (2019).

[11] Khalili, A. & Rezai, P. Microfluidic Devices for Embryonic and Larval Zebrafish Studies. Briefings in functional genomics **18**, 419–432, DOI: 10.1093/bfgp/elz006 (2019).

[12] Markaki, M. & Tavernarakis, N. Modeling Human Diseases in *Caenorhabditis elegans*. Biotechnology Journal **5**, 1261–1276, DOI: 10.1002/biot.201000183 (2010).

[13] Youssef, K., Bayat, P., Peimani, A. R., Dibaji, S. & Rezai, P. Miniaturized Sensors and Actuators for Biological Studies on Small Model Organisms of Disease. In Environmental, Chemical and Medical Sensors, 199–225, DOI: 10.1007/978-981-10-7751-7_9 (Springer, 2018).

[14] Youssef, K., Tandon, A. & Rezai, P. Studying Parkinson's Disease Using *Caenorhabditis elegans* Models in Microfluidic Devices. Integrative biology : quantitative biosciences from nano to macro **11**, 186–207, DOI: 10.1093/intbio/zyz017 (2019).

[15] Li, J. & Le, W. Modeling Neurodegenerative Diseases in *Caenorhabditis elegans*. Experimental Neurology **250**, 94–103, DOI: 10.1016/j.expneurol.2013.09.024 (2013).

[16] Wolozin, B., Gabel, C., Ferree, A., Guillily, M. & Ebata, A. Watching Worms Whither: Modeling Neurodegeneration in *C. elegans*. In Progress in Molecular Biology and Translational Science, vol. 100, 499–514, DOI: 10.1016/B978-0-12-384878-9.00015-7 (Elsevier, 2011).

[17] Chen, X., Barclay, J. W., Burgoyne, R. D. & Morgan, A. Using *C. elegans* to Discover Therapeutic Compounds for Ageing-associated Neurodegenerative Diseases. Chemistry Central Journal **9**, 65, DOI: 10.1186/s13065-015-0143-y (2015).

[18] AU - Margie, O., AU - Palmer, C. & AU - Chin-Sang, I. *C. elegans* Chemotaxis Assay. JoVE e50069, DOI: 10.3791/50069 (2013).

[19] Ward, A., Liu, J., Feng, Z. & Xu, X. Z. S. Light-sensitive Neurons and Channels Mediate Phototaxis in *C. elegans*. Nature neuroscience **11**, 916–922, DOI: 10.1038/nn.2155 (2008).

[20] Hedgecock, E. M. & Russell, R. L. Normal and Mutant Thermotaxis in the Nematode *Caenorhabditis elegans*. Proceedings of the National Academy of Sciences **72**, 4061–4065, DOI: 10.1073/pnas.72.10.4061 (1975).

[21] Schafer, W. R. Mechanosensory Molecules and Circuits in *C. elegans*. Pflügers Archiv-European Journal of Physiology **467**, 39–48, DOI: 10.1007/s00424-014-1574-3 (2015).

[22] Shanmugam, M. M. Galvanotaxis of *Caenorhabditis elegans*: Current Understanding and Its Application in Improving Research. Biology, Engineering and Medicine **2**, 1–5, DOI: 10.15761/bem.1000111 (2017).

[23] Sukul, N. C. & Croll, N. A. Influence of Potential Difference and Current on the Electrotaxis of *Caenorhaditis elegans*. Journal of nematology **10**, 314–317, DOI: 19305860 (1978).

[24] Gabel, C. V. et al. Neural Circuits Mediate Electrosensory Behavior in *Caenorhabditis elegans*. Journal of Neuroscience **27**, 7586–7596, DOI: 10.1523/JNEUROSCI.0775-07.2007 (2007).

[25] Chrisman, S. D., Waite, C. B., Scoville, A. G. & Carnell, L. *C. elegans* Demonstrates Distinct Behaviors Within a Fixed and Uniform Electric Field. PLoS ONE **11**, DOI: 10.1371/journal.pone.0151320 (2016).

[26] Rezai, P., Siddiqui, A., Selvaganapathy, P. R. & Gupta, B. P. Electrotaxis of *Caenorhabditis elegans* in a Microfluidic Environment. Lab on a Chip **10**, 220–226, DOI: 10.1039/b917486a (2010).

[27] Whitesides, G. M. The Origins and the Future of Microfluidics. Nature **442**, 368–373, DOI: 10.1038/nature05058 (2006).

[28] Rezai, P., Siddiqui, A., Selvaganapathy, P. R. & Gupta, B. P. Behavior of *Caenorhabditis elegans* in Alternating Electric Field and Its Application to Their Localization and Control. Applied Physics Letters **96**, 153702, DOI: 10.1063/1.3383223 (2010).

[29] Liu, D., Gupta, B. & Selvaganapathy, P. R. An Automated Microfluidic System for Screening Caenorhabditis elegans Behaviors Using Electrotaxis. Biomicrofluidics **10**, 14117, DOI: 10.1063/1.4941709 (2016).

[30] Tong, J., Rezai, P., Salam, S., Selvaganapathy, P. R. & Gupta, B. P. Microfluidic-based Electrotaxis for On-demand Quantitative Analysis of *Caenorhabditis elegans'* Locomotion. Journal of visualized experiments : JoVE e50226, DOI: 10.3791/50226 (2013).

[31] Rezai, P. Microfluidic Devices for Nematode-Based Behavioural Assays. Ph.D. thesis, McMaster University (2012).

[32] Han, B., Kim, D., Ko, U. H. & Shin, J. H. A Sorting Strategy for *C. elegans* Based on Size-dependent Motility and Electrotaxis in a Micro-structured Channel. Lab on a chip **12**, 4128–4134, DOI: 10.1039/c2lc40209b (2012).

[33] Wang, X. et al. Highly Efficient Microfluidic Sorting Device for Synchronizing Developmental Stages of *C. elegans* Based on Deflecting Electrotaxis. Lab on a Chip **15**, 2513–2521, DOI: 10.1039/c5lc00354g (2015).

[34] Chuang, H. S., Kuo, W. J., Lee, C. L., Chu, I. H. & Chen, C. S. Exercise in An Electrotactic Flow Chamber Ameliorates Age-related Degeneration in *Caenorhabditis elegans*. Scientific Reports **6**, 1–11, DOI: 10.1038/srep28064 (2016).

[35] Ma, H., Jiang, L., Shi, W., Qin, J. & Lin, B. A Programmable Microvalve-based Microfluidic Array for Characterization of Neurotoxin-induced Responses of Individual *C. elegans*. Biomicrofluidics **3**, 44114, DOI: 10.1063/1.3274313 (2009).

[36] Shi, W. et al. Droplet Microfluidics for Characterizing the Neurotoxin-induced Responses in Individual *Caenorhabditis elegans*. Lab on a Chip **10**, 2855–2863, DOI: 10.1039/c0lc00256a (2010).

[37] Salam, S. et al. A Microfluidic Phenotype Analysis System Reveals Function of Sensory and Dopaminergic Neuron Signaling in *C. elegans* Electrotactic Swimming Behavior. In Worm, vol. 2, e24558, DOI: 10.4161/worm.24558 (Taylor & Francis, 2013).

[38] Youssef, K., Archonta, D. & Rezai, P. Microfluidic Devices to Study the Effect of Electric Field on *Caenorhabditis elegans* and *Danio rerio*. In Xinyu, L. & Sun, Y. (eds.) Micro and Nano Systems for Biophysical Studies of Cells and Small Organisms, chap. 15 (Elsevier "Underreview", 2021).

[39] Collins, K. M. et al. Activity of the *C. elegans* Egg-laying Behavior Circuit is Controlled By Competing Activation and Feedback Inhibition. eLife **5**, e21126, DOI: 10.7554/eLife.21126 (2016).

[40] Schafer, W. R. Genetics of Egg-Laying in Worms. Annual Review of Genetics **40**, 487–509, DOI: 10.1146/annurev.genet.40.110405.090527 (2006).

[41] Schlotterer, A. et al. *C. elegans* as model for the study of high glucose–mediated life span reduction. Diabetes **58**, 2450–2456, DOI: 10.2337/db09-0567 (2009).

[42] Youssef, K., Archonta, D., Kubiseski, T. J., Tandon, A. & Rezai, P. Semi-mobile *C. elegans* Electrotaxis Assay for Movement Screening and Neural Monitoring of Parkinson's Disease Models. Sensors and Actuators, B: Chemical **316**, 128064, DOI: 10.1016/j.snb.2020.128064 (2020).

[43] Youssef, K., Archonta, D., Kubiseski, T., Tandon, A. & Rezai, P. Parallel-Channel Electrotaxis and Neuron Screening of *Caenorhabditis elegans*. Micromachines **11**, 756, DOI: 10.3390/mi11080756 (2020).

[44] Youssef, K., Archonta, D., Kubiseski, T. J., Tandon, A. & Rezai, P. Electric Egg-laying: a New Approach for Regulating *C. elegans* Egg-laying Behaviour in a Microchannel Using Electric Field. Lab on a chip DOI: 10.1039/D0LC00964D (2021).

[45] Youssef, K., Archonta, D., Kubiseski, T. J., Tandon, A. & Rezai, P. Microplastic Toxicity at the Neuronal, Behavioural and Physiological Levels Investigated on *C. elegans* in a Multi-Nematode Lab-on-a-Chip Device with Population and Single-Worm Screening Capability. Science of the Total Environment "Under review" (2021).

[46] Wu, W. I., Rezai, P., Hsu, H. H. & Selvaganapathy, P. R. Materials and Methods for the Microfabrication of Microfluidic Biomedical Devices. In Microfluidic Devices for Biomedical Applications, 3–62, DOI: 10.1533/9780857097040.1.3 (Elsevier, 2013).

[47] Rezai, P., Wu, W. I. & Selvaganapathy, P. R. Microfabrication of Polymers for BioMEMS. In Mems for Biomedical Applications, 3–45, DOI: 10.1533/9780857096272.1.3 (Elsevier, 2012).

[48] Xia, Y. & Whitesides, G. M. Soft Lithography. Annual Review of Materials Science **28**, 153–184, DOI: 10.1146/annurev.matsci.28.1.153 (1998).

[49] Gerhart, P. M., Gerhart, A. L. & Hochstein, J. I. Munson, Young and Okiishi's Fundamentals of Fluid Mechanics (John Wiley & Sons, 2016).

[50] Schulman, R. D., Backholm, M., Ryu, W. S. & Dalnoki-Veress, K. Dynamic Force Patterns of An Undulatory Microswimmer. Physical Review E **89**, 50701, DOI: 10.1103/PhysRevE.89.050701 (2014).

[51] Aryasomayajula, A., Bayat, P., Rezai, P. & Selvaganapathy, P. R. Microfluidic Devices and Their Applications BT - Springer Handbook of Nanotechnology. 487–536, DOI: 10.1007/978-3-662-54357-3_16 (Springer Berlin Heidelberg, Berlin, Heidelberg, 2017).

[52] Altun-Gultekin, Z. et al. A Regulatory Cascade of Three Homebox Genes, *Ceh-10*, *Ttx-3* and Ceh-23, Controls Cell Fate Specification of a Defined Interneuron Class in *C. elegans*. Development **128**, 1951–1969 (2001).

[53] Pu, P. & Le, W. Dopamine Neuron Degeneration Induced By MPP+ is Independent of CED-4 Pathway in *Caenorhabditis elegans*. Cell Research **18**, 978–981, DOI: 10.1038/cr.2008.279 (2008).

[54] Van Ham, T. J. et al. *C. elegans* Model Identifies Genetic Modifiers of Alpha-synuclein Inclusion Formation During Aging. PLoS Genetics **4**, e1000027, DOI: 10.1371/journal.pgen.1000027 (2008).

[55] Stiernagle, T. Maintenance of *C. elegans*. Wormbook **2**, 51–67 (1999).

[56] Porta-de-la Riva, M., Fontrodona, L., Villanueva, A. & Cerón, J. Basic *Caenorhabditis elegans* Methods: Synchronization and Observation. Journal of Visualized Experiments e4019, DOI: 10.3791/4019 (2012).

[57] Youssef, K., Archonta, D., Kubiseski, T. J., Tandon, A. & Rezai, P. Egg Laying Neuron Mediates Electrosensation in *Caenorhabditis elegans*. In µTAS 2020, 911–912 (USA, 2020).

[58] Altun, Z. & Hall, D. Nervous System, General Description. WormAtlas **103908** (2011).

[59] Schafer, W. R. Egg-laying. In WormBook: The Online Review of *C. elegans* Biology [Internet] (WormBook, 2005).

[60] Teshiba, E., Miyahara, K. & Takeya, H. Glucose-induced Abnormal Egg-laying Rate in *Caenorhabditis elegans*. Bioscience, Biotechnology, and Biochemistry **80**, 1436–1439, DOI: 10.1080/09168451.2016.1158634 (2016).

[61] Sussarellu, R. et al. Oyster Reproduction is Affected By Exposure to Polystyrene Microplastics. Proceedings of the National Academy of Sciences **113**, 2430 LP – 2435, DOI: 10.1073/pnas.1519019113 (2016).

[62] Prüst, M., Meijer, J. & Westerink, R. H. S. The Plastic Brain: Neurotoxicity of Micro- and Nanoplastics. Particle and Fibre Toxicology **17**, 24, DOI: 10.1186/s12989-020-00358-y (2020).

[63] Hu, J. et al. The Toxicity of (Nano)Microplastics on *C. elegans* and Its Mechanisms. In He, D. & Luo, Y. (eds.) Microplastics in Terrestrial Environments: Emerging Contaminants and Major Challenges, 259–278, DOI: 10.1007/698_2020_452 (Springer International Publishing, Cham, 2020).

[64] Lei, L. et al. Microplastic Particles Cause Intestinal Damage and Other Adverse Effects in Zebrafish *Danio rerio* and Nematode *Caenorhabditis elegans*. Science of the Total Environment **619-620**, 1–8, DOI: 10.1016/j.scitotenv.2017.11.103 (2018).

[65] Schöpfer, L. et al. Microplastics Effects on Reproduction and Body Length of the Soil-Dwelling Nematode *Caenorhabditis elegans*. Frontiers in Environmental Science **8**, 41, DOI: 10.3389/fenvs.2020.00041 (2020).

[66] Lei, L. et al. Polystyrene (nano)microplastics Cause Size-dependent Neurotoxicity, Oxidative Damage and Other Adverse Effects in *Caenorhabditis elegans*. Environmental Science: Nano **5**, 2009–2020, DOI: 10.1039/c8en00412a (2018).

[67] Kim, S. W., Kim, D., Jeong, S. W. & An, Y. J. Size-dependent Effects of Polystyrene Plastic Particles on the Nematode *Caenorhabditis elegans* As Related to Soil Physicochemical Properties. Environmental Pollution **258**, 113740, DOI: 10.1016/j.envpol.2019.113740 (2020).

[68] Yu, Y. et al. Polystyrene Microplastics (PS-MPs) Toxicity Induced Oxidative Stress and Intestinal Injury in Nematode *Caenorhabditis elegans*. Science of the Total Environment **726**, 138679, DOI: 10.1016/j.scitotenv.2020.138679 (2020).

[69] Shang, X. et al. Microplastic (1 and 5 M) Exposure Disturbs Lifespan and Intestine Function in the Nematode *Caenorhabditis elegans*. Science of the Total Environment **705**, 135837, DOI: 10.1016/j.scitotenv.2019.135837 (2020).

[70] Mondal, S. et al. Large-scale Microfluidics Providing High-resolution and High-throughput Screening of *Caenorhabditis elegans* Poly-glutamine Aggregation Model. Nature Communications **7**, 13023, DOI: 10.1038/ncomms13023 (2016).

[71] Mondal, S. et al. High-Content Microfluidic Screening Platform Used to Identify 2R/Tmem97 Binding Ligands That Reduce Age-Dependent Neurodegeneration in *C. elegans* SC-APP Model. ACS Chemical Neuroscience **9**, 1014–1026, DOI: 10.1021/acschemneuro.7b00428 (2018).

[72] Kim, D. K. et al. Anti-aging Treatments Slow Propagation of Synucleinopathy By Restoring Lysosomal Function. Autophagy **12**, 1849–1863, DOI: 10.1080/15548627.2016.1207014 (2016).

[73] Kim, D. K. et al. Cell-to-cell Transmission of Polyglutamine Aggregates in *C. elegans*. Experimental Neurobiology **26**, 321–328, DOI: 10.5607/en.2017.26.6.321 (2017).

[74] Tyson, T. et al. Novel Animal Model Defines Genetic Contributions for Neuron-to-neuron Transfer of Alpha-synuclein. Scientific Reports **7**, 1–10, DOI: 10.1038/s41598-017-07383-6 (2017).

[75] Wang, H., Zhao, Y. & Zhang, Z. Age-dependent Effects of Floxuridine (FUdR) on Senescent Pathology and Mortality in the Nematode *Caenorhabditis elegans*. Biochemical and biophysical research communications **509**, 694–699, DOI: 10.1016/j.bbrc.2018.12.161 (2019).

APPENDICES

Appendix A

Review Paper and Book Chapter for Literature Review in Chapter 2

A.1 Studying Parkinson's Disease Using *Caenorhabditis elegans* Models in Microfluidic Devices

Youssef, K., Tandon, A., & Rezai, P. (2019). Studying Parkinson's disease using *Caenorhabditis elegans* models in microfluidic devices. Integrative Biology, 11(5), 186-207.

Integrative Biology, 2019, 11(5), 186–207

doi: 10.1093/intbio/zyz017
Advance Access publication June 7, 2019
Review Article

REVIEW ARTICLE

Studying Parkinson's disease using *Caenorhabditis elegans* models in microfluidic devices

Khaled Youssef[1], Anurag Tandon[2,3], and Pouya Rezai*[1]

[1]Department of Mechanical Engineering, York University, Toronto, ON, Canada, [2]Tanz Centre for Research in Neurodegenerative Diseases, Toronto, ON, Canada, and [3]Department of Medicine, University of Toronto, Toronto, ON, Canada

*Corresponding author. Tel: +416–736-2100 ext. 44703; E-mail: prezai@yorku.ca

Abstract

Parkinson's disease (PD) is a progressive neurological disorder associated with the loss of dopaminergic neurons (DNs) in the substantia nigra and the widespread accumulation of α-synuclein (α-syn) protein, leading to motor impairments and eventual cognitive dysfunction. *In-vitro* cell cultures and *in-vivo* animal models have provided the opportunity to investigate the PD pathological hallmarks and identify different therapeutic compounds. However, PD pathogenesis and causes are still not well understood, and effective inhibitory drugs for PD are yet to be discovered. Biologically simple but pathologically relevant disease models and advanced screening technologies are needed to reveal the mechanisms underpinning protein aggregation and PD progression. For instance, *Caenorhabditis elegans* (*C. elegans*) offers many advantages for fundamental PD neurobehavioral studies including a simple, well-mapped, and accessible neuronal system, genetic homology to humans, body transparency and amenability to genetic manipulation. Several transgenic worm strains that exhibit multiple PD-related phenotypes have been developed to perform neuronal and behavioral assays and drug screening. However, in conventional worm-based assays, the commonly used techniques are equipment-intensive, slow and low in throughput. Over the past two decades, microfluidics technology has contributed significantly to automation and control of *C. elegans* assays. In this review, we focus on *C. elegans* PD models and the recent advancements in microfluidic platforms used for manipulation, handling and neurobehavioral screening of these models. Moreover, we highlight the potential of *C. elegans* to elucidate the *in-vivo* mechanisms of neuron-to-neuron protein transfer that may underlie spreading Lewy pathology in PD, and its suitability for *in-vitro* studies. Given the advantages of *C. elegans* and microfluidics technology, their integration has the potential to facilitate the investigation of disease pathology and discovery of potential chemical leads for PD.

Insight

This review paper is providing insight on the use of the model organism *Caenorhabditis elegans (C. elegans)* to investigate the neurotoxin and protein aggregation-based neurodegeneration and movement impairment in Parkinson's Disease (PD). The potential of using *C. elegans* for toxicology and drug screening in PD is also of importance in this paper. The main advantages of using *C. elegans*, in addition to biological suitability, are its simplicity and small size, making it amenable to high-throughput and high-content screening for PD pathology studies and drug screening. While conventional methods are limited in this front, the emergence and integration of the reviewed microfluidic devices have provided the technological innovation required to target *in-vitro* and *in-vivo* PD studies with *C. elegans*.

Received November 14, 2018; **revised** April 30, 2019; **editorial decision** May 11, 2019; **accepted** May 16, 2019

INTRODUCTION

Parkinson [1] was the first to describe the Shaking Palsy in 1817, which was later renamed to Parkinson's disease (PD). In 1895, Brissuad [2] hypothesized that PD pathologically affects the substantia nigra (SN) pars compacta (Fig. 1), causing different motor defects like tremor, shaking, rigid muscles, bradykinesia and impaired balance, which was also described by Parkinson in the original essay. Afterwards, Lewy [3] originated how diagnostically the SN pars compacta is affected by describing the formation of specific protein clumps in multiple areas of PD patient brains. In 1919, Trétiakoff [4] examined post-mortem tissues and validated Brissuad's and Lewy's theories by describing specific protein aggregates in the SN, termed Lewy bodies (LBs). In 1997, Spillantini [5] identified α-syn as the major component of LBs, which are the main pathological hallmarks of PD, as shown in Fig. 1.

α-syn is a small protein (14 kDa) of the synuclein family of proteins, which also includes β- and γ-synuclein. It is abundantly expressed at the presynaptic terminals in the central nervous system, constituting 1% of the brain total cytosolic proteins [6], where it is involved in neurotransmitter storage and release. The protein comprises three structurally distinct regions, i.e. an amino terminus α-helical domain (N-terminal amino acids 1–65), a central hydrophobic component (non-amyloid component (NAC) amino acids 66–95), and a highly negatively charged carboxyl tail (C-terminal amino acids 96–140). The central NAC region provides the protein's ability to form rigid β-sheet structures prone to self-assembly into multimeric fibrils, which are the major component of LBs [6]. Moreover, A53T, A30P, and E46K are three α-syn mutations in the α-helical domain that show early PD onset due to their ability to aggregate and form fibrils [6].

Based on genetic approaches, PD researchers have focused on understanding the role of α-syn in PD and its potential as a target for neuroprotective therapeutics by presenting multiple animal models in which various forms of α-syn are overexpressed. Today, there are several transgenic murine lines with α-syn overexpression that show some degree of neurodegeneration [7]. Using these animal models, recent studies have demonstrated the compelling evidence that α-syn is involved in both cases of PD pathogenesis, i.e. familial and sporadic, by inducing either dysfunction or loss of various neurons including DNs [8]. This evidence heralded a new era in PD research and, since then, multiple mammalian models have been developed to replicate and investigate several key motor and pathological features of PD [7]. These models have revealed fundamental aspects underpinning the disease causes and progression by using α-syn gene mutation [7, 9–11] or exposure to multiple environmental compounds [12–16] (e.g. neurotoxins and heavy metals) to induce PD-like neurodegeneration. For instance, Luk *et al.* [17] found that a single inoculation of synthetic α-syn fibrils showed a parkinsonian-like effect in a mouse model and led to α-syn cell-to-cell transmission in physically interconnected regions. However, detecting PD pathological hallmarks and performing large-scale drug screening using vertebrate mammalian models is ethically restricted, expensive and intricate due to their brain complexity and the large number of neuron interactions.

To address the limitations above, *in-vitro* cell culture assays have been developed to ease investigating the neuronal interconnections and elucidating how α-syn is accumulated [10, 18, 19]. These studies have suggested that α-syn moves from neuron to neuron with α-syn aggregation happening at axon-dendrite connections. Desplats *et al.* [10] demonstrated that α-syn aggregates are secreted from neuronal cells via exocytosis and taken up by neighboring cells via endocytosis. A similar transfer was implicated by the post-mortem detection of LB in fetal graft tissue implanted into brains of PD patients [20, 21], and supported by other models [22, 23]. Moreover, Freundt *et al.* [18] studied the role of axonal transport in α-syn transmission using a microfluidic device which consisted of two chambers interconnected with multiple microchannels to allow axonal growth. Their results supported the concept that PD pathology could be propagated by the interneuronal spread of α-syn.

Translation of results from 2D *in-vitro* cell cultures to *in-vivo* applications is critical but difficult to achieve due to the large gap between cell cultures and mammalian animal models. In this regard, simple invertebrate and vertebrate model organisms such as *Caenorhabditis elegans* [24, 25], *Drosophila melanogaster* [26], and *Danio rerio* [27, 28] have offered several advantages including cellular and neuronal simplicity, genetic homology to humans, rapid and low-cost growth and maintenance in labs, body transparency for microscopy, and amenability to genetic manipulation. In this paper, we provide a review of *C. elegans*-based conventional and microfluidic approaches to study α-syn overexpression and neurotoxicity effects in PD. We have summarized the worm-based microfluidic technologies for studying neurodegenerative diseases that aided in high-throughput screening of drugs. A number of exemplary reviews have already been published on *C. elegans* as a model for PD studies [29–34] and microfluidics-based *C. elegans* studies [35–50]. However, a review article focused on *C. elegans in-vitro* and *in-vivo* protein aggregation and the associated neurobehavioral affects, studied by the use of microfluidic technologies, is currently lacking.

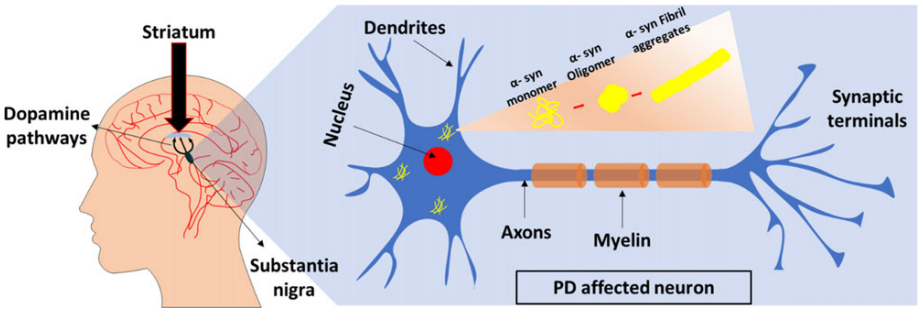

Figure 1. Toxicity of α-syn aggregation in human brain which affects the dopamine pathways between substantia nigra and striatum, focusing on single neuron to show the process of α-syn aggregation.

CAENORHABDITIS ELEGANS AS A MODEL ORGANISM FOR NEUROLOGICAL AND PD STUDIES

Caenorhabditis elegans is a round worm that has become a reliable invertebrate model organism for biological studies [51, 52]. Normally, *C. elegans* are cultured on agar plates seeded with a food source of *E. coli* OP50 strain bacteria with various nutrients, as shown in Fig. 2 [53]. They offer multiple experimental advantages such as possessing a simple and thoroughly mapped system of 302 neurons in hermaphrodites with DNs located in their head (4 cephalic (CEP) and 2 anterior deirid (ADE)) and tail (2 posterior deirid (PDE)), optical transparency permitting *in-vivo* imaging of cells by fluorescent microscopy, and short lifespan of approximately 3 weeks for age-based investigations. *C. elegans* also offers a small size of approximately 1 mm in length of adult worms, amenability to a plethora of genetic tools, a fully sequenced genome, and fast reproduction time of approximately 3 days from embryo to adult stage. Moreover, *C. elegans* can be cultivated and maintained with simple laboratory techniques in nonsterile environments at indoor temperatures without the need of controlling the humidity. These advantages have attracted the molecular, cellular and system biology researchers to adopt the worm model for performing comprehensive fundamental and applied studies that are not feasible rapidly and at low cost with complex mammalian models [54].

In addition to the experimental features above, the basic neuronal functions of *C. elegans* are conserved in vertebrates. *C. elegans* have 56 cholinergic, 19 GABAnergic, 4 serotonergic and 8 DNs that produce different neurotransmitters including glutamate, GABA, dopamine and acetylcholine. DNs are responsible for modulating the locomotion behavior in different environmental conditions [54]. Additionally, the worm's amenability to molecular genetic tools and the high level of preserved orthologs between the nematode and vertebrates allow mimicking multiple biological processes and diseases through the creation of transgenic and mutant strains. Therefore, an insight into neurotoxicity and neurodegenerative disease pathologies, pathogenesis, mechanisms and pathways is attainable by studying the worm model [54].

In neurobiology studies, *C. elegans* have made significant contributions from modeling disease pathology to drug screening, mainly due to their body transparency which allows direct imaging of neurons and protein expression using fluorescence microscopy. Molecular mechanisms underlying these diseases are not fully understood but are crucial for developing treatments. Biologists have exploited *C. elegans* in the last two decades using conventional experimental techniques (e.g. plate-based assays, glue-based method for immobilization and imaging, pharyngeal pumping rate, etc.) to understand the molecular, cellular and behavioral mechanisms behind PD [29–34]. Two general approaches, i.e. genetic mutation and neurotoxin exposure, are mostly used in worm studies to induce neuronal malfunction, degeneration or death [55]. Genetic mutation studies are outside the scope of this paper; therefore, we will focus on traditional and microfluidic technologies used to study neurotoxin-induced and α-syn overexpression-based models of *C. elegans* for PD studies.

Neurotoxin exposure or α-syn overexpression in *C. elegans* models for PD studies

Genetic analysis in *C. elegans* has showed that their genome contains six orthologs of established genes associated with familial PD in humans (i.e. *Parkin*, *DJ-1*, *PINK1*, *UCHL-1*, *LRRK2*, *PARK 9* and *NURR1*) [29, 56]. Subsequently, exploiting *C. elegans*

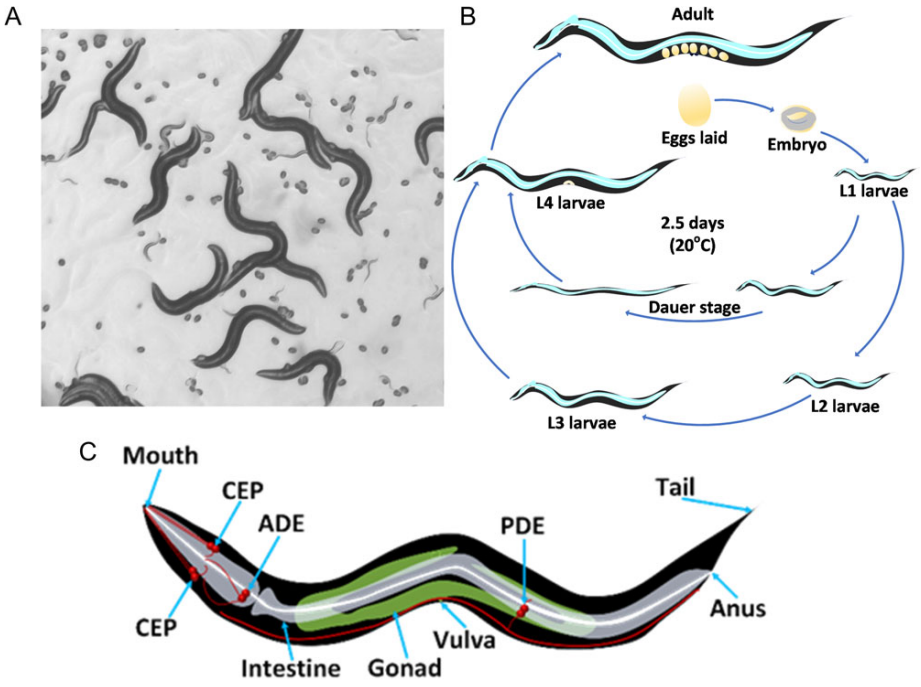

Figure 2. *Caenorhabditis elegans* and its life cycle. (A) A normal culture on an agar plate showing different worm stages; (B) *C. elegans* life cycle at 20°C, which is approximately three weeks including embryogenesis, four larval stages and adulthood; (C) A schematic showing the worm's general anatomy and the dopaminergic neurons in the head and tail (ADE, CEP and PDE).

in PD research has emerged through developing a variety of transgenic *C. elegans* strains using genetics to overexpress human wild type (WT) or A53T α-syn in either DNs or all neurons, despite the natural absence of an α-syn ortholog [29–34]. A number of commonly used transgenic worms for PD studies are listed in Table 1. Lakso *et al.* [57] were the first to overexpress WT and A53T α-syn in the worms' neuronal system (aex-3) and DNs (dat-1), and study their effects on the worms' phenotypic behavior. α-syn overexpression in all neurons induced locomotion deficits, but it showed no effect on the motor activities of the DN strain [57]. Yet, a significant neuronal loss was observed in the worms with WT and A53T α-syn expressed in all or specifically in the DNs. These worm models have been extensively used to determine the link between α-syn toxicity and multiple environmental compounds and to investigate the effect of different potential PD drugs [58]. Through these studies, the worm bioactivities such as growth, lethality, locomotion speed and other movement characteristics have been used for assessment of different drug compounds in multi-well plates. For instance, assessment of DNs survival could be achieved by measuring the Green Fluorescent Protein (GFP) intensity of the dopamine transporter gene, dat-1. Using these methods, a number of neurotoxins including 6-hydroxydopamine (6-OHDA), 1-methyl-4-phenyl-1,2,3,6-tetrahydropyridine (MPTP) and rotenone have been used to induce various behavioral deficiencies that might serve as proxies for PD relevant neurodegeneration [34].

Drug screening has been achieved to identify different neuroprotective compounds using neurotoxin-exposed *C. elegans* models. Braungart *et al.* [58] established the MPP^+-based *C. elegans* model expressing GFP in DNs that showed mobility defects resembling PD phenotypes to investigate the effect of several anti-PD drugs. They found that different compounds at various concentrations mitigated the MPP+-induced phenotypes, such as using low concentration (0.05 mM) of lisuride, apomorphine (dopamine receptor agonists) and rottlerin (protein kinase C inhibitor) and high concentration (0.5 mM) of Nomifensine (dopamine transporter inhibitor), Nicotine (acetylcholine receptor antagonist), Selegiline (Monoamine Oxidase B inhibitor), MPEP (metabotropic glutamate receptor inhibitor), Amantadine, α-Lipoic acid (antioxidant) and Ascorbic acid. Moreover, Marvanova *et al.* [67] studied the effect of two DN receptor agonists, bromocriptine and quinpirole, on a 6-OHDA-exposed *C. elegans* strain and found that these agonists alleviated the behavioral defects. Locke *et al.* [68] used UA18 strain (human α-syn expression in the DNs) and reported the significant effect of acetaminophen, as a neuroprotective, in ameliorating the worm's behavior against 6-OHDA, however, it did not affect α-syn protein aggregation. Kautu *et al.* [69] tested valproic acid, a chemical compound used as a drug for epilepsy and bipolar disorder, to protect DNs against α-syn aggregation and found, through genetic analysis, that the protection is attributed to the signal-regulated kinase (ERK), MPK-1, in the dopaminergic neurons.

Fu *et al.* [24] evaluated the potential use of Acetylcorynolin, a chemical compound extracted from the traditional Chinese medical herb *Corydalis bungeana*, to attenuate DNs degeneration and α-syn accumulation by exploiting BZ555 (GFP expression in DNs) and OW13 (human α-syn expression in the muscle cells) strains, respectively. Significant reduction in α-syn accumulation in OW13 and DNs degeneration in BZ555 due to 6-OHDA exposure was reported by exposing the worms to 10 mM Acetylcorynolin. Moreover, Acetylcorynolin helped in restoring the Basal Slowing Response (BSR) of N2, recovering the lipid content of OW13 and prolonging the lifespan of 6-OHDA-treated N2 worms without causing any toxic effects on the worms. The same group tested the effect of n-Butylidenephthalide, a natural chemical extracted from *Angelica sinensis* [70]. Their investigations showed similar effects to Acetylcorynolin on both strains. Both chemicals exerted their effect by blocking egl-1, an apoptosis mediator, to hinder apoptosis pathways and enhancing rpn-5 and rpn-6, two proteasome subunits, expression to augment the proteasomes activity. Moreover, Tsai *et al.* [71] interrogated the effect of Betulin, birch tree bark, on ameliorating PD pathogenesis on transgenic *C. elegans* models. Reduction of α-syn accumulation and 6-OHDA-induced DNs degeneration as well as enhanced BSR and lifespan were reported and attributed to the promotion of rpn1 expression, a proteasome subunit, and the down-regulation of egl-1, an apoptosis pathway gene.

Liu *et al.* [72] demonstrated the neuroprotective effects of the cultivated red seaweed *Chondrus crispus*, commonly known as *Irish Moss* and found in Northern Atlantic, on UA57 (expressing GFP in the DNs) and NL5901 (α-syn expression in the muscle cells) *C. elegans* strains. Significant reduction in DNs degeneration, caused by 6-OHDA, and α-syn accumulation in NL5901

Table 1. Commonly used *C. elegans* strains for studying PD and their availability at the Caenorhabditis Genetics Center (CGC).

Strain	Genotype	Description	CGC availability	Ref
BY200	dat-1p::GFP, pRF4(rol-6(su1006))	GFP expression in DNs	No	[59]
BY250	dat-1p::GFP	GFP expression in DNs	No	[60]
BY273	baEx18[dat-1p::GFP+dat-1p::WT α-syn]	α-syn GFP expression in the DNs	No	[61]
BZ555	egIs1 [dat-1p::GFP]	GFP expression in DNs	Yes	[62]
DDP1	uonEx1 [unc-54:: α-syn::CFP + unc-54:: α-syn::YFP(Venus)]	α-syn YFP expression in the muscle cells when a CFP tag gets very close to a YFP tag within an aggregate	Yes	[63]
N2	Wild-isolate Bristol	Wild type	Yes	
NL5901	pkIs2386 [unc-54p:: α-syn::YFP + unc-119(+)]	α-syn YFP expression in the muscle cells	Yes	[64]
OW13	pkIs2386 [unc-54p:: α-syn::YFP + unc-119(+)]	α-syn YFP expression in the muscle cells	Yes	[64]
UA18	baEx18[dat-1p::GFP+dat-1p:: α-syn]	α-syn GFP expression in the DNs	No	[65]
UA196	sid-1(pk3321) dat-1p:: α-syn, dat-1p::GFP; dat-1p::sid1, Pmyo2::mCherry	α-syn, GFP, and SID-1 expression in the dopaminergic neurons	No	[66]
UA30	baEx30 [dat-1p::GFP]	GFP expression in DNs	No	[65]
UA31	baEx31 [dat-1p::GFP+dat-1p:: α-syn]	α-syn GFP expression in the DNs	No	[65]
UA44	baIn11 [dat-1p::GFP+dat-1p:: α-syn]	α-syn GFP expression in the DNs	No	[65]
UA57	baIs4 [dat-1p::GFP + dat-1p::CAT-2]	GFP expression in DNs	Yes	[58]

upon exposure to Methanolic extract of *Chondrus crispus* was demonstrated using fluorescence intensity measurement, as shown in Fig. 3. These effects were attributed to the up-regulation of the oxidative stress response genes, sod-3 and skn-1, utilizing gene expression analysis by performing quantitative polymerase chain reaction (qPCR).

Cheon *et al.* [73] studied the effect of the methanol extracts of *Sorbus Alnifolia* (MESA), a densely branched ornamental tree commonly known as *Korean mountain ash*, on rat pheochromocytoma PC12 cells and two *C. elegans* transgenic mutants, BZ555 and UA57, after 48 h exposure to MPP+. Exposure to MESA recovered the MPP + treated PC12 cells and both *C. elegans* strains with approximate efficiencies of 85% and 54%, respectively, and enhanced the worms' lifespan by almost 26%. Worms pre-exposed to MESA were protected against DNs degeneration. However, no obvious reduction in the α-syn protein aggregation was reported in the transgenic strain NL5901 under exposure to MESA [73].

Chalorak *et al.* [74] utilized the C. elegans strains BZ555 and NL5901 to examine the anti-Parkinsonian effect of the sea cucumber extracts, Holothuria scabra, including whole body-ethyl acetate (WBEA), body wall-ethyl acetate (BWEA), viscera-ethyl acetate (VIEA), whole body butanol (WBBU), body wall-butanol (BWBU), and viscera-butanol (VIBU), on the DNs degeneration and α-syn accumulation. DNs degeneration of the 6-OHDA treated worms and α-syn aggregation in NL5901 were mitigated by 1.5-fold using 500 μg/ml of WBEA and BWEA which was comparable to the effect of levodopa. Furthermore, the extracts aided in restoring the worm BSR and the lipid content which were inhibited by DNs degeneration.

Altogether, Table 2 summarizes multiple compounds that show PD therapeutic effects in *C. elegans*. Despite many advantages offered by this organism, technological deficiencies in achieving automated, sensitive, high-throughput, simple and low-cost screening have hindered the widespread use of this model in drug discovery and toxicology. Thus, microfluidic techniques have been developed to fulfill the technical gap associated with *C. elegans* research which are reviewed in the next section.

MICROFLUIDICS FOR *C. ELEGANS* STUDIES

Microfluidics is the science and technology of exploiting miniaturized features, including microchannels, microchambers and microvalves, to precisely handle fluids and suspended or dissolved substances, and to study any associated phenomenon at the micrometer to millimeter scale. Microfluidic devices offer various advantages including precise handling of fluids, low consumption of analytes, high-throughput and automation of assays and experimental user-friendliness, simplicity and time efficiency. Using microfluidics, laboratory-based conventional assays on *C. elegans* have been automated by incorporating various actuation and sensing mechanisms to enhance the assay precision and sensitivity. These lab-on-a-chip devices have contributed to understanding of various molecular, cellular and behavioral processes in *C. elegans*.

When using *C. elegans* as a model organism, not only are the cellular and neuronal activities important, but the phenotypic screening of behaviors like locomotion can provide a more comprehensive understanding of the diseases that involve motor dysfunctions, e.g. in PD. However, the worm's small size and continuous crawling and swimming behavior poses a significant challenge in developing precise and high-throughput

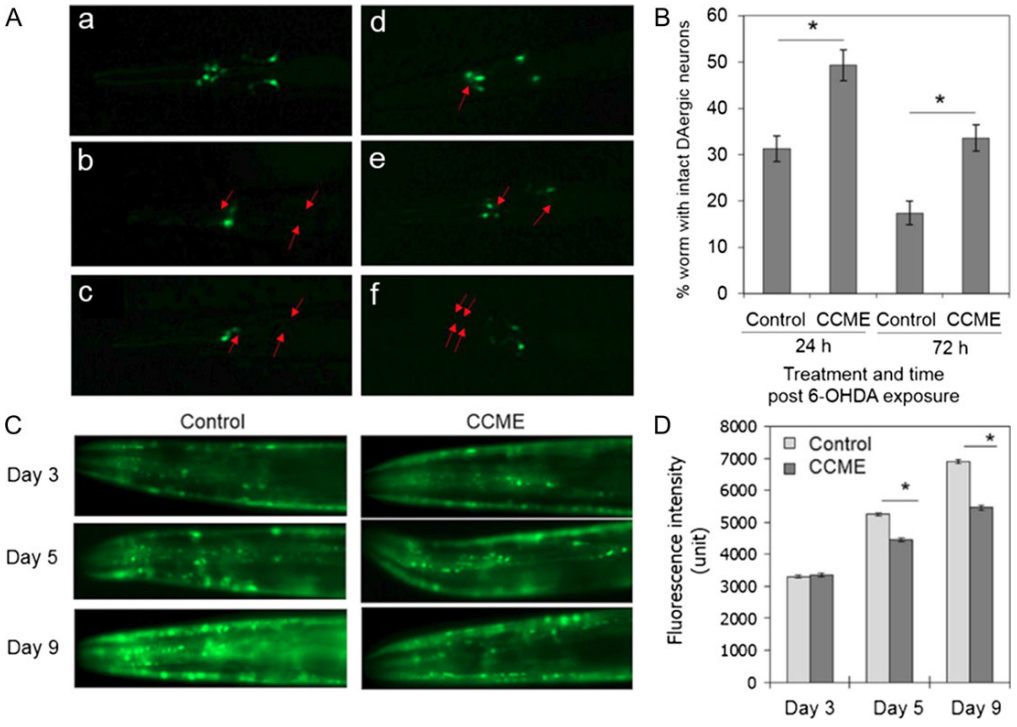

Figure 3. The methanolic extract of Chondruc crispus rescues 6-OHDA induced DNs degeneration and reduces α-syn accumulation in NL5901. (A) GFP expression in DNs of transgenic *C. elegans* strain UA57. (a) image for the intact DNs, (b-f) DNs loss under the exposure to 6-OHDA, with the red arrows indicating the degenerated/missing neurons. (B) Percentage of worms with intact DNs under exposure to 6-OHDA for one hour prior to culturing for 24 or 72 h in the presence and absence of Chondruc crispus, (C) Images of α-syn accumulation over time in the presence and absence of Chondruc crispus, (D) Quantification of YFP expression in muscle cells [72]. (Permission under the terms of the Creative Commons Attribution Non-Commercial License (http://creativecommons.org/licenses/by-nc/4.0))

Table 2. A list of published neuroprotective compounds and their mechanisms of action tested on *C. elegans* under exposure to different neurotoxins. All chemical structures were obtained from PubChem- https://pubchem.ncbi.nlm.nih.gov.

Year	*C. elegans* strains	Chemical treatment or Molecular manipulation (see [a] for symptoms)	Neuroprotective compound	Proposed mechanism of action or mammalian pharmacology [b]	Tested with another model	Ref.
2004	cat-2::gfp	MPP+	Lisuride $C_{20}H_{26}N_4O$	Dopamine receptor agonist	Yes [75]	[58]
			Apomorphine $C_{17}H_{17}NO_2$	Dopamine receptor agonist	Yes [76]	
			Rottlerin $C_{30}H_{28}O_8$	Protein kinase C inhibitor	Yes [77]	
			Nomifensine $C_{16}H_{18}N_2$	Dopamine transporter inhibitor	Yes [78]	
			Nicotine $C_{10}H_{14}N_2$	nACh receptor antagonist	Yes [79]	
			Selegiline $C_{13}H_{17}N$	MAO-B inhibitor	Yes [80]	
			MPEP $C_{14}H_{11}N$	mGluR-5 inhibitor	Yes [81]	
2006	BY250	6-OHDA	Bromocriptine mesylate $C_{33}H_{44}BrN_5O_8S$	D2R agonist	Yes [67]	[67]
			Dihydrexidine hydrochloride C17H18ClNO2	D1R agonist		
			57-OH DPAT hydrobromide C16H26BrNO	D3R agonist		
			SCH23390 hydrochloride $C_{17}H_{19}Cl_2NO$	D1R antagonist		
			Raclopride hydrochloride $C_{15}H_{21}Cl_3N_2O_3$	D2/D3R antagonist		
			Memantine hydrochloride $C_{12}H_{22}ClN$	NMDAR antagonist		
2008	UA18	6-OHDA α-Syn	Acetaminophen $C_8H_9NO_2$	Limiting oxidative stresses. Not protective against α-syn aggregation.	Yes [82]	[68]
2011	BZ555 NL5901	6-OHDA α-Syn	Bacopa monnieri	Activation of bcl-2, maintaining the stability of MMP, and decreasing the activation of caspase-3 through the mitochondria dependent pathway.	Yes [83]	[84]
2012	NL5901	α-Syn	10-O-trans-p-Coumaroylcatalpol $C_{20}H_{24}O_{12}$	Activation of longevity promoting transcription factor DAF-16.	No	[85]
201[3	UA44 UA196	α-Syn	Valproic acid $C_8H_{16}O_2$	Via the MAP extracellular signal-regulated kinase (ERK-MAPK) signaling	Yes [86]	[69]
2014	BZ555 UA44	α-Syn	Spermidine $C_7H_{19}N_3$	Induction of autophagy, suggesting that this cytoprotective process may be responsible for the beneficial effects of spermidine.	Yes [87]	[87]]
2014	BZ555 OW1 3N2	6-OHDA	Acetylcorynoline $C_{23}H_{23}NO_6$	Decreasing egl-1 expression to suppress apoptosis pathways and increasing rpn5 expression to enhance the activity of proteasomes.	No	[24]
2014	BZ555 OW13 N2	6-OHDA	n-Butylidenephthalide $C_{12}H_{12}O_2$	Blocking egl-1 expression to inhibit apoptosis pathways and raising rpn-6 expression to enhance the activity of proteasomes.	Yes [88]	[70]
2015	N2	MPP+	*Myrciaria dubia*	Upregulation expression of superoxide dismutase (SOD-3 and SOD-4) and catalases (CTL-1; CTL-2; CTL-3)	No	[89]
2015	N2 UA57 NL5901	6-OHDA α-Syn	*Chondrus crispus*	Enhancement of oxidative stress tolerance and up-regulation of the stress response genes, sod-3 and skn-1	No	[72]
2016	NL5901	α-Syn	Isoliquiritigenin and liquiritin $C_{15}H_{12}O_4$- $C_{21}H_{22}O_9$	Due to the presence of phenolic hydroxyls. (Anti-oxidants)	Yes [90]	[91]

(*Continued*)

Table 2. (Continued)

Year	*C. elegans* strains	Chemical treatment or Molecular manipulation (see [a] for symptoms)	Neuroprotective compound	Proposed mechanism of action or mammalian pharmacology [b]	Tested with another model	Ref.
2016	N2 NL5901 UA57 BZ555	MPP+ α-Syn	Sorbus alnifolia	Neuroprotection by a DAT-independent mechanism. Failed to inhibit α-syn aggregation	Yes [73]	[73]
2017	NL5901 BZ555	6-OHDA α-Syn	β-amyrin $C_{30}H_{50}O$	Effects of β-amyrin might be regulated via LGG-1 involved autophagy pathway in *C. elegans*.	No	[92]
2017	NL5901 N2	α-Syn	*Shatavarin IV* $C_{45}H_{74}O_{17}$	Increased mRNA expression of stress responsive genes namely sod-1, sod-2, sod-3, gst-4, gst-7 and ctl-2 suggesting its anti-oxidant property that might be contributed in the modulation of oxidative stress and promoting lifespan. Utilizing ubiquitin-mediated proteasomal system and attenuating oxidative stress by up-regulating PD-associated genes pdr-1, ubc-12 and pink-1.	No	[25]
2017	N2 BZ555 OW13	6-OHDA α-Syn	Betulin $C_{30}H_{50}$ O_2	Promoting rpn1 expression and downregulation of the apoptosis pathway gene, egl-1.	No	[71]
2017	N2 NL5901	α-Syn	*Silymarin*$C_{25}H_{22}O_{10}$	Up-regulation of longevity and stress related genes daf-16, sod-3, gst-4 and skn-1.Mitigation of free radicals through pdr-1 mediated recruitment of ubiquitin proteasome system	Yes [93]	[94]]
2017	N2 BZ555 NL5901	6-OHDA α-Syn	*Holothuria scabra*	Due to the presence of antioxidant activity of the contained phenolic compounds, triterpene glycosides, glycosaminoglycans and polysaccharides.	No	[74]
2019	N2 BZ555 NL5901	6-OHDA	*Holothuria leucospilota*	Up-regulation of cat-2 gene (Dopamine synthesis) and sod-3 gene (the free radical scavenging), and downregulation of egl-1 gene (apoptosis). Due to the presence of antioxidant bioactive compounds such as alkaloids, flavonoids, terpenoids, phenols, steroids, saponins (triterpenoids), and glycosides.	No	[95]

[a]The symptoms induced under exposure to 6-OHDA, MPP+, MPTP and α-syn are DNs degeneration, mobility defects, lethality and α-syn accumulation in DNs or body wall muscles. Moreover, DNs degeneration reduction, α-syn aggregation reduction, enhancing the basal slowing response, recovering the lipid content and prolonging the worm's life span were the parameters used to identify the efficacy of each drug.
[b]The mechanism of action for some chemicals were not given in their respective publications, therefore their mammalian pharmacology definition is used instead.

behavioral assays. Therefore, it is inevitable that a variety of microsystems have been developed to manipulate and analyze the neurobehavioral responses of *C. elegans* in response to various external stimulations. Worm immobilization, synchronization, body orientation and stimulus exposure are the common manipulation functionalities needed in these assays. Conventionally, biologists restrict the worm's motion by using glue [96] or anesthetics [97–99]. Despite their common use, these low-throughput methods are slow, irreversible, and inapplicable for long-term immobilization of the worm. Therefore, for the sake of high-throughput research, microfluidic engineers have offered technologies to ease the worm manipulation and imaging. These techniques are reviewed below while we have focused on the methodologies that can be utilized for *C. elegans* PD studies in the future.

Caenorhabditis elegans immobilization on a chip

High resolution imaging and screening of dynamic processes throughout the worms' lifespan are particularly important in neurodegeneration studies to track the protein aggregation and neuron degeneration over prolonged periods. For example, the DNs are spread spatially in the head and tail regions of *C. elegans* and imaging them at high resolution is necessary for determination of any drug-induced degeneration or neuroprotection. Thus, secure immobilization in a high-throughput manner and without affecting the worm physiological conditions is highly valuable. This has been achieved via the use of various mechanical, chemical, thermal or electrical methods.

Mechanical attempts have been performed by restraining the worm motion in a tapered microchannel or by applying

pressure on the worm's cuticle. For instance, Hulme *et al.* [100] developed a microfluidic device for worm immobilization in a 10 μm tapered channel for further morphological analysis and fluorescence imaging. Their device was fabricated from a single Polydimethylsiloxane (PDMS) layer reversibly bonded to a glass substrate. It consisted of 128 parallel tapering channels for immobilization and imaging of approximately 100 worms in 15 minutes. The system was designed in a way to achieve desirable pressure drops in each channel for trapping the worms without excessive force. Lifespan assessment showed that the worms were not physiologically affected by this technique. Although this chip enabled worm immobilization for imaging at high resolution and without any active components, it was difficult to simultaneously image multiple worms in a microscopic field of view, because worms were not located at identical places inside the channels, and the channels were not densely packed. Moreover, it hindered the ability of food and chemical delivery to the worms to enable long-term monitoring that is required in age-associated diseases such as PD. To overcome this challenge, Lee *et al.* [101] designed a chip, shown in Fig. 4A, with 140 tapered channels arrayed in 20 parallel columns and 7 rows, to increase the ability of imaging and stimulating multiple worms simultaneously. These tapered channels were connected in series by a single serpentine channel to supply the food and chemical stimuli. Worm loading, immobilization and recovery were successfully achieved by a pressure driven passive flow with an efficiency of 80%. The abilities for simultaneous imaging of multiple worms, on-chip culturing and controlled stimulus delivery are suitable for neuroscience studies and drug screening applications. As a proof of concept, neuron ablation was tested by measuring the fluorescence signal of a transgenic worm strain with GFP expressed in the mechanosensory neurons ALM and PLM. In 2017, Gokce *et al.* [102] presented a single PDMS layer device incorporated with 20 tapered channels for femtosecond laser axotomy and high resolution imaging of the immobilized worms. The chip, called *Worm Hospital*, consisted of two main compartments, the first was for worm immobilization, axotomy, and imaging while the second had a large chamber for worm culturing and recovery after surgery. Transgenic worms were analyzed to determine whether axonal growth was affected by various genes, and their results showed no significant effect after the laser surgery of ALM and PLM neurons. Moreover, Lockery *et al.* [103] developed a novel technique for whole-worm chemical screening using electrophysiological readouts of the pharynx by mechanical trapping of *C. elegans* head into a tiny channel. The electrodes were attached to eight channels, arranged in a tree-like array, each containing a single worm for recording the electrical activities of the pharynx. The same channels were used for chemical perfusion, while recording the worms' pharyngeal contractions in the presence and absence of anthelmintic, an anti-nematode drug. The above-mentioned mechanical immobilization techniques have the potential to be used in PD studies. Worms expressing α-syn in various neurons can be immobilized, exposed to various neurotoxins and neuroprotection agents, and neuron regrowth after ablation and pharyngeal pumping behavior can be studied.

Guo *et al.* [104] exploited the flexibility of PDMS for *C. elegans* immobilization in an anesthetic-free environment. The paper demonstrated an on-chip femtosecond laser nano-axotomy for studying nerve regeneration of *C. elegans* in a high-throughput manner (60 worms per hour). The developed microfluidic system, called nano-axotomy, was designed to perform neurosurgery and high-resolution imaging in an immobilized worm by applying pressure to deflect a flexible PDMS membrane and trap the worm. The chip incorporated a feeding module for recovery of the ablated worms for further analysis. Fluorescently tagged neurons were utilized for tracking the targeted neurons and monitoring the regeneration process in the absence of anesthetics. The anesthetics-free environment showed much faster axonal regeneration and regrowth of the distal fragments. Collectively, the work revolutionized the field of *in-vivo* neuroscience by combining high-resolution imaging capabilities with microfluidic technologies. Followed after, Chokshi *et al.* [105] used both the flexibility and porosity of PDMS and developed a microfluidic device to investigate two different immobilization approaches. The first approach was achieved by using a deflection PDMS membrane to push the worm towards the channel walls while the other allowed for CO_2 gas diffusion as an anesthetic for worm immobilization, as shown in Fig. 4b. The flexible membrane was sandwiched between two PDMS layers, one layer held the worm flow channel and the other contained the pneumatic control channels for deflecting the membrane and ceasing the worm motion and for applying CO_2. A behavioral characterization module was incorporated inside the device for

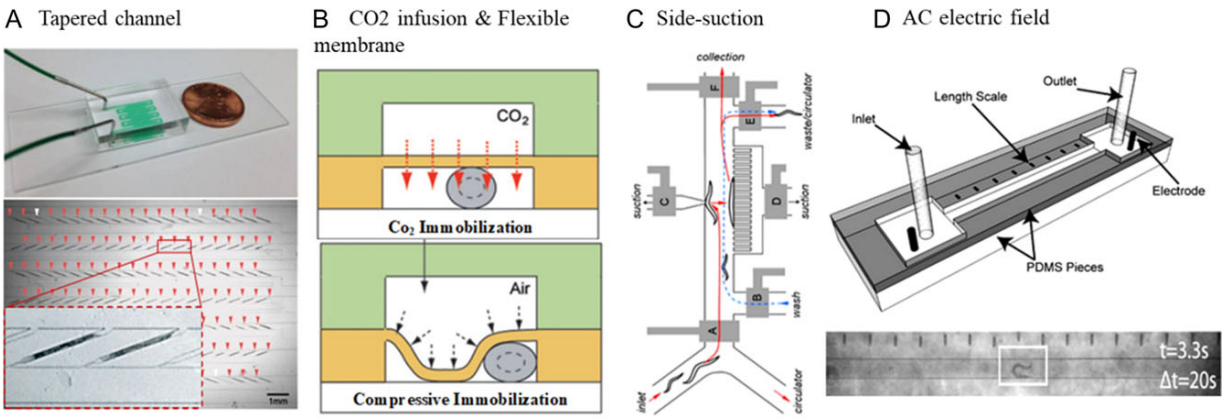

Figure 4. *Caenorhabditis elegans* immobilization approaches in microfluidic devices involving (A) multiple tapered channels loaded with *C. elegans*. (Red triangles indicate successful loading) [101], (B) Co_2 infusion and flexible membrane compression under high pressure (25 psi) [105], (C) side suction channels used for worm sorting and imaging [106], and (D) alternating current electric field used to localize worms [118, 119]. (Figures were adapted from ref [101, 105, 106, 118], with permission from the Royal Society of Chemistry)

determining the worm's behavior before and after immobilization. Their results showed that both methods were efficient for short-term (minutes) immobilization, while long-term (1–2 hours) immobilization was only achievable by using the CO_2 approach. However, the lethality rate for CO_2-based immobilization extending beyond 3 h was reported to be high.

Rohde *et al.* [106] demonstrated a microfluidic device for worm sorting, immobilization, and exposure to different biochemical compounds for imaging. The worm was longitudinally immobilized by utilizing tiny side suction channels along the body of the worm, as shown in Fig. 4c. The authors demonstrated the potential of this chip for phenotypic analysis and worm imaging by tracking neural degeneration and regeneration after femtosecond laser microsurgery of axons. McCormick *et al.* [107] utilized the same immobilization technique to clamp the worm at its midsection, leaving its head and tail free to move for behavioral screening when exposed to chemical, thermal and osmotic gradients. The main feature of this device was that the worm was located at the point of confluence with a stimulus at two different concentrations forming a step-like gradient at the free moving part of the worm. Individual head swings were used as the behavioral readout. Moreover, Hu *et al.* [108] designed a *C. elegans* stimulus delivery system using a multi-layer PDMS device consisting of a T-junction channel, supported by a comb-shaped valve, for worm immobilization to investigate the effect of different gases (O_2, CO_2) and odors (1-Octanol) on the *C. elegans* neuronal system. Their investigations showed that BAG†[109], (Low O_2 sensory neurons) neuronal activities inhibition by CO_2 causes anesthesia symptoms while URX‡[109], (High O_2 sensory neurons) neuronal responses were induced by 10–21% O_2 level as confirmed previously by Zimmer *et al.* [110] and after that by Wang *et al.* [111] In addition, several researchers have combined multiple techniques to precisely immobilize the worm such as developing chips with integrated suction channels and a flexible membrane [106, 112, 113] or a tapering channel [114].

Most of the previously discussed approaches successfully immobilized adult worms in a precise manner. However, when it comes to small *C. elegans* larval stages, these techniques need to be scaled down which is not easily achievable. Krajnuiak *et al.* [115] maneuvered this issue and availed the use of Pluronic F127 (PF127), a temperature-sensitive biocompatible polymer that reversibly transforms from solution to gel phase by raising its temperature above 17°C. The microfluidic chip was developed to perform high-resolution imaging of L1 stage worms in a benign environment. Two PDMS layers were used to develop the chip, the first was the main flow layer for introducing the worms, nutrients and gel flow. The second was the flow control layer which contained the pneumatic valves for controlling inlets and outlets. Eight worm traps were designed to be filled with PF127 for worm immobilization by controlling the gel temperature. As a validation step, a transgenic worm strain expressing GFP was used for fluorescent imaging. Their investigations showed that the gel had no effect on the quality of the produced images when compared with the conventional methods of using an agar pad with sodium azide for immobilization. Aubry *et al.* [116] developed a microfluidic device for encapsulating the small larvae in droplets of PF127. By controlling the gel temperature, L1 larvae were immobilized within the droplets. This microfluidic platform consisted of a T junction channel for droplet generation and worm encapsulation, followed by a serpentine channel for immobilization of 80 to 250 worms at the same time and finally a worm sorting unit. At first, the device temperature was kept at 12°C for liquefying the gel to flow easily through the device. Meanwhile, another fluid was injected as a spacer between the gel droplets for eliminating the coalescence possibility of the PF127 droplets. Then, for imaging purposes, the flow was stopped, and the device was brought into room temperature at which the gel solidified for immobilizing multiple worms. Finally, as a proof of concept, mutants that express GFP in URX sensory neurons were used for high-resolution imaging of 50 worms in a single run within the device.

Recently, Dong *et al.* [117] introduced two mechanical compliance approaches for worm immobilization. The first exploited the PDMS elasticity to securely restrict the worm's motion by applying tensile stress along the channel. The second method was designed for all *C. elegans* stages by using a height-tunable chip. The height tunable chip consisted of a PDMS-glass based device, mounted in a screw adjustable polymethyl methacrylate (PMMA) holder for compressing the PDMS layer. The PDMS layer was enhanced with multiple crescent shape micropillars that restrained the worm motion in the compression phase. The authors demonstrated the capability of their devices for *in-vivo* developmental imaging by monitoring the transition from oocyte to embryo stage on a chip. Also, they demonstrated that the two approaches had no apparent physical or physiological effects on the worms.

Rezai *et al.* [118, 119] demonstrated the response of *C. elegans* to electricity, called electrotaxis, in a straight channel, showing that the worm swims towards the negative pole of a direct current electric field or stops when exposed to an alternating current electric field at low frequency, as shown in Fig. 4d. Their investigations showed that this behavior is attributed to specific sensory neurons. Additionally, there are other microfluidic techniques used for immobilization including testing a variety of anesthetics (e.g. levamisole and sodium azide) [97–99], cooling down the worm's body to 4°C by flowing a cold liquid through an adjacent channel [48] or raising the worm temperature to 37°C using an optoelectrical microchip [120]. However, these techniques are not amenable to long term immobilization without affecting the worms' behavior. Thus, they are omitted from this review since they are less useful to studying neurodegeneration.

As detailed in this section, different approaches have been developed for worm immobilization over the last two decade. The main objectives have been to achieve high-throughput immobilization without affecting the worms' physiological conditions and fecundity, and to enable high resolution imaging of all the developmental stages of *C. elegans*. While all techniques are effective in immobilizing the worms, one needs to select an appropriate method when studying *C. elegans* PD models introduced in Tables 1 and 2. Under conditions where lower throughput assays are being developed that require perfect immobilization of the worms for high-magnification imaging or laser-based ablation of neurons such as DNs, the side suction channel or membrane deflection technique are recommended. Tapered channels are more suitable for high-throughput experiments where behaviors such as pharyngeal pumping, low-magnification images of neurons and organs, and electrophysiological readouts are of interest. If age-associated processes such as α-syn accumulation and neuron degeneration over larval stages are being investigated in worms, one needs to use the phase changing hydrogels or the PDMS compliance-based techniques that are compatible with worms at various ages and sizes.

Caenorhabditis elegans synchronization on a chip

The possibility of obtaining synchronized populations is a considerable advantage of *C. elegans* as a model organism. It is a very useful feature for studying age-related diseases such as PD where the neurobehavioral status of the model or patient is progressively worsening by age. Conventionally, synchronization is attained by bleaching gravid adult worms using sodium hypochlorite while the intact eggs are kept to hatch and cultured on a new plate for growing into a specific developmental stage [53]. However, this conventional method is time consuming and labor intensive. The COPAS (Complex Object Parametric Analyzer and Sorter) machine, an automatic small organism and cell sorter, has been used to sort worms with a technique similar to fluorescence–activated-cell-sorting (FACS) [121]. Using COPAS, large-scale optical data could be generated to isolate 100 mutants per second based on gene expressing fluorescence signals [122]. Although this equipment offers valuable advantages, it uses a one-dimensional scanning approach and an active imaging-based feedback function which hinder its ability to image the worms' three-dimensional cellular and subcellular features. The tool is also bulky, expensive in the order of few hundred thousand dollars and operationally sophisticated.

Microfluidic devices have offered different approaches to overcome the aforementioned challenges in worm synchronization. Recently, multiple platforms have been developed for *C. elegans* sorting and synchronization based on age or mutation. Rezai *et al.* [123] developed a sorting microfluidic chip by exploiting the use of their DC electrotaxis method, described previously, on sorting large populations of *C. elegans*. They designed a single 100 μm height PDMS layer device, consisting of two parallel chambers interconnected with 20 microchannels, as shown in Fig. 5a. A population of worms (L3, L4, muscle mutant or neuron mutant worms mixed with young adult WT) was loaded into the device and a specific electric field was applied across the device which electrically stimulated the worms to swim through the microchannels towards the separation chamber. The high electric field generated in microchannels selectively prevented the older stages of worms from passing through the microchannels. Age- and mutant-based sorting were effectively achieved with a throughput of 78 worms/minute. Han *et al.* [124] investigated the worms' electrotaxis effect on sorting mixed populations of *C. elegans* in a single PDMS layer microfluidic device. The chip consisted of multiple parallel arrays of channels containing hexagonal arrayed micro-bumps (Fig. 5b). These micro-bumps were designed to enhance the worms' swimming behavior and, with the aid of electrotaxis, the worms were guided through three different channels, in which only the targeted age/size could pass. Followed by that, Wang *et al.* [125] developed a sorting microfluidic chip by taking advantage of the investigations reported by Gabel *et al.* [126] who showed that worms crawl from the anode to the cathode at a specific angle depending on their age/size and the electric field strength. This criterion was termed deflecting electrotaxis. The developed monolayer chip consisted of 20 symmetrical microchannels tilted with specific angles ranging from –50° to 50° for worm sorting, as shown in Fig. 5c. When the electric field was applied, mixed populations of L2, L3, L4, young adult, and mutants were simultaneously sorted. A question that still needs to be answered in this field is the biological pathways that are involved in electrotaxis. If the genes, neurons and muscles involved in PD are also mediating electrotaxis, a new line of research can evolve in which electrotaxis can be used to evoke biological responses on-demand to investigate various genetic, molecular and cellular processes.

Mechanical approaches have been exploited to passively or actively sort different worm stages. Solvas *et al.* [127] developed a passive technique to sort worms based on their size taking advantage of the phenotypic differences between adults and larvae. Their chip, termed 'smart mazes' and shown in Fig. 6a, consisted of a network of interconnected channels tilted 45° to x-axis and oriented towards the desired sorting channel. The interconnected channels were designed to disturb the hydrodynamic movement of different worm stages and passively sort them towards the targeted outlets based on their size, just like a method in cell and particle sorting called 'Deterministic Lateral Displacement (DLD)' [128]. Successful separation of adult worms from larvae was achieved at 200–300 worms per minute with 94% efficiency and 0.2% contamination. Additionally, the authors stated the potential of their device to process 1200 worms/minute combined with a reduction in the device sorting efficiency. Another study developed by Ai *et al.* [129] reported efficient sorting of a worm population containing a mixture of L1 to adult stage with a throughput of 130 to 180 worms/minute. A passive flow filtration approach was demonstrated by incorporating micro-pillar structures optimized to pass specific stages of worms, as shown in Fig. 6b. Multiple devices were fabricated to deal with two consecutive developmental stages and, by combining these devices in series, mixed worm populations

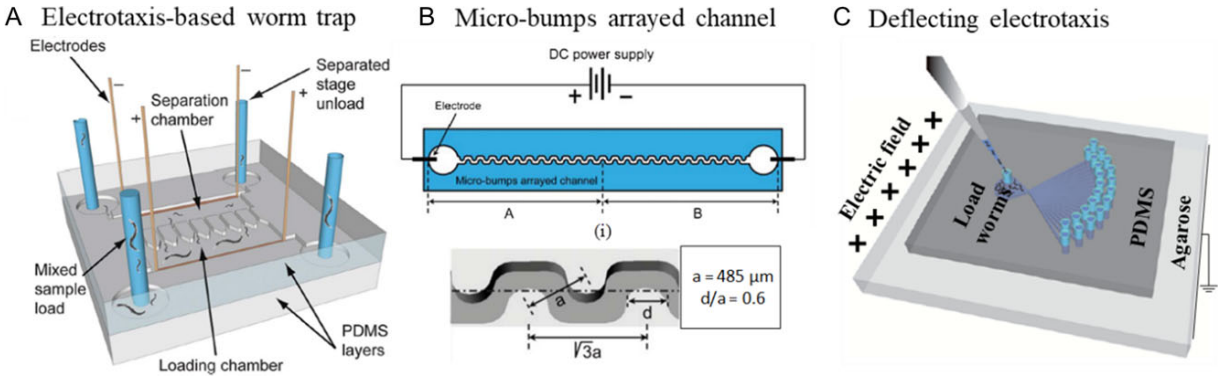

Figure 5. Different electric-based microfluidic devices for *C. elegans* sorting. (A) Worm electrotactic sorter using narrowing channels with enhanced electric field called electric traps [123]. (B) A micro-bump electrotaxis-based worm sorter with the reported best design for adult worm sorting [124]. (C) worm sorting based on the deflecting electrotaxis behavior [125] (Figures were adapted from ref [123–125]. with permission from the Royal Society of Chemistry)

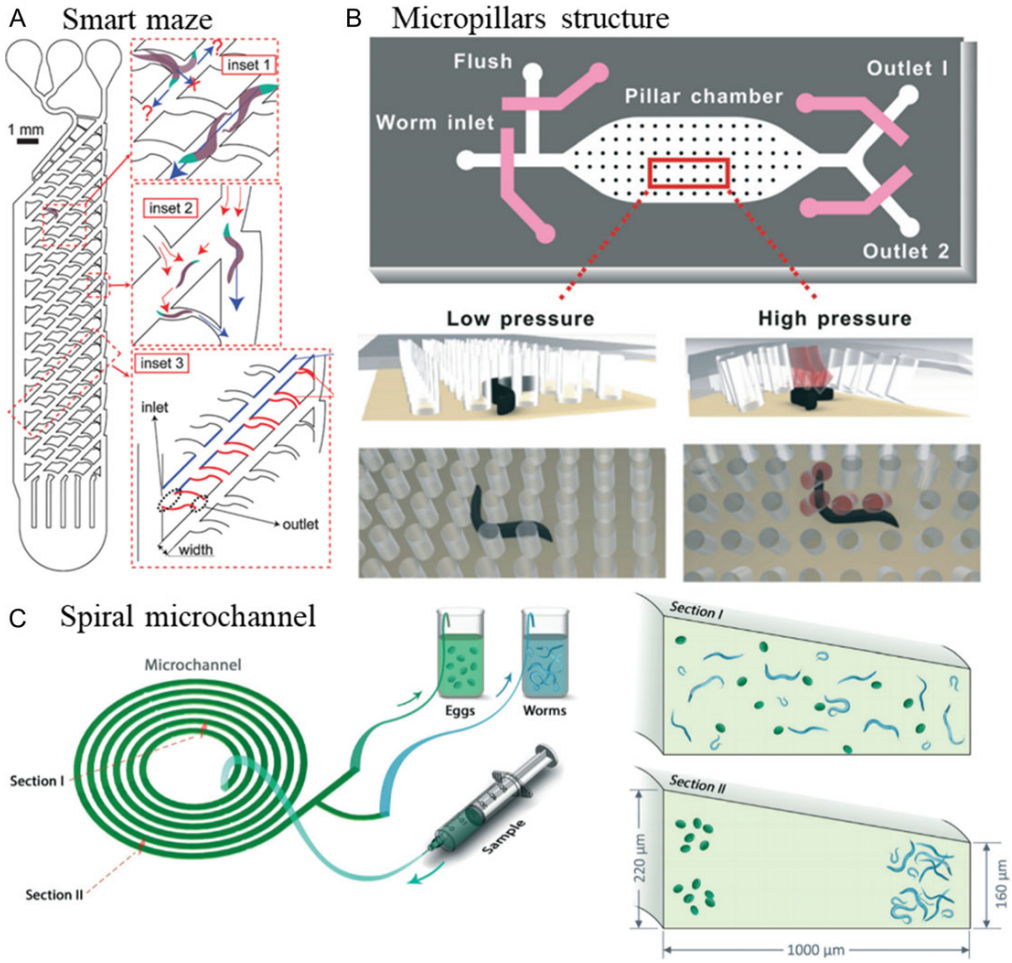

Figure 6. Schematic illustration of different passive microfluidic devices for *C. elegans* sorting. (A) smart maze concept for adult worm sorting [127]. (B) micropillars-based sorting technique [129]. (C) spiral microfluidic channel to extract eggs from a worm population [130]. (Figures were adapted from ref [127, 129, 130], with permission from the Royal Society of Chemistry)

were successfully sorted. Recently, Sofela *et al.* [130] reported an efficient and high-throughput (4200 worms/minute) method for egg extraction from a mixed worm population by focusing the eggs along the channel inner wall based on the use of inertial focusing in a spiral microfluidic chip shown in Fig. 6c. These mechanical approaches are suitable in PD worm studies where age-synchronized samples are needed either for exposure to neurotoxins or for investigating the time-dependent effects on size throughout the worm lifespan. However, synchronizing mutant worms with size similarity or distinguishing samples with degenerated neurons or locomotion defects in PD cannot be performed with mechanical sorters.

Despite the advances offered by these approaches, none of them reported the sorting of transgenic animals based on their fluorescence expression. This functionality is very important in PD assays for isolating the worms with different levels of α-syn aggregation and neuron degeneration based on fluorescent reporters, especially because the effect of neurotoxins is often inconsistent even among the worms of a single population. For this purpose, Rohde *et al.* [106] developed a whole-animal genetic and drug screening platform, able to perform high-resolution fluorescent imaging along with a rapid worm sorting platform. The worm sorter was manipulated with pressure-driven microvalves in a sequential process to randomly capture a single worm, immobilize it using side suction channels, and sort it based on the phenotypic feature of interest. Then, Chung *et al.* [131] adopted a similar technique integrated with customized software to precisely image and sort transgenic worms without human intervention. The device consisted of an inlet port, an immobilization channel and a Y-shaped outlet channel, all manipulated by pressure-controlled valves. Their chip was designed to immobilize the worm by cooling it to 4 C, image it for fluorescent signal detection, and operate the valves sequentially for successful sorting based on the worm phenotype. The system achieved a throughput of approximately 150 worms/hour. Finally, Yan *et al.* [132] developed a fully automated fluorescent-based sorting microfluidic chip, shown in Fig. 7, with a sorting efficiency of 100% and a throughput of 60 worms/minute. The developed chip consisted of a single PDMS layer, incorporated with worm inlet channels, two fluidic control channels for worm sorting, Y-shaped outlet channels and four optical fiber inlets. The GFP signal was detected by the optical fibers and, upon receiving the signal, the worms were sorted by altering the pressure of two opposing channels B and C, as shown in Fig. 7.

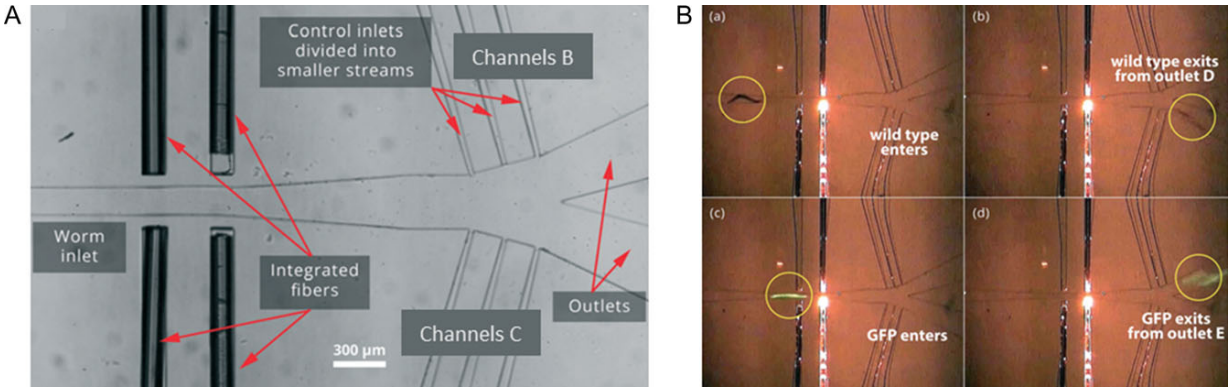

Figure 7. Microfluidic sorting device based on the worms' fluorescent signal. (A) Image of the device with integrated optical fibers. (B) Snapshots of (a–b) a WT worm and (c–d) a GFP worm being sorted in the device [132]. (Figures were adapted from ref [132], with permission from the Royal Society of Chemistry)

Altogether, the approaches discussed in this section reported high-throughput sorting of mixed populations of worms based on size and phenotypic responses as well as medium-throughput sorting based on fluorescence signal. Although sorting of transgenic strains is done at a lower throughput, high-throughput sorting is highly desirable in many experiments that require transgenic animals expressing fluorescent reporters, like in PD studies of protein aggregation and neuron degeneration/protection. Thus, active methods like electrotaxis and fluorescence-based sorting are more anticipated in *C. elegans*-based neurobiology studies.

Caenorhabditis elegans orientation on a chip

In addition to immobilization and synchronization, worm orientation poses a challenge when imaging specific locations within the worm, such as studies of *C. elegans* chemosensation neurons or DNs in PD, which are located near the anterior and posterior regions of the worm. Thus, in many applications such as laser ablation, neurodegenerative studies and microinjection, longitudinal and lateral worm orientation have been a focus of investigation. Although confocal microscopy can be used to avoid the need for orientation, but due to the lack of access to this microscopy technique in most *C. elegans* and microfluidics labs, and due to the need for performing imaging faster to facilitate high-throughput screening, researchers have developed microfluidic techniques to achieve a specific orientation on a chip. With these devices, in addition to multi-directional imaging, one can perform simultaneous stimulation with various chemical and physical signals that is not easily achievable in confocal microscopy.

Rezai *et al.* [118] demonstrated the use of direct and alternate current electrotaxis in longitudinally orienting the worms. Ardeshiri *et al.* [114] demonstrated a novel microfluidic chip for on-demand manipulation of *C. elegans* by exploiting the electrotaxis effect to longitudinally orient the worm in a microchannel incorporated with a rotatable glass capillary to trap the worm's head for orientation in any favorable lateral direction, as shown in Fig. 8a. Successful optical and fluorescence imaging of different body locations such as worms' vulva and ventral nerve cord were demonstrated. A 100% and 76% success rate for longitudinal and lateral orientation were reported, respectively. Ahmed *et al.* [133] developed an acoustic-based on-chip manipulation method using a piezoelectric transducer and a simple microfluidic channel to manipulate microparticles, cells and *C. elegans*, as shown in Fig. 8b. They precisely rotated *C. elegans* by using either continuous or stepwise power supply, allowing the worm orientation at any desired angle. Using on-chip rotation, they differentiated and examined mutant worms from mixed populations by imaging the structure of the worms' vulva. Cáceres *et al.* [134, 135] utilized a curved microchannel to passively orient *C. elegans* into lateral body positions along their dorso-ventral body axis in a simple and robust operation, as shown in Fig. 8c. The curved microchannel aided in adjusting the worm body within the microscope field of view to image morphological features along its entire body. For achieving passive flow control, a multi-layer PDMS chip was fabricated to control the worm's flow and mutants' isolation by utilizing on-chip valves based on the deformable PDMS membrane technique mentioned previously. A mixture of worms was introduced into the device including six neurodegenerative mutants for lateral orientation with 84% efficiency. Successful isolation of these mutants was achieved based on their neurodegenerative defects without altering their physiological conditions, by activating mutant type (MT) channel, as shown in Fig. 8c.

Recently, Martin *et al.* [136] developed a novel acousto-optical deflector-based imaging technique using the line excitation array detection (LEAD) microscopy that eliminates the need for *C. elegans* immobilization and orientation to capture 3D *C. elegans* images at 0.8 million frames per second. The system was coupled with a flow-based microfluidic platform to work as a flow cytometer for imaging randomly oriented free-flowing worms at speeds over 1 m/s. A HD worm model with polyglutamine protein aggregations was used to assess the system's potential for phenotypic and drug screening under exposure to dronedarone, a drug for arrhythmias in humans [137]. Precise 3D *in-vivo* imaging of aggregation localization was achieved for drug-free and drug-treated worms revealing that dronedarone reduces the polyglutamine aggregation in a dose-dependent manner as reported earlier [138]. Moreover, the technique's potential for brain imaging was implemented using brain slices from Arc-dVenus transgenic mice [139].

In neurodegenerative studies, all the manipulation techniques reviewed in this section are needed for high resolution imaging of the worm body, organs and cells in various orientations and for behavioral investigations. In the next section, we will review the studies related to neurodegeneration with *C. elegans* with a focus on PD.

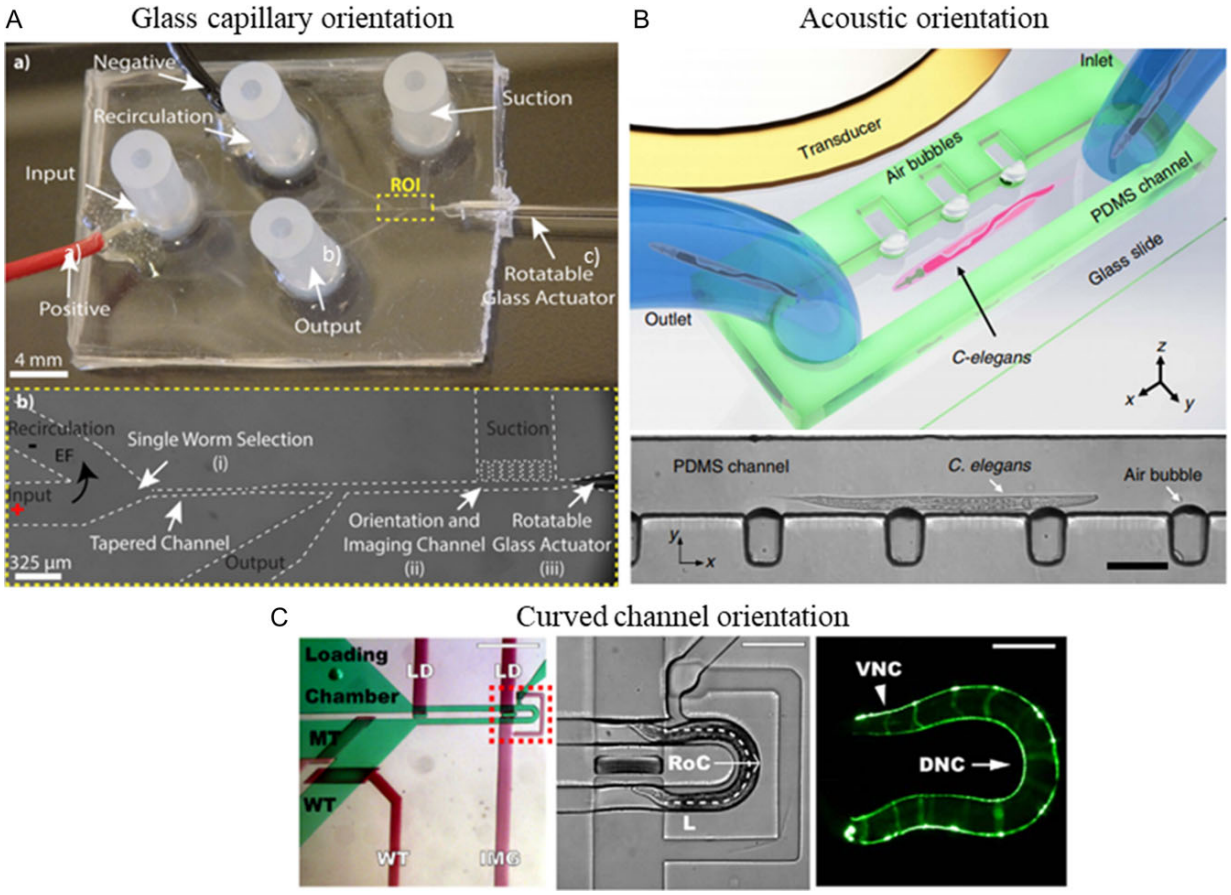

Figure 8. Microfluidic devices for *C. elegans* lateral and longitudinal orientation. (A) on-demand manipulation of *C. elegans* using a rotatable glass capillary [114]. (B) Acoustic manipulation using a piezoelectric transducer [133]. (C) A curved microchannel to passively orient *C. elegans* into lateral body positions [134]. (Figures were adapted from ref [114, 133, 134], with permission from AIP publishing and Creative Commons Attribution 4.0 International License http://creativecommons.org/licenses/by/4.0/)

MICROFLUIDIC DEVICES FOR STUDYING PD AND OTHER NEURODEGENERATIVE DISEASES USING *C. ELEGANS*

Thanks to the *C. elegans* simple and unique nervous system, ongoing research with the worm has contributed to the discovery of different pathological mechanisms related to neurodegenerative diseases. Most of the neurodegenerative diseases are known by the loss or malfunction of specific neurons in the central nervous system due to the uncontrolled aggregation of various proteins. The effect of different neurotoxins and neuroprotective compounds on the aggregation or misfolding of the protein of interest have been studied in worms using microfluidic devices.

Ma *et al.* [140] used the deflecting membrane technique for trapping multiple worms in parallel channels by activating programmable microvalves incorporated into the chip, as shown in Fig. 9a. The immobilization channels were designed for trapping the worm and allowing its movement in a controlled environment for achieving real-time and long-term monitoring of the examined worms. Transgenic worms expressing GFP in DNs were exposed to different concentrations of the neurotoxin MPP + prior to entering the chip. The worms' mobility and neurons fluorescence intensity were investigated simultaneously over their lifespan without causing any harm in the device. Their findings demonstrated that MPP+ induced DNs degeneration and mobility defects in *C. elegans*. Shi *et al.* [141]. investigated the effect of 6-OHDA on *C. elegans* movement behavior and neuronal fluorescence by utilizing a droplet-based microfluidic device integrated with a tapered channel for worm immobilization and imaging, as shown in Fig. 9b. Worms were exposed to 6-OHDA before being encapsulated within droplets; then, using a novel floatage-based trap, worms were transferred to the trap section and immobilized for imaging. 6-OHDA-induced mobility defects and DNs degeneration were observed and quantified in their device.

Cornaglia *et al.* [142] proposed a novel temperature-controlled multi-functional platform, shown in Fig. 10, integrated with chambers for worm isolation, channels for food delivery and PF127 gelation for worm immobilization. This platform was utilized to perform precise *in-vivo* imaging and tracking of protein growth and aggregation in amyotrophic lateral sclerosis (ALS) and Huntington's disease (HD) using AM725 (rmIs290 [unc-54p::Hsa-sod-1 (127X)::YFP]) and AM140 (rmIs132 [unc-54p::Q35::YFP]) strains, respectively. A continuous food delivery system and chambers for individual worm isolation allowed performing the experiments for a long period of time (> 90 h) and monitoring protein aggregate size over multiple days. Moreover, the effect of

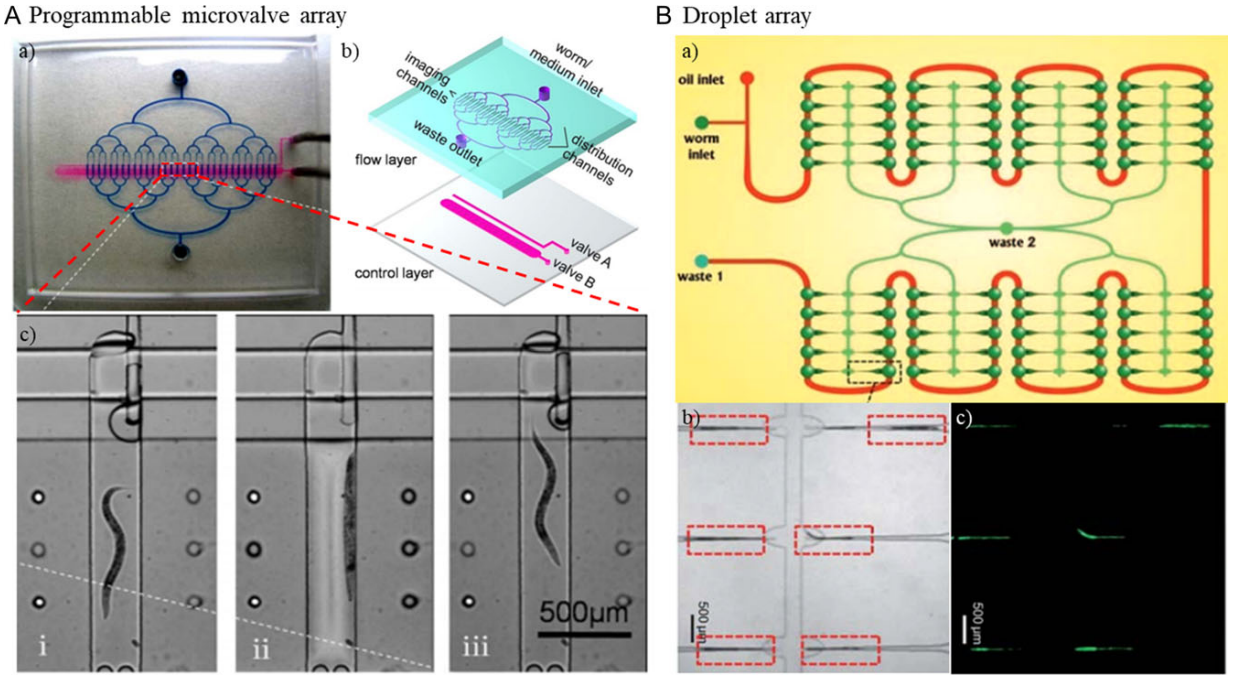

Figure 9. Microfluidic devices for investigation of neurotoxins' effect on *C. elegans*. (A) Programmable microvalve-based microfluidic chip for characterization of neurotoxin-induced responses of individual *C. elegans* [140]. (B) Schematic of the droplet-based microfluidic chip for 6-OHDA exposure and neurobehavioral screening [141]. (Figures were adapted from ref [140, 141], with permission from AIP publishing and the Royal Society of Chemistry, respectively)

doxycycline, a common antibiotic, on protein aggregation in an ALS model was investigated and proved to reduce the size of protein aggregates over time.

Mondal *et al.* [138] developed a high-throughput and high-resolution imaging microfluidic chip with a 96-well format to be compatible with automated liquid handling systems, as shown in Fig. 11. Every single well embraced a set of 40 parallel channels for worm immobilization and imaging. Each channel was designed precisely to immobilize the worm in the lateral orientation by axially reducing the height and width of the channel and keeping its aspect ratio to 1. The chip efficacy was tested by performing a drug screening for HD (polyglutamate aggregation) using a *C. elegans* model and 1000 FDA-approved compounds. Four compounds were identified for polyglutamate aggregation reduction. Moreover, the same chip was successfully used to identify neuroprotective drugs for other neurodegenerative diseases [143]. The same group has recently developed a novel 3D high-speed imaging platform discussed earlier that is also suitable for drug screening using PD-worm models [144].

Most of the aforementioned studies focus on correlating the neurotoxins effects on the neurons by using fluorescently labeled cells while paying less attention to the sensory-motor behavioral responses. Therefore, Salam *et al.* [145] were the first to utilize the instinctive electrotaxis response of *C. elegans* to crawl towards the cathode, when exposed to DC electric field, for analyzing different mutants and worms treated with neurotoxins such as 6-OHDA, MPTP and rotenone, and neuroprotective compounds such as acetaminophen. Transgenic worms with defective sensory and dopaminergic neurons showed noticeable reduction in electrotaxis speed, i.e. 30–80% slower when compared to wild type. Worms treated with neurotoxins presented movement disorder while their behavior was preserved by pre-exposing them to acetaminophen.

Although the free movement of worm is beneficial for phenotypic behavioral studies, enhancing the throughput of this method is very challenging. Accordingly, we developed a microfluidic device for detecting the neurobehavioral effects of 6-OHDA and α-syn overexpression on neurodegeneration and electrotaxis movement impairment of semi-mobile worms, as a model for PD [146]. Our microfluidic device, shown Fig. 12A, composed of a 70μm-thick PDMS layer bonded to a glass substrate. This layer (Fig. 12B) included a worm loading channel, a tapered worm trapping channel, an electrotaxis channel with end electrodes, and comb-shaped channel for immobilization and fluorescent imaging. The loading process, shown in Fig. 12C (i), was used to load individual worms into the trapping channel from their tail side, leaving almost 70% of their body free-to-move inside the electrotaxis channel, as shown in Fig. 12C (ii-iii). Following the electrotaxis assay, the worms were immobilized and imaged by applying negative pressure at the comb-shaped channels, as shown in Fig. 12C (iv-v). Our results showed that exposing the worms to 100 μM of 6-OHDA affected both neurons and their electrotaxis behavior significantly while the most commonly used 6-OHDA concentrations in the literature are exceeding 5 mM. Another advantage of this method is its potential for parallelization of worm traps to achieve higher throughput worm screening devices that are needed for drug screening in PD assays. Moreover, one can easily assess the neuronal properties and behavioral phenotypes of worms by keeping their identity in the chip, an advantage that had not been achieved by the previous electrotaxis screening devices.

The use of active methods such as electrotaxis and phototaxis [99] to evoke movement is beneficial in controlling and assessing the voluntary locomotion of worms in neurodegenerative disease studies. However, a major challenge is to ensure that the biological pathways mediating these sensory-motor processes are also

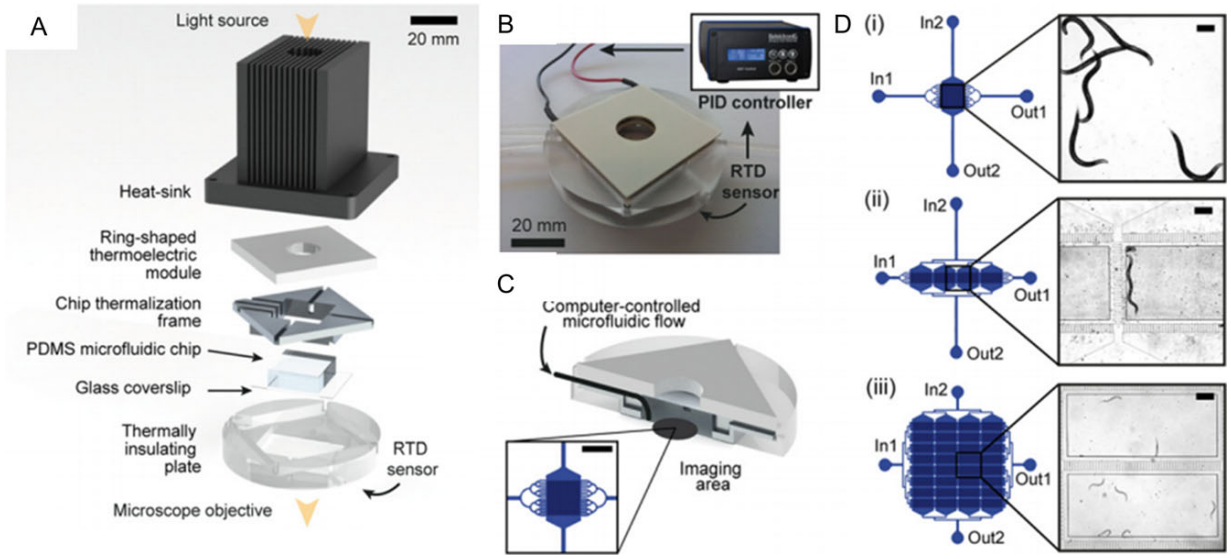

Figure 10. (A) Schematic illustration of a thermally-controlled microfluidic device and its assembled components. (B) & (C) Actual device image with a cross section view of the device, focusing on the microfluidic device inside the assembly. (D) Different microfluidic chips designed to be assembled with (i) 1, (ii) 4 and (iii) 32 worm culture chambers. Scale bars = 200 μm [142]. (Permission under the terms of the Creative Commons Attribution Non-Commercial License (http://creativecommons.org/licenses/by-nc/4.0))

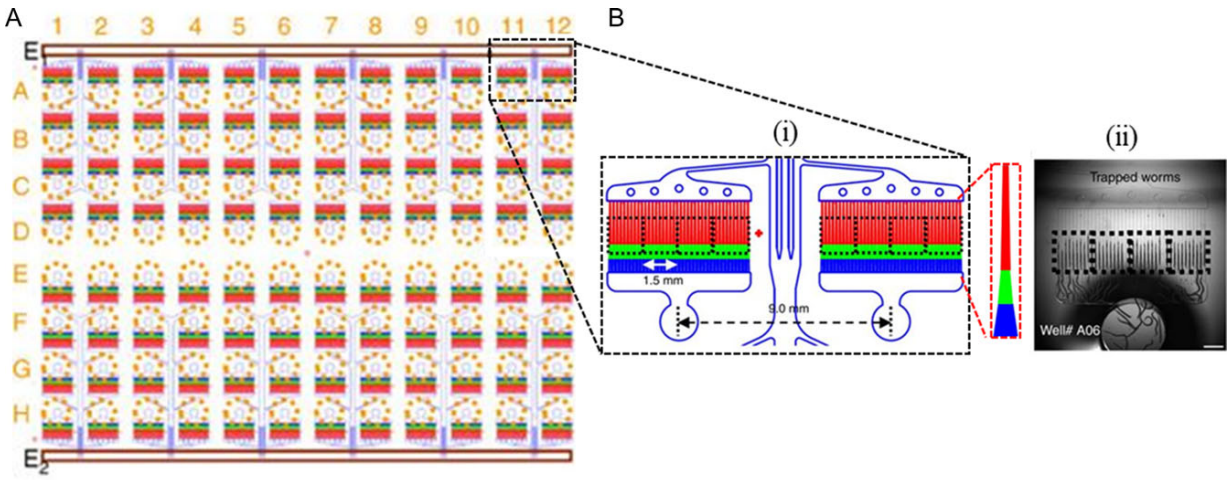

Figure 11. Schematic of a high-throughput *C. elegans* immobilization and imaging chip for chemical screening. (A) schematic of the overall chip with two main exits E_1 and E_2. (B) (i) A closer image of the actual traps connected to a single exit, (ii) an actual image of a well with 40worms immobilized [138]. (Permission under the terms of the Creative Commons Attribution Non-Commercial License (http://creativecommons.org/licenses/by-nc/4.0))

involved in the targeted disease. At a technical level, achieving behavioral investigations with electrotaxis and phototaxis techniques at a high-throughput is a limitation that requires more research.

FUTURE TRENDS OF *IN-VIVO* AND *IN-VITRO C. ELEGANS* ASSAYS

α-syn accumulation, lewy-body formation and their spread throughout the brain have been characterized as a cause for PD [147]. Moreover, misfolding α-syn cell-to-cell transfer has been suggested to contribute to the pathogenesis of PD. However, the *in-vivo* mechanisms involved in this progression are yet to be explained in detail. *Caenorhabditis elegans* has proven to be a powerful tool for investigation of PD and other neurodegenerative diseases at the molecular, cellular and behavioral levels. To investigate the mechanisms of α-syn transmission *in-vivo*, *C. elegans* models have been developed to study the cell-to-cell transmission of different proteins, owing to its transparency [148–150]. For instance, recently, two groups have used the bimolecular fluorescence complementation (BiFC) technique to develop worm models for studying protein cell-to-cell transfer in PD and HD [148–150]. In BiFC technique, the two halves of a fluorescent protein (e.g., GFP or YFP) are fused to the protein of interest (e.g., α-syn), as shown in Fig. 13A. The hybrid proteins will only emit fluorescence when the two complementary GFP halves are brought together by α-syn self-assembly, thereby reconstituting their function as a single protein to emit

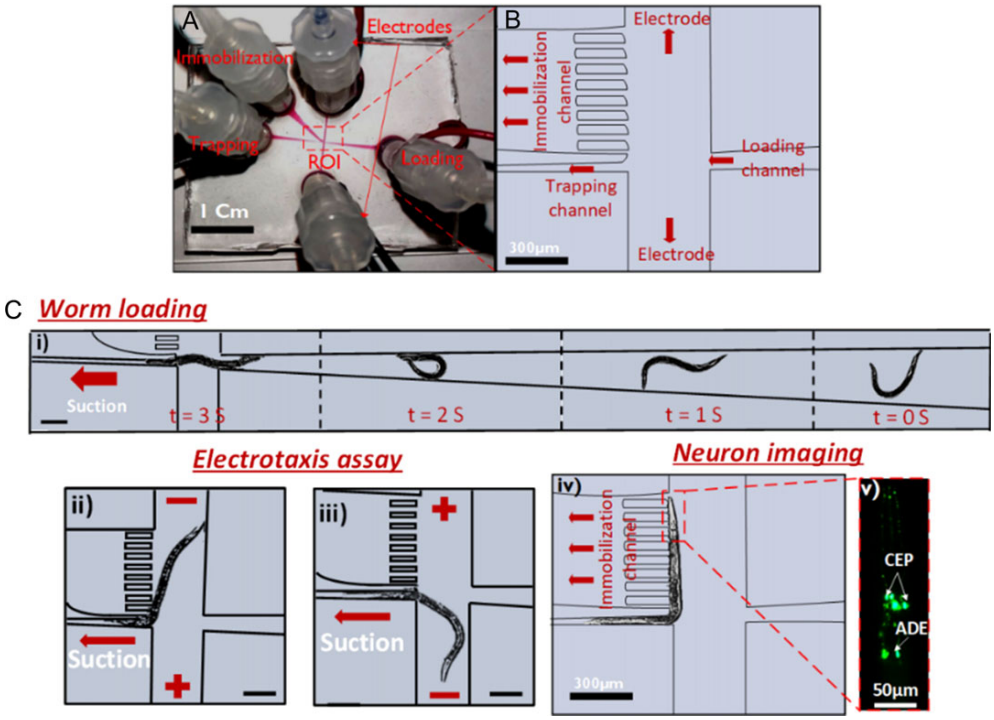

Figure 12. (A-B) Microfluidic device consisting of one inlet, two suction channels and a phenotypic analysis channel for electrotaxis screening and worm immobilization. (C) (i) Time-lapsed images showing the worm loading process, (ii-iii) Worm facing the cathode during the electrotaxis assay, (iv-v) Worm immobilization using the side-suction channel and imaging under 20x magnification, showing the CEP and ADE intact neurons of the BZ555 strain in the absence of any neurotoxin [146].

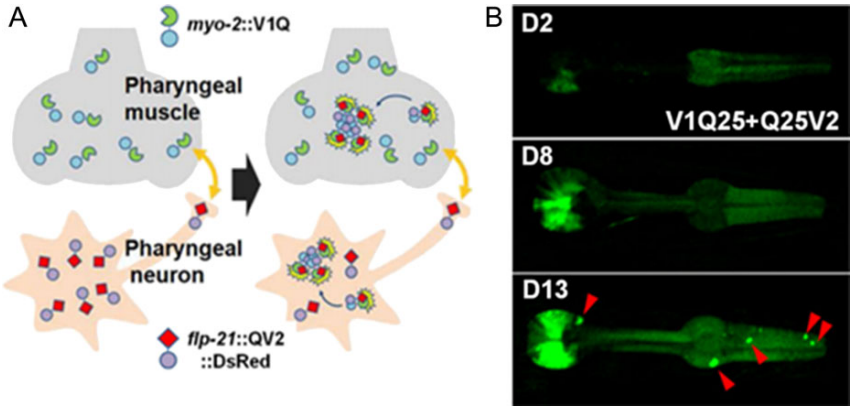

Figure 13. (A) BiFC technique to study cell-to-cell protein transmission. (B) BiFC fluorescence in the aging-related mutants from day 2 to day 13 [149]. (Permission under the terms of the Creative Commons Attribution Non-Commercial License (http://creativecommons.org/licenses/by-nc/4.0))

fluorescence. Hence, this technique has contributed in developing *C. elegans* models to study cell-to-cell interaction.

In *C. elegans*, two BiFC-based α-syn proteins were expressed either in two separate neurons or in two different cell types. As an example, Kim *et al.* [148] studied the effect of aging on cell-to-cell α-syn protein transmission by utilizing the BiFC technique to develop a unique worm strain that expresses fluorescence in pharyngeal muscles and their related neurons only if α-syn proteins interact together. As a result, they suggested the use of anti-aging approaches as a remedy for inhibiting or reducing the progression of PD. Later, the same group developed a *C. elegans* strain to study the transmission of polyglutamine aggregates in real time for HD, as shown in Fig. 13B [149]. Tyson *et al.* [150] exploited the same technique to study the neuron-to-neuron spreading of misfolded α-syn. Interestingly, they showed that silencing different PD-related genes, including *ATP13A2*, *dj-1*, *lrk-1* and *pdr-1*, using RNAi caused an increase in α-syn accumulation over time. Given that neuron-to-neuron transfer occurs *in-vivo* in *C. elegans*, this model can now be implemented not only for PD investigations but also for other neurodegenerative diseases [151–153]. Integration of this technique with the reviewed microfluidics devices for worm manipulation is a potential way to enhance the speed and quality of the assays.

As shown previously, *C. elegans* has been extensively used to test the effect of different neurotoxins on neuron degeneration by using fluorescently labeled strains. These studies have focused on specific sets of neurons (e.g. DNs) without considering the neurotoxins effect on other neurons. Different neuronal subtypes may be accessed by the toxin due to their anatomical placement within the intact nematode body or the cuticle permeability. Thus, to overcome this challenge, primary cultures of *C. elegans* neurons are crucial to determine whether neuron degeneration happens *in-vitro* in a same way as *in-vivo*. However, access to *C. elegans* larval and adult cells is difficult due to the worm's tough and thick cuticle, which is composed of collagens, highly cross-linked cuticlins, and surface glycoproteins [154]. For embryos, early attempts have showed that isolation and culture of embryonic cells are possible for short periods [155, 156]. Following up with this work, Bloom et.al [157] tried multiple large scale embryonic cell isolation techniques. This pioneering work showed successful occurrence of morphological differentiation in these cells. However, some difficulties of cells adhesion to the substrate and poor cell survival were reported. Therefore, Bloom's method was optimized to finally establish a high-throughput method for large scale embryonic cell isolation and culture [158]. Eventually, this protocol illustrated that embryonic cells can be easily isolated by treating adult nematodes with an alkaline hypochlorite solution. This solution aided in lysing the worm cuticle which releases the eggs out of the body. Then, by pelleting the eggs in a chitinase solution, the eggshells were digested, and early embryo cells were collected and cultured. The aforementioned protocol has enhanced and supported *C. elegans* as a model organism [158], because researchers have been able to conduct electrophysiological analysis of cultured neurons on specific type of cells that are marked with GFP and sorted by FACS [159]. Moreover, Caldwell *et al.* [160] extracted and cultured embryonic *C. elegans* cells to study the effect of a common soil bacterium on DNs neurodegeneration *in-vitro* and showed a significant decrease in DNs with age upon exposure to the bacteria.

Despite the great advances offered by embryonic cell cultures, post embryonic studies are also crucial to understand the developmental events in later larval stages which is not assessable with embryonic cells. Dissection of individual animals has been used previously for larval cell isolation [161, 162]. However, this approach was labor-intensive and time consuming and was not applicable for large scale studies. Therefore, an efficient chemical lysis protocol developed by Jeff Kuhn's laboratory has successfully proven its applicability in generating large quantities of viable cells from *C. elegans* larvae (L1 to L4) as an alternative approach to dissection [163]. For breaking down the cuticle, Cox et. al [164] concluded that lysis solution of 0.25% Sodium dodecyl sulfate (SDS) and 5% ß-mercaptoethanol reducing agent successfully solubilized 69% of the cuticle. Jeff Kuhn's group used 0.25% SDS and 3% dithiothreitol (DTT) reducing agent for 2 to 4 minutes to weaken the cuticle without extensive worm death. They provided analysis for the effect of SDS-DTT on worm survival at different larval stages. Their results showed that the majority of L1 worms survived within 2–3 minutes of SDS-DTT treatment, while, for L2-L4, 90% of the worms were still alive after 4 minutes of SDS-DTT treatment. This investigation was justified by the increase in L4 cuticle thickness of 2.5x more than L1 cuticle which shows that L4 cuticle is more resistant to the SDS-DTT treatment. However, the lysis solution was not capable of dissolving the cuticle without the use of proteinase pronase that can digest 70% to 96% of the cuticle and release the cells. Large quantity of viable cells (7×10^6 cells per pellet) were extracted and cultured, while it was reported that 81% of the extracted cells were muscle cells. However, using this protocol, they were not able to successfully isolate low abundance cells. Building upon this pioneering work, Spencer and colleagues [159] enhanced Jeff Kuhn's protocol for rapid adherence of cells to the culture dish and successful isolation of rare neurons were reported.

We envision that *C. elegans* embryonic and larval cells will be used in the future in microfluidic devices, using the developed techniques of tissue engineering and organ on a chip, to study the cellular and molecular basis of protein aggregation and neurodegeneration in PD and other neural disorders. These microfluidic devices can provide 3D microenvironments and culturing of the cells in synthetic and natural extracellular matrices to better mimic *in-vivo* conditions of the extracted cells. These parallel *in-vitro* and *in-vivo* studies using *C. elegans* can shed light on many unanswered biological questions in the field of neurodegeneration. Despite many of the experimental advantages offered by the reviewed microfluidic technologies in this paper, we acknowledge that these devices have not been fully adopted by the biologists and scientists to replace their time-consuming and labor-intensive techniques. The microfluidic community needs to address the gap in technology implementation by communicating and collaborating with scientists and working on scientific questions that are unanswered and more compelling to the biologists. For a microfluidic device to be fully adopted, it must provide appealing criteria from the economic and technical points of view. From an economic perspective, issues related to cost-effectiveness, integrability, and adaptability are needed to be addressed in microfluidic devices. While the cost of microfluidic devices can be relatively low, the technology integrability within the biologists' laboratories and adaptability with existing facilities in the lab are significantly important. For instance, and as shown by a few recent papers, microfluidic devices need to be compatible with the existing pipetting-based fluid handling and multiwell plate-based screening techniques in biology laboratories. However, it will add a remarkable cost to integrate the supporting equipment and to provide the required personnel training to use microfluidic devices under these settings. From a technical perspective, most of the current microfluidic technologies are sophisticated and yet not stand-alone or fully automated to be used by minimally-trained personnel. Standardization and robustness of device operation are other barriers to microfluidics implementation in end-user labs. It appears that technology adoption by small laboratories can be achieved easier with less complicated devices. For instance, droplet microfluidics and neuronal cell culture platforms have been commercialized for DNA amplification [165] and studying cell-to-cell interaction [18], respectively, because of their low-cost, ease of use, integrability, portability, and robustness. While smaller labs may require devices that can assay a few worms at a time, many of the larger scale end users demand technologies with high-throughput and high-content screening capabilities, which are yet to be fully achieved with microfluidics in many of the *C. elegans* assays.

CONCLUSION

Parkinson's disease is a chronic long-term nervous system syndrome characterized by a constellation of clinical symptoms. To date, the exact roots of PD are yet to be known; however, by using cell, animal and human based models, a variety of environmental and genetic causes have been identified to lead to α-syn protein accumulation, neuron degeneration and movement

disorder in PD. *Caenorhabditis elegans* is an invaluable model organism with a great acquiescence to genetic mutation and a mapped nervous system that is easy to grow in a lab and cost-efficient for neurological and behavioral research, especially in neurodegenerative disease investigations and chemical screening. These advantages make *C. elegans* a prime model for studying the effect of different neurotoxins and protein misfolding, aggregation and cell-to-cell transfer in PD and other neurodegenerative diseases. Over the past decade, a wide assortment of microfluidic devices has been developed to phase out tedious laboratory-based techniques for achieving automated assays with accurate quantitative analyses of the neurobehavioral responses of *C. elegans* to various external stimulations. In this paper, we comprehensively reviewed the available *C. elegans*-based research, focusing on determining the effect of various neurotoxins and α-syn aggregation on neuron dysfunction and movement impairment of worms using conventional and microfluidic-based approaches. Moreover, we provided review on the recent trends and advancements on *C. elegans in-vivo* and *in-vitro* studies. We showed that recent *C. elegans* cell isolation protocols have enhanced the quality of embryonic and larval cell culture and extended the research towards cell sorting, co-culture and post-embryonic development. However, these isolation techniques are expensive and time- and labor-intensive. Thus, microfluidics can be used for developing automated and high-throughput cell extraction and assay techniques that will allow localized chemical stimulation of single cell types and investigation of protein migration *in-vitro*. Results can be confirmed easily in parallel *in-vivo* assays on whole-worms to enhance our understanding of neurotoxicity and its correlation with movement disorder. We envision that microfluidic devices will become increasingly integrated in *C. elegans* assays, and opportunities to understand complex biological processes from molecular to whole-animal level will be on the rise in near future. However, implementation of microfluidic devices in end user laboratories is impeded by various economical and technical challenges that are needed to be addressed via collaborations between engineers and biologists who are using *C. elegans* as a disease model.

ACKNOWLEDGMENT

This project has received funding support from the Ontario Thrilium Scholarship to KY.

Notes

* Orthologs: gene sequences found in different species related to a common ancestral gene that conserve the same function

† According to Worm Atlas: 'Two neurons with cell bodies that are situated sub-dorsally in the pseudocoelomic cavity just posterior to the ring neuropile.'

‡ According to Worm Atlas: 'Two neurons with ciliated endings, in the head, with elliptical, closed, sheet-like processes near the cilium, which envelop a piece of hypodermis.'

References

1. Parkinson J. An essay on the shaking palsy (Printed by Whittingham and Rowland for Sherwood, Neely, and Jones). *J Neuropsychiatry Clin Neurosci* 1817;**14**:223–236.
2. Brissaud E. Leçons Sur Les Maladies Nerveuses (Salpêtrière, 1893–94); 1895.
3. Lewy FH. Paralysis agitans. I. Pathologische anatomie. *Handb der Neurol* 1912;**3**:920–958.
4. Trétiakoff C. Contribution à l'étude de l'anatomie pathologique du locus niger de Soemmering avec quelques déductions relatives à la pathogénie des troubles du tonus musculaire et de la maladie de Parkinson. *Theses de Paris*. 1919.
5. Spillantini MG, Schmidt ML, Lee VM-Y et al. α-synuclein in Lewy bodies. *Nature* 1997;**388**:839–840.
6. Watts JC, Tandon A, Fraser PE. The biology and pathobiology of α-synuclein. *Protein Fold Disord Cent Nerv Syst* 2017:109.
7. Visanji NP, Brotchie JM, Kalia LV et al. α-Synuclein-based animal models of Parkinson's disease: challenges and opportunities in a new era. *Trends Neurosci* 2016;**39**:750–762.
8. Goetz CG. The history of Parkinson's disease: early clinical descriptions and neurological therapies. *Cold Spring Harb Perspect Med* 2011;**1**:a008862.
9. Lee Y, Dawson VL, Dawson TM. Animal models of Parkinson's disease: vertebrate genetics. *Cold Spring Harb Perspect Med* 2012:a009324. doi:10.1101/cshperspect.a009324.
10. Degenhardt J, Hiltpold I, Köllner TG et al. Restoring a maize root signal that attracts insect-killing nematodes to control a major pest. *Proc Natl Acad Sci* 2009;**106**:pnas-0906365106.
11. Rey NL, Petit GH, Bousset L et al. Transfer of human α-synuclein from the olfactory bulb to interconnected brain regions in mice. *Acta Neuropathol* 2013;**126**:555–573.
12. Zhang Z, Miah M, Culbreth M et al. Autophagy in neurodegenerative diseases and metal neurotoxicity. *Neurochem Res* 2016;**41**:409–422.
13. Daniel G, Musso A, Tsika E et al. α-Synuclein-induced dopaminergic neurodegeneration in a rat model of Parkinson's disease occurs independent of ATP13A2 (PARK9). *Neurobiol Dis* 2015;**73**:229–243.
14. Cheng L, Chen L, Wei X et al. NOD2 promotes dopaminergic degeneration regulated by NADPH oxidase 2 in 6-hydroxydopamine model of Parkinson's disease. *J Neuroinflammation* 2018;**15**:243. doi:10.1186/s12974–018-1289-z.
15. Johnson S, Park H, DaSilva N et al. Levodopa-reduced Mucuna pruriens seed extract shows neuroprotective effects against Parkinson's disease in murine microglia and human neuroblastoma cells, Caenorhabditis elegans, and Drosophila melanogaster. *Nutrients* 2018;**10**:1139.
16. Peng S, Wang C, Ma J et al. Achyranthes bidentata polypeptide protects dopaminergic neurons from apoptosis in Parkinson's disease models both in vitro and in vivo. *Br J Pharmacol* 2018;**175**:631–643.
17. Luk KC, Song C, Brien PO et al. PNAS-2009-Luk-20051–6.pdf. *Proc Natl Acad Sci* 2009;**106**:20051–20056.
18. Freundt EC, Maynard N, Clancy EK et al. Neuron-to-neuron transmission of α-synuclein fibrils through axonal transport. *Ann Neurol* 2012;**72**:517–524. doi:10.1002/ana.23747.
19. Hansen C, Angot E, Bergström A-L et al. α-Synuclein propagates from mouse brain to grafted dopaminergic neurons and seeds aggregation in cultured human cells. *J Clin Invest* 2011;**121**:715–725.
20. Li J-Y, Englund E, Holton JL et al. Lewy bodies in grafted neurons in subjects with Parkinson's disease suggest host-to-graft disease propagation. *Nat Med* 2008;**14**:501.
21. Kordower JH, Chu Y, Hauser RA et al. Lewy body–like pathology in long-term embryonic nigral transplants in Parkinson's disease. *Nat Med* 2008;**14**:504.
22. Outeiro TF, Putcha P, Tetzlaff JE et al. Formation of toxic oligomeric α-synuclein species in living cells. *PLoS One* 2008;**3**:e1867.

23. Reyes JF, Olsson TT, Lamberts JT et al. A cell culture model for monitoring α-synuclein cell-to-cell transfer. *Neurobiol Dis* 2015;**77**:266–275.
24. Fu R-H, Wang Y-C, Chen C-S et al. Acetylcorynoline attenuates dopaminergic neuron degeneration and α-synuclein aggregation in animal models of Parkinson's disease. *Neuropharmacology*. 2014;**82**:108–120.
25. Smita SS, Raj Sammi S, Laxman TS et al. Shatavarin IV elicits lifespan extension and alleviates Parkinsonism in Caenorhabditis elegans. *Free Radic Res* 2017;**51**:954–969.
26. Siddique YH, Jyoti S, Naz F et al. Protective effect of apigenin in transgenic Drosophila melanogaster model of Parkinson's disease. *Pharmacology* 2011;**3**:790–795.
27. Xi Y, Noble S, Ekker M. Modeling neurodegeneration in zebrafish. *Curr Neurol Neurosci Rep* 2011;**11**:274–282.
28. Feng C-W, Wen Z-H, Huang S-Y et al. Effects of 6-Hydroxydopamine Exposure on Motor Activity and Biochemical Expression in Zebrafish (*Danio Rerio*) Larvae. *Zebrafish* 2014;**11**:227–239. doi:10.1089/zeb.2013.0950.
29. Markaki M, Tavernarakis N. Modeling human diseases in Caenorhabditis elegans. *Biotechnol J*. 2010;**5**:1261–1276.
30. Wolozin B, Gabel C, Ferree A et al. Watching worms whither: modeling neurodegeneration in C. elegans. In: Progress in Molecular Biology and Translational Science, Vol 100. Amsterdam, Netherlands: Elsevier, 2011, 499–514.
31. Li J, Le W. Modeling neurodegenerative diseases in Caenorhabditis elegans. *Exp Neurol*. 2013;**250**:94–103.
32. Alexander AG, Marfil V, Li C. Use of C. elegans as a model to study Alzheimer's disease and other neurodegenerative diseases. *Front Genet* 2014;**5**:279.
33. Giráldez-Pérez RM, Antolín-Vallespín M, Muñoz MD et al. Models of α-synuclein aggregation in Parkinson's disease. *Acta Neuropathol Commun* 2014;**2**:1–17. doi:10.1186/s40478–014-0176–9.
34. Chen X, Barclay JW, Burgoyne RD et al. Using C. elegans to discover therapeutic compounds for ageing-associated neurodegenerative diseases. *Chem Cent J* 2015;**9**:65.
35. Gupta B, Rezai P. Microfluidic approaches for manipulating, imaging, and screening C. elegans. *Micromachines* 2016;**7**:123.
36. Hamon M, Hong JW. New tools and new biology: recent miniaturized systems for molecular and cellular biology. *Mol Cells* 2013;**36**:485–506.
37. San-Miguel A, Lu H. Microfluidics as a tool for C. elegans researchMicrofluidics as a tool for C. elegans research. *WormBook* 2014:1–18. doi:10.1895/wormbook.1.
38. Bakhtina NA, Korvink JG. Microfluidic laboratories for C. elegans enhance fundamental studies in biology. *Rsc Adv* 2014;**4**:4691–4709.
39. Aubry G, Lu H. A perspective on optical developments in microfluidic platforms for Caenorhabditis elegans research. *Biomicrofluidics* 2014;**8**:11301.
40. Lagoy RC, Albrecht DR. Microfluidic devices for behavioral analysis, microscopy, and neuronal imaging in Caenorhabditis elegans. In: *C. Elegans*. Springer, 2015, 159–179.
41. Youssef K, Bayat P, Peimani AR et al. Miniaturized sensors and actuators for biological studies on small model organisms of disease, in environmental. In: *Environmental, Chemical and Medical Sensors*. Springer, 2018, 199–225. doi:10.1007/978–981-10–7751-7_9.
42. Muthaiyan Shanmugam M, Subhra Santra T. Microfluidic devices in advanced Caenorhabditis elegans research. *Molecules* 2016;**21**:1006.
43. Ghorashian N, Gökçe SK, Ben-Yakar A. Microfluidic systems for whole-animal screening with C. elegans. *Micro-and nanosyst. Biotechnol* 2016:2.
44. Stanley CE, Grossmann G. i Solvas XC. Soil-on-a-Chip: microfluidic platforms for environmental organismal studies. *Lab Chip* 2016;**16**:228–241.
45. Cornaglia M, Lehnert T, Gijs MAM. Microfluidic systems for high-throughput and high-content screening using the nematode Caenorhabditis elegans. *Lab Chip* 2017;**17**:3736–3759.
46. Kamili F, Lu H. Recent advances and trends in microfluidic platforms for C. elegans biological assays. *Annu Rev Anal Chem* 2018;**11**:245–264.
47. Chronis N. Worm chips: microtools for C. elegans biology. *Lab Chip* 2010;**10**:432–437.
48. Crane MM, Chung K, Stirman J et al. Microfluidics-enabled phenotyping, imaging, and screening of multicellular organisms. *Lab Chip* 2010;**10**:1509–1517.
49. Shi W, Wen H, Lin B et al. Microfluidic platform for the study of Caenorhabditis elegans. In: *Microfluidics*. Berlin, Heidelberg: Springer, 2011, 323–338.
50. Wlodkowic D, Khoshmanesh K, Akagi J et al. Wormometry-on-a-chip: Innovative technologies for in situ analysis of small multicellular organisms. *Cytom Part A*. 2011;**79**:799–813.
51. O'reilly LP, Luke CJ, Perlmutter DH et al. C. elegans in high-throughput drug discovery. *Adv Drug Deliv Rev* 2014;**69**:247–253.
52. Kinser HE, Pincus Z. High-throughput screening in the C. elegans nervous system. *Mol Cell Neurosci* 2017;**80**:192–197.
53. Stiernagle T. Maintenance of C. elegans. *C elegans* 1999;**2**:51–67.
54. Teschendorf D, Link CD. What have worm models told us about the mechanisms of neuronal dysfunction in human neurodegenerative diseases? *Mol Neurodegener* 2009;**4**:38.
55. Dimitriadi M, Hart AC. Neurodegenerative disorders: insights from the nematode Caenorhabditis elegans. *Neurobiol Dis* 2010;**40**:4–11.
56. Harrington AJ, Hamamichi S, Caldwell GA et al. C. elegans as a model organism to investigate molecular pathways involved with Parkinson's disease. *Dev Dyn an Off Publ Am Assoc Anat* 2010;**239**:1282–1295.
57. Lakso M, Vartiainen S, Moilanen A et al. Dopaminergic neuronal loss and motor deficits in Caenorhabditis elegans overexpressing human α-synuclein. *J Neurochem* 2003;**86**:165–172.
58. Braungart E, Gerlach M, Riederer P et al. Caenorhabditis elegans MPP+ model of Parkinson's disease for high-throughput drug screenings. *Neurodegener Dis* 2004;**1**:175–183.
59. Nass R, Hall DH, Miller DM et al. Neurotoxin-induced degeneration of dopamine neurons in Caenorhabditis elegans. *Proc Natl Acad Sci* 2002;**99**:3264–3269.
60. Nass R, Hahn MK, Jessen T et al. A genetic screen in Caenorhabditis elegans for dopamine neuron insensitivity to 6-hydroxydopamine identifies dopamine transporter mutants impacting transporter biosynthesis and trafficking. *J Neurochem* 2005;**94**:774–785.
61. Settivari R, LeVora J, Nass R. The divalent metal transporter homologues SMF-1/2 mediates dopamine neuron sensitivity in Caenorhabditis elegans models of manganism and Parkinson's disease. *J Biol Chem* 2009;**284**:jbc-M109.
62. Pu P, Le W. Dopamine neuron degeneration induced by MPP + is independent of CED-4 pathway in Caenorhabditis elegans. *Cell Res* 2008;**18**:978.
63. Bodhicharla R, Nagarajan A, Winter J et al. Effects of α-synuclein overexpression in transgenic Caenorhabditis elegans strains. *CNS Neurol Disord Targets (Formerly Curr Drug Targets-CNS Neurol Disord* 2012;**11**:965–975.

64. Van Ham TJ, Thijssen KL, Breitling R et al. C. elegans model identifies genetic modifiers of α-synuclein inclusion formation during aging. *PLoS Genet* 2008;**4**:e1000027.
65. Cao S, Gelwix CC, Caldwell KA et al. Torsin-mediated protection from cellular stress in the dopaminergic neurons of Caenorhabditis elegans. *J Neurosci* 2005;**25**:3801–3812.
66. Wang S, Zhang S, Xu C et al. Chemical compensation of mitochondrial phospholipid depletion in yeast and animal models of Parkinson's disease. *PLoS One* 2016;**11**:e0164465.
67. Marvanova M, Nichols CD. Identification of neuroprotective compounds of Caenorhabditis elegans dopaminergic neurons against 6-OHDA. *J Mol Neurosci* 2007;**31**:127–137.
68. Locke CJ, Fox SA, Caldwell GA et al. Acetaminophen attenuates dopamine neuron degeneration in animal models of Parkinson's disease. *Neurosci Lett* 2008;**439**:129–133.
69. Kautu BB, Carrasquilla A, Hicks ML et al. Valproic acid ameliorates C. elegans dopaminergic neurodegeneration with implications for ERK-MAPK signaling. *Neurosci Lett* 2013;**541**: 116–119.
70. Fu R-H, Harn H-J, Liu S-P et al. n-Butylidenephthalide protects against dopaminergic neuron degeneration and α-synuclein accumulation in Caenorhabditis elegans models of Parkinson's disease. *PLoS One* 2014;**9**:e85305.
71. Tsai C-W, Tsai R-T, Liu S-P et al. Neuroprotective effects of betulin in pharmacological and transgenic Caenorhabditis elegans models of Parkinson's disease. *Cell Transplant* 2017; **26**:1903–1918.
72. Liu J, Banskota AH, Critchley AT et al. Neuroprotective effects of the cultivated Chondrus crispus in a C. elegans model of Parkinson's disease. *Mar Drugs* 2015;**13**:2250–2266.
73. Cheon S-M, Jang I, Lee M-H et al. Sorbus alnifolia protects dopaminergic neurodegeneration in Caenorhabditis elegans. *Pharm Biol* 2017;**55**:481–486.
74. Chalorak P, Jattujan P, Nobsathian S et al. Holothuria scabra extracts exhibit anti-Parkinson potential in C. elegans: A model for anti-Parkinson testing. *Nutr Neurosci* 2018;**21**:427–438.
75. Rinne UK. Lisuride, a dopamine agonist in the treatment of early Parkinson's disease. *Neurology* 1989;**39**:336.
76. Frankel JP, Lees AJ, Kempster PA et al. Subcutaneous apomorphine in the treatment of Parkinson's disease. *J Neurol Neurosurg Psychiatry* 1990;**53**:96–101.
77. Zhang D, Anantharam V, Kanthasamy A et al. Neuroprotective effect of protein kinase Cδ inhibitor rottlerin in cell culture and animal models of Parkinson's disease. *J Pharmacol Exp Ther* 2007;**322**:913–922.
78. Bedard P, Parkes JD, Marsden CD. Nomifensine in Parkinson's disease. *Br J Clin Pharmacol* 1977;**4**:187S–190S.
79. Kelton MC, Kahn HJ, Conrath CL et al. The effects of nicotine on Parkinson's disease. *Brain Cogn* 2000;**23**:1641–1652.
80. Pålhagen S, Heinonen E, Hägglund J et al. Selegiline slows the progression of the symptoms of Parkinson disease. *Neurology* 2006;**66**:1200–1206.
81. Morin N, Grégoire L, Gomez-Mancilla B et al. Effect of the metabotropic glutamate receptor type 5 antagonists MPEP and MTEP in parkinsonian monkeys. *Neuropharmacology* 2010;**58**:981–986.
82. Tripathy D, Grammas P. Acetaminophen inhibits neuronal inflammation and protects neurons from oxidative stress. *J Neuroinflammation* 2009;**6**:10.
83. Singh B, Pandey S, Yadav SK et al. Role of ethanolic extract of Bacopa monnieri against 1-methyl-4-phenyl-1, 2, 3, 6-tetrahydropyridine (MPTP) induced mice model via inhibition of apoptotic pathways of dopaminergic neurons. *Brain Res Bull* 2017;**135**:120–128.
84. Jadiya P, Khan A, Sammi SR et al. Anti-Parkinsonian effects of Bacopa monnieri: insights from transgenic and pharmacological Caenorhabditis elegans models of Parkinson's disease. *Biochem Biophys Res Commun* 2011;**413**:605–610.
85. Shukla V, Phulara CS, Yadav D et al. Iridoid compound 10-O-trans-p-coumaroylcatalpol extends longevity and reduces alpha synuclein aggregation in Caenorhabditis elegans. *CNS Neurol Disord Targets (Formerly Curr Drug Targets-CNS Neurol Disord* 2012;**11**:984–992.
86. Ximenes JCM, Neves KRT, Leal LK et al. Valproic acid neuroprotection in the 6-OHDA model of Parkinson's disease is possibly related to its anti-inflammatory and HDAC inhibitory properties. *J Neurodegener Dis* 2015;**2015**:1–14.
87. Büttner S, Broeskamp F, Sommer C et al. Spermidine protects against α-synuclein neurotoxicity. *Cell cycle* 2014;**13**: 3903–3908.
88. Chi K, Fu R-H, Huang Y-C et al. Adipose-derived stem cells stimulated with n-butylidenephthalide exhibit therapeutic effects in a mouse model of Parkinson's disease. *Cell Transplant* 2018;**27**:0963689718757408.
89. Azevêdo JCS, Borges KC, Genovese MI et al. Neuroprotective effects of dried camu-camu (Myrciaria dubia HBK McVaugh) residue in C. elegans. *Food Res Int* 2015;**73**:135–141.
90. Lee Y-I, Lee Y, Kim H et al. Phytochemical and pharmacological role of liquiritigenin and isoliquiritigenin from Radix Glycyrrhizae in human health and disease models. *Front Aging Neurosci* 2018;**10**:348.
91. Liao M, Zhao Y, Huang L et al. Isoliquiritigenin and liquiritin from Glycyrrhiza uralensis inhibit α-synuclein amyloid formation. *Rsc Adv* 2016;**6**:86640–86649.
92. Wei C-C, Chang C-H. Liao VH-C. Anti-Parkinsonian effects of β-amyrin are regulated via LGG-1 involved autophagy pathway in Caenorhabditis elegans. *Phytomedicine* 2017;**36**:118–125.
93. Ullah H, Khan H. Anti-Parkinson potential of silymarin: Mechanistic insight and therapeutic standing. *Front Pharmacol* 2018;**9**:422.
94. Srivastava S, Sammi SR, Laxman TS et al. Silymarin promotes longevity and alleviates Parkinson's associated pathologies in Caenorhabditis elegans. *J Funct Foods* 2017;**31**: 32–43.
95. Malaiwong N, Chalorak P, Jattujan P et al. Anti-Parkinson activity of bioactive substances extracted from Holothuria leucospilota. *Biomed Pharmacother* 2019;**109**:1967–1977.
96. Kerr R, Lev-Ram V, Baird G et al. Optical imaging of calcium transients in neurons and pharyngeal muscle of C. elegans. *Neuron* 2000;**26**:583–594.
97. Carr JA, Parashar A, Gibson R et al. A microfluidic platform for high-sensitivity, real-time drug screening on C. elegans and parasitic nematodes. *Lab Chip* 2011;**11**:2385–2396.
98. Mondal S, Ahlawat S, Rau K et al. Imaging in vivo neuronal transport in genetic model organisms using microfluidic devices. *Traffic* 2011;**12**:372–385.
99. Chuang H-S, Raizen DM, Lamb A et al. Dielectrophoresis of Caenorhabditis elegans. *Lab Chip* 2011;**11**:599–604.
100. Hulme SE, Shevkoplyas SS, Apfeld J et al. A microfabricated array of clamps for immobilizing and imaging C. elegans. *Lab Chip* 2007;**7**:1515–1523.
101. Lee H, Kim SA, Coakley S et al. A multi-channel device for high-density target-selective stimulation and long-term monitoring of cells and subcellular features in C. elegans. *Lab Chip* 2014;**14**:4513–4522.
102. Gokce SK, Hegarty EM, Mondal S et al. A multi-trap microfluidic chip enabling longitudinal studies of nerve regeneration in Caenorhabditis elegans. *Sci Rep* 2017;**7**:9837.

103. Lockery SR, Hulme SE, Roberts WM et al. A microfluidic device for whole-animal drug screening using electrophysiological measures in the nematode C. elegans. *Lab Chip* 2012;**12**:2211–2220.
104. Guo SX, Bourgeois F, Chokshi T et al. Femtosecond laser nanoaxotomy lab-on-a-chip for in vivo nerve regeneration studies. *Nat Methods* 2008;**5**:531–533.
105. Chokshi TV, Ben-Yakar A, Chronis N. CO 2 and compressive immobilization of C. elegans on-chip. *Lab Chip* 2009;**9**:151–157.
106. Rohde CB, Zeng F, Gonzalez-Rubio R et al. Microfluidic system for on-chip high-throughput whole-animal sorting and screening at subcellular resolution. *Proc Natl Acad Sci* 2007;**104**:13891–13895.
107. McCormick KE, Gaertner BE, Sottile M et al. Microfluidic devices for analysis of spatial orientation behaviors in semi-restrained Caenorhabditis elegans. *PLoS One* 2011;**6**:e25710.
108. Hu L, Wang J, Feng X et al. Microfluidic device for analysis of gas-evoked neuronal sensing in C. elegans. *Sensors Actuators B Chem* 2015;**209**:109–115.
109. Altun ZF, Hall DH WormAtlas. URL http://www.wormatlas.org.
110. Zimmer M, Gray JM, Pokala N et al. Neurons detect increases and decreases in oxygen levels using distinct guanylate cyclases. *Neuron*. 2009;**61**:865–879.
111. Wang J, Feng X, Du W et al. Microfluidic worm-chip for in vivo analysis of neuronal activity upon dynamic chemical stimulations. *Anal Chim Acta* 2011;**701**:23–28.
112. Zeng F, Rohde CB, Yanik MF. Sub-cellular precision on-chip small-animal immobilization, multi-photon imaging and femtosecond-laser manipulation. *Lab Chip*. 2008;**8**:653–656.
113. Gilleland CL, Rohde CB, Zeng F et al. Microfluidic immobilization of physiologically active Caenorhabditis elegans. *Nat Protoc*. 2010;**5**:1888.
114. Ardeshiri R, Mulcahy B, Zhen M et al. A hybrid microfluidic device for on-demand orientation and multidirectional imaging of C. elegans organs and neurons. *Biomicrofluidics*. 2016;**10**:64111.
115. Krajniak J, Lu H. Long-term high-resolution imaging and culture of C. elegans in chip-gel hybrid microfluidic device for developmental studies. *Lab Chip*. 2010;**10**:1862–1868.
116. Aubry G, Zhan M, Lu H. Hydrogel-droplet microfluidic platform for high-resolution imaging and sorting of early larval Caenorhabditis elegans. *Lab Chip*. 2015;**15**:1424–1431.
117. Dong L, Zhang J, Cornaglia M et al Elegans immobilization using deformable microfluidics for in vivo studies of early embryogenesis and intestinal microbiota. In: *Micro Electro Mechanical Systems (MEMS), 2017 IEEE 30th International Conference On*. Ieee; 2017:616–619.
118. Rezai P, Siddiqui A, Selvaganapathy PR et al. Electrotaxis of Caenorhabditis elegans in a microfluidic environment. *Lab Chip*. 2010;**10**:220–226.
119. Rezai P, Siddiqui A, Selvaganapathy PR et al. Behavior of Caenorhabditis elegans in alternating electric field and its application to their localization and control. *Appl Phys Lett* 2010;**96**:153702.
120. Chuang H-S, Chen H-Y, Chen C-S et al. Immobilization of the nematode caenorhabditis elegans with addressable light-induced heat knockdown (ALINK). *Lab Chip*. 2013;**13**:2980–2989.
121. Mayer G, Ahmed M-SL, Dolf A et al. Fluorescence-activated cell sorting for aptamer SELEX with cell mixtures. *Nat Protoc* 2010;**5**:1993.
122. Pulak R. *Techniques for Analysis, Sorting, and Dispensing of C. elegans on the COPAS Flow-Sorting System*. Totowa, NJ, USA: Humana Press, 2006, 275–286. doi:10.1385/1–59745-151–7:275.
123. Rezai P, Salam S, Selvaganapathy PR et al. Electrical sorting of Caenorhabditis elegans. *Lab Chip* 2012;**12**:1831–1840.
124. Han B, Kim D, Ko UH et al. A sorting strategy for C. elegans based on size-dependent motility and electrotaxis in a micro-structured channel. *Lab Chip* 2012;**12**:4128–4134.
125. Wang X, Hu R, Ge A et al. Highly efficient microfluidic sorting device for synchronizing developmental stages of C. elegans based on deflecting electrotaxis. *Lab Chip* 2015;**15**:2513–2521.
126. Gabel CV, Gabel H, Pavlichin D et al. Neural circuits mediate electrosensory behavior in Caenorhabditis elegans. *J Neurosci* 2007;**27**:7586–7596.
127. Geier FM, Leroi AM, Bundy JG et al. High-throughput age synchronisation of Caenorhabditis elegans. *Chem Commun (Camb)* 2011;**47**:9801–9803.
128. Huang LR, Cox EC, Austin RH et al. Continuous particle separation through deterministic lateral displacement. *Science (80-)* 2004;**304**:987–990.
129. Ai X, Zhuo W, Liang Q et al. A high-throughput device for size based separation of C. elegans developmental stages. *Lab Chip* 2014;**14**:1746–1752.
130. Sofela S, Sahloul S, Rafeie M et al. High-throughput sorting of eggs for synchronization of C. elegans in a microfluidic spiral chip. *Lab Chip* 2018;**18**:679–687.
131. Chung K, Crane MM, Lu H. Automated on-chip rapid microscopy, phenotyping and sorting of C. elegans. *Nat Methods* 2008;**5**:637.
132. Yan Y, Ng LF, Ng LT et al. A continuous-flow C. elegans sorting system with integrated optical fiber detection and laminar flow switching. *Lab Chip* 2014;**14**:4000–4006.
133. Ahmed D, Ozcelik A, Bojanala N et al. Rotational manipulation of single cells and organisms using acoustic waves. *Nat Commun* 2016;**7**:11085.
134. de Carlos Cáceres I, Valmas N, Hilliard MA et al. Laterally orienting C. elegans using geometry at microscale for high-throughput visual screens in neurodegeneration and neuronal development studies. *PLoS One* 2012;**7**:e35037.
135. de Carlos Cáceres I, Porto DA, Gallotta I et al. Automated screening of C. elegans neurodegeneration mutants enabled by microfluidics and image analysis algorithms. *Integr Biol* 2018;**10**:539–548.
136. McGorty R, Liu H, Kamiyama D et al. Open-top selective plane illumination microscope for conventionally mounted specimens. *Opt Express* 2015;**23**:16142–16153.
137. Pikto-Pietkiewicz W. The effect of dronedarone on the frequency of cardiovascular events in patients with atrial fibrillation-ATHENA studies. *Kardiol Pol* 2009;**67**:455.
138. Mondal S, Hegarty E, Martin C et al. Large-scale microfluidics providing high-resolution and high-throughput screening of Caenorhabditis elegans poly-glutamine aggregation model. *Nat Commun* 2016;**7**:13023.
139. Eguchi M, Yamaguchi S. In vivo and in vitro visualization of gene expression dynamics over extensive areas of the brain. *Neuroimage* 2009;**44**:1274–1283.
140. Ma H, Jiang L, Shi W et al. A programmable microvalve-based microfluidic array for characterization of neurotoxin-induced responses of individual C. elegans. *Biomicrofluidics* 2009;**3**:44114.

141. Shi W, Wen H, Lu Y et al. Droplet microfluidics for characterizing the neurotoxin-induced responses in individual Caenorhabditis elegans. *Lab Chip* 2010;**10**:2855–2863.
142. Cornaglia M, Krishnamani G, Mouchiroud L et al. Automated longitudinal monitoring of in vivo protein aggregation in neurodegenerative disease C. elegans models. *Mol Neurodegener* 2016;**11**:17.
143. Mondal S, Hegarty E, Sahn JJ et al. High-content microfluidic screening platform used to identify σ2R/Tmem97 binding ligands that reduce age-dependent neurodegeneration in C. elegans SC_APP model. *ACS Chem Neurosci* 2018;**9**: 1014–1026.
144. Martin C, Li T, Hegarty E et al. Line excitation array detection fluorescence microscopy at 0.8 million frames per second. *Nat Commun* 2018;**9**:4499.
145. Salam S, Ansari A, Amon S et al. A microfluidic phenotype analysis system reveals function of sensory and dopaminergic neuron signaling in C. elegans electrotactic swimming behavior. In: *Worm*, Vol 2. Milton Park, Abingdon-on-Thames, Oxfordshire, UK: Taylor & Francis, 2013, e24558.
146. Youssef K, Archonta D, Tandon A et al. Neuronal and Behavioural Effects of Alpha-Synuclein Protein and 6-OHDA Neurotoxin in Parkinson's Disease Investigated with a C. elegans Electrotaxis Microfluidic Assay. In: *The Twenty Second International Conference on Miniaturized Systems for Chemistry and Life Sciences*; 2018:In Press.
147. Cooper JF, Van Raamsdonk JM. Modeling Parkinson's disease in C. elegans. *J Parkinsons Dis*. 2018;**8**:17–32. doi:10.3233/JPD-171258.
148. Kim D-K, Lim H-S, Kawasaki I et al. Anti-aging treatments slow propagation of synucleinopathy by restoring lysosomal function. *Autophagy* 2016;**12**:1849–1863.
149. Kim D-K, Cho K-W, Ahn WJ et al. Cell-to-cell transmission of polyglutamine aggregates in C. elegans. *Exp Neurobiol* 2017;**26**:321–328.
150. Tyson T, Senchuk M, Cooper JF et al. Novel animal model defines genetic contributions for neuron-to-neuron transfer of α-synuclein. *Sci Rep* 2017;**7**:1–10. doi:10.1038/s41598–017-07383–6.
151. Nussbaum-Krammer CI, Neto MF, Brielmann RM et al. Investigating the spreading and toxicity of prion-like proteins using the metazoan model organism C. elegans. *J Vis Exp JoVE* 2015;**95**:1–15.
152. Nussbaum-Krammer CI, Morimoto RI. Caenorhabditis elegans as a model system for studying non-cell-autonomous mechanisms in protein-misfolding diseases. *Dis Model Mech*. 2014;**7**:31–39.
153. Nussbaum-Krammer CI, Park K-W, Li L et al. Spreading of a prion domain from cell-to-cell by vesicular transport in Caenorhabditis elegans. *PLoS Genet*. 2013;**9**:e1003351.
154. Strange K. From genes to integrative physiology: ion channel and transporter biology in Caenorhabditis elegans. *Physiol Rev* 2003;**83**:377–415.
155. Edgar LG, McGhee JD. DNA synthesis and the control of embryonic gene expression in C. elegans. *Cell* 1988;**53**: 589–599.
156. Goldstein B. Induction of gut in Caenorhabditis elegans embryos. *Nature* 1992;**357**:255.
157. Bloom L. Massachusetts Institute of Technology. 1993.
158. Christensen M, Estevez A, Yin X et al. A primary culture system for functional analysis of C. elegans neurons and muscle cells. *Neuron* 2002;**33**:503–514.
159. Spencer WC, McWhirter R, Miller T et al. Isolation of specific neurons from C. elegans larvae for gene expression profiling. *PLoS One* 2014;**9**:e112102.
160. Caldwell KA, Tucci ML, Armagost J et al. Investigating bacterial sources of toxicity as an environmental contributor to dopaminergic neurodegeneration. *PLoS One* 2009;**4**: e7227.
161. Nickell WT, Pun RYK, Bargmann CI et al. Single ionic channels of two Caenorhabditis elegans chemosensory neurons in native membrane. *J Membr Biol* 2002;**189**:55–66.
162. Brockie PJ, Mellem JE, Hills T et al. The C. elegans glutamate receptor subunit NMR-1 is required for slow NMDA-activated currents that regulate reversal frequency during locomotion. *Neuron* 2001;**31**:617–630.
163. Zhang S, Banerjee D, Kuhn JR. Isolation and culture of larval cells from C. elegans. *PLoS One* 2011;**6**:e19505.
164. Cox GN, Kusch M, Edgar RS. Cuticle of Caenorhabditis elegans: its isolation and partial characterization. *J Cell Biol* 1981;**90**:7–17.
165. Heyries KA, Tropini C, VanInsberghe M et al. Megapixel digital PCR. *Nat Methods* 2011;**8**:649–651.

A.2 Microfluidic Devices to Study the Effect of Electric Field on *Caenorhabditis elegans* and *Danio rerio*

Youssef, Khaled, Daphne Archonta, and Pouya Rezai. "Microfluidic Devices to Study the Effect of Electric Field on *Caenorhabditis elegans* and *Danio rerio*." ElSeiver, 2021 "Under review".

Chapter 15

Microfluidic Devices to Study the Effect of Electric Field on *Caenorhabditis elegans* and *Danio rerio*

Khaled Youssef, Daphne Archonta, and Pouya Rezai*

Department of Mechanical Engineering, York University, Toronto, ON, Canada

* Corresponding Author: BRG 433B, 4700 Keele St, Toronto, ON, M3J 1P3, Canada; Tel: 416-736-2100 ext. 44703; Email: prezai@yorku.ca

Abstract

Electrotaxis or galvanotaxis is the movement of unicellular and multicellular organisms towards a desired direction under exposure to direct or alternating current electric fields. The mechanisms underpinning how electrical stimulus evokes taxis response are not fully understood in animal models due to their complexities. *Caenorhabditis elegans* (*C. elegans*) and *Danio rerio* (*D. rerio*) have been used as model organisms to understand basic biological processes in electrotaxis due to their simple sensory and motor systems. However, their small size and continuous movement have limited the development of effective experimental techniques to study electrotaxis. Thus, microfluidics has been adopted to study electrosensation of *C. elegans* and *D. rerio* and develop various electric-based application devices. In this chapter, we provide an up to date review on the developed techniques to interrogate and use the electrosensation of *C. elegans* and *D. rerio* for the development of various manipulation and drug screening tools. The content of this chapter can be useful to worm and fish biologists for understanding the advanced screening technologies and to microfluidic engineers for improving their devices.

Keywords: *C. elegans*, *D. rerio*, Electrosensation, Electrotaxis, Galvanotaxis, Electric field, Microfluidics, Organism-on-a-Chip.

1. Introduction

Organisms' movement is affected by the complexity of the environment where they reside, imposing a milieu of complex stimuli. The organisms ability to sense and interact with the external environment has been studied extensively for understanding various physiological activities and their underlying biological processes in genetic and drug discovery applications [1]. Different stimuli such as chemical, optical, thermal, mechanical, and electrical cues have been shown to affect organisms' sensorimotor activities. Chemotaxis is how organisms move under the influence of chemicals; light sensation and response towards or away from it is termed phototaxis; and the directional movement induced by temperature gradient is known as thermotaxis. The focus of this chapter is on electrotaxis or galvanotaxis, i.e. movement towards a desired direction under exposure to direct current (DC) or alternating current (AC) electric field (EF). The mechanisms underpinning how various stimuli evoke taxis responses are not fully understood. However, due to the high-controllability and ease of application, EF is one of the effective tools to interrogate the neuronal and muscular basis of stimulated response.

Electrotaxis has been identified in many unicellular and multicellular organisms, including aquatic animals such as sharks and terrestrial organisms such as cockroaches and bees [2–8]. Considerable experimental investigations have been recently conducted to provide insights into the biological mechanisms of cells' response to EF [9]. It is shown that EF-induced collective cell movement is involved in processes such as embryogenesis [10,11] and wound healing [12]. Many cell types, such as cancer cells, epithelial cells, fibroblasts, and leukocytes have ability to detect and migrate in response to EF [9,13]. A well-known example of wound healing is the migration of endothelial cells towards the injured location due to the generation of endogenous directional EFs towards the wound [13]. An exogenous electric stimulus has also been shown to accelerate the rate of wound-healing [14]. For instance, human neural stem cells were guided using small exogenous EFs toward wounded sites in the central nervous system [15]. It has also been observed that different cancer cell lines have different migratory patterns in the presence of EF, which have been

correlated to their metastasis rate [16]. For instance, CL1-5, a highly invasive lung cancer cell line, migrated to the anode, whereas CL1-0, a less invasive cancer cell line, had no electrotaxis [16].

Electrotaxis is not specific to cells but also observed in whole organisms for environmental navigation, food recognition, and predator detection. For instance, *Caenorhabditis elegans* (*C. elegans* or the roundworm) and *Danio rerio* (zebrafish) demonstrate movement phenotypes in the presence of EF [17,18]. These small-scale organisms are genetically homologous to humans, amenable to genetic manipulation, transparent and easy to maintain in laboratory conditions, and possess simple cellular and neuronal systems rendering them ideal for studies of neurobehavioral processes such as electrotaxis [19]. In terms of complexity, they fit in nicely between unicellular organisms and higher vertebrate models. Investigating these small model organisms has helped us improve our understanding of many biological processes, efficiently aiding transition of knowledge from cells to complex animal models and even humans.

Researchers have developed various experimental setups to study electrotaxis in petri dishes due to their widespread use in culturing small organisms in laboratories [8]. Despite many advantages offered by these assays, they possess various drawbacks such as EF non-uniformity, susceptibility to media evaporation, and low throughput. Due to the small size of *C. elegans*, in the range of tens of micrometers to a millimeter, microfluidics was first adopted in 2010 for studying electrotaxis while providing well-controlled microenvironments for precise phenotypic assays [18]. Microfluidics is the science of utilizing microfabricated structures, such as microchannels, valves, and pumps, for the manipulation and handling of fluids and solids at the micrometer to millimeter scale. It provides advantages of precise control of the organisms and the EF, low chemical consumption, amenability to high-throughput assays, and ease of use. Therefore, various electrotaxis-based microfluidic devices have been offered over the past two decades to study the electrosensation of *C. elegans* and *D. rerio* to DC and AC EFs.

In this chapter, we present the recent research on electrosensation of the two commonly used model organisms, i.e. *C. elegans* and *D. rerio*, with a focus on the use of microfluidics, termed on-chip assays. We divide the chapter into three main sections of (i) electric field in microchannels, (ii) *C. elegans* electrotaxis, and (iii) *D. rerio* electrosensation. We review the off- and on-chip systems developed to date for investigating the electric-induced behavior of each organism. We elaborate on the recent findings on the neuronal basis of electrosensation in *C. elegans* and shed light on the promising applications of the electrotaxis assay in disease pathology and drug screening. Zebrafish cell [20] and whole organism [21]responses to EF were recently reported, hence we will provide a relatively brief summary on the findings on this model organism. We hope that the knowledge acquired through the chapter will aid scientists and researchers in implementing these platforms for various biological applications.

2. Electric Field in Microchannels

Before proceeding with the EF effect on the two model organisms, here, we would like to give a brief introduction about the working principles of EF inside a microchannel. Microchannels are mostly fabricated in silicon, glass, or polymers with rectangular cross-sections and specific lengths, widths, and heights depicted by L, W, and H, respectively [22]. Metal electrodes are either microfabricated -n-channel or wire-connected from a power supplier to the inlet and outlet reservoirs for EF application. In the latter simpler case, the distance between the two electrodes is equal to the channel length (L). In the case of uniform electric charge density, Eq. 1 can be used to estimate the electrical potential difference, V , between the two electrodes.

$$V = -\int_{1}^{2} E \,.\, dl \tag{1}$$

where E is the EF intensity at any point along the path l. According to Eq. 1 and for a microchannel with a constant cross section, E will dependent on the applied external electric potential V and the distance L between the electrodes.

$$E = \frac{V}{I} \tag{2}$$

In addition to *E* and *V*, it is often required to know the electric current and the power dissipation in the channel. The channel electric resistance, *R*, can be used for this purpose; *R* is dependent on the channel dimensions (L, W and H) and the electrical resistivity of the buffer (ρ). For a rectangular microchannel, *R* can be expressed as:

$$R = \frac{\rho L}{A} \tag{3}$$

The current flowing through the microchannel and the power dissipated to the media can be calculated based on Eq. 4 and Eq. 5, respectively.

$$I = \frac{V}{R} \tag{4}$$

$$P = \frac{V^2}{R} = \frac{E^2.\mathbb{V}}{\rho} \tag{5}$$

where $\mathbb{V}$ $(= L \times H \times W)$ is approximated as the microchannel volume.

3. *C. elegans*

C. elegans as a model organism offers various advantages such as small dimensions ranging from 17-60 µm in diameter and 100-1000 µm in length with full-body transparency [23,24]. They offer a plethora of phenotypes that have been extensively investigated, and, owing to its transparency, correlated with specific neuron and muscle activities through cellular imaging. Moreover, *C. elegans* was the first organism with its genome fully sequenced, with ~65% homology to human genes, permitting the creation of specific mutants mimicking disease-specific symptoms for disease pathway investigations and drug screening [25]. *C. elegans'* simple and fully mapped sensory system has been found capable of sensing different stimuli such as chemical [26], optical [27], thermal [28], mechanical [29], and electrical [30] cues through their amphid, phasmid, labial, and mechanosensory neurons.

3.1. *C. elegans* electrotaxis

Several behaviors of the worm have been used in disease pathology and drug screening including motility, pharyngeal pumping, and egg-laying [31]. *C. elegans* motility can be controlled on-demand using DC EF in a phenomenon termed electrotaxis [8]. In the mid-twentieth century, electrotaxis was observed for various nematodes crawling mostly towards the anode once exposed to EF [32]. Overtime several on-plate and on-chip techniques have been developed to investigate the worms' response to DC and AC EF.

In 1978, Sukul and Croll [8] were the first to report a single nematode-tracking technique for studying the *C. elegans* electrotaxis. Young-adult (YA) *C. elegans* were transferred individually to 5-cm-diameter agar petri dishes with two 3-cm apart platinum electrodes. Different combinations of electric currents (0.02-0.4mA) and voltages (2-6V) were applied by adjusting the buffer electric resistivity. At low and high currents (0.02, 0.04, and 0.4mA), the worms showed preference to swim towards the anode, whereas, at medium currents (0.06-0.3 mA) and voltages between 3 to 4V, cathodal movement was dominant. It was also shown that the worms were consistently stopping 2mm away from the electrode while engaging in continuous reversals. Their observations confirmed that electrotaxis is an inert response that is not attributed to electrophoresis or electric activation of the muscles. Electrotaxis was claimed to be mediated by the amphid neurons through sensing the ionic changes. For instance, the robust cathodal movements were related to the continuous discharge of potassium and chloride ions at the electrodes, and the worms' ability to sense the ions mobility. In an interesting experiment by Klein, Kim and Meyer [32], worms on an agarose gel filled with M9 buffer were exposed to EF and a biphasic movement towards the cathode was reported. At an EF of 0.7V/cm, a random movement towards the cathode was observed, whereas, at 4V/cm, the worms moved rapidly in a V-shape pattern with 45^o angle towards the cathode. Moreover, L1 worms showed no response to EF. L2 and L3 showed a weaker response with a haphazard movement towards the cathode, whereas L4, adult worms, and males had the strongest response. In a pursuit to figure out the causes underpinning electrotaxis, various mutants were tested, leading to the discovery of defective electrotaxis in some mutants (*lin-32 (u282)* and *n1754*) which were defective in chemotaxis and thermotaxis as well. However, the normal electrotaxis response observed in *n1937* and *n1938* strains, demonstrating defective chemotaxis, suggested that chemotaxis and electrotaxis do not share the same exact pathways in *C. elegans*.

In 2007, Gabel et al. [30] investigated and mapped the possible genetic and neuronal basis of *C. elegans* electrosensation through imaging of intracellular calcium dynamics. The developed experimental setup, shown in Figure 1A-i, consisted of a gel electrophoresis chamber with a centered agarose pad for loading the worms. YA worms were picked individually and placed on the surface of the agar, made with various salt concentrations to allow for distinction between current and volt applications. The EF strength and direction were precisely controlled through

four platinum electrodes placed in a cross-like configuration. Upon EF stimulation, a robust electrosensory behavior was observed with directional movement towards the cathode, with an angle proportional to the EF strength. For instance, below 3V/cm, the worms showed limited electrotactic response, but from 4 to 14V/cm, the worms moved towards the cathode with an increasing angle from 15° to 60° (Figure 1A-ii). It was reported that *C. elegans* exploit two reorientation maneuvers when exposed to EF, omega turns and slight backward motion with a change in EF direction. Furthermore, to investigate the frequency range of *C. elegans* electrosensation, worms were exposed to sinusoidal waveform EFs at various frequencies. At frequencies >16Hz, *C. elegans* showed a DC-like electrotaxis, whereas, at frequencies <16Hz, wide reorientation angles were observed as worms could sense the change in EF direction. A step-wise EF rotation technique was also used to screen various mutants for defective electrotaxis. Laser ablation of genes such as *che-2*, *che-13*, *osm-3*, *osm-5*, *osm-6*, and *tax-6* resulted in defective electrosensation, chemosensation and osmosensation. To map the neuronal circuit of electrosensation, intracellular calcium dynamics recording, and laser ablation were used on transgenic worms expressing fluorescent calcium-binding protein in the amphid sensory neurons. Figure 1A-iii shows the hierarchical structure of the neuronal circuit involved in *C. elegans* electrosensation which consists of three phases for EF-detection, motility decision-making, and movement execution. Next, Manière et al. [33] used a similar technique to investigate the age-dependent electrotaxis deficiency. Worms of ages beyond the YA stage responded directionally towards the cathode but with a 70% decrease in the average velocity at day 8 (D8) post YA (Figure 1B).

Further analysis by Chrisman et al. [34] revealed the involvement of pairs of AWC neurons in *C. elegans* electrotaxis. *ceh-36* mutants which are defective in the terminal differentiation of both AWC pairs showed a partial flaw in electrosensation. Worms with complete ablation of the AWC neurons were able to distinguish the EF, whereas worms with an asymmetric loss of function were severely impaired, highlighting the role of AWC neurons in electrotaxis. Moreover, the increase in EF-induced angled motion of *C. elegans* was attributed to the preference of the worms to stay within an EF of ~ 5V/cm. In the same year, Risley et al. [35] developed an electric shock assay for introducing *C. elegans* as a convulsion model for anticonvulsant drug screening. The experiment was conducted by connecting two electrodes to a 9cm Tygon micro-bore tubing filled with M9 buffer. YA worms were exposed for 3s to a EF shock of 47V at 200HZ inside the tubing. During the electric shock, worms exhibited paralysis with elongation and convulsions, inducing a seizure like effect. Once the stimulus was removed, the time to regain natural swimming pattern was measured. Testing of two mutants with loss of function in the GABAergic neurotransmission showed a struggle recovering after the shock, revealing the role of the neurotransmitter GABA in the recovery process. This deficiency was improved by exposing worms to pentylenetetrazol, a common convulsant agent for evoking seizures in animals.

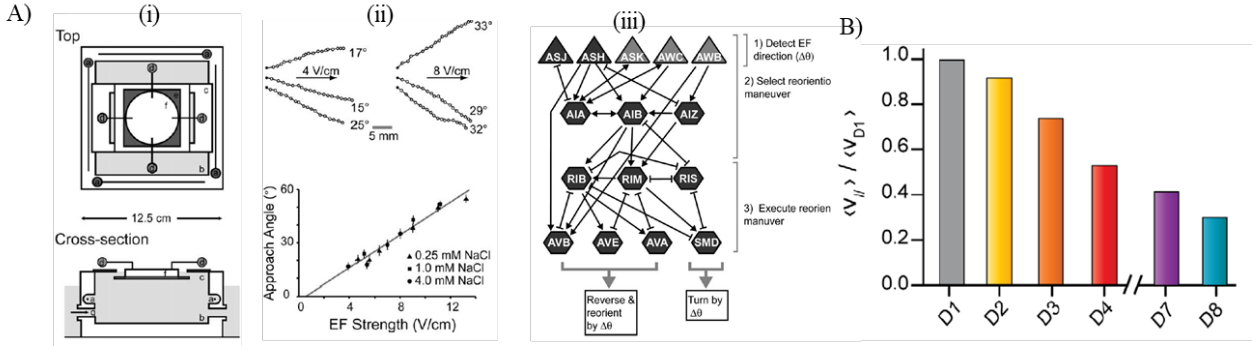

Figure 1: Off-chip electrotaxis in C. elegans. (A) Experimental setup (i) and results obtained by Gabel et al. [30] *(ii) C. elegans tracks and angle of movement at different EFs; (iii) Electrosensation neuronal pathways. (B) Aging effect on the worms' average electrotactic speed from day 1 to day 8 post YA* [33]. *Figures were adapted from ref.* [30,33] *with permission under the terms of the Creative Commons Attribution Non-Commercial License (http://creativecommons.org/licenses/by-nc/4.0).*

Due to the worms' small size and continuous movement, miniaturized platforms were implemented to further investigate *C. elegans* electrotaxis in a controlled manner. For instance, Rezai et al. [18] were the first to investigate electrotaxis in microfluidics, demonstrating that the worms move towards the negative pole in a confined microenvironment. A single layer polydimethylsiloxane (PDMS)-based microfluidic channel (300µm-wide, 80µm-deep, and 5cm-long) was fabricated and copper electrodes were attached for EF stimulation (Figure 2A). Age

synchronized worms from L1 to YA stage were loaded individually into the device and exposed to EF for electrotaxis assay. It was observed that different developmental stages respond uniquely to different EF strengths and with variable speeds. For instance, early-stage worms (L1 and L2) showed no electrotaxis, which was attributed to their premature neuronal system or the insufficient EF strength used in the channel. At later stages (L3 to YA), the response was consistent towards the cathode with a age-dependent increase in sensitivity to EF and electrotaxis speed. Moreover, the cellular basis of electrotaxis was investigated using two mutants (*unc-6(e78)* and *unc-54(s74)*), and it was concluded that the electrosensory response is neuron mediated. Post-exposure to EF, all worms exhibited a normal motility behavior, life cycle, and fecundity. The investigation expanded to pulse DC EF in microchannels, demonstrating that *C. elegans* and *C. briggsae* show electrotactic behavior even at a low EF duty cycle of 30% [36]. Followed by that, the same experimental setup was exploited to characterize the effect of AC EF on the worms' movement with variable frequencies between 20mHz and 3kHz [37]. At low frequencies between 20 and 100mHz, worms could sense the directionality change between the positive and negative half-cycles and, consequently, adjust their swimming direction. At frequencies between 100mHz and 1Hz, worms moved with a "stop and go" pattern as they swim towards the cathode during the positive-half of the AC cycle and localize or severely reduce their speed in the negative half of the cycle. However, at higher frequencies of 1Hz to 3kHz, worms were localized even though they appeared to sense the change in EF polarity. An age-dependent study showed that all stages except L1 responded similarly to the AC EF with a difference in their localization range.

The above-mentioned systems integrated microscopy techniques and image analysis for recording and quantifying the worms electrotaxis phenotypes. In 2016, Jung et al. [38] developed a stand-alone technique to measure *C. elegans* undulatory motion on-chip without microscopy. To measure the speed, a microfluidic device consisting of three PDMS layers (Figure 2B) was developed to convert *C. elegans* motion into electrical signals. The top layer comprised of a sinusoidal wavy channel complimenting the worms' motion. The middle layer contained a square wave-like electrode to correlate the worms' movement to the change in electric resistance. The bottom layer contained a straight channel to permit the electrode layer deflection due to the worms' motion. Using this device, the velocity of the worm could be obtained by measuring the change in the electrical resistance without the need for worm imaging.

Gabel et al. [30] mapped part of the electrosensory circuit of *C. elegans* and hypothesized that the neurons are predominantly located at the head region. Therefore, Chokshi et al. [39] developed a microfluidic device to probe the effect of DC EF strength and polarity on the age-dependent functionalities of ASH neuron, located at the head. The developed microfluidic device consisted of a tapered channel for single worm trapping and imaging, and three electrodes located at the head, mid body, and tail for EF stimulation. Worms of different ages (1-5 days post-L4) were exposed with head-to-tail orientation to a 10s DC signal and the intracellular calcium levels of ASH neurons were shown to increase by age. This was attributed to either the increase in the density of voltage gated Ca^{2+} with age or the age-dependent deficiency in the Ca^{2+} regulatory mechanisms. Moreover, when a negative polarity was applied (tail-to-head orientation), a current threshold was observed. Increasing the current to higher or lower than 0.01µA hyperpolarized and depolarized the neuron, respectively. Interestingly, they observed a spatial exposure dependency in ASH activation which was high when the worms were stimulated between the head and the mid-body.

Previous studies, performed by exposing the whole worm to EF, did not consider that certain body segments might respond differently to the EF. Therefore, we developed a simple microfluidic device that allowed for exposure of specific body parts to EF for investigating the neurons involved in electrosensation [40,41]. The developed T-shaped monolayer microfluidic device comprised of two perpendicular channels, a 300µm-wide 2cm-long straight channel for EF stimulation and a tapered perpendicular channel for worms' head or tail capturing (Figure 2C). WT worms were captured by either tail or head allowing the rest of the body to move freely in the main channel and be exposed to EF. Tail-trapped worms showed a robust cathodal orientation when subjected to EF, confirming that electrotaxis is mediated by sensory neurons at the head. Surprisingly, the head-trapped worms demonstrated a directional but weak tail response towards the cathode, highlighting that the mid body neurons might be contributing to *C. elegans* electrosensation. Therefore, *MT1082* mutants, lacking the hermaphrodite-specific neurons (HSN) located at the vulva and mediating the egg-laying behavior, were tested. These tail-trapped worms demonstrated a directional response with significantly lower sensing ability, supporting the mid-body HSN' involvement in electrosensation.

Building upon the fact that a part of the egg-laying circuit in *C. elegans* might be responsible for electrosensation, we recently investigated the EF effect on the *C. elegans* egg-laying circuit in a phenomenon termed "electric egg-laying" [42,43]. We showed that egg-laying circuit could be activated on-demand using DC EF. A wide microchannel incorporating a narrow electrical trap in its mid-section (Figure 2D) was developed to investigate the effect of EF strength, direction, and pulse duration as well as worm age (D1 to D4 post-YA) on egg-laying. Worms were tested

facing either the anode or the cathode. EF exposure was found to be associated with various induced behaviors such as body length reduction, head movement frequency changes, and egg deposition. Interestingly, worms were stimulated to lay eggs only when facing the anode. A 6V/cm EF appeared to be most effective for egg-laying with a significant body length reduction and decrease in the head movement frequency. Egg-count was not altered by changing the pulse duration, whereas the egg-deposition rate was proportional to the increase in pulse duration. In other words, increasing the pulse duration stimulated the worms to deposit more eggs faster. Moreover, adult worms showed a significant decrease in the egg-count from D1 to D4 post YA stage. Next, fluorescent imaging of intracellular calcium dynamics in the neuronal circuit of egg-laying including vulva muscles, ventral cord neurons and HSN showed their involvement in electrosensation.

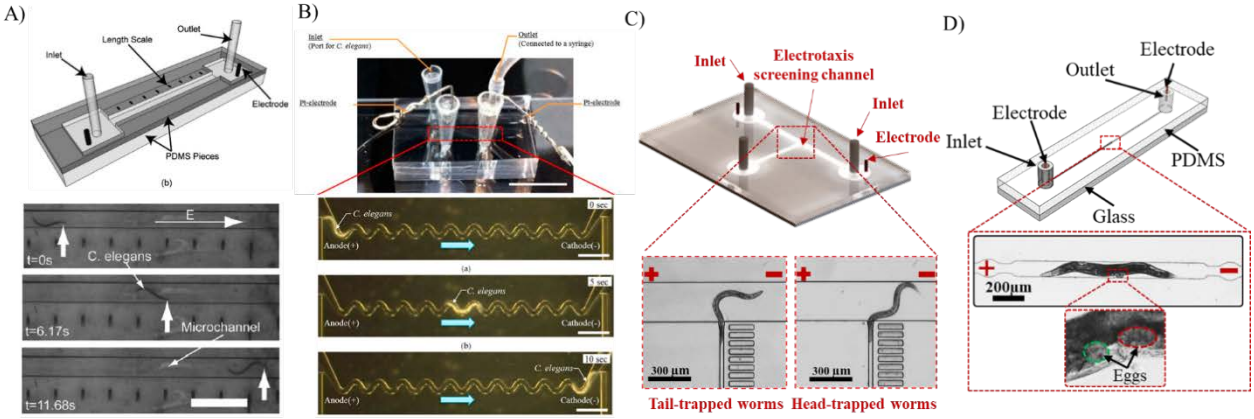

Figure 2: Microfluidic devices to study C. elegans electrotaxis and egg-laying. (A) DC, pulsed DC and AC signals investigated in a straight channel [18,36,37]. *(B) Measuring C. elegans electrotaxis speed with on-chip electrodes* [38]. *(C) Semi-mobile electrotaxis assay chip* [40,41]. *(D) Electric egg-laying on-a-chip* [42,43]. *Figures were adapted from ref.* [18,38] *with permission from Royal Society of Chemistry and the terms of the Creative Commons Attribution Non-Commercial License (http://creativecommons.org/licenses/by-nc/4.0)*

3.2. Applications of *C. elegans* Electrotaxis

C. elegans electrotaxis in microchannels has been utilized for the development of immobilization, orientation, sorting, and drug and genetic screening devices [1,25,32] which will be discussed in this section.

C. elegans is raised on agar plates with a mixed population of all ages, and obtaining a synchronized population is required to study age-related diseases [25]. Conventionally, a synchronized population is obtained by washing gravid adults with sodium hypochlorite solution to isolate unhatched eggs and grow them on new plates to desired stages. Due to the laborious nature of this technique and inaccessibility of automated worm sorters (such as the COPAS technology), various on-plate or microfluidic sorting methods have been developed using mechanical or electric field-based filtration. In 2011, Manière et al. [33] exploited electrotaxis of *C. elegans* to measure their velocity over a swimming distance of 5cm using an electrophoresis chamber. For instance, WT worms showed an average crawling speed of 110µm/s, whereas, *unc-29, acr-16, and unc-29/acr-16* mutants showed reduced crawling speeds of 80µm/s, 35µm/s, and 15µm/s, respectively. Accordingly, a novel technique to perform sorting of large populations of worms based on electrotaxis velocity was reported.

In 2011, Rezai et al. [44,45] were the first to develop a microfluidic device for *C. elegans* continuous sorting using the difference in their electrotactic behaviors. Their previous studies showed that each worm stage responded to a specific EF range [18]. Building upon that, a straight microfluidic channel incorporating a narrow region in its midsection serving as an electrical trap was developed. The difference in the EF between the main channel and the trap allowed for younger worms in a population to pass through. As a proof of concept, a mixed population of L3 and YA worms were loaded into the device, and EFs of 6V/cm and 18V/cm where applied in the main channel and the trap, respectively. In a matter of minutes, L3 worms were swimming through the trap, whereas YA worms were partially paralyzed at its entrance. To increase the throughput, a microfluidic device (Figure 3A) consisting of loading

and collection chambers connected through 20 parallel electric traps was successfully used to obtain synchronized L3, L4 and YA worms with a minimum throughput of 78 worms per minute. Lastly, neuron- (*unc-6(e78)*) or muscle-defective (*unc-54(s74)*) mutants were separated from WT worms. Next, Han et al. [46] exploited the electrotaxis effect and the precise microfabrication techniques to develop a size-dependent worm sorter (Figure 3B). The chip consisted of parallel arrays of hexagonally designed microchannels termed "micro-bumps" to match the swimming frequency of certain worm ages, hence enhancing their swimming behavior. With the aid of electrotaxis, worms were guided through the channels, where only the targeted age could swim through. Followed by that, Wang et al. [47] proposed a novel sorting technique termed "deflecting electrotaxis", exploiting the findings of Gabel et al. [30] who showed that worms crawl towards the cathode at a specific angle based on their age and EF strength. The fan-shaped microfluidic device (Figure 3C) was fabricated with PDMS-agarose layers, incorporating 20 symmetrical channels at specific angles (-50° to 50°) for worm separation. As a proof of concept, mixed populations of worms (L2, L3, L4, YA, and mutants) were tested and, once exposed to EF, age/mutation synchronization was achieved using the concept of deflecting electrotaxis. In 2018, the same group developed a PDMS-agarose microfilter for *C. elegans* synchronization with the aid of electrotaxis as a driving force [48]. The microfluidic device (Figure 3D) consisted of multiple microfilter stages to work as a sieve for the worms. Parametric investigation was conducted to maximize the sorting efficiency by optimizing the proper combination of EF strength, flow rate, and the decreasing gap size between consecutive filtering stages according to the expected age. The EF of 6V/cm, flow rate of 3µL/s, and gap sizes of 100, 55, 40, 25, and 15µm were found to efficiently (>96%) separate L2, L3, L4 and YA worms with an average throughput of 120 worms per minute. Later, in 2019, Yoon et al. [49] developed a microfluidic device for analyzing the electrotaxis behavior of *C. elegans* populations and for separating various strains. The developed straight microchannel was divided into three zones, i.e. two side ones with and the middle one without EF. Exposure to 4V/cm induced WT and *unc-54(s74)* worms to move towards the EF-free zone, whereas *unc-6(e78)*, a netrin gene mutation, showed no response to EF, allowing for separation and screening of mutants.

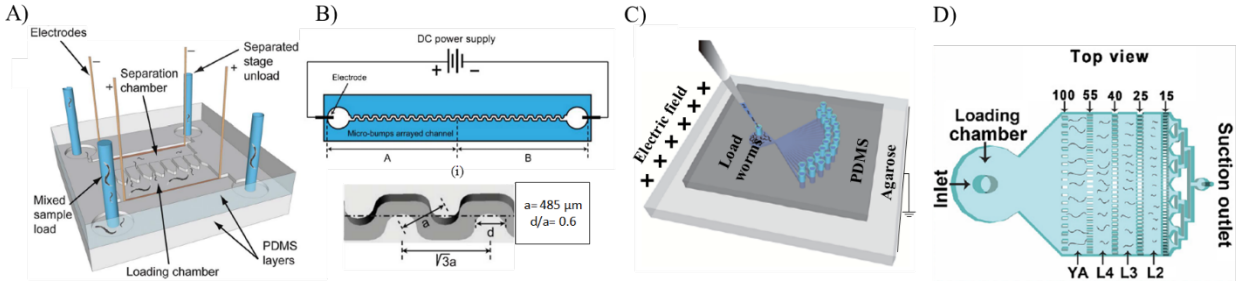

Figure 3: Different electrotaxis-based C. elegans sorting microfluidic devices based on (A) electrical traps [44,45], *(B) zigzag frequency-matching channels* [46], *(C) deflecting electrotaxis* [47], *and (D) electric sieving* [48] *techniques. Figures were adapted from ref.* [44,46–48] *with permission from Royal Society of Chemistry and Elsevier*

Naturally, *C. elegans* crawl stochastically on their left or right side, hindering the possibility of tracking specific body organs such as the gonad for microinjection [50]. Very commonly, worms are immobilized using glue or anesthetics, then manually maneuvered with a worm picking tool for obtaining a preferred orientation. However, these immobilization and orientation techniques are irreversible, low-throughput, labor-intensive and time-consuming. In 2016, Ardeshiri et al. [50] developed an electrotaxis-based on-demand orientation technique for adjusting the worm in any desired orientation, allowing for imaging of different body organs and neurons. Their PDMS-microdevice (Figure 4A) consisted of a electrotaxis-based worm selection channel, a rotatable orientation glass needle and an imaging channel. Using electrotaxis, a single worm was longitudinally oriented and loaded from a synchronized population into the imaging channel, then the incorporated rotatable capillary was used to pneumatically hold the worm from its head or tail. The capillary was then turned by any specific degrees to bring the organ or neuron of interest into focus for imaging. To demonstrate the ability of the device to properly orient and image the worm, different body organs such as vulva and ventral cord were imaged optically and fluorescently. In 2018, Huang et al. [51] reported a microfluidic method for on-demand, rapid, and reversible immobilization of *C. elegans* using the dielectrophoresis phenomena introduced earlier by Chuang et al. [52]. The developed multi-layer straight channel microfluidic device incorporated either a pair of thick spiked or thin flat electrodes (Figure 4B) fabricated from PDMS mixed with carbon black nanoparticles for EF application. Various EF strengths and frequencies were tested to immobilize *C. elegans* at different ages from L1 to L4. At smaller ages, lower EF strength was needed for worm trapping because the DEP force had to surpass the worms' muscular force, which improves with age. As a proof of

concept, high-resolution bright field and fluorescent images were obtained at 60x magnification without affecting the worms' health.

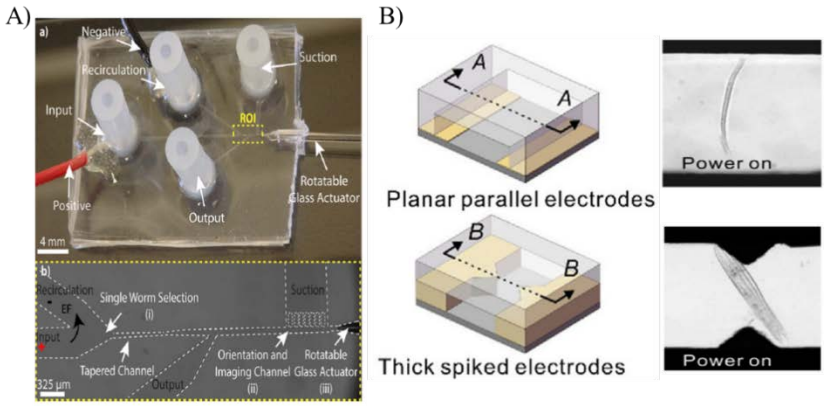

Figure 4: Electric-based orientation and immobilization techniques using (A) a rotatable glass capillary [50] *and (B) dielectrophoresis* [51]. *Figures were adapted from ref.* [50,51] *with permission from AIP Publishing and Elsevier*

C. elegans is a promising model organism for studying pathological mechanisms related to different diseases [53]. Different phenotypes such as swimming and crawling speed, body bend frequency, and movement characteristics have been used as readouts for drug screening [31]. Electrotaxis is an effective method for on-demand control of the voluntary movement of worms, hence useful for chemical screening assays. Carr et al. [54] were the first to exploit electrotaxis in a microfluidic device for chemical screening of *C. elegans* and *Oesophagotomum dentatum (O. dentatum)*. The device, depicted in Figure 5A, consisted of a straight electrotaxis screening channel connected to an inlet and a drug well via a tapered channel. Worms were loaded into the screening channel, and their pre-exposure electrotactic behaviors were recorded and quantified. Then, electrotaxis was used to guide the worms into and out from the drug well for exposure. During and after drug exposure, the worms' electrotactic behaviors were recorded, providing a real-time observation tool for drug screening. As a proof of concept, the device was used for screening anthelmintic drugs like levamisole on *C. elegans* and *O. dentatum*, using levamisole resistant or sensitive strains for each organism. The proposed method offered a robust, sensitive, and high-resolution assay that is amenable to replication for high-throughput dose-response studies in different nematodes. Later, the same device was utilized by Lycke et al. [55] to test the effect of four anthelmintic drugs (pyrantel, levamisole, tribendimidine, and methyridine) on worm paralysis.

Salam et al. [56] used the microfluidic device developed by Rezai et al. [18] (Figure 2A) to establish a worm model of Parkinson's disease (PD). Worm mutants with defective sensory and dopaminergic neurons (DNs) were tested and demonstrated defective electrotactic behaviors of reduced speed and body bend frequency. Their results suggested the involvement of the dopaminergic pathways in electrosensation. Thus, PD models were developed by exposing worms to various neurotoxins such as 6-hydroxydopamine (6-OHDA), 1-methyl-4-phenyl 1,2,3,6-tetrahydropyridine (MPTP), and rotenone, and neuroprotective compounds such as acetaminophen were tested against them. Worms treated with neurotoxins were investigated using on-chip electrotaxis and off-chip fluorescence imaging to correlate the electrotactic behavior with the DNs function. They demonstrated noticeable reductions in the electrotactic behavior and DNs fluorescent expression that were alleviated by pre-exposing worms to acetaminophen. The proposed technique provided an on-demand screening tool for monitoring movement behaviors and cellular processes, but its manual operation and low throughput made it labor-intensive and time-consuming, hindering its practicality. Thus, Liu et al. [57] developed a multi-layer microfluidic device integrated with various computer controlled microvalves and electrodes to perform a fully automated worm loading, isolation, and electrotaxis testing with a throughput of 20 worms per hour (Figure 5B). Next, Chuang et al. [58] proposed a novel usage of electrotaxis for driving *C. elegans* to exercise their muscles through swimming in a microfluidic chamber called "worm treadmill". A worm model of Alzheimer's disease was used to show that, although degeneration is inevitable, it could be slowed in exercise-treated worms compared to their control counterparts.

The abovementioned devices showed the potential for application of *C. elegans* electrotaxis to drug screening. However, they were based on testing single animals with no on-chip imaging and a maximum throughput of 20 worms per hour, hindering the possibility of using electrotaxis for high-throughput drug screening. To increase the electrotaxis

assay's throughput and incorporate on-chip imaging, two methods have been developed by us to either increase the number of worms tested simultaneously or shorten the assay time by performing the electrotaxis test in a more confined environment. The first method proposed a parallel assay that allows for electrotaxis testing and neuronal imaging of up to 16 worms simultaneously (Figure 5C) [59,60]. The monolayer microfluidic device consisted of 16 straight electrotaxis channels connected through tapered channels to tree-like inlets and outlets. The tapered channels were used for single worm loading before and imaging after the electrotaxis assay. Several phenotypes including swimming speed, body bend frequency, electrotaxis time index, electrotaxis turning time, and neuronal fluorescence intensity were analyzed. Worms exposed to 6-OHDA demonstrated a noticeable decrease in electrotaxis and neuron fluorescent expression. The device showed the potential to reach a throughput of up to 100 worms/hr. The second method introduced an alternative to the free movement-based electrotaxis assay by semi-immobilizing the worm from its tail while allowing its head to respond to EF, achieving a faster assay in a more confined space (Figure 2C) [40]. The device incorporated an electrotaxis channel and a tapered channel for worm capturing and imaging, allowing for correlating the electrotaxis behaviors with the neuronal processes in worm models of PD exposed to neurotoxins and neuroprotective compounds. Electrotaxis of tail-trapped worms at an EF of 4V/cm was studied followed by their immobilization and neuron imaging in the tapered channel. The results showed that exposing the worms to 100 and 250µM 6-OHDA affected their electrotaxis behavior and the neurons. Pre- and post- exposure to 1mM levodopa, a commonly used drug for PD, ameliorated the electrotaxis behavior and protected the neurons' fluorescent expression.

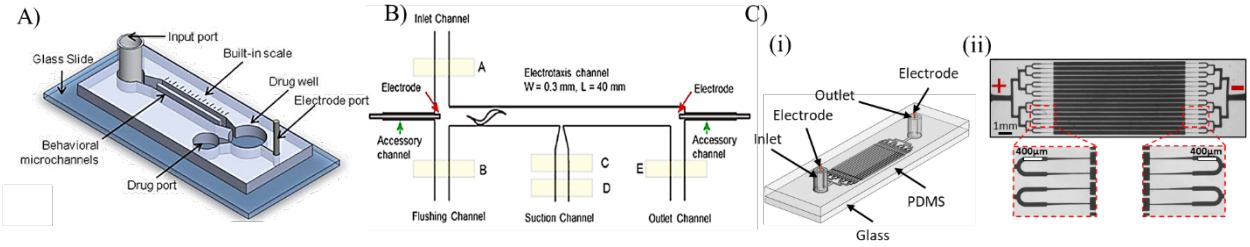

Figure 5: Microfluidic devices for drug screening using C. elegans electrotaxis [54,57,59,60]. *Figures were adapted from ref.* [54,57,59,60] *with permission from AIP publishing and the terms of the Creative Commons Attribution Non-Commercial License (http://creativecommons.org/licenses/by-nc/4.0)*

4. *D. rerio*

D. rerio or zebrafish is a vertebrate model organism that has emerged as a candidate for bridging the gap between invertebrates such as *C. elegans* or *D. melanogaster* and mammalian models. Compared to invertebrates, the zebrafish neuronal system is more complex, allowing for recapitulating many functions of the human brain and studying the neural basis of behavior. Moreover, their translucency during larval stages facilitates imaging and recording of the cellular and internal organ activities such as the heart and the brain [1]. Different stimuli such as chemicals, mechanical force, light, and EF have been shown to evoke the zebrafish central nervous system (CNS), leading to various behaviors [61]. In this section, the recent applications of EF to study zebrafish off and on microfluidic chips are discussed in detail.

4.1. Off-chip Studies

Various *in-vitro* and *in-vivo* assays have been developed to investigate the effect of EF on zebrafish cells and movement behaviors. For instance, Cormie et al. [20] extracted the embryonic zebrafish spinal neurons and investigated the effect of EF on their growth and movement. The extracted neurons were cultured on laminin-coated glass dishes and exposed to EF of 100mV/mm for 4 or 20hr through the insertion of electrodes into the culture medium. No directional movement or noticeable increase in the number of neurons were reported post EF exposure. Next, Huang et al. [62] investigated the EF-induced directed migration of cells using zebrafish keratocytes, aiming to understand the mechanisms governing cell galvanotaxis. The extracted keratocytes instantaneously migrated towards the cathode in the presence of a DC EF as low as 7mV/mm. The directed movement was independent of the cell size

and was attributed to the hydrodynamic forces generated on the cell membrane because of the EF-induced osmotic flow.

The integrity of the CNS can be assessed by recording the brain's electrical activity, which is easier to be performed on simpler organisms like zebrafish. Thus, Issa et al. [63] developed an experimental setup to monitor the zebrafish escape neural circuit upon stimulating the fish with a water jet. The setup consisted of a test chamber where the fish could swim in, a picospritzer to adjust the chamber's flow rate, a differential amplifier connected to two electrodes placed in the chamber for recording the EF, and a high-speed camera for recording zebrafish's behavior. The escape behavior was evoked by applying a water jet to the zebrafish's head. The evoked response generated unique EF potentials at slow and fast escapes. Fish with unilaterally ablated trigeminal neurons were tested at different days and showed escape behavior deficiency at one- and three-days post-ablation. However, at 7-days, the escape behavior enhanced significantly, demonstrating the ability to reconfigure the escape circuitry. Next, Kim et al. [64] investigated the effect of pulsed electromagnetic fields (PEMFs) on stimulating the pigmentation process in zebrafish, introducing zebrafish as a model organism for melanogenesis. For exposure to PEMFs, a Helmholtz coil was used to generate a magnetic field with 2, 4, and 20 gausses (G). It was shown that a 4G, the magnetic field significantly upregulated pigmentation by increasing the melanin content. The proposed technique demonstrated its application as a tool for hyperpigmentation-related skin disorder therapy.

4.2. Microfluidics-based Assays

Despite the remarkable advancements in zebrafish research, the conventional techniques used for the organism's manipulation, immobilization, orientation, and imaging are laborious, time-consuming, and tedious, hindering the usage of zebrafish for high-throughput studies. Microfluidics has been introduced as a promising technology for the development of accurate, high-throughput, and non-invasive methods for zebrafish assays [61]. Recently, several papers have shown the use of microfluidic devices to investigate the effects of EF on zebrafish and introduced novel techniques for CNS studies and drug screening.

Hong et al. [65] developed a non-invasive multichannel electrophysiology unit, called iZAP, for parallel neural recording of zebrafish larvae. The iZAP consisted of a microfluidic network of channels, a multielectrode layer, and a multichannel amplifier (Figure 6A). The microfluidic network was comprised of inlet and outlet parallel channels connected through 12 perpendicular half-cylindrical channels with tapered endings. The larvae were autonomously head-loaded and aligned over electrodes for long-term electroencephalographic recording. The unit was integrated with a custom-developed software to precisely detect the real-time electrophysiological characteristics of seizure in zebrafish larvae. As a proof of concept, exposure to pentylenetetrazole induced abrupt bursts in the electroencephalogram signal, which were found to be associated with unique eye and tail movement artifacts. Moreover, *scn1Lab* Dravet syndrome zebrafish mutants were tested with two antiepileptic drugs (Valproic acid and Topiramate) to monitor epileptogenic progression, providing a model for drug screening using the iZAP system.

We were the first to report the effect of EF on freely moving zebrafish larvae in a microfluidic channel with two end electrodes [17,66]. Zebrafish larvae were exposed to electric currents of 1-25µA while the cathode was at the larva's head. Electric currents of 3-15 µA stimulated the larvae in the daytime to instantaneously turn and swim towards the anode. However, at night, zebrafish demonstrated a significant decline in the electric-induced behavior. Exposure to apomorphine, a dopamine agonist, revived the response at night, demonstrating the involvement of dopamine receptors in zebrafish electrosensation. Next, the roles of D1- and D2-like receptors were investigated by exposing the fish to D1-selective agonist SKF-38393 and D2-selective agonist Quinpirole. They showed a significant involvement of the D2 receptor in electrosensation due to the corresponding increase in larvae's electric response at night after exposure to Quinpirole.

Recently, our head trap and tail screening design in Figure 6B, which was first proposed by Nady et al. [67], was used by us to study the effect of EF on semi-mobile zebrafish larvae [66]. The device contained three layers; the top layer consisted of two electrode spots, loading and trapping channels, a screening pool, and an outlet channel. The bottom layer contained a trapping valve with one L-shaped channel. A thin PDMS layer was sandwiched between the two layers to serve as a deformable membrane for larva trapping. Zebrafish larvae were loaded with their tail towards the screening pool, and once exposed to electric currents, an oscillatory tail movement with various C- and J-bend patterns were observed. In addition to these patterns, two quantitative parameters of tail beat frequency (TBF) and response duration (RD) were measured. The highest TBF and RD were recorded at 1µA and 3µA, respectively. Next, we used

this platform for genetic and drug screening [68]. Exposure to 250μM 6-OHDA induced alterations in the electric response of zebrafish that was successfully rescued by post-exposure to 1mM levodopa, a commonly used PD drug. The results demonstrated the application of the microfluidic electric assay to chemical screening of zebrafish movement disorder models. Moreover, a *panx1a* knockout zebrafish model was tested and showed an electric response deficiency, suggesting its role in governing the behavior and the application of the method to gene screening. In 2020, we incorporated a right-angle prism for recording and imaging the zebrafish's heart, providing a microfluidic device for multi-phenotypic and bi-directional imaging of zebrafish [69]. During EF stimulation, a noticeable increase in the heart beating frequency was observed and ameliorated after the end of the stimulus. Exposure to ethanol and 6-OHDA induced significant decreases in the heart rate, demonstrating the application of our technique not only to behavioral studies but also for organ-level screening.

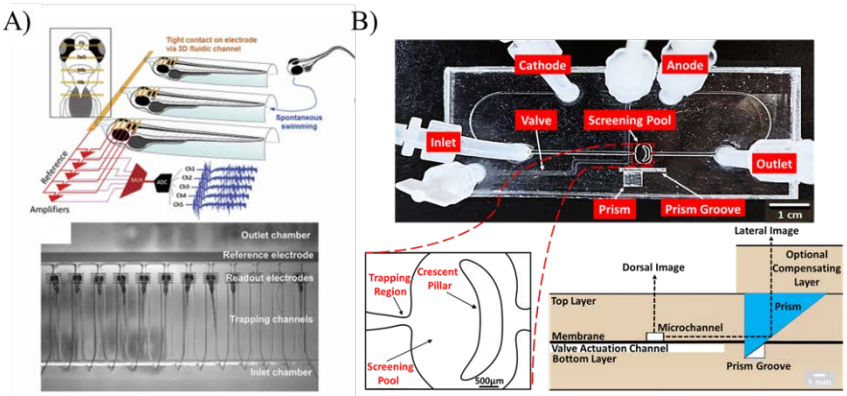

Figure 6: Experimental methods used for on-chip electrical studies of zebrafish. (A) A non-invasive multichannel electrophysiology unit (iZAP) [65]. *(B) A microfluidic device for electric response* [66] *and heart screening* [69] *of semi-mobile zebrafish larvae. Figure A was adapted from ref.* [65] *and permission under the terms of the Creative Commons Attribution Non-Commercial License (http://creativecommons.org/licenses/by-nc/4.0)*

5. Conclusions and Future Remarks

The central nervous system allows organisms to perceive the world by integrating and processing sensory information into motor outputs. The neuronal processes that guide a particular behavior like navigation are not well understood in humans and higher animal models due to their complexities. Model organisms such as *C. elegans* and *D. rerio* have made these investigations feasible due to their simple sensory and motor systems. Different stimuli such as heat, light, sound, mechanical force, and electrical signals have been used to probe the organism's sensing and movement mechanisms and processes. Electrical stimulation is of interest due to its suitability to stimulate nerves and muscles precisely and controllably. However, due to the small size and continuous stochastic movement of these model organisms, and the complexity of their environment, electrical stimulation has been limited in the existing experimental assays. Microfluidics has offered various platforms to interrogate the effect of electric stimulation on small model organisms in an automated, high-throughput, and accurate manner. In this chapter, we reviewed the majority of the conventional and microfluidic techniques developed to date to investigate the neuronal circuits involved in electrosensation of *C. elegans* and *D. rerio*. Moreover, we reviewed the promising electric-based applications for on-demand manipulation and screening of these organisms. Our assessment of the field reveals that despite the noteworthy research on electrosensation and electrotaxis, many fundamental and applied questions and gaps are yet to be addressed. The major ones are the underlying pathways of electrotaxis, the limitations of electric sensorimotor screening, enhancing the throughput of electrotactic technologies and developing phenotypic assays that are specific towards organisms' identity.

Reference:

[1] K. Youssef, P. Bayat, A.R. Peimani, S. Dibaji, P. Rezai, Miniaturized Sensors and Actuators for Biological Studies on Small Model Organisms of Disease, in: Environmental, Chemical and Medical Sensors, Springer, 2018: pp. 199–225. https://doi.org/10.1007/978-981-10-7751-7_9.

[2] N.U. Czech-Damal, G. Dehnhardt, P. Manger, W. Hanke, Passive electroreception in aquatic mammals, Journal of Comparative Physiology A. 199 (2013) 555–563.

[3] N.U. Czech-Damal, A. Liebschner, L. Miersch, G. Klauer, F.D. Hanke, C. Marshall, G. Dehnhardt, W. Hanke, Electroreception in the Guiana dolphin (Sotalia guianensis), Proceedings of the Royal Society B: Biological Sciences. 279 (2012) 663–668.

[4] J.D. Pettigrew, Electroreception in monotremes, Journal of Experimental Biology. 202 (1999) 1447–1454.

[5] L.J. Shanley, P. Walczysko, M. Bain, D.J. MacEwan, M. Zhao, Influx of extracellular Ca2+ is necessary for electrotaxis in Dictyostelium, Journal of Cell Science. 119 (2006) 4741–4748.

[6] P.L. Newland, E. Hunt, S.M. Sharkh, N. Hama, M. Takahata, C.W. Jackson, Static electric field detection and behavioural avoidance in cockroaches, Journal of Experimental Biology. 211 (2008) 3682–3690.

[7] D. Clarke, H. Whitney, G. Sutton, D. Robert, Detection and learning of floral electric fields by bumblebees, Science. 340 (2013) 66–69.

[8] N.C. Sukul, N.A. Croll, Influence of potential difference and current on the electrotaxis of Caenorhaditis elegans., Journal of Nematology. 10 (1978) 314–317.

[9] Y.-S. Sun, Studying electrotaxis in microfluidic devices, Sensors. 17 (2017) 2048.

[10] T. Kimura, M. Sakai, K. Tabu, L. Wang, R. Tsunematsu, M. Tsuda, H. Sawa, K. Nagashima, H. Nishihara, S. Hatakeyama, Human synovial sarcoma proto-oncogene Syt is essential for early embryonic development through the regulation of cell migration, Laboratory Investigation. 89 (2009) 645–656.

[11] J.R. Tran, X. Zheng, Y. Zheng, Lamin-B1 contributes to the proper timing of epicardial cell migration and function during embryonic heart development, Molecular Biology of the Cell. 27 (2016) 3956–3963.

[12] R. Riahi, Y. Yang, D.D. Zhang, P.K. Wong, Advances in wound-healing assays for probing collective cell migration, Journal of Laboratory Automation. 17 (2012) 59–65.

[13] C.D. McCaig, A.M. Rajnicek, B. Song, M. Zhao, Controlling cell behavior electrically: current views and future potential, Physiological Reviews. (2005).

[14] Y.-S. Sun, S.-W. Peng, J.-Y. Cheng, In vitro electrical-stimulated wound-healing chip for studying electric field-assisted wound-healing process, Biomicrofluidics. 6 (2012) 34117.

[15] J. Feng, J. Liu, X. Zhang, L. Zhang, J. Jiang, J. Nolta, M. Zhao, Guided migration of neural stem cells derived from human embryonic stem cells by an electric field, Stem Cells. 30 (2012) 349–355.

[16] Y.-S. Sun, S.-W. Peng, K.-H. Lin, J.-Y. Cheng, Electrotaxis of lung cancer cells in ordered three-dimensional scaffolds, Biomicrofluidics. 6 (2012) 14102.

[17] A.R. Peimani, G. Zoidl, P. Rezai, A microfluidic device to study electrotaxis and dopaminergic system of zebrafish larvae, Biomicrofluidics. 12 (2018) 14113.

[18] P. Rezai, A. Siddiqui, P.R. Selvaganapathy, B.P. Gupta, Electrotaxis of Caenorhabditis elegans in a microfluidic environment, Lab on a Chip. 10 (2010) 220–226. https://doi.org/10.1039/b917486a.

[19] K. Youssef, P. Bayat, A.R. Peimani, S. Dibaji, P. Rezai, Miniaturized Sensors and Actuators for Biological Studies on Small Model Organisms of Disease, in: Environmental, Chemical and Medical Sensors, Springer, 2018: pp. 199–225. https://doi.org/10.1007/978-981-10-7751-7_9.

[20] P. Cormie, K.R. Robinson, Embryonic zebrafish neuronal growth is not affected by an applied electric field in vitro, Neuroscience Letters. 411 (2007) 128–132.

[21] A.R. Peimani, G. Zoidl, P. Rezai, A microfluidic device to study electrotaxis and dopaminergic system of zebrafish larvae, Biomicrofluidics. 12 (2018) 14113. https://doi.org/10.1063/1.5016381.

[22] A. Aryasomayajula, P. Bayat, P. Rezai, P.R. Selvaganapathy, Microfluidic Devices and Their Applications, in: Springer Handbook of Nanotechnology, Springer, 2017: pp. 487–536.

[23] L.P. O'Reilly, C.J. Luke, D.H. Perlmutter, G.A. Silverman, S.C. Pak, C. elegans in high-throughput drug discovery, Advanced Drug Delivery Reviews. 69–70 (2014) 247–253. https://doi.org/10.1016/j.addr.2013.12.001.

[24] J. Spieth, D. Lawson, P. Davis, G. Williams, K. Howe, Overview of gene structure in C. elegans, in: WormBook : The Online Review of C. Elegans Biology, 2014: pp. 1–18. https://doi.org/10.1895/wormbook.1.65.2.

[25] K. Youssef, A. Tandon, P. Rezai, Studying Parkinson's disease using Caenorhabditis elegans models in microfluidic devices, Integrative Biology : Quantitative Biosciences from Nano to Macro. 11 (2019) 186–

207. https://doi.org/10.1093/intbio/zyz017.
[26] O. Margie, C. Palmer, I. Chin-Sang, C. elegans chemotaxis assay, JoVE (Journal of Visualized Experiments). (2013) e50069.
[27] A. Ward, J. Liu, Z. Feng, X.Z.S. Xu, Light-sensitive neurons and channels mediate phototaxis in C. elegans, Nature Neuroscience. 11 (2008) 916–922.
[28] E.M. Hedgecock, R.L. Russell, Normal and mutant thermotaxis in the nematode Caenorhabditis elegans, Proceedings of the National Academy of Sciences. 72 (1975) 4061–4065.
[29] W.R. Schafer, Mechanosensory molecules and circuits in C. elegans, Pflügers Archiv-European Journal of Physiology. 467 (2015) 39–48.
[30] C. V. Gabel, H. Gabel, D. Pavlichin, A. Kao, D.A. Clark, A.D.T. Samuel, Neural Circuits Mediate Electrosensory Behavior in Caenorhabditis elegans, Journal of Neuroscience. 27 (2007) 7586–7596. https://doi.org/10.1523/JNEUROSCI.0775-07.2007.
[31] M. Maulik, S. Mitra, A. Bult-Ito, B.E. Taylor, E.M. Vayndorf, Behavioral phenotyping and pathological indicators of Parkinson's disease in C. elegans models, Frontiers in Genetics. 8 (2017) 77. https://doi.org/10.3389/fgene.2017.00077.
[32] M.M. Shanmugam, Galvanotaxis of Caenorhabditis elegans: current understanding and its application in improving research, Biology, Engineering and Medicine. 2 (2017) 1–5. https://doi.org/10.15761/bem.1000111.
[33] X. Manière, F. Lebois, I. Matic, B. Ladoux, J.-M. Di Meglio, P. Hersen, Running worms: C. elegans self-sorting by electrotaxis, PloS One. 6 (2011).
[34] S.D. Chrisman, C.B. Waite, A.G. Scoville, L. Carnell, C. elegans demonstrates distinct behaviors within a fixed and uniform electric field, PLoS ONE. 11 (2016). https://doi.org/10.1371/journal.pone.0151320.
[35] M.G. Risley, S.P. Kelly, K. Jia, B. Grill, K. Dawson-Scully, Modulating behavior in C. elegans using electroshock and antiepileptic drugs, PLoS One. 11 (2016) e0163786.
[36] P. Rezai, S. Salam, P.R. Selvaganapathy, B.P. Gupta, Effect of pulse direct current signals on electrotactic movement of nematodes Caenorhabditis elegans and Caenorhabditis briggsae, Biomicrofluidics. 5 (2011) 44116.
[37] P. Rezai, A. Siddiqui, P.R. Selvaganapathy, B.P. Gupta, Behavior of Caenorhabditis elegans in alternating electric field and its application to their localization and control, Applied Physics Letters. 96 (2010) 153702. https://doi.org/10.1063/1.3383223.
[38] J. Jung, M. Nakajima, M. Takeuchi, Z. Najdovski, Q. Huang, T. Fukuda, Microfluidic device to measure the speed of C. elegans using the resistance change of the flexible electrode, Micromachines. 7 (2016) 50.
[39] T.V. Chokshi, D. Bazopoulou, N. Chronis, Probing the physiology of ASH neuron in Caenorhabditis elegans using electric current stimulation, Applied Physics Letters. 99 (2011) 53702.
[40] K. Youssef, D. Archonta, T.J. Kubiseski, A. Tandon, P. Rezai, Semi-mobile C. elegans electrotaxis assay for movement screening and neural monitoring of Parkinson's disease models, Sensors and Actuators, B: Chemical. (2020). https://doi.org/10.1016/j.snb.2020.128064.
[41] K. Youssef, D. Archonta, A. Tandon, T. Kubiseski, P. Rezai, Neuronal and Behavioural Effects of Alpha-Synuclein Protein and 6-OHDA Neurotoxin in Parkinson's Disease Investigated with a C. elegans Electrotaxis Microfluidic Assay, in: Mtas2018, Kaohsiung, Taiwan, 2018: pp. 115–118.
[42] K. Youssef, D. Archonta, T.J. Kubiseski, A. Tandon, P. Rezai, Electric Egg-Laying: Effect of Electric Field in a Microchannel on C. elegans Egg-Laying Behavior, BioRxiv. (2020).
[43] K. Youssef, D. Archonta, T. Kubiseski, A. Tandon, P. Rezai, On-Demand Electric Field Induced Egg Laying of CAENORHABDITIS ELEGANS, in: Mtas 2019, Basel, Switzerland, 2019: pp. 392–393.
[44] P. Rezai, S. Salam, B.P. Gupta, P.R. Selvaganapathy, Electrical sorting of caenorhabditis elegans, 15th International Conference on Miniaturized Systems for Chemistry and Life Sciences 2011, MicroTAS 2011. 2 (2011) 723–725.
[45] P. Rezai, S. Salam, P.R. Selvaganapathy, B.P. Gupta, Electrical sorting of Caenorhabditis elegans, Lab on a Chip. 12 (2012) 1831–1840.
[46] B. Han, D. Kim, U.H. Ko, J.H. Shin, A sorting strategy for C. elegans based on size-dependent motility and electrotaxis in a micro-structured channel., Lab on a Chip. 12 (2012) 4128–4134. https://doi.org/10.1039/c2lc40209b.
[47] X. Wang, R. Hu, A. Ge, L. Hu, S. Wang, X. Feng, W. Du, B.F. Liu, Highly efficient microfluidic sorting device for synchronizing developmental stages of C. elegans based on deflecting electrotaxis, Lab on a Chip. 15 (2015) 2513–2521. https://doi.org/10.1039/c5lc00354g.
[48] X. Wang, A. Ge, L. Hu, X. Feng, W. Du, B.-F. Liu, A microfluidic microfilter chip driven by electrotaxis

and fluid flow for size-dependent C. elegans sorting with high purity and efficiency, Sensors and Actuators B: Chemical. 260 (2018) 311–319.
[49] S. Yoon, M. Yeo, H. Kim, T. Jeon, S.M. Kim, Effectively controlled microfluidic trap for spatiotemporal analysis of the electrotaxis of Caenorhabditis elegans, Electrophoresis. 40 (2019) 431–436.
[50] R. Ardeshiri, B. Mulcahy, M. Zhen, P. Rezai, A hybrid microfluidic device for on-demand orientation and multidirectional imaging of C. elegans organs and neurons, Biomicrofluidics. 10 (2016) 64111. https://doi.org/10.1063/1.4971157.
[51] L. Huang, P. Zhao, J. Wu, H.S. Chuang, W. Wang, On-demand dielectrophoretic immobilization and high-resolution imaging of C. elegans in microfluids, Sensors and Actuators, B: Chemical. 259 (2018) 703–708. https://doi.org/10.1016/j.snb.2017.12.106.
[52] H.S. Chuang, D.M. Raizen, A. Lamb, N. Dabbish, H.H. Bau, Dielectrophoresis of Caenorhabditis elegans, Lab on a Chip. 11 (2011) 599–604. https://doi.org/10.1039/c0lc00532k.
[53] C.D. Link, C. elegans models of age-associated neurodegenerative diseases: Lessons from transgenic worm models of Alzheimer's disease, Experimental Gerontology. 41 (2006) 1007–1013. https://doi.org/10.1016/j.exger.2006.06.059.
[54] J.A. Carr, A. Parashar, R. Gibson, A.P. Robertson, R.J. Martin, S. Pandey, A microfluidic platform for high-sensitivity, real-time drug screening on C. elegans and parasitic nematodes, Lab on a Chip. 11 (2011) 2385–2396. https://doi.org/10.1039/c1lc20170k.
[55] R. Lycke, A. Parashar, S. Pandey, Microfluidics-enabled method to identify modes of Caenorhabditis elegans paralysis in four anthelmintics, Biomicrofluidics. 7 (2013) 64103.
[56] S. Salam, A. Ansari, S. Amon, P. Rezai, P.R. Selvaganapathy, R.K. Mishra, B.P. Gupta, A microfluidic phenotype analysis system reveals function of sensory and dopaminergic neuron signaling in C. elegans electrotactic swimming behavior , in: Worm, Taylor & Francis, 2013: p. e24558. https://doi.org/10.4161/worm.24558.
[57] D. Liu, B. Gupta, P.R. Selvaganapathy, An automated microfluidic system for screening Caenorhabditis elegans behaviors using electrotaxis, Biomicrofluidics. 10 (2016) 14117. https://doi.org/10.1063/1.4941709.
[58] H.S. Chuang, W.J. Kuo, C.L. Lee, I.H. Chu, C.S. Chen, Exercise in an electrotactic flow chamber ameliorates age-related degeneration in Caenorhabditis elegans, Scientific Reports. 6 (2016) 1–11. https://doi.org/10.1038/srep28064.
[59] K. Youssef, D. Archonta, T. Kubiseski, A. Tandon, P. Rezai, A Microfluidic Device To Enhance the Throughput of Electrotaxis Screening With Caenorhabditis Elegans Models of Parkinson ' S Disease, in: Mtas 2019, Basel, Switzerland, 2019: pp. 382–383.
[60] K. Youssef, D. Archonta, T. Kubiseski, A. Tandon, P. Rezai, Parallel-Channel Electrotaxis and Neuron Screening of Caenorhabditis elegans, Micromachines. 11 (2020) 756.
[61] A. Khalili, P. Rezai, Microfluidic devices for embryonic and larval zebrafish studies, Briefings in Functional Genomics. 18 (2019) 419–432. https://doi.org/10.1093/bfgp/elz006.
[62] L. Huang, P. Cormie, M.A. Messerli, K.R. Robinson, The involvement of Ca2+ and integrins in directional responses of zebrafish keratocytes to electric fields, Journal of Cellular Physiology. 219 (2009) 162–172.
[63] F.A. Issa, G. O'Brien, P. Kettunen, A. Sagasti, D.L. Glanzman, D.M. Papazian, Neural circuit activity in freely behaving zebrafish (Danio rerio), Journal of Experimental Biology. 214 (2011) 1028–1038.
[64] Y.-M. Kim, H.-M. Lim, H.-S. Ro, G.-E. Ki, Y.-K. Seo, Pulsed electromagnetic fields increase pigmentation through the p-ERK/p-p38 pathway in zebrafish (Danio rerio), International Journal of Molecular Sciences. 19 (2018) 3211.
[65] S. Hong, P. Lee, S.C. Baraban, L.P. Lee, A novel long-term, multi-channel and non-invasive electrophysiology platform for zebrafish, Scientific Reports. 6 (2016) 1–10.
[66] A.R. Peimani Foroushani, Microfluidic Devices for Investigation of Zebrafish Larvaes Electrotaxis and their Applications to Dopamine System Studies, (2017).
[67] A. Nady, A.R. Peimani, G. Zoidl, P. Rezai, A microfluidic device for partial immobilization, chemical exposure and behavioural screening of zebrafish larvae, Lab on a Chip. 17 (2017) 4048–4058.
[68] A. Khalili, A.R. Peimani, N. Safarian, K. Youssef, G. Zoidl, P. Rezai, Phenotypic chemical and mutant screening of zebrafish larvae using an on-demand response to electric stimulation, Integrative Biology. 11 (2019) 373–383.
[69] A. Khalili, E. van Wijngaarden, G.R. Zoidl, P. Rezai, Multi-phenotypic and bi-directional behavioral screening of zebrafish larvae, Integrative Biology. (2020).

Appendix B

Research Papers and Submitted Manuscripts related to Chapter 4

B.1 Paper I: Parallel-Channel Electrotaxis and Neuron Screening of *Caenorhabditis elegans*

Youssef, K., Archonta, D., Kubiseski, T., Tandon, A., & Rezai, P. (2020). Parallel-Channel Electrotaxis and Neuron Screening of *Caenorhabditis elegans*. Micromachines, 11(8), 756.

micromachines

MDPI

Article

Parallel-Channel Electrotaxis and Neuron Screening of *Caenorhabditis elegans*

Khaled Youssef [1], Daphne Archonta [1], Terrance Kubiseski [2], Anurag Tandon [3] and Pouya Rezai [1,*]

[1] Department of Mechanical Engineering, York University, Toronto, ON M3J 1P3, Canada; kyoussef@yorku.ca (K.Y.); daphnea@my.yorku.ca (D.A.)
[2] Department of Biology, York University, Toronto, ON M3J 1P3, Canada; tkubises@yorku.ca
[3] Tanz Center for Research in Neurodegenerative Diseases, Toronto, ON M5T 0S8, Canada; a.tandon@utoronto.ca
* Correspondence: prezai@yorku.ca; Tel.: +1-416-736-2100 (ext. 44703)

Received: 14 July 2020; Accepted: 30 July 2020; Published: 4 August 2020

Abstract: In this paper, we report a novel microfluidic method to conduct a *Caenorhabditis elegans* electrotaxis movement assay and neuronal imaging on up to 16 worms in parallel. *C. elegans* is a model organism for neurodegenerative disease and movement disorders such as Parkinson's disease (PD), and for screening chemicals that alleviate protein aggregation, neuronal death, and movement impairment in PD. Electrotaxis of *C. elegans* in microfluidic channels has led to the development of neurobehavioral screening platforms, but enhancing the throughput of the electrotactic behavioral assay has remained a challenge. Our device consisted of a hierarchy of tree-like channels for worm loading into 16 parallel electrotaxis screening channels with equivalent electric fields. Tapered channels at the ends of electrotaxis channels were used for worm immobilization and fluorescent imaging of neurons. Parallel electrotaxis of worms was first validated against established single-worm electrotaxis phenotypes. Then, mutant screening was demonstrated using the NL5901 strain, carrying human α-synuclein in the muscle cells, by showing the associated electrotaxis defects in the average speed, body bend frequency (BBF), and electrotaxis time index (ETI). Moreover, chemical screening of a PD worm model was shown by exposing the BZ555 strain, expressing green fluorescence protein (GFP) in the dopaminergic neurons (DNs), to 6-hydroxydopamine neurotoxin. The neurotoxin-treated worms exhibited a reduction in electrotaxis swimming speed, BBF, ETI, and DNs fluorescence intensity. We envision our technique to be used widely in *C. elegans*-based movement disorder assays to accelerate behavioral and cellular phenotypic investigations.

Keywords: *C. elegans*; microfluidics; electrotaxis; Parkinson's disease

1. Introduction

High-throughput screening (HTS) is a crucial drug discovery process that aims to test large compound libraries on a specific target in a sensitive, fast, and cost-effective manner [1]. Typically, preliminary hits are achieved by using in-vitro cell-based assays. The positive hits are then tested on whole-animal mammalian models to evaluate the chemical potency and toxicity before preliminary clinical trials [2]. Very commonly, these compounds are found to be impractical on whole animals due to the drug toxicity, metabolism complications, or poor target engagement, thereby rendering the process expensive and tedious [2]. Model organisms such as *Caenorhabditis elegans* (*C. elegans*) [1,3,4], *Drosophila melanogaster* [5,6], and *Danio rerio* [7] have shown promising outcomes to fill the gap between in-vitro cell-based and in-vivo whole-animal studies.

C. elegans is a free-living worm and a promising model for studying human diseases due to its genetic homology with humans, small size, short life cycle, cost-effective maintenance, fecundity, and whole-life body transparency for fluorescent imaging of neuron and muscle cells [8,9]. Moreover, *C. elegans* continues to be of importance in drug discovery due to a fully sequenced genome, genetic tractability, and many other experimental advantages [8,9]. *C. elegans* behavioral phenotypes such as mobility, body morphology, pharyngeal pumping, brood size, and development, along with in-vivo fluorescently labeled cells, have been quantified for drug efficacy testing [10–13]. For instance, *C. elegans* share various gene orthologues for many of the neurological disorders. Therefore, they have been exploited extensively as models for neurodegenerative diseases (NDs), such as Parkinson's disease (PD) [14–17], Alzheimer's disease (AD) [18], and Huntington's disease (HD) [10]. Various mutants have been created to help reveal the causes underpinning these NDs and to identify novel neuroprotective compounds [19].

Microfluidics have contributed to *C. elegans*-based ND research by offering various manipulation and screening platforms. The prevision offered by microfluidics in delivering external stimuli and maintaining highly controllable test conditions has facilitated its use in evoking the worms' neurobehavioral phenotypes for chemical screening. For example, Ma et al. [20] and Shi et al. [21] investigated the effects of 1-methyl-4-phenylpyridinium (MPP+) and 6-hydroxydopamine (6-OHDA), respectively, on worms' mobility and neurodegeneration rate to study worm models of PD using microfluidic platforms. Recently, Mondal et al. [22] invented a novel drug screening platform based on the worms' fluorescently tagged neurons to screen for various drugs in a short time. The chip was designed in a 96-well plate format to fit within an automated liquid handling system, and a worm model of HD was used to screen for positive hits out of 1000 FDA-approved compounds.

In addition to the natural behaviors of the worm investigated in the papers above, induced responses by different stimuli, such as chemicals, light, temperatures, magnetic fields, and electric fields have also attracted attention [8,23–26]. For instance, Salam et al. [27] exploited the innate response of *C. elegans* towards the cathode under the effect of a direct current (DC) electric field in a microchannel, termed electrotaxis [28], as an on-demand method for drug testing. Various PD-related neurotoxins were utilized to validate the use of electrotaxis in assessing neurobehavioral processes. To enhance the speed of this technique, Li et al. [29] developed an automated system to achieve a throughput of 20 worms/h in a single-channel single-worm device and validated the system using a worm model of PD. Worms' electrotaxis behavior on open-surface substrates has been shown to be relatively complex due to electric field nonuniformity and multidirectional movement of worms, but in the above microfluidic approaches, microchannels have provided uniform and consistent stimulus exposure and movement pathways to guide worms directionally for easy phenotypic quantification.

Up until now, electrotaxis assays on freely moving worms have been done on a single worm at a time, and no on-chip imaging along with electrotaxis screening has been reported. Testing of multiple worms to enhance the throughput of electrotaxis screening and simultaneous neuron imaging to correlate movement malfunctions with neuron and muscle degeneration, preferably at single animal resolution, is still needed. To address these gaps, we report a simple and easy-to-use microfluidic electrotaxis-based chip to investigate the behavior and neuron degeneration of 16 worms in parallel. In this context, we showed the applicability of our device for genetic, chemical, and neuronal screening after validating it against the single-worm electrotaxis assay.

2. Materials and Methods

2.1. Chemicals and Materials

For the lithography procedures, a set of 4-inch diameter and 500–550 µm thick silicon (Si) wafers was obtained from Wafer World Incorporation (West Palm Beach, FL, USA). SU8 developer and the negative photoresist SU8-2035 were procured from MicroChem Corporation (Newton, MA, USA). Polydimethylsiloxane (PDMS) was ordered from Dow corning Corporation (Auburn, MI, USA).

All other chemicals were ordered from Sigma-Aldrich (St. Louis, MO, USA). Typically, *C. elegans* M9 buffer was prepared by autoclaving a 1 L solution of 3 g of KH_2PO_4, 6 g Na_2HPO_4, and 5 g NaCl in distilled H_2O, followed by the addition of 1 ml of 1 M $MgSO_4$. *C. elegans'* food source of *Escherichia coli (E. coli)* strain OP50 was prepared in L-broth, a bacterial food source. L-broth was obtained by autoclaving a 1 L mixture of 10 g of Bacto-tryptone, 5 g of Bacto-yeast, and 5 g of NaCl in distilled H_2O. For neurodegeneration, 6-OHDA (636-00-0, Sigma-Aldrich), a known neurotoxin for degenerating the dopaminergic neurons, was used by obtaining a 10 mM stock solution using 5 mg of 6-OHDA in 2 mL of autoclaved M9. 6-OHDA solution was prepared in a dark room and stored at −20 °C.

2.2. C. elegans Strains, Maintenance, Synchronization, and Chemical Exposure

Wild-type N2, BZ555, and NL5901 strains (obtained from the *Caenorhabditis* Genetics Center (University of Minnesota, Minneapolis, MN, USA)) (Table 1) were grown on standard nematode-growth media agar plates seeded with OP50 as a food source at 25 °C. For all assays, worms were synchronized by Alkaline hypochlorite treatment, as previously described. [30] Briefly, gravid adult hermaphrodites were washed off the plate using M9 buffer and centrifuged for bacterial removal. Then, the worms' pellet was treated with a commercial bleach-based solution (1 mL of commercial bleach, 125 µL of NaOH, and 3.875 mL of double-distilled water) for egg-extraction. The extracted eggs were allowed to hatch into L1 larve overnight in 1 mL of M9 buffer. In the following day, the hatched larvae (L1 stage) were treated with 250 µM of 6-OHDA (975 µL M9 and 25 µL 6-OHDA from our prepared 10 mM stock solution) in a dark room for 1 h [27]. The control batches were only treated with M9 for 1 h in the darkroom to maintain the same test conditions. The worms were incubated for 40 h at 25 °C to be tested at the young adult stage.

Table 1. *Caenorhabditis elegans* strains used in this study.

Strain	Genotype	Description	Ref.
N2	WT Bristol	Wild type	
NL5901	*pkIs2386 [unc-54p:: α-syn::YFP+unc-119(+)]*	α-syn YFP expression in muscle cells	[31]
BZ555	*egIs1 [dat-1p::GFP]*	GFP expression in DNs	[32]

2.3. Experimental Setup and Device Design

The experimental setup used to perform this study is illustrated in Figure 1. It consisted of a microfluidic device (Figure 2A) with two end electrodes connected to a Keithley 2410 DC sourcemeter (Keithley Instruments Inc., Austin, TX, USA). Imaging of worms inside the device was done by an upright microscope (Leica MZ10F fluorescence microscope, Leica, Wetzlar, Germany). The mono-layer device was fabricated from (PDMS) using conventional soft lithography [33,34] and irreversible bonding to a glass slide using O_2 plasma [23] (see Appendix A for details). Our device consisted of four-channel sections, each 60 µm-thick, as shown in Figure 2B, i.e., (1) branching channels for worm loading and distribution; (2) 16 parallel 300 µm-wide electrotaxis screening channels; (3) tapering channels, from 40 to 20 µm, for worm immobilization and imaging; and (4) branching channels for unloading the worms. The electrotaxis screening channels were designed according to the results of Rezai et al. [28] to allow proper worm swimming and turning (see Appendix C for details). Electrodes were installed in inlet and outlet reservoirs for electric field stimulation.

The critical design criteria of our chip were to smoothly load the worms and provide a constant electric field throughout all the 16 screening channels for electrotaxis studies. This was achieved by embracing a loading technique inspired by Hulme et al. [35] through a hierarchy of channels that helped maintaining equal hydrodynamic and electrical resistances for each path. Hydrodynamic resistance determines the path each worm follows at each bifurcation in the network. An occupied path will lead the next worm to be loaded into another vacant channel. Constant channel dimensions at each bifurcation were used to maintain the same pressure and voltage drop up to the electrotaxis

screening channels using Hagen–Poiseuille's and Ohm's laws [36]. The pressure and voltage drops were defined by Equations (1) and (2), respectively.

$$\triangle P = R_f Q, \quad R_f = \frac{128\mu l}{\pi D^4} \tag{1}$$

$$\triangle V = R_e I, \quad R_e = \frac{\rho l}{A} \tag{2}$$

where Q is the flow rate, R_f is the fluid flow resistance, D is the channel hydraulic diameter, l is the channel length, μ is the fluid dynamic viscosity, A is the cross-sectional area, R_e is the electrical resistance, I is the electric current, and ρ is the electric resistivity.

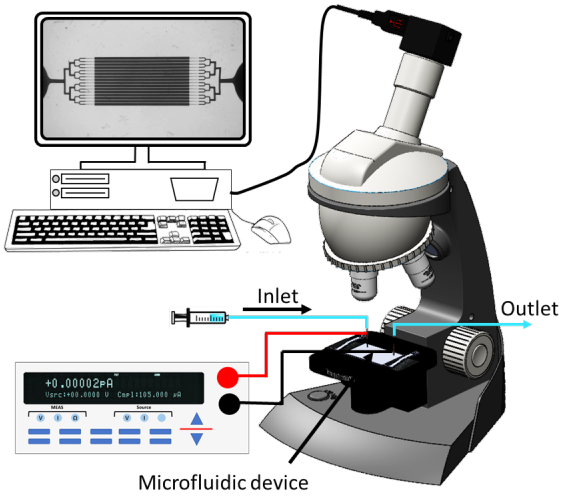

Figure 1. Sketch of our experimental setup consisting of our microfluidic device, a microscope, a camera, a sourcemeter, and a computer.

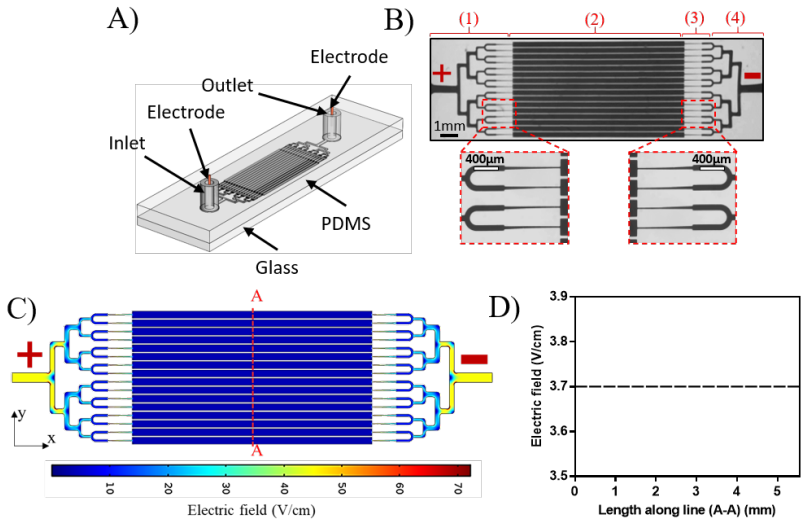

Figure 2. (**A**) Schematic of the parallel electrotaxis microfluidic chip (3 cm × 1.5 cm) consisting of one inlet and one outlet that are connected by four modules shown in (**B**): (1) worm loading and distribution channels, (2) 16 parallel electrotaxis screening channels, (3) tapered channels for worm immobilization and imaging, and (4) unloading channels. (**C**) Electric field distribution throughout the chip simulated using COMSOL by applying 50 V to achieve a constant electric field of 3.7 V/cm in electrotaxis screening channels (**D**).

Two-dimensional steady-state COMSOL simulations (accessed via CMC Microsystems) were conducted to estimate the electric field across the channels (see Appendix B for details). Fluid electric conductivity was obtained experimentally using a 3 cm-long and 300 µm-wide channel. Using custom-written MATLAB code, various voltages were applied, and the electric current across the channel was obtained to calculate the channel's electric resistance. Using the electric resistance and the known channel dimensions in Equation (2), the fluid electric conductivity was found to be approximately 1.6 siemens/m. Figure 2C shows the electric field distribution across the microfluidic chip at a constant electric voltage of 5 0V. No electric field variation was observed along line A-A in Figure 2C, and the electric field (EF) was 3.7 V/cm across all the channels (Figure 2D). The obtained EF satisfied the required EF range of 2–4 V/cm needed for young adult *C. elegans'* electrotaxis [28].

2.4. Experimental Methodology

Young adult worms were loaded into the microchannel using a syringe and pushed slowly until all the tapered entrance channels were occupied by worms (Supplementary Materials Video S1). Next, the worms were manually pressure-pulsed and placed in the screening channels (Figure 3A). In 5 trials, N = 12 $\pm$ 3 worms were successfully loaded into channels.

To permit free swimming, the flow rate was brought to zero by releasing the loading pressure and letting the worms stabilize in the channel. A constant DC electric field of 3.7 V/cm was applied in the screening channels, which initiated the worms' movement towards the cathode for 10 mm (Figure 3A shown for 6-OHDA exposed worms). Once the worms reached the end of the electrotaxis channel, the electric field was reversed, thereby triggering the worms to turn and swim in the opposite direction (Supplementary Materials Video S1). This was repeated twice, and behavioral phenotypes were determined and reported as described below.

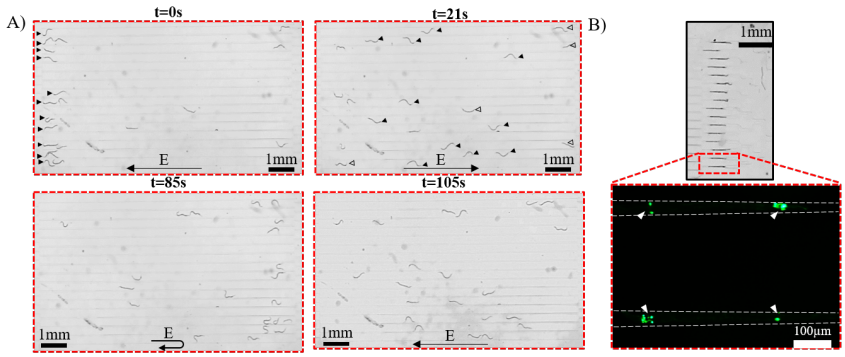

Figure 3. (**A**) Time-lapse images showing electrotaxis of N2 worms in parallel channels after exposure to 250 µM 6-OHDA. Black arrows indicate worms responding towards the cathode, while empty arrows show worms with different phenotypes, such as uncoordinated movement and sudden freezing due to 6-OHDA exposure (EF = 3.7 V/cm). (**B**) Worms trapped in the tapered channels, with a zoom-in on two immobilized BZ555 worms, fluorescently imaged in a healthy state. Arrowheads are showing the dopaminergic neurons (DNs).

The electrotaxis swimming speed and body bend frequency (BBF) were quantified using the automated Worm Tracker plugin in ImageJ software [37]. The electrotaxis turning time (ETT) and electrotaxis time index (ETI) [23,27] were calculated for all conditions and averaged over the three electric field exposure cycles. ETT is the time at which the worm successfully performed a complete turn after an electric field reversal and started to swim towards the cathode. ETI is the ratio between the actual swimming time towards the cathode to the total time of the experiment. It was defined to account for the intermittent stops and reversals happening during the movement towards the cathode. For fluorescent imaging, the worms were aspirated into the trapping channels for imaging (Figure 3B and Video V1).

2.5. Data Analysis

2.5.1. Quantification of Neuron Degeneration

Neurodegeneration was assayed by simultaneously immobilizing the worms using parallel tapered channels (Figure 3B). The worms were imaged using fluorescent microscopy. The images were quantified in terms of their fluorescence intensity using ImageJ software (national institute of Health, NIH, Bethesda, MD, USA) [37]. Briefly, ImageJ software was used to subtract the background of each image using the built-in rolling ball algorithm [38] and we calculated the mean fluorescence intensity (MFI) of the entire image. The drug-treated worms' MFIs were normalized with the control experiments using Microsoft Excel (Microsoft Corp., Redmond, WA, USA).

2.5.2. Statistical Analysis

All the results are presented as mean ± standard error of the mean (SEM), while the difference among the two populations was compared using the Mann–Whitney test. The data were deemed significantly different at a p-value of less than 0.05. The star-based notation was used to identify the significance level as follows: * for $p < 0.05$, ** for $p < 0.01$, *** for $p < 0.001$, and **** for $p < 0.0001$.

3. Results and Discussion

The performance of our device was first confirmed by investigating the electrotaxis responses of wild type worms. As shown in Figure 4, N2 worms showed an average speed of 406 ± 36 µm/s, turning time of 3.5 ± 0.48 s, and BBF of 1.6 ± 0.125 Hz. These results matched the previously published electrotaxis results in a single channel device with an electric field of 4 V/cm [29] (see Appendix C for details), highlighting the applicability of our method for multi-worm electrotaxis screening. N = 12 ± 3 worms could be successfully loaded and tested in our device, with the assay taking on average six minutes for all worms. This significantly reduced the electrotaxis test time for each worm from 3–4 min [28] to about 30 s in our parallel-channel device.

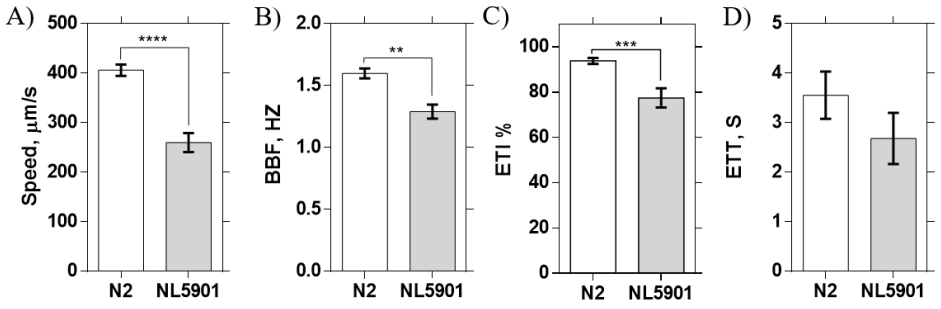

Figure 4. Application of the microfluidic device to mutant screening using NL5901 strain expressing α-syn (N = 19/21 responders) at EF = 3.7V/cm. (**A**) Worm speed, (**B**) body bend frequency (BBF), (**C**) electrotaxis time index (ETI) of responder worms, and (**D**) electrotaxis turning time (ETT). Error bars are SEM; *: $p < 0.05$; **: $p < 0.01$; ***: $p < 0.001$; ****: $p < 0.0001$.

3.1. α-syn Aggregation Effect on C. elegans' Electrotaxis

Parallel electrotaxis was then used to perform mutant screening. We conducted experiments on NL5901 worms expressing α-syn in muscle cells. α-syn is a protein that aggregates to create insoluble fibrils that coalesce in cytoplasmic inclusions called Lewy bodies, a pathological hallmark of PD [17,39]. Transgenic worm lines expressing α-syn have been reported to show reduced lifespans, motility, and pharyngeal pumping rates. [40] Thus, we aimed to examine whether α-syn overexpression in muscles alters stimuli-evoked behavioral responses, such as electrotaxis, to identify genetically-induced

movement deficits. Figure 4 shows that α-syn overexpression induced significant decreases in the worms' average speed, BBF, and ETI, whereas no effect on the ETT was observed. These findings implied that α-syn aggregation in muscles affect the worms' response to the electric field, causing a decrease in worm motility and difficulty for the worm to maintain continuous swimming towards the cathode (as per low ETI). In the future, it would be interesting to test a strain with α-syn overexpression in DNs to interrogate the behavioral effect of protein aggregation inside the neurons.

3.2. Chemical Screening Using a PD-Related Neurotoxin

To further demonstrate the application of our device in chemical screening, worms' electrotaxis response after exposure to 6-OHDA was studied. 6-OHDA is a neurotoxin that has been reported to induce PD-like symptoms by selectively degenerating the DNs. [19] DNs take up 6-OHDA through the dopamine transporter DAT-1, which leads to oxidative stresses and cell death. [41] Changes in dopamine levels will result in various neurological disorders, including PD. In this test, N2 and the transgenic strain BZ555, which expressed GFP in the DNs, were used to screen for mobility defects upon electric field stimulation (Figure 5A) and neurodegeneration upon exposure to 250 µM 6-OHDA. Typically, the untreated N2 and BZ555 worms exhibited normal swimming speed, BBF, and ETT, and high ETI, attributed to their healthy state, whereas the 6-OHDA treated worms showed a slower response in terms of swimming speed, BBF, and ETI. After electrotaxis screening of BZ555 worms, the DNs were fluorescently imaged in the tapered channels (Figure 3B and Figure 5B-i), and their MFI was quantified (Figure 5B-ii). The untreated worms' DNs were intact with strong GFP expression, contrary to the treated worms, which showed a reduction in the MFI due to the partial loss of DNs upon exposure to the neurotoxin.

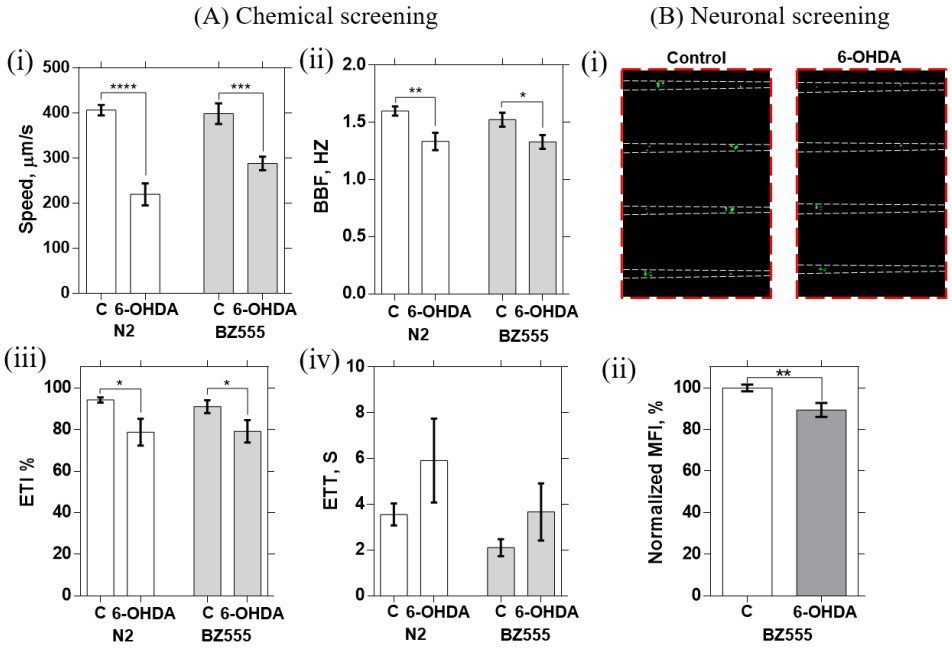

Figure 5. Application of the microfluidic device to chemical and neural screening at EF = 3.7 V/cm using N2 (wild-type) (N = 16/17 responders for control and N = 27/29 responders for exposed worms) and BZ555 strain (N = 19/20 responders for control and N = 24/29 responders for exposed worms) exposed to 250 µM 6-OHDA (controls are shown by "C"). (i) Worm speed, (ii) body bend frequency (BBF), (iii) rlectrotaxis turning time (ETT), and (iv) electrotaxis time index (ETI). Error bars are SEM; *: $p < 0.05$; **: $p < 0.01$; ***: $p < 0.001$; ****: $p < 0.0001$.

4. Conclusions

In conclusion, this work demonstrated an easy to operate, simple to fabricate, and reusable microfluidic device for the analysis of the electrotaxis responses of multiple worms at single animal resolution. We showed that this device can be used in a wide range of *C. elegans* assays wherein movement and cellular phenotypes need to be investigated on large groups of specimens, such as neurodegenerative disease studies and chemical screening. Moreover, considering the limitations associated with microfluid devices' integrability in biological laboratories, we developed our device to be simple to use by an end-user with the aid of syringes and a power supply; it also increased the number of worms that can be tested simultaneously, achieving at least nine worms every 5 min, which has not been achieved previously for electrically induced-behavioral assays even with automated systems. We envision that although automating this system will add complexity to it, it could help the throughput to reach to more than 100 worms per hour in the future.

Supplementary Materials: The following are available at http://www.mdpi.com/2072-666X/11/8/756/s1, Video S1: Worm loading, electrotaxis testing, and the neuron imaging procedure in the microfluidic device.

Author Contributions: K.Y.: methodology, investigation, formal analysis, validation, data curation, visualization, and writing—original draft. D.A.: data curation and writing—original draft. T.K.: conceptualization and writing—review and editing. A.T.: supervision, validation, and writing—review and editing. P.R.: conceptualization, methodology, validation, resources, writing—review and editing, supervision, and funding acquisition. All authors have read and agreed to the published version of the manuscript.

Funding: This work was supported by Natural Sciences and Engineering Research Council (NSERC) of Canada, the Ontario Early Researcher Award to P.R., and the Ontario Trillium Scholarship to K.Y.

Acknowledgments: We would like to acknowledge CMC Microsystems for the provision of products that facilitated this research, including COMSOL Multiphysics®.

Conflicts of Interest: The authors declare no conflict of interest.

Appendix A. Microfluidic Chip Fabrication

The conventional photolithography [34] technique was used to fabricate a 60 µm-thick monolayer SU8-mold. A pre-treated 4 inch Si wafer was used as a substrate. Four milliliters of the negative SU-8 2035 photoresist was poured and pre-spun at 500 rpm for five seconds. Then, to achieve a thickness of 60 µm, the spinning speed increased to 1700 rpm for 30 s, followed by soft-backing at 65 °C for 1.5 min and 95 °C for 7.5 min. A computer-aided design was sketched and printed as a 25,000 DPI transparency photomask (CAD\Art Services Inc., USA). UV-KUB2 (KOLE, France) was used to expose the Si wafer, using the transparency mask, to ultraviolet light at 365 nm with a power of 10 mW/cm^2 for 18 seconds, followed by post-backing at 65 °C for one minute and 95 °C for six minutes. Finally, the wafer was rinsed with SU8-developer, followed by IPA, and hard-baked at 200 °C for 10 min. A Bruker optical profilometer was used (Bruker Optics, USA) to confirm the wafer's thickness.

The PDMS device was fabricated using the standard soft lithography technique.[33] The inlet and outlet were prepared by attaching a piece of Masterflex tubing (L/S 14 size, Gelsenkirchen, Germany) over the reservoirs on the master mold. A mixture of PDMS elastomer base and curing agent in the ratio of 10:1 was prepared, de-gasified, poured over the Si wafer, and left to cure for two hours at 80 °C. The cured PDMS was peeled off the wafer and bonded irreversibly to glass using oxygen plasma (PDC-001-HP Harrick Plasma, USA) at 870 mTorr pressure and 30 W for 30 s. The electric wires were connected to the inlet and outlet tubes, for electric field stimulation, by punching through the PDMS and sealing with liquid PDMS.

Appendix B. Numerical Simulation of the Electric Field

The commercial software COMSOL Multiphysics® was used to predict the electric field distribution in the microfluidic device. Two-dimensional (2D) numerical simulations were conducted to solve Ohm's law using the steady-state direct-current electric module to obtain the electric field within a conductive media. SOLIDWORKS® software was utilized to generate the computational

domain (Figure 2 of the paper), which was then imported into the COMSOL Multiphysics software for the mesh generation and boundary conditioning. Three boundary condition types were adopted: an electric potential of 50V at one of the end reservoirs, ground for the other end, and electric insulation for all other boundaries. M9 was used as the conductive media, and its electric conductivity was found experimentally to be approximately 1.6 siemens/meter. The number of meshes was set to be approximately 1.5×10^6 after conducting a mesh independency study. Figure 2C of the main paper illustrated the electric field distribution across the microfluidic device, showing that the electric field is constant across each electrotaxis channel and consistent across other channels.

Appendix C. Comparison of Multi-Worm and Single Worm Electrotaxis Assay

In the conventional electrotaxis assay, a single worm can be stimulated to swim towards the negative pole, and some behavioral phenotypes, including speed, body bend frequency (BBF), electrotaxis time index (ETI), and electrotaxis turning time (ETT) are quantified. Here, we present a multi-worm electrotaxis assay for 16 worms in parallel that can provide information for the same phenotypes and image the worms fluorescently using a tapered channel immobilization technique, which has not been achieved previously in the single worm electrotaxis assay.

C. elegans electrotaxis has been studied in terms of crawling on open agar gel surfaces or swimming in media inside microfluidic devices. For instance, in 2007, Gabel et al. [24] studied the electrotaxis behavior of *C. elegans* on open gel surfaces using two stereotyped maneuvers, but movement speed was not reported. Then, Manière et al. [25] studied the same behavior in open gel surfaces and reported a crawling speed of 110 ± 50 μm/s towards the negative pole. Crawling speed is expected to be lower than swimming speed. Using microfluidic devices, different groups have studied electrotaxis swimming and established that the 300 μm channel width is the optimum dimension for obtaining a proper swimming speed [26–29]. Therefore, we adopted the same channel dimensions and replicated them to make 16 parallel channels for our experiments. In order to verify our technique, we compared the results obtained in our device for wild-type worms with the results obtained by other groups in terms of swimming speed. As shown in Figure A1, we obtained an average swimming speed of 406 ± 36 μm/s; compare that to the results obtained by Rezai et al.[28] and Liu et al. [29] in single channels. That supports the fact that the 300 μm channel is not affecting the worms' movement and the worms in our device are responding normally to the EF as the single-worm electrotaxis assay. It should also be mentioned that the channel width in the range of 300–500 μm has been reported not to have any significant effect on the worms' electrotaxis speed, while channels larger than 300 μm may cause some complexity in the response since the worms will gain freedom to move laterally in the channel and orient themselves at an angle with the electric field. It should also be mentioned that the differences between our results and those of Manière et al. [25] in Figure A1 may stem from differences between swimming and crawling, respectively.

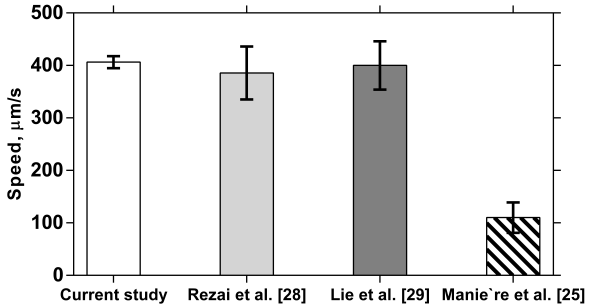

Figure A1. Comparison of the swimming speeds obtained using the multi-worm assay in the current study, and the single worm electrotaxis assays from Rezai et al. [28] and Liu et al. [29], plus the off-chip crawling electrotaxis speed on agar surfaces from Manie 're et al. [25].

References

1. Kinser, H.E.; Pincus, Z. High-throughput screening in the *C. elegans* nervous system. *Mol. Cell. Neurosci.* **2017**, *80*, 192–197. [CrossRef] [PubMed]
2. Leung, C.K.; Wang, Y.; Malany, S.; Deonarine, A.; Nguyen, K.; Vasile, S.; Choe, K.P. An ultra high-throughput, whole-animal screen for small molecule modulators of a specific genetic pathway in *Caenorhabditis elegans*. *PLoS ONE* **2013**, *8*, e62166.
3. O'Reilly, L.P.; Luke, C.J.; Perlmutter, D.H.; Silverman, G.A.; Pak, S.C. *C. elegans* in high-throughput drug discovery. *Adv. Drug Deliv. Rev.* **2014**, *69*, 247–253.
4. Youssef, K.; Tandon, A.; Rezai, P. Studying Parkinson's disease using *Caenorhabditis elegans* models in microfluidic devices. *Integr. Biol.* **2019**, *11*, 186–207. [CrossRef] [PubMed]
5. Wu, Q.; Kumar, N.; Velagala, V.; Zartman, J.J. Tools to reverse-engineer multicellular systems: Case studies using the fruit fly. *J. Biol. Eng.* **2019**, *13*, 33. [CrossRef]
6. Zabihihesari, A.; Hilliker, A.J.; Rezai, P. Fly-on-a-Chip: Microfluidics for Drosophila melanogaster Studies. *Integr. Biol.* **2019**, *11*, 425–443. [CrossRef]
7. Khalili, A.; Rezai, P. Microfluidic devices for embryonic and larval zebrafish studies. *Brief. Funct. Genom.* **2019**. [CrossRef]
8. Youssef, K.; Bayat, P.; Peimani, A.R.; Dibaji, S.; Rezai, P. Miniaturized Sensors and Actuators for Biological Studies on Small Model Organisms of Disease. In *Environmental, Chemical and Medical Sensors*; Springer: Singapore, 2018; pp. 199–225.
9. Gupta, B.P.; Rezai, P. Microfluidic approaches for manipulating, imaging, and screening *C. elegans*. *Micromachines* **2016**, *7*, 123. [CrossRef]
10. Li, J.; Le, W. Modeling neurodegenerative diseases in Caenorhabditis elegans. *Exp. Neurol.* **2013**, *250*, 94–103. [CrossRef]
11. Wolozin, B.; Gabel, C.; Ferree, A.; Guillily, M.; Ebata, A. Watching worms whither: Modeling neurodegeneration in C. elegans. In *Progress in Molecular Biology and Translational Science*; Elsevier: Amsterdam, The Netherlands, 2011; Volume 100, pp. 499–514.
12. Markaki, M.; Tavernarakis, N. Modeling human diseases in Caenorhabditis elegans. *Biotechnol. J.* **2010**, *5*, 1261–1276. [CrossRef]
13. Chen, X.; Barclay, J.W.; Burgoyne, R.D.; Morgan, A. Using C. elegans to discover therapeutic compounds for ageing-associated neurodegenerative diseases. *Chem. Cent. J.* **2015**, *9*, 65. [CrossRef] [PubMed]
14. Giráldez-Pérez, R.M.; Antolín-Vallespín, M.; Muñoz, M.D.; Sánchez-Capelo, A. Models of α-synuclein aggregation in Parkinson's disease. *Acta Neuropathol. Commun.* **2014**, *2*, 176. [CrossRef]
15. Lee, Y.; Dawson, V.L.; Dawson, T.M. Animal models of Parkinson's disease: Vertebrate genetics. *Cold Spring Harb. Perspect. Med.* **2012**, *2*, a009324. [CrossRef] [PubMed]
16. Harrington, A.J.; Hamamichi, S.; Caldwell, G.A.; Caldwell, K.A. *C. elegans* as a model organism to investigate molecular pathways involved with Parkinson's disease. *Dev. Dyn. Off. Publ. Am. Assoc. Anat.* **2010**, *239*, 1282–1295.
17. Visanji, N.P.; Brotchie, J.M.; Kalia, L.V.; Koprich, J.B.; Tandon, A.; Watts, J.C.; Lang, A.E. α-Synuclein-based animal models of Parkinson's disease: Challenges and opportunities in a new era. *Trends Neurosci.* **2016**, *39*, 750–762. [CrossRef]
18. Alexander, A.G.; Marfil, V.; Li, C. Use of *Caenorhabditis elegans* as a model to study Alzheimer's disease and other neurodegenerative diseases. *Front. Genet.* **2014**, *5*, 279. [CrossRef] [PubMed]
19. Cooper, J.F.; Van Raamsdonk, J.M. Modeling Parkinson's Disease in *C. elegans*. *J. Park. Dis.* **2018**, *8*, 17–32. [CrossRef]
20. Ma, H.; Jiang, L.; Shi, W.; Qin, J.; Lin, B. A programmable microvalve-based microfluidic array for characterization of neurotoxin-induced responses of individual *C. elegans*. *Biomicrofluidics* **2009**, *3*, 044114. [CrossRef]
21. Shi, W.; Wen, H.; Lu, Y.; Shi, Y.; Lin, B.; Qin, J. Droplet microfluidics for characterizing the neurotoxin-induced responses in individual *Caenorhabditis elegans*. *Lab A Chip* **2010**, *10*, 2855–2863. [CrossRef]
22. Mondal, S.; Hegarty, E.; Martin, C.; Gökce, S.K.; Ghorashian, N.; Ben-Yakar, A. Large-scale microfluidics providing high-resolution and high-throughput screening of *Caenorhabditis elegans* poly-glutamine aggregation model. *Nat. Commun.* **2016**, *7*, 1–11. [CrossRef]

23. Youssef, K.; Archonta, D.; Kubiseski, T.J.; Tandon, A.; Rezai, P. Semi-mobile *C. elegans* electrotaxis assay for movement screening and neural monitoring of Parkinson's disease models. *Sens. Actuators B Chem.* **2020**, *316*, 128064. [CrossRef]
24. Gabel, C.V.; Gabel, H.; Pavlichin, D.; Kao, A.; Clark, D.A.; Samuel, A.D. Neural circuits mediate electrosensory behavior in *Caenorhabditis elegans*. *J. Neurosci.* **2007**, *27*, 7586–7596. [CrossRef] [PubMed]
25. Manière, X.; Lebois, F.; Matic, I.; Ladoux, B.; Di Meglio, J.M.; Hersen, P. Running worms: *C. elegans* self-sorting by electrotaxis. *PLoS ONE* **2011**, *6*, e16637. [CrossRef] [PubMed]
26. Han, B.; Kim, D.; Ko, U.H.; Shin, J.H. A sorting strategy for *C. elegans* based on size-dependent motility and electrotaxis in a micro-structured channel. *Lab Chip* **2012**, *12*, 4128–4134. [CrossRef] [PubMed]
27. Salam, S.; Ansari, A.; Amon, S.; Rezai, P.; Selvaganapathy, P.R.; Mishra, R.K.; Gupta, B.P. A Microfluidic Phenotype Analysis System Reveals Function of Sensory and Dopaminergic Neuron Signaling in C. elegans Electrotactic Swimming Behavior. In *Worm*; Taylor & Francis: Abingdon, UK, 2013; Volume 2, p. e24558.
28. Rezai, P.; Siddiqui, A.; Selvaganapathy, P.R.; Gupta, B.P. Electrotaxis of *Caenorhabditis elegans* in a microfluidic environment. *Lab A Chip* **2010**, *10*, 220–226. [CrossRef] [PubMed]
29. Liu, D.; Gupta, B.; Selvaganapathy, P.R. An automated microfluidic system for screening Caenorhabditis elegans behaviors using electrotaxis. *Biomicrofluidics* **2016**, *10*, 014117. [CrossRef]
30. Porta-de-la Riva, M.; Fontrodona, L.; Villanueva, A.; Cerón, J. Basic Caenorhabditis elegans methods: Synchronization and observation. *JoVE J. Vis. Exp.* **2012**, e4019. [CrossRef]
31. Van Ham, T.J.; Thijssen, K.L.; Breitling, R.; Hofstra, R.M.; Plasterk, R.H.; Nollen, E.A. *C. elegans* model identifies genetic modifiers of α-synuclein inclusion formation during aging. *PLoS Genet.* **2008**, *4*, e1000027. [CrossRef]
32. Pu, P.; Le, W. Dopamine neuron degeneration induced by MPP+ is independent of CED-4 pathway in *Caenorhabditis elegans*. *Cell Res.* **2008**, *18*, 978–981. [CrossRef]
33. Xia, Y.; Whitesides, G.M. Soft lithography. *Annu. Rev. Mater. Sci.* **1998**, *28*, 153–184. [CrossRef]
34. Rezai, P.; Wu, W.; Selvaganapathy, P. Microfabrication of polymers for bioMEMS. In *Mems for Biomedical Applications*; Woodhead Publishing: Cambridge, UK, 2012; pp. 3–45.
35. Hulme, S.E.; Shevkoplyas, S.S.; Apfeld, J.; Fontana, W.; Whitesides, G.M. A microfabricated array of clamps for immobilizing and imaging *C. elegans*. *Lab A Chip* **2007**, *7*, 1515–1523. [CrossRef] [PubMed]
36. Oh, K.W.; Lee, K.; Ahn, B.; Furlani, E.P. Design of pressure-driven microfluidic networks using electric circuit analogy. *Lab A Chip* **2012**, *12*, 515–545. [CrossRef] [PubMed]
37. Schindelin, J.; Arganda-Carreras, I.; Frise, E.; Kaynig, V.; Longair, M.; Pietzsch, T.; Preibisch, S.; Rueden, C.; Saalfeld, S.; Schmid, B.; et al. Fiji: An open-source platform for biological-image analysis. *Nat. Methods* **2012**, *9*, 676–682. [CrossRef] [PubMed]
38. Vitulano, S.; Di Ruberto, C.; Nappi, M. Biomedical image processing human perception modeling. In Proceedings of the Third International Conference on Electronics, Circuits, and Systems, Rodos, Greece, 13–16 October 1996; Volume 2, pp. 1116–1119.
39. Kavallaris, M.; Ng, D.; Byrne, F. *Cytoskeleton and Human Disease*; Humana Press: Totowa, NJ, USA, 2012.
40. Bodhicharla, R.; Nagarajan, A.; Winter, J.; Adenle, A.; Nazir, A.; Brady, D.; Vere, K.; Richens, J.; O'Shea, P.; R Bell, D.; et al. Effects of α-synuclein overexpression in transgenic *Caenorhabditis elegans* strains. *CNS Neurol. Disord.-Drug Targets (Formerly Curr. Drug Targets-CNS Neurol. Disord.* **2012**, *11*, 965–975. [CrossRef]
41. Offenburger, S.L.; Ho, X.Y.; Tachie-Menson, T.; Coakley, S.; Hilliard, M.A.; Gartner, A. 6-OHDA-induced dopaminergic neurodegeneration in *Caenorhabditis elegans* is promoted by the engulfment pathway and inhibited by the transthyretin-related protein TTR-33. *PLoS Genet.* **2018**, *14*, e1007125. [CrossRef]

B.2 Paper II: Semi-mobile *C. elegans* electrotaxis assay for movement screening and neural monitoring of Parkinson's disease models

Youssef, K., Archonta, D., Kubiseski, T. J., Tandon, A., & Rezai, P. (2020). Semi-mobile *C. elegans* Electrotaxis Assay for Movement Screening and Neural Monitoring of Parkinson's Disease Models. Sensors and Actuators B: Chemical, 316, 128064.

Sensors & Actuators: B. Chemical 316 (2020) 128064

Contents lists available at ScienceDirect

Sensors and Actuators B: Chemical

journal homepage: www.elsevier.com/locate/snb

Semi-mobile *C. elegans* electrotaxis assay for movement screening and neural monitoring of Parkinson's disease models

Khaled Youssef[a], Daphne Archonta[a], Terrance J. Kubiseski[b], Anurag Tandon[c,d], Pouya Rezai[a,*]

[a] Department of Mechanical Engineering, York University, Toronto, ON, Canada
[b] Department of Biology, York University, Toronto, ON, Canada
[c] Tanz Centre for Research in Neurodegenerative Diseases, Toronto, Ontario, Canada
[d] Department of Medicine, University of Toronto, Toronto, Ontario, Canada

ARTICLE INFO

Keywords:
Microfluidics
C. elegans electrotaxis
Parkinson's model
Movement impairment
Neurodegeneration

ABSTRACT

Microfluidic-based electrotaxis assay is a quantitative movement phenotyping technique for behavioral studies on *Caenorhabditis (C.) elegans* which is currently space-consuming and limited for cell imaging. To address these limitations and show applications in Parkinson's Disease (PD) studies, we introduce a novel microfluidic device to investigate the electrotaxis of semi-mobile *C. elegans* and image them immediately after the behavioral assay. The device consisted of an electrotaxis screening channel integrated with a perpendicular tapered microchannel that was used for worm tail or head trapping for electrotaxis screening and full-body immobilization for neuron imaging. Semi-mobile *C. elegans* with trapped tails demonstrated electrotaxis orientation towards the cathode. Interestingly, the response of head-trapped worms was also with the tail towards the cathode, implying the involvement of the mid-body to tail sensory neurons in electrotaxis. Moreover, semi-mobile *C. elegans* electrotaxis assay time is 3-folds shorter and 20-folds less space-consuming, compared to our freely moving assay. This makes the technique amenable to parallelization for the design of multi-worm electrotaxis and neuronal screening devices. For biological application to PD studies, we showed that human α-synuclein protein accumulation or exposure to neurotoxin 6-OHDA affected the electrotaxis phenotypes of semi-mobile worms. Moreover, L-DOPA rescued the electrotaxis of 6-OHDA exposed worms. The above behavioral effects of 6-OHDA and L-DOPA corresponded well with the degeneration of dopaminergic neurons and rescue of dopamine transmission, confirmed by on-chip fluorescent imaging. Our technique can be used for PD pathology studies and potentially for other neurobehavioral disorders modeled in *C. elegans*.

1. Introduction

C. elegans is a small-size (~1 mm) roundworm and a promising model organism for biological studies, owing to its experimental advantages of short life span (~ 25 days), fast growth (~ 2–3 days from L1 to the adult stage), and body transparency for in-vivo imaging [1–7]. *C. elegans* connectome has revealed the high level of conserved human orthologs that permit imitating multiple diseases using genetic modifications [3]. For instance, *C. elegans* neuronal system consists of 8 dopaminergic neurons (DNs) and 4 serotonergic neurons. Therefore, it has been used as a model organism for various neurodegenerative diseases such as Alzheimer's disease (AD) [8], Parkinson's disease (PD) [7] and Huntington's disease (HD) [9,10]. *C. elegans* motor responses can be evoked through stimulation of sensory amphid, phasmid, and labial neurons, as well as mechanosensory neurons for behavioural studies, using different stimuli such as chemical compounds, temperature, light, touch and electric field [11].

The ability of an organism to sense an electric field and move towards a desired direction is called electrotaxis or galvanotaxis [12]. It was found to be utilized for navigation and food search across many species like aquatic animals, amphibians, cockroaches, bees, and *C. elegans* [12]. In 1978, Sukul and Croll [13] studied the electrotaxis of *C. elegans* on agar plates and found that cathodal movement was substantial in the range of 3–4 volts. Klein et al. studied the electrotaxis behaviour of L1 to young adult *C. elegans* on agar plates at low and high electric fields [12]. At 0.7 V/cm, the worms moved randomly towards the cathode, while, at 4 V/cm, the worms robustly moved towards the cathode in a specific angle, which formed a V-shaped movement pattern. The behavioral response diminished in L1 and increased with age until it reached the most robust response for L4 and adult worms. Next, Gabel et al. [14] attempted to explore the involvement of genetic and neuronal bases in electrotaxis using the step-wise rotation electric field

* Corresponding author at: BRG 433B, 4700 Keele St, Toronto, ON, M3J 1P3, Canada.
E-mail address: prezai@yorku.ca (P. Rezai).

https://doi.org/10.1016/j.snb.2020.128064
Received 16 December 2019; Received in revised form 26 March 2020; Accepted 30 March 2020
Available online 07 May 2020
0925-4005/

method. Mutation or laser ablation in some genes and sensory neurons showed that genes such as che-2, che-13, eat-4, osm-3, osm-5, osm-6, osm-10 and tax-6 are involved in electrotaxis, and different neurons such as ASJ, ASH, AWC, ASK, and AWB are essential for the electrotactic motor decision making [14].

Microfluidics has emerged as a powerful tool to address the limitations of conventional worm assays by integrating various sensing and actuation techniques on a single chip [15–20]. The sensitivity and precision of microfluidics in immobilizing, stimulating, and imaging the worm have aided in its adoption to develop neural and behavioral screening assays [21,22]. For instance, Johari et al. [17] have developed a force sensing technique using elastomeric PDMS micropillars to measure *C. elegans* muscular forces and locomotion metrics. Qui et al. [19] have exploited the developed sensing technique integrated with optogenetic stimulation of *C. elegans* neuronal system to study muscular forces and locomotion patterns. Recently, Sofela et al. [23] have exploited similar technique to partially immobilize a worm while measuring the changes in the worms' thrashing forces in response to various glucose concentrations. Rezai et al. [24,25] developed microfluidic devices to examine the swimming behaviour of *C. elegans* using direct current or alternate current electric fields while maintaining controlled test conditions in terms of electric field uniformity and strength as well as worms' movement direction. Different developmental stages of *C. elegans* were tested at a wide range of electric fields. It was found that the sensitivity in electrosensation increases with age in microfluidic environments, just like the observation reported by Klein et al. [12]. Ever since, electrotaxis has been used to sort worms based on their age or to demonstrate that electrotaxis impairment is an indicator of *C. elegans* neuron degeneration [16,26–31]. Many neurological disorders, such as PD, result in sensory-motor system malfunctions and behavioural deficiencies such as uncoordinated movement. Therefore, stimulated behavioural responses like electrotaxis can be used as readouts for nervous system investigations and drug screening. For instance, Salam et al. [22] employed electrotaxis of freely moving worms to investigate the movement of neurotoxin-exposed *C. elegans* PD models. Later on, Liu et al. [26] developed a fully automated system for electrotaxis screening of freely moving worms at a throughput of 20 worms per hour. Recently, Chuang et al. [16] exploited electrotaxis to study the effect of exercise in improving age-related degeneration using a worm model of AD in a microfluidic flow chamber.

Although electrotaxis has been proven to be a suitable technique for on-demand sensory-motor screening, the current devices have large footprints and the assays are slow due to the need for the worm to swim for a few centimeters along a channel, especially when multiple worms are required to be monitored. Moreover, previous electrotaxis assays have been conducted by exposing the entire worm to electric field, limiting the possibility of investigating the involvement of neurons or muscles in certain body parts in electrotaxis via exposing desired parts of the worm to electric field. Lastly, on-chip neuronal imaging of the same population of the worms that have been electrotactically screened has not been demonstrated, which is preferred for determining the correlation of electrotaxis deficiency with neurondegeneration.

In this paper, we have addressed the limitations of the electrotaxis assay speed, spatial exposure to electric field, and on-chip neuron imaging using the novel method of semi-mobile worm electrotaxis. For this, a microfluidic device was developed for trapping a worm from its tail or head in a tapered microchannel perpendicular to a main electrotaxis movement monitoring channel. Neural imaging was accomplished by full immobilization of the worm in the trapping channel after electrotaxis monitoring. Pharmacological and genetic PD worm models were studied in our device to show the applicability of semi-mobile worm electrotaxis assay for studying neurodegenerative diseases. We also show the suitability of our technique for screening multiple worms in parallel by replicating the worm trap along the main channel. Our technique has the potential to be integrated with automated worm handling microfluidic systems and data acquisition and analysis tools for future development of parallelized neurobehavioural screening platforms with single-animal monitoring resolution.

2. Experimental

2.1. Chemicals and materials

All chemicals were purchased from Sigma-Aldrich, USA. M9 buffer was obtained by adding 3 g KH_2PO_4, 6 g Na_2HPO_4, 5 g NaCl, and 1 mL 1 M $MgSO_4$ in 1 L distilled water. Bacterial were cultured in L-Broth, prepared by mixing 10 g Bacto-tryptone, 5 g Bacto-yeast, and 5 g NaCl in 1 L distilled water. M9 buffer and L-broth were sterilized by autoclaving. A stock solution of 10 mM 6-hydrodoxybamine (6-OHDA, 636 − 00-0, Sigma-Aldrich) and 0.01 % (w/v) ascorbic acid was prepared by adding 2 mL of autoclaved M9 buffer to 5 mg of 6-OHDA and storing at -20 °C. A 10 mM stock solution of L-DOPA (59-92-7, Sigma-Aldrich) was freshly prepared in M9 buffer.

Silicon (Si) wafers with 4 in diameter and 500 − 550 µm thickness were procured from Wafer World Incorporation, USA. Negative photoresist SU-8 2075 and SU-8 developer were ordered from MicroChem Corporation, USA. Polydimethylsiloxane (PDMS) was purchased from Dow Corning Corporation, USA.

2.2. C. elegans strains, maintenance, and synchronization

C. elegans were grown on standard nematode-growth medium (NGM) agar plates containing *Escherichia coli* (*E. coli*) strain OP50 as a food source at 20 °C. The food source was prepared by inoculating L-Broth media using a single colony of *E. coli* and culturing overnight at 37 °C on a shaker-incubator. As shown in Table 1, wild-type (WT) Bristol N2, NW1229, BZ555, and NL5901 *C. elegans* strains were obtained from the *Caenorhabditis* Genetics Center (University of Minnesota, USA) and used in our studies.

For all the assays, synchronized worms were prepared by Alkaline hypochlorite treatment (bleach-treatment) as previously described [35]. Briefly, eggs were obtained from gravid hermaphrodites by treating them with a solution of 1 mL commercial bleach (125 µL of NaOH and 3.875 mL of double-distilled water) for 10 min. Then, eggs were incubated at 20 °C overnight in 1 mL of M9 buffer and allowed to hatch into L1 larvae. L1 larvae were used either as a control group or exposed to the desired chemical for further testing with our microfluidic chip.

2.3. Chemical exposure of C. elegans

N2, NW1229 and BZ555 strains were treated with a combination of 6-OHDA and L-DOPA trials starting at the L1 stage as per protocols reported by Salam et al. [22]. L1 larvae were collected after synchronization in a microcentrifuge tube and exposed to 100 µM (990 µL of M9 and 10 µL of 6-OHDA stock solution) or 250 µM (975 µL of M9 and 25 µL of 6-OHDA stock solution) 6-OHDA for 1 h in a dark room with gentle mixing and pipetting every 10 min. For L-DOPA testing, the worms were pre- or post-exposed for 1 h to freshly prepared 100µM L-

Table 1
C. elegans strains used in this study.

Strain	Genotype	Description	Ref
N2	WT Bristol	Wild type	
NW1229	evIs111 [F25B3.3::GFP + dpy-20(+)]	Pan-neuronal GFP expression	[32]
BZ555	egIs1 [dat-1p::GFP]	GFP expression in DNs	[33]
NL5901	pkIs2386 [unc-54p:: α-syn::YFP + unc-119(+)]	α-syn YFP expression in muscle cells	[34]

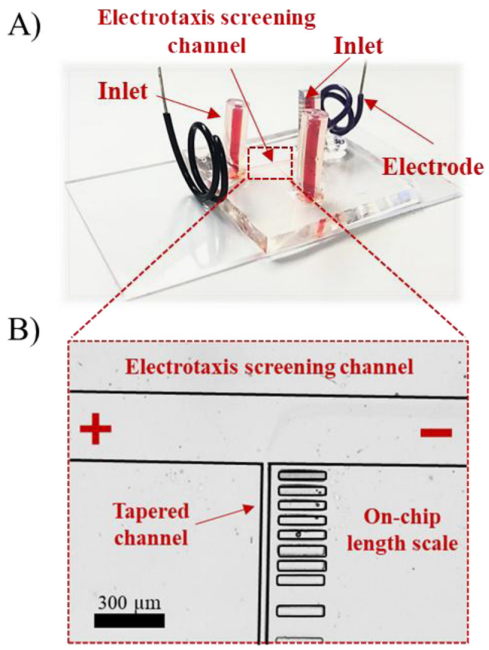

Fig. 1. Microfluidic device for investigating the electrotaxis response of semi-mobile *C. elegans*. (A) 3D schematic of the microfluidic chip consisting of the electrotaxis screening channel with end electrodes and a perpendicular tapered channel for worm partial and full trapping as well as imaging. (B) The T-junction region of the device shown under 5x microscope magnification.

DOPA solutions. After treatment, the worms were washed three times with M9 buffer and incubated for 52 h at 20 °C on OP50/NGM plates. Young adults were washed off the plates and collected for further dilution before the experiments.

2.4. Microfluidic chip design and fabrication

The microfluidic device shown in Fig. 1A was intended to study the electrotaxis response of semi-mobile *C. elegans* in response to a Direct Current (DC) electric field and to image the worm fluorescently. It consisted of two perpendicular 60 µm-thick PDMS microchannels, including an electrotaxis screening channel and a mid-region tapered channel for worm trapping, immobilization and fluorescent imaging (Fig. 1B). The electrotaxis screening channel (2 cm long and 300 µm wide) was connected to two copper-wire electrodes that were used for applying electric field along the channel. To ensure smooth turning of the worm, three different channel widths (300, 400, and 500 µm) were tested primarily. A young adult worm could be trapped from its tail or head using a negative pressure inside the tapered channel, narrowing from 30 µm to 25 µm, leaving the rest of the worm's body free to move inside the electrotaxis channel. An on-chip length scale was incorporated to ensure maintaining the same length of each worm captured during experiments. The same tapered channel was also used to immobilize the whole worm and image it by applying an increased suction pressure after each electrotaxis assay.

To fabricate the microfluidic chip shown in Fig. 1A, a single 60 µm-thick SU-8 layer was fabricated on a Si wafer master mold using the photolithography technique [36]. Then, a negative replica of the master mold was fabricated using the standard soft lithography process [37]. PDMS mixture was poured over the master mold and cured. Then, the peeled PDMS layer was irreversibly bonded to a glass substrate. For electric field stimulation, two copper electrodes were inserted into the inlet and outlet reservoirs of the electrotaxis screening channel (see Section 1 of the Supplementary File for detailed fabrication process).

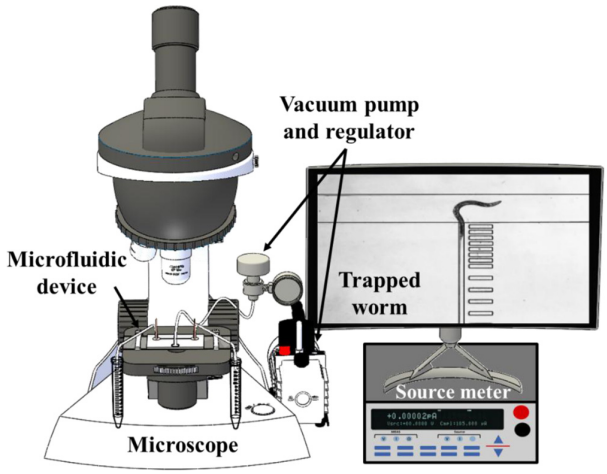

Fig. 2. Experimental setup consisting of the microfluidic chip, a manipulation system (electric sourcemeter, two centrifuge tubes filled with M9, and vacuum pump with a vacuum pressure regulator) and an image acquisition system (inverted Leica microscope, Leica camera, and a monitoring screen).

2.5. Experimental setup and procedures

Fig. 2 shows the experimental setup used to investigate the electrotaxis behaviour of semi-mobile worms with post-screening fluorescent imaging of neurons. The setup consisted of the microfluidic device, a worm manipulation system, and an image acquisition system. The worm manipulation system consisted of a DC sourcemeter (KEITHLEY 2410, Keithley Instruments Inc., USA) and a vacuum pressure regulator (41585K43, Mcmaster-CARR, USA) connected to a vacuum pump (KNF™ Neuberger UN86KTP115 V, USA). Based on the electrotaxis [25] response of freely moving young adult worms, the DC sourcemeter was used to supply an electric voltage of 8 V (equivalent to 4 V/cm electric field) for testing the electrotaxis response of the semi-mobile worms. The electric field polarity was easily reversed using the sourcemeter. The vacuum pump was regulated by a manual controllable vacuum pressure regulator. The image acquisition system consisted of an inverted microscope (DMIL LED Inverted Routine Fluorescence Microscope, Leica, Germany) coupled with a color camera (MC170 HD, Leica, Germany), which was used for capturing fluorescent images and movie clips for neuronal and behavioural analyses, respectively.

The full worm loading procedure is shown in Fig. 3A and Supplementary Video 1. Briefly, a single worm was picked from a synchronized population (Table 1) and loaded into the device already filled with M9 buffer. With the aid of a 15 Kpa negative pressure at the trapping channel and the worms' rheotaxis behavior to swim against the flow, the loaded worm was guided towards the tapered channel. The pressure was lowered to 5–10 Kpa when the worm approached the tapered channel, and it was captured from its tail at the tapered channel. Within a pressure range of 5–10 Kpa used for trapping of worms with slight deviation in their sizes, up to 30 % of the worm's length could be aspired into the tapered channel and immobilized (over 60 % captured at 20 %–30 % of their length). For trapping the head (needed in preliminary assays), the worm was released and recaptured when the head was in the vicinity of the tapered channel. Once the worm was trapped and acclimated to the environment, DC electric field of 4 V/cm [25,38] was applied for 30 s using the sourcemeter, and the worm ability to sense the electric field and turn its free end towards one of the electrodes was investigated (Fig. 3B). Then, the electric field was reversed and maintained for another 30 s while the worm's response was always video recorded (Supplementary Video 1). This was repeated three times for each worm during which the pressure value was not altered. Following the electrotaxis test, the vacuum pressure in the trap

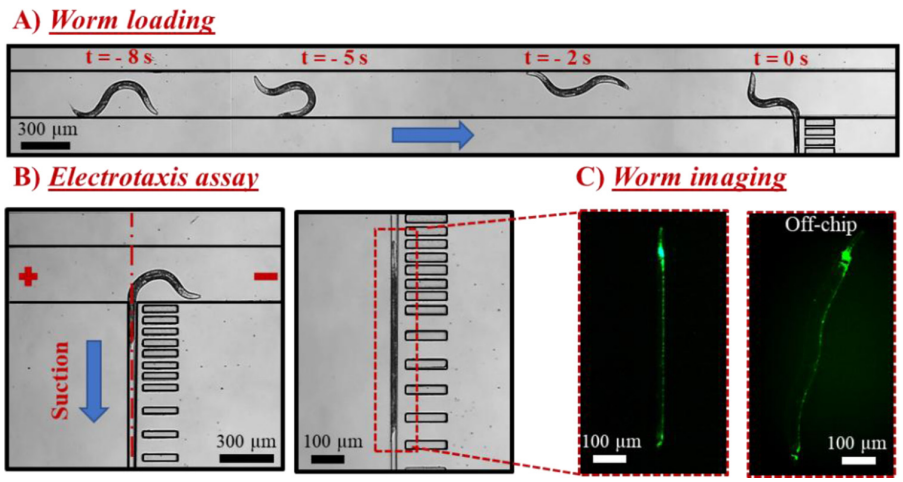

Fig. 3. Operating procedures for capturing and electrotactic testing of semi-mobile *C. elegans*. (A) Time-lapse images of the worm showing a rheotaxis rotation response against the flow (arrow) and orientation with the tail towards the trapping channel right before capturing. (B) Electrotaxis response of a semi-mobile tail-trapped worm under exposure to a 4 V/cm DC electric field (head towards cathode). (C) Immobilized NW1229 worm and fluorescent images inside and outside the microfluidic device.

was increased to approximately 20 kPa, and the worm was pulled into the tapered channel for complete immobilization and fluorescent imaging (Fig. 3C and Supplementary Video 1). Then, the worm was flushed out of the device, and the next worm was loaded for testing. The same procedure was conducted for the 6-OHDA, and L-DOPA treated worms, and their results were compared with their respective control groups.

2.6. Data analysis

2.6.1. Electrotaxis phenotyping

Two phenotypes, namely the worms' Electrotaxis Time Index (ETI) and Electrotaxis Turning Time (ETT), were extracted from the recorded experimental videos to quantify the worms' response to the electric field. These phenotypes were inspired by the work of Salam et al. [22]. ETI was defined as the time consumed by the worm to face the cathode divided by the total time of the experiment, presented in percentiles. Therefore, this phenotype represented the time-lapse behaviour and the worms' ability to maintain a directional preference while the electric field was being applied. ETT was defined as the time taken by the worm to change direction towards the cathode as soon as the electric field was reversed in the channel. Hence, this phenotype represented the spontaneous behaviour of the worms in terms of the speed with which they were able to sense and turn towards a preferred direction. The worm was considered to face the cathode when the head or tail crossed the centerline of the trapping region, shown in Fig. 3B. Overall, three consecutive turns were conducted for each worm, and the ETI and ETT were quantified as an average of the three turns.

2.6.2. Neuron imaging

Following the electrotaxis assay, the worm was immobilized inside the tapered channel and imaged fluorescently. ImageJ software [39] was used to quantify the fluorescence intensity and normalize the data relative to control experiments. Specifically, each raw image was loaded into the software, and the entire image was background subtracted, leaving behind the fluorescent regions of the worm. The subtraction was achieved by the built-in rolling-ball algorithm [40] in ImageJ. Then, the average mean fluorescent intensity (MFI) was calculated for the entire image. This was done three times for each worm to enhance accuracy. All the results were transferred to Microsoft Excel (Microsoft Corp., WA, USA) for normalizing the data with control experiments.

2.6.3. Statistical analysis

Sample size calculation was achieved using the GPower [41] software based on a pilot study and confirmed using the equations presented by Charan et al. [42]. Twenty worms were used in each experiment. All the results were presented as mean ± standard error of the mean (SEM), while the differences among multiple or two populations were compared using one-way ANOVA analysis or Mann-Whitney test, respectively. The groups were considered significantly different at P-value less than 0.05. The significance level was identified by stars, i.e. * for p-value < 0.05, ** for p-value < 0.01, *** for p-value < 0.001, and **** for p-value < 0.0001.

3. Results and discussion

3.1. Electrotaxis of semi-mobile C. elegans

The response of freely moving *C. elegans* to the electric field was studied previously either using a straight microchannel [24,25] or on an agar plate [14]. Movement of the worm for a few centimeters and challenges associated with manipulating it after behavioral assay have made these methods slow, space-consuming and not suitable for neuron imaging. Here, we sought to address these limitations by investigating the electrotaxis of semi-mobile worms, which could make the assay faster and amenable to worm imaging right after electrotaxis phenotyping. In this investigation, we also aimed to study the effect of selective exposure of the worm's head or tail to electricity to explore whether partial exposure will result in a directional electrotaxis behaviour.

Microfluidic devices with different electrotaxis screening channel widths of 300, 400, and 500 µm were fabricated and tested. The 300 µm-wide channel aided in proper guidance of the worm towards the tapered channel and its smooth electrotaxis turning. On the other hand, the 400 and 500 µm wide channels appeared to be large and inappropriate for worm capturing, while the worms sometimes experienced sporadic fluctuations between the cathode and the anode. The same channel width of 300 µm was previously reported to be the most effective size for electrotaxis of freely moving worms by Rezai et al. [25], then used by Han et al. [29] for electrotactic sorting of the worms.

WT young adult *C. elegans* were used to study the electrotaxis response of tail- or head-trapped worms in a device with a screening channel width of 300 µm and under an electric field of 4 V/cm. In the absence of electric field, erratic flapping behavior was observed, and the worms were not able to sustain a specific direction (Supplementary Video 2). Numerical modeling (Supplementary Figure S1) confirmed that the trap had no effect on the electric field distribution in the screening channel when the voltage was applied across the electrotaxis screening channel. As shown in Fig. 4A, a tail-trapped worm responded to the electric field by repeatedly orienting towards the cathode, as reported earlier by Rezai et al. [25] for freely moving *C. elegans*. Out of

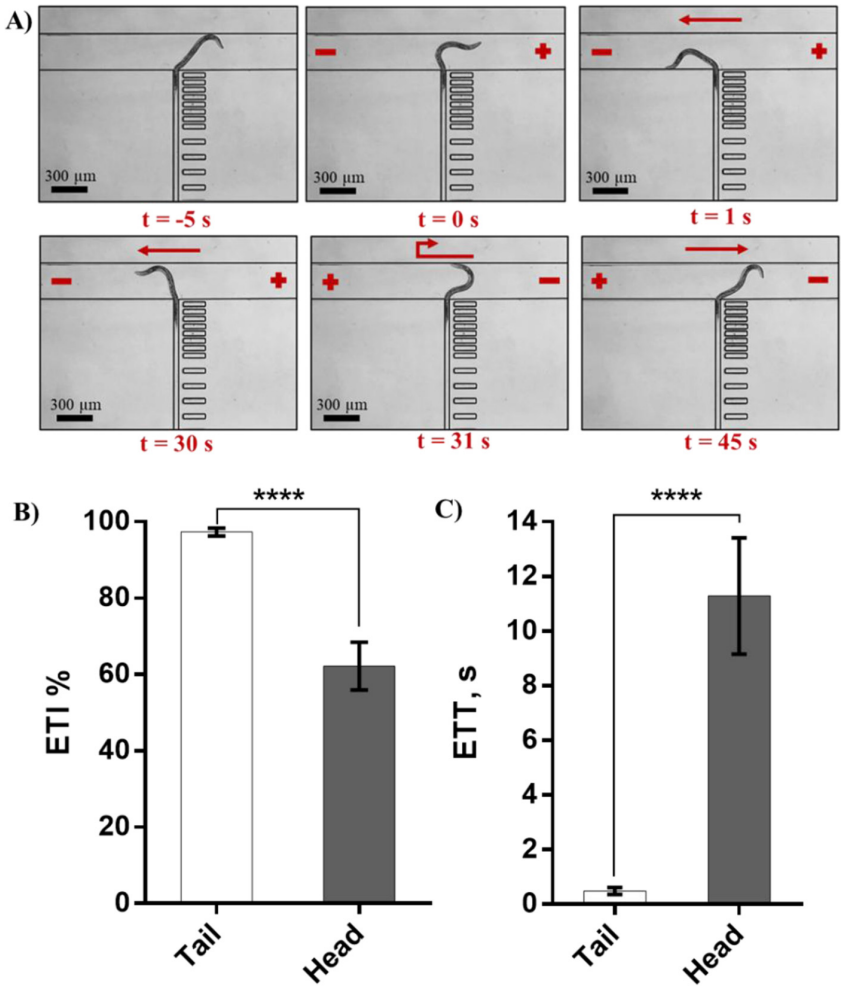

Fig. 4. Electrotaxis response of semi-mobile WT *C. elegans* in the microfluidic device. (A) Time-lapse images showing the electrotaxis response of a semi-mobile tail-trapped *C. elegans* for two consecutive electric field (4 V/cm) reversals at t = 0 s and t = 30 s. Electrotaxis turning time was less than 1 s in both cases. During electric field application, the worm maintained its head towards the cathode, while this behaviour was very sporadic when no electric field was applied. (B) Electrotaxis Time Index (ETI) and (C) Electrotaxis Turning Time (ETT) of responding *C. elegans* (N = 10/10 for tail-trapped and N = 7/10 for head-trapped worms). Error bars are SEM; ****: $p < 0.0001$.

N = 10 tail-trapped worms, all oriented towards the cathode attempting to swim away from the tapered channel (Supplementary Video 3). To our surprise, out of N = 10 head-trapped worms, seven oriented their tails towards the cathode again (Supplementary Video 4). According to Fig. 4B, the head-trapped worms had difficulty maintaining their orientation towards the cathode for an extended period (lower ETT) and showed a significantly slower response time (higher ETI) compared to the tail-trapped worms. These results indicated that either head-trapping severely affected the electrotaxis response of semi-mobile *C. elegans*, or the neurons involved in sensing the electric field direction may be predominantly located at the head to the mid-body of *C. elegans*. Nevertheless, despite the earlier report of electrotaxis sensory neurons being in the head region [14], our results show that excluding the head exposure still results in directional electrotaxis. Further investigation of this hypothesis requires designing devices to control the electrical exposure of worms with higher spatial resolution while applying less mechanical force to the head.

In our conventional electrotaxis assay [25], swimming speed of the worm towards the cathode is quantified along a 3 − 4 cm long microchannel. With an average speed of 350 µm/s [25] for young adult worms and the need for two electric field reversals, each assay takes between 257 s to 343 s to complete. In contrast, our new device enables studying electrotaxis within 90 s inside a more confined area of 1.8 mm by 1.8 mm (see Supplementary Figure S2 for comparison between the two techniques). This will become advantageous in the future for developing parallelized electrotaxis screening microdevices that require arraying and controlling many worms under the microscope field of view (Supplementary Figure S3). In terms of limitations, our device requires worm trapping that may add complexity in operation and is not capable of determining the electrotaxis swimming speed. However, swimming speed has been shown to lack sensitivity for chemical screening while we will show later that phenotypic analysis is achievable by quantification of ETI and ETT parameters in our device.

Due to a more robust response, experiments were continued with tail-trapped worms, starting with investigating the effect of body trapping length on electrotaxis. In these experiments, the worms were captured from their tails in the tapered channel using a suction pressure. Due to the worms' slight variation in length (740–820 µm) and their continuous movement in the device, there was a small variation in their trapped lengths, even though we maintained the suction pressure at a constant value during each experiment. In order to examine if variation in the capturing length influenced the response of the worms, we analyzed the ETI and ETT responses of control strains by categorizing them into four groups with different captured lengths as shown in Fig. 5. It is worth mentioning that out of N = 100 worms analyzed, 61 were captured at approximately 20 %–30 % of their lengths. Based on an ANOVA test between all the groups in Fig. 5, and with no statistical significance detected, we concluded that trapping the worms up to 30 % of their length did not significantly affect their electrotaxis response rate, while the response was diminished when the worms were trapped at or beyond their vulva (data not shown). This result further confirmed our hypothesis of mid-body neurons being involved in electrotaxis, but

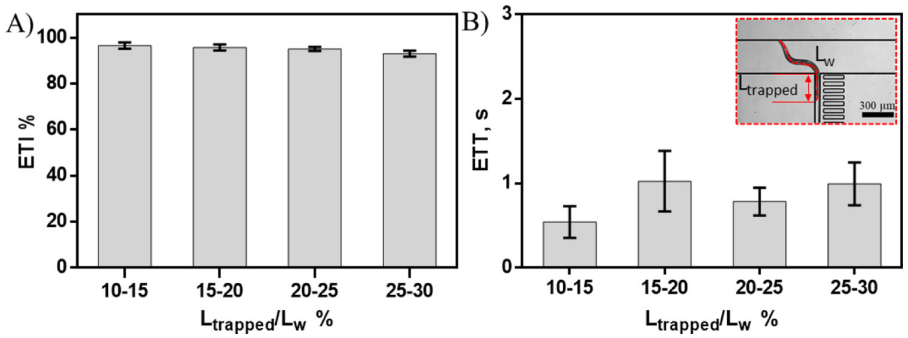

Fig. 5. Effect of worm trapping length ($L_{trapped}$) on the electrotaxis behaviour. (A) Electrotaxis Time Index (ETI), (B) Electrotaxis Turning Time (ETT). Error bars are SEM.

the finding needs further investigation with mutant strains for determining whether the vulva neurons are contributing to electrotaxis, or the behavior deteriorates solely due to the worm confinement. According to this result, the confinement length of the tail-trapped worms was fixed at 20–30 % of the worms' body length for the rest of the experiments. These experiments were conducted with a 300 µm wide electrotaxis screening channel, and ETI and ETT phenotypes of the worms were used to investigate the application of our method in PD worm model studies.

3.2. Effect of α-syn aggregation on the electrotaxis of semi-mobile C. elegans

A variety of transgenic strains have been developed to study the effect of α-syn protein aggregation on the worm's physiological and behavioral responses as a model of PD [43,44]. Here, we asked if α-syn aggregation in muscles (due to availability at the *Caenorhabditis* Genetics Center) affects *C. elegans* electrotaxis and whether our technique is appropriate and sensitive for behavioral phenotyping of this model. NL5901 worms (Table 1) expressing α-syn in muscle cells were loaded into the microfluidic device, and their ETI and ETT phenotypes were determined and compared with WT worms as shown in Fig. 6.

As shown in Fig. 6A, the ETI of NL5901 worms was decreased by ~15 % compared to the WT worms. This indicates that the NL5901 worms spent slightly less time facing the cathode while the electric field was maintained in the device. ETI represents the ability of the worms to maintain electrotaxis directionality for an extended period. Since muscles have been shown to be involved in electrotactic swimming (e.g., mutants with defective muscles reduce electrotaxis speed [22,25,27]), low ETI of NL5901 can be attributed to a small level of α-syn toxicity on their muscles and deteriorated ability to maintain directional motility for a long time, which could be sensed sensitively with our device.

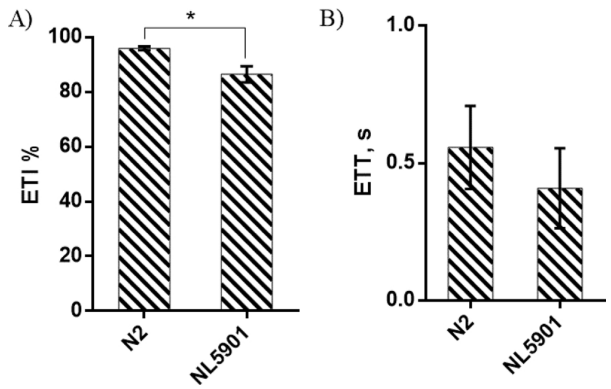

Fig. 6. α-syn aggregation in muscles moderately affects the electrotaxis of *C. elegans* in comparison to the WT worms by reducing their (A) Electrotaxis Time Index (ETI). (B) Electrotaxis Turning Time (ETT) of the worms was not significantly altered by α-syn aggregation in muscles. Error bars are SEM; *: $p < 0.05$.

According to Fig. 6B, the ETT of NL5901 worms in response to the electric field reversal was fast and similar to that of the WT worms. Electrotaxis has been shown to be mediated by sensory neurons [14,25] which are intact in NL5901 strain [43]. Therefore, NL5901 worms were able to sense the electric field reversal in our assay and turn towards the cathode spontaneously just like the WT worms. All in all, α-syn aggregation in muscles did not affect the ability of the worms to sense and turn quickly towards the cathode but slightly affected their ability to maintain a directional preference for an extended period (requiring engaging the muscles for a long time).

Our results, in terms of α-syn overexpression slightly altering the worms' electrotaxis, match with the earlier reports on the natural locomotion behavior of NL5901 worms. For instance, α-syn overexpression has been shown to significantly reduce the lifespan, locomotor activity, and pharyngeal pumping of NL5901 [27,43]. Altogether, our results indicated the potential of our technique to be used for mutant screening using electrotaxis of semi-mobile worms as an on-demand, phenotypic, and quantitative behavioral assay. An interesting line of research that can be pursued in the future is on worms overexpressing α-syn in DNs, which are also known to be affected in PD.

3.3. Effect of 6-OHDA on the electrotaxis of semi-mobile C. elegans and its relation to neurodegeneration

The neurotoxin 6-OHDA has been proven to induce DNs degeneration and cause PD-like symptoms in various vertebrates and invertebrates [45,46]. In *C. elegans*, eight DNs are anatomically located in the head (two pairs of cephalic deirids (CEPs) and a pair of anterior deirids (ADEs)) and the tail (a pair of posterior deirids (PDEs)) regions. Thus, *C. elegans* has been exploited as a pharmacological model to screen for different antiparkinsonian drugs [44]. Our goal was to study the unknown effect of 6-OHDA on the electrotaxis of semi-mobile worms and its possible correlation with neurodegeneration using WT and two transgenic strains, i.e., NW1229 and BZ555 (Table 1). In each experiment, synchronized worms were randomly picked from the plates without any preferences and loaded into the device. Their electrotaxis ETI and ETT phenotypes as well as their neurodegeneration in response to 6-OHDA at 100 and 250 µM concentrations were investigated in comparison to unexposed control animals. The results are shown in Fig. 7.

Our behavioral results in Fig. 7A showed that the untreated worms exhibited a strong response to the electric field as demonstrated by their high ETIs (N2: 96 %, NW: 98 %, BZ: 95 %) and fast ETTs (N2: 0.8 s, NW: 0.55 s, BZ: 0.5 s). However, the worms treated with 6-OHDA exhibited

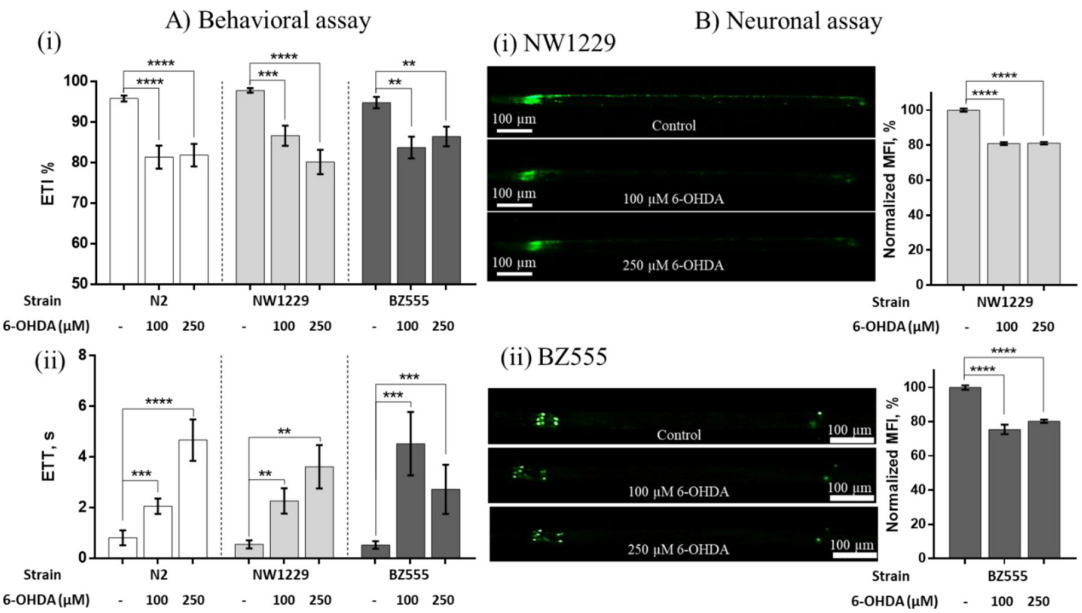

Fig. 7. Electrotaxis response and neurodegeneration of three *C. elegans* strains treated with 100μM and 250μM 6-OHDA. (A) Electrotaxis response of semi-mobile *C. elegans* phenotypically characterized in terms of (i) ETI and (ii) ETT. (B) 6-OHDA induced neuron degeneration of (i) NW1229 and (ii) BZ555 worms shown by fluorescent images and normalized mean fluorescent intensities (MFI). Error bars are SEM; **: $p < 0.01$; ***: $p < 0.001$; ****: $p < 0.0001$.

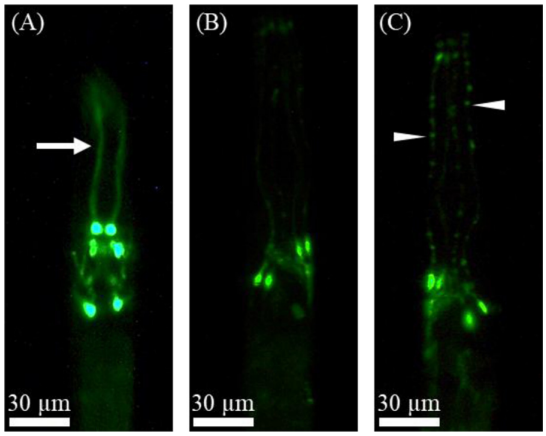

Fig. 8. DNs degeneration in 6-OHDA treated BZ555 worms, demonstrated by dat-1::GFP expression. (A) An untreated control worm showing strong GFP signal in DNs and dendrites (white arrow). 100 and 250 μM 6-OHDA treated worms showed a significant decrease in GFP expression with (B) missing and (C) blebbing dendrites with spotty appearance of GFP signal (white arrowheads).

noticeable electrotaxis defects. This is indicated by their significantly lower ETIs to maintain electrotaxis orientation for a long time, and slower ETTs to respond to electric field reversals in a rapid manner. Moreover, the 100μM and 250μM 6-OHDA concentrations induced similar effects on the ETI and ETT, showing that the effect of 6-OHDA on the electrotaxis behaviour of semi-mobile worms is dose-independent at the examined range.

Some qualitative behaviors that we observed were complete paralysis (Supplementary Video 5), sluggishness (Supplementary Video 6), and uncoordinated movement (distracted flapping) (Supplementary Video 7) upon exposure of the worms to 6-OHDA. On the Petri dish, most of the worms seemed vigorous without any alteration in normal locomotion, providing that electrically evoked responses are useful for qualitative assessment of worms as needed in some assays. The frequency of paralysis and sluggish movement increased with exposure of the worms to 6-OHDA. Since we were interested in quantifying the effect of this toxicant on electrotaxis, worms with complete paralysis and uncoordinated movement were excluded from our phenotypic analysis. Worms with sluggish but coordinated movement were analyzed since the effect of this behaviour was captured by the ETI and ETT parameters in Fig. 7A, resulting in lowering the ETI and increasing the ETT of the exposed worms.

To investigate the relationship between the 6-OHDA induced electrotactic response deficiency with neurons degeneration, NW1229 and BZ555 strains which respectively express GFP in all neurons (Fig. 7B–i) and the eight DNs (Fig. 7B–ii) were tested. Following the electrotaxis test, worms were immobilized in the trapping region of the device for fluorescent imaging. The overall GFP intensities in various 6-OHDA exposure conditions were normalized by the values obtained for the control untreated worms. The untreated worms showed intact neurons with strong and consistent GFP signals and healthy-looking ventral cord neuron (VCN) and DNs. However, the treated worms showed significant 6-OHDA induced GFP signal loss (~20 %) at 100μM and 250μM concentrations, shown in Fig. 7B, as well as the disappearance of the VCN and exhibition of discontinuous dendrites. Reduction in GFP expression has been repeatedly linked with neuron degeneration in *C. elegans* 6-OHDA models [4,5,47–49]. Other abnormal phenotypes that were observed in the BZ555 treated worms were blebbing and missing dendrites as shown in Fig. 8.

Similar to the electrotaxis behavior, the two 6-OHDA concentrations showed indifferent neuronal degeneration effects. Interestingly, a decrease of approximately 20 % was obtained for both GFP expression of neurons and the ETI after exposure of the worms to 6-OHDA. This analogy between the level of neuronal degeneration and the deficiency in electrotaxis behaviour supports the appropriateness of our technique for neurobehavioural screening of *C. elegans*.

Our results in Fig. 7B show that the effect of 6-OHDA at 100–250 μM concentration is not specific towards the DNs. Once the 6-OHDA effect is established, all the neurons (including DNs) gradually degenerate, and the worms show defective ETI and ETT responses. These results are in-line with previously-published off-chip and on-chip assays that presented defective foraging behaviour [45] and locomotor rate [22] of *C.*

elegans in exposure to 6-OHDA. However, due to the high sensitivity of our assay, we were able to detect these effects at an order of magnitude lower concentrations of 6-OHDA in contrary to the reported off-chip assays that are commonly conducted at 5 – 50 mM 6-OHDA. These concentrations usually induce catastrophic defects and lethality. For instance, N2 worms were exposed to 5 mM 6-OHDA and tested using our chip. However, the worms showed a high degree of electrotaxis deficiency and were paralyzed when exposed to electric field, which hindered our ability to perform the phenotypic electrotaxis assay (Supplementary Video 8). Accordingly, our microfluidic platform appears to be a delicate and sensitive tool to study neurodegeneration and detect behavioral and neuronal abnormalities at low concentration levels of drugs. All in all, our assay has provided an electrotaxis-based screening technique integrated with worm immobilization which enhances the conventional electrotaxis assays in terms of speed and capability of fluorescent imaging.

3.4. Effect of L-DOPA against 6-OHDA induced neurodegeneration and electrotaxis impairment in semi-mobile C. elegans

DNs release dopamine, a neurotransmitter responsible for transmitting signals between nerve cells to control body movements [50]. Disruption in the dopamine level causes PD-related movement disorders. The most effective therapeutic way to adjust the dopamine level for PD patients involves screening of small molecules that unlike dopamine, can cross the blood-brain barrier and palliate the disease symptoms. L-DOPA is the precursor to dopamine and is commonly used as a drug for PD. The therapeutic effect of L-DOPA against 6-OHDA has been shown using the behavioral phenotypes and cellular markers of *C. elegans* [45]. Here, we aimed to determine the unknown effect of L-DOPA on the electrotaxis behavior, taking both approaches of using the drug as a pre- and post-treatment. For this, NW1229 and BZ555 worms, treated with 250 μM 6-OHDA, were pre- and post-exposed to 100 μM L-DOPA for 1 h and tested in our device. The results of our behavioral and neuronal assays are shown in Fig. 9.

Fig. 9A demonstrates that pre- and post-treatment of 6-OHDA worms with L-DOPA improved electrotaxis phenotypes in a similar trend for both strains. Exposure of NW1229 and BZ555 worms to 250μM 6-OHDA resulted in significantly lower ETIs and slower ETTs. Pre-treatment of these worms with L-DOPA resulted in slight enhancement of ETIs and reduction of ETTs (Fig. 9A). The ETIs of the L-DOPA pre-treated worms were not significantly different from 6-OHDA exposed worms (Fig. 9A–i). The ETT of the NW1229 worms returned to a level equivalent to the control animals, contrary to the ETT of the BZ555 worms which showed improvement but with no significant difference from the 6-OHDA treated worms (Fig. 9A–ii). For both strains, post-treatment of the worms with L-DOPA resulted in a substantial revitalization of the worm's response to the electric field, recognized by their high ETI (Fig. 9A–i) and fast ETTs (Fig. 9A–ii). The results for both strains showed similar trends in terms of ETI and ETT improvement with L-DOPA, giving credence to the test robustness and sensitivity.

Fig. 9B shows the fluorescent-based neuronal screening results for assessing the effect of L-DOPA on 6-OHDA exposed neurons. The untreated worms showed a strong GFP signal, while 250 μM 6-OHDA treated worms demonstrated a significant loss in the neurons. Pre-treatment of these worms with L-DOPA showed a slight enhancement of GFP level but with no statistically significant difference. Post-treatment with L-DOPA significantly rescued dopamine transmission, visible by significant enhancement in the GFP signal (Fig. 9B). This enhancement might be attributed to the increased level of exogenous dopamine that stimulated the dopamine receptors and recompensed the decrease in the endogenous dopamine level. Moreover, we observed an interesting analogy between the behavioral and neuronal assay results for the 6-OHDA/L-DOPA model in our device.

4. Conclusion

C. elegans electrotactic activities have been recently exploited as promising readouts for behavioral and genetic studies within microfluidic platforms. However, the worms' continuous movement hinders

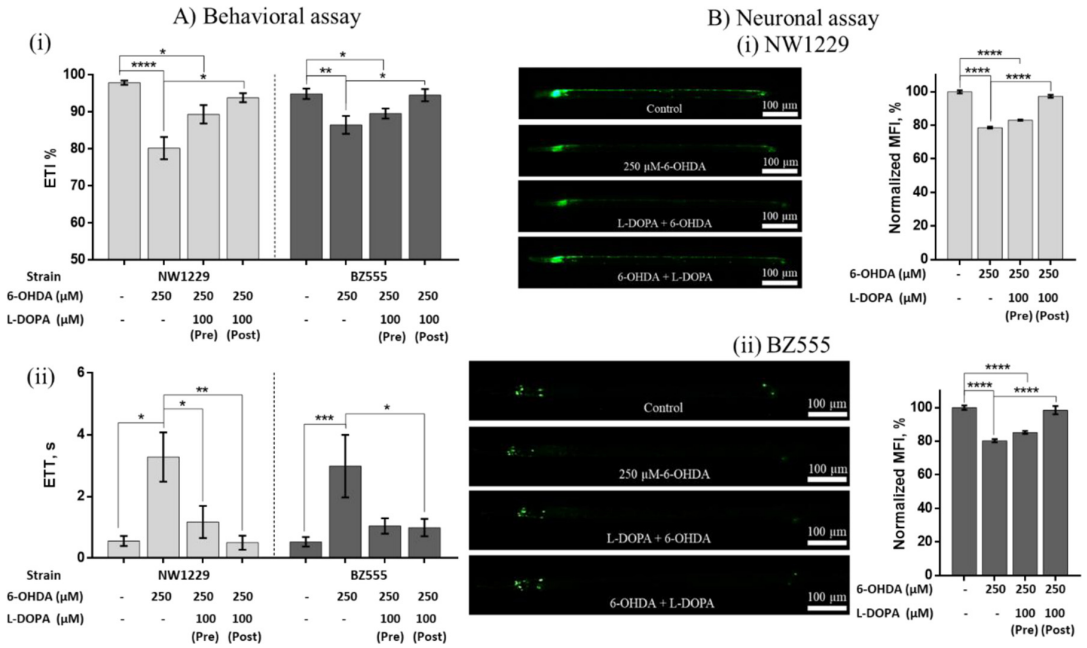

Fig. 9. Electrotaxis response and GFP expression of NW1229 and BZ555 *C. elegans* treated with 250 μM 6-OHDA and 100 μM L-DOPA before (pre) or after (post) 6-OHDA treatment. (A) Electrotaxis response of L-DOPA treated *C. elegans* phenotypically characterized in terms of (i) ETI and (ii) ETT. (B) L-DOPA rescued dopamine transmission of (i) NW1229 and (ii) BZ555 worms shown by fluorescent images and normalized mean fluorescent intensities (MFI). Error bars are SEM; *: $p < 0.05$; **: $p < 0.01$; ***: $p < 0.001$; ****: $p < 0.0001$.

the ability to image cells and leads to a tedious and time-consuming assay. Thus, we proposed a technique in which the worm is captured from one end while the rest of the body is exposed to electric current with the advantages of fluorescently imaging the worm and spatially controlling the electrical signal exposure. Our results demonstrated that the tail-trapped worms show a robust response towards the cathode, just like the freely swimming worms, but at a 3-fold faster rate within a 20-fold smaller assay area. This makes our technique amenable to development of parallelized neurobehavioral screening tools with proof of concept shown in Section 4 of the Supplementary File. Moreover, contrary to what was expected when head-trapped worms are exposed to electric field, we found that they also orient their tails towards the cathode, potentially indicating that the mid-body sensory-motor neurons are contributing to electrotaxis. The capability of our technique was phenotypically tested using *C. elegans* models of PD. The results showed that both Electrotaxis Time Index (ETI) and Electrotaxis Turning Time (ETT) alter by α-syn overexpression in *C. elegans* muscles and worms' exposure to 100–250 μM 6-OHDA. Moreover, implementing imaging within an electrotaxis screening chip was not achieved before, which adds an advantage to our device. At each condition, the worms were fluorescently imaged and assayed to relate neural degeneration to electrotaxis impairment. Pre- and post-exposure of 6-OHDA treated worms to 100 μM L-DOPA, a commonly prescribed drug for PD, rescued dopamine transmission and revitalized electrotaxis response in worms. In the future, we aim to determine the pathway of action behind electrotaxis and its relationship with different PD-related genes. We also envision that by further developing a semi-automated multi-worm chip, we can enhance the throughput of the electrotaxis-based neurobehavioral screening assays.

CRediT authorship contribution statement

Khaled Youssef: Methodology, Investigation, Formal analysis, Validation, Data curation, Visualization, Writing - original draft. **Daphne Archonta:** Data curation, Writing - original draft. **Terrance J. Kubiseski:** Conceptualization, Writing - review & editing. **Anurag Tandon:** Supervision, Validation, Writing - review & editing. **Pouya Rezai:** Conceptualization, Methodology, Validation, Resources, Writing - review & editing, Supervision, Funding acquisition.

Declaration of Competing Interest

The author(s) declared no conflict of interest.

Acknowledgements

This work was supported by Natural Sciences and Engineering Research Council (NSERC) of Canada and the Early Researcher Award to PR and the Ontario Trillium Scholarship to KY.

Appendix A. Supplementary data

Supplementary material related to this article can be found, in the online version, at doi:https://doi.org/10.1016/j.snb.2020.128064.

References

[1] D. Teschendorf, C.D. Link, What have worm models told us about the mechanisms of neuronal dysfunction in human neurodegenerative diseases? Mol. Neurodegener. 4 (2009) 38, https://doi.org/10.1186/1750-1326-4-38.
[2] B. Wolozin, C. Gabel, A. Ferree, M. Guillily, A. Ebata, Watching worms whither: modeling neurodegeneration in C. elegans, Progress in Molecular Biology and Translational Science, Elsevier, 2011, pp. 499–514, https://doi.org/10.1016/B978-0-12-384878-9.00015-7.
[3] A.G. Alexander, V. Marfil, C. Li, Use of C. elegans as a model to study Alzheimer's disease and other neurodegenerative diseases, Front. Genet. 5 (2014), https://doi.org/10.3389/fgene.2014.00279 pp.279.
[4] X. Chen, J.W. Barclay, R.D. Burgoyne, A. Morgan, Using C. elegans to discover therapeutic compounds for ageing-associated neurodegenerative diseases, Chem. Cent. J. 9 (2015), https://doi.org/10.1186/s13065-015-0143-y pp.65.
[5] J.F. Cooper, J.M. Van Raamsdonk, Modeling Parkinson's disease in C. elegans, J. Parkinsons Dis. 8 (2018) 17–32, https://doi.org/10.3233/JPD-171258.
[6] R.M. Giráldez-Pérez, M. Antolín-Vallespín, M.D. Muñoz, A. Sánchez-Capelo, Models of α-synuclein aggregation in Parkinson's disease, Acta Neuropathol. Commun. 2 (2014) 1–17, https://doi.org/10.1186/s40478-014-0176-9.
[7] A.J. Harrington, S. Hamamichi, G.A. Caldwell, K.A. Caldwell, C. elegans as a model organism to investigate molecular pathways involved with Parkinson's disease, Dev. Dyn. 239 (2010) 1282–1295, https://doi.org/10.1002/dvdy.22231.
[8] C.D. Link, C. elegans models of age-associated neurodegenerative diseases: lessons from transgenic worm models of Alzheimer's disease, Exp. Gerontol. 41 (2006) 1007–1013, https://doi.org/10.1016/j.exger.2006.06.059.
[9] K.M. Collins, A. Bode, R.W. Fernandez, J.E. Tanis, J.C. Brewer, M.S. Creamer, M.R. Koelle, Activity of the C. elegans egg-laying behavior circuit is controlled by competing activation and feedback inhibition, ELife 5 (2016), https://doi.org/10.7554/eLife.21126 pp.e21126.
[10] C. Voisine, H. Varma, N. Walker, E.A. Bates, B.R. Stockwell, A.C. Hart, Identification of potential therapeutic drugs for Huntington's disease using Caenorhabditis elegans, PLoS One 2 (2007), https://doi.org/10.1371/journal.pone.0000504 pp.e504.
[11] K. Youssef, P. Bayat, A.R. Peimani, S. Dibaji, P. Rezai, Miniaturized sensors and actuators for biological studies on small model organisms of disease, Environ. Chem. Med. Sens. (2018) 199–225, https://doi.org/10.1007/978-981-10-7751-7_9 Springer.
[12] M.M. Shanmugam, Galvanotaxis of Caenorhabditis elegans: current understanding and its application in improving research, Biol. Eng. Med. 2 (2017), https://doi.org/10.15761/bem.1000111.
[13] N.C. Sukul, N.A. Croll, Influence of potential difference and current on the electrotaxis of Caenorhaditis elegans, J. Nematol. 10 (1978) 314–317.
[14] C.V. Gabel, H. Gabel, D. Pavlichin, A. Kao, D.A. Clark, A.D.T. Samuel, Neural circuits mediate electrosensory behavior in Caenorhabditis elegans, J. Neurosci. 27 (2007) 7586–7596, https://doi.org/10.1523/JNEUROSCI.0775-07.2007.
[15] B.P. Gupta, P. Rezai, Microfluidic approaches for manipulating, imaging, and screening C. elegans, Micromachines 7 (2016), https://doi.org/10.3390/mi7070123 pp.123.
[16] H.S. Chuang, W.J. Kuo, C.L. Lee, I.H. Chu, C.S. Chen, Exercise in an electrotactic flow chamber ameliorates age-related degeneration in Caenorhabditis elegans, Sci. Rep. 6 (2016) 1–11, https://doi.org/10.1038/srep28064.
[17] S. Johari, V. Nock, M.M. Alkaisi, W. Wang, On-chip analysis of C. elegans muscular forces and locomotion patterns in microstructured environments, Lab Chip 13 (2013) 1699–1707, https://doi.org/10.1039/c3lc41403e.
[18] A. Ghanbari, V. Nock, S. Johari, R. Blaikie, X. Chen, W. Wang, A micropillar-based on-chip system for continuous force measurement of C. elegans, J. Micromech. Microeng. 22 (2012), https://doi.org/10.1088/0960-1317/22/9/095009 pp. 95009.
[19] Z. Qiu, L. Tu, L. Huang, T. Zhu, V. Nock, E. Yu, X. Liu, W. Wang, An integrated platform enabling optogenetic illumination of Caenorhabditis elegans neurons and muscular force measurement in microstructured environments, Biomicrofluidics 9 (2015), https://doi.org/10.1063/1.4908595 pp.14123.
[20] L. Huang, P. Zhao, J. Wu, H.S. Chuang, W. Wang, On-demand dielectrophoretic immobilization and high-resolution imaging of C. elegans in microfluids, Sens. Actuators B Chem. 259 (2018) 703–708, https://doi.org/10.1016/j.snb.2017.12.106.
[21] L. Hu, J. Wang, X. Feng, W. Du, B.F. Liu, Microfluidic device for analysis of gas-evoked neuronal sensing in C. elegans, Sens. Actuators B Chem. 209 (2015) 109–115, https://doi.org/10.1016/j.snb.2014.11.081.
[22] S. Salam, A. Ansari, S. Amon, P. Rezai, P.R. Selvaganapathy, R.K. Mishra, B.P. Gupta, A Microfluidic Phenotype Analysis System Reveals Function of Sensory and Dopaminergic Neuron Signaling in C. Elegans Electrotactic Swimming Behavior, Taylor & Francis, Worm, 2013, https://doi.org/10.4161/worm.24558 p. e24558.
[23] S. Sofela, S. Sahloul, C. Stubbs, A. Orozaliev, F.S. Refai, A.M. Esmaeel, H. Fahs, M.O. Abdelgawad, K.C. Gunsalus, Y.A. Song, Phenotyping of the thrashing forces exerted by partially immobilized: C. elegans using elastomeric micropillar arrays, Lab Chip 19 (2019) 3685–3696, https://doi.org/10.1039/c9lc00660e.
[24] P. Rezai, A. Siddiqui, P.R. Selvaganapathy, B.P. Gupta, Behavior of Caenorhabditis elegans in alternating electric field and its application to their localization and control, Appl. Phys. Lett. 96 (2010), https://doi.org/10.1063/1.3383223 pp. 153702.
[25] P. Rezai, A. Siddiqui, P.R. Selvaganapathy, B.P. Gupta, Electrotaxis of Caenorhabditis elegans in a microfluidic environment, Lab Chip 10 (2010) 220–226, https://doi.org/10.1039/b917486a.
[26] D. Liu, B. Gupta, P.R. Selvaganapathy, An automated microfluidic system for screening Caenorhabditis elegans behaviors using electrotaxis, Biomicrofluidics 10 (2016), https://doi.org/10.1063/1.4941709 pp.14117.
[27] J. Tong, P. Rezai, S. Salam, P.R. Selvaganapathy, B.P. Gupta, Microfluidic-based electrotaxis for on-demand quantitative analysis of Caenorhabditis elegans' locomotion, J. Visual. Exp. (2013), https://doi.org/10.3791/50226 pp.e50226.
[28] P. Rezai, Microfluidic Devices for Nematode-Based Behavioural Assays, McMaster University, 2012.
[29] B. Han, D. Kim, U.H. Ko, J.H. Shin, A sorting strategy for C. elegans based on size-dependent motility and electrotaxis in a micro-structured channel, Lab Chip 12 (2012) 4128–4134, https://doi.org/10.1039/c2lc40209b.
[30] A.R. Peimani, G. Zoidl, P. Rezai, A microfluidic device to study electrotaxis and dopaminergic system of zebrafish larvae, Biomicrofluidics 12 (2018), https://doi.

org/10.1063/1.5016381 pp.14113.
[31] X. Wang, R. Hu, A. Ge, L. Hu, S. Wang, X. Feng, W. Du, B.F. Liu, Highly efficient microfluidic sorting device for synchronizing developmental stages of C. elegans based on deflecting electrotaxis, Lab Chip 15 (2015) 2513–2521, https://doi.org/10.1039/c5lc00354g.
[32] Z. Altun-Gultekin, Y. Andachi, E.L. Tsalik, D. Pilgrim, Y. Kohara, O. Hobert, A regulatory cascade of three homebox genes, ceh-10, ttx-3 and ceh-23, controls cell fate specification of a defined interneuron class in C. elegans, Development 128 (2001) 1951–1969.
[33] P. Pu, W. Le, Dopamine neuron degeneration induced by MPP+ is independent of CED-4 pathway in Caenorhabditis elegans, Cell Res. 18 (2008) 978–981, https://doi.org/10.1038/cr.2008.279.
[34] T.J. Van Ham, K.L. Thijssen, R. Breitling, R.M.W. Hofstra, R.H.A. Plasterk, E.A.A. Nollen, C. elegans model identifies genetic modifiers of α-synuclein inclusion formation during aging, PLoS Genet. 4 (2008), https://doi.org/10.1371/journal.pgen.1000027 pp.e1000027.
[35] M. Porta-de-la-Riva, L. Fontrodona, A. Villanueva, J. Cerón, Basic Caenorhabditis elegans methods: synchronization and observation, J. Vis. Exp. (2012), https://doi.org/10.3791/4019 pp.e4019.
[36] P. Rezai, W.I. Wu, P.R. Selvaganapathy, Microfabrication of polymers for bioMEMS, Mems for Biomedical Applications, Elsevier, 2012, pp. 3–45.
[37] Y. Xia, G.M. Whitesides, Soft lithography, Annu. Rev. Mater. Sci. 28 (1998) 153–184, https://doi.org/10.1146/annurev.matsci.28.1.153.
[38] P. Rezai, S. Salam, B.P. Gupta, P.R. Selvaganapathy, Electrical sorting of caenorhabditis elegans, MicroTAS 2011, 15th International Conference on Miniaturized Systems for Chemistry and Life Sciences 2011, 2 2011, pp. 723–725.
[39] J. Schindelin, I. Arganda-Carreras, E. Frise, V. Kaynig, M. Longair, T. Pietzsch, S. Preibisch, C. Rueden, S. Saalfeld, B. Schmid, J.Y. Tinevez, D.J. White, V. Hartenstein, K. Eliceiri, P. Tomancak, A. Cardona, Fiji: An open-source platform for biological-image analysis, Nat. Methods 9 (2012) 676–682, https://doi.org/10.1038/nmeth.2019.
[40] S. Vitulano, C. Di Ruberto, M. Nappi, Biomedical image processing, Proceedings of the IEEE International Conference on Electronics, Circuits, and Systems 2 (1996), pp. 1116–1119, https://doi.org/10.4018/jhisi.2012010105.
[41] F. Faul, E. Erdfelder, A.G. Lang, A. Buchner, G*Power 3: a flexible statistical power analysis program for the social, behavioral, and biomedical sciences, Behav. Res. Methods 39 (2007) 175–191, https://doi.org/10.3758/BF03193146.
[42] A. Ge, X. Wang, M. Ge, L. Hu, X. Feng, W. Du, B.F. Liu, Profile analysis of: C. elegans rheotaxis behavior using a microfluidic device, Lab Chip 19 (2019) 475–483, https://doi.org/10.1039/c8lc01087k.
[43] R. Bodhicharla, A. Nagarajan, J. Winter, A. Adenle, A. Nazir, D. Brady, K. Vere, J. Richens, P. O'Shea, D.R. Bell, D. de Pomerai, Effects of α-synuclein over-expression in transgenic Caenorhabditis elegans strains, CNS Neurol. Disord. - Drug Targets 11 (2013) 965–975, https://doi.org/10.2174/1871527311211080005.
[44] K. Youssef, A. Tandon, P. Rezai, Studying Parkinson's disease using Caenorhabditis elegans models in microfluidic devices, Integr. Biol.: Quantitative Biosci. Nano Macro. 11 (2019) 186–207, https://doi.org/10.1093/intbio/zyz017.
[45] P. Chalorak, P. Jattujan, S. Nobsathian, T. Poomtong, P. Sobhon, K. Meemon, Holothuria scabra extracts exhibit anti-Parkinson potential in C. elegans: a model for anti-Parkinson testing, Nutr. Neurosci. 21 (2018) 427–438, https://doi.org/10.1080/1028415X.2017.1299437.
[46] F. Jin, Q. Wu, Y.F. Lu, Q.H. Gong, J.S. Shi, Neuroprotective effect of resveratrol on 6-OHDA-induced Parkinson's disease in rats, Eur. J. Pharmacol. 600 (2008) 78–82, https://doi.org/10.1016/j.ejphar.2008.10.005.
[47] S.L. Offenburger, X.Y. Ho, T. Tachie-Menson, S. Coakley, M.A. Hilliard, A. Gartner, 6-OHDA-induced dopaminergic neurodegeneration in Caenorhabditis elegans is promoted by the engulfment pathway and inhibited by the transthyretin-related protein TTR-33, PLoS Genet. 14 (2017), https://doi.org/10.1371/journal.pgen.1007125 pp.e1007125.
[48] R.H. Fu, H.J. Harn, S.P. Liu, C.S. Chen, W.L. Chang, Y.M. Chen, J.E. Huang, R.J. Li, S.Y. Tsai, H.S. Hung, W.C. Shyu, S.Z. Lin, Y.C. Wang, N-Butylidenephthalide protects against dopaminergic neuron degeneration and α-synuclein accumulation in Caenorhabditis elegans models of Parkinson's disease, PLoS One 9 (2014), https://doi.org/10.1371/journal.pone.0085305 pp.e85305.
[49] R.H. Fu, Y.C. Wang, C.S. Chen, R.T. Tsai, S.P. Liu, W.L. Chang, H.L. Lin, C.H. Lu, J.R. Wei, Z.W. Wang, W.C. Shyu, S.Z. Lin, Acetylcorynoline attenuates dopaminergic neuron degeneration and α-synuclein aggregation in animal models of Parkinson's disease, Neuropharmacology 82 (2014) 108–120, https://doi.org/10.1016/j.neuropharm.2013.08.007.
[50] W. Schultz, Multiple functions of dopamine neurons, F1000 Biol. Rep. 2 (2010), https://doi.org/10.3410/B2-2.

Khaled Youssef is a Ph.D. candidate at the Mechanical Engineering Department, York University under the supervision of Dr. P. Rezai and Dr. A. Tandon. He obtained his Bachelor and Master of Science degrees in Mechanical Engineering, both from Ain Shams University, Egypt. He has received multiple prestigious scholarships including the Ontario Trillium and Carswell Scholarships to conduct his Ph.D. in developing microfluidic platforms for investigation of *C. elegans* electrotaxis and its applications to disease studies and chemical screening.

Daphne-Eleni Archonta is a second-year mechanical engineering student at York University. Daphne received the Lassonde Scholar award as well as the President's scholarship upon starting her post secondary studies. She joined the Advanced Center for Microfluidics Technology and Engineering laboratory in 2017, during her high school education, as a part of the Sanofi Biogenius Canada Competition and was ranked first in the provincial round in Ontario. Her research interests focus in the field of biomedical engineering.

Dr. Terrance Kubiseski graduated with a Ph.D. from the Department of Biochemistry of Queen's University in Kingston, Ontario and then pursued his postdoctoral training at the Samuel Lunenfeld Research Institute in the Programme in Molecular Biology and Cancer under the guidance of Dr. Tony Pawson. He is currently an Associate Professor in the Department of Biology at York University, where he is studying the genetic regulation of the oxidative stress response using *Caenorhabditis elegans* as a model organism.

Dr. Anurag Tandon obtained his Ph.D. from the Department of Pharmacology and Therapeutics at McGill University. He subsequently undertook postdoctoral training at the Scripps Research Institute in La Jolla, California, where he investigated the regulation of protein and vesicular trafficking with Dr. William Balch. He is currently an Associate Professor in the Department of Medicine, with a laboratory at the Tanz Centre for Research in Neurodegenerative Diseases. The main focus of Dr. Tandon's research is to understand the early events that lead to neurodegeneration in Parkinson's disease using cell and molecular biology techniques. In addition, his laboratory is developing gene therapies to modulate asyn expression levels and solubility in vivo as a means to prevent disease progression.

Dr. Pouya Rezai obtained his PhD from the Department of Mechanical Engineering at McMaster University, Canada. He then joined the Public Health Agency of Canada as an NSERC Visiting Fellow in Guelph, Canada, where he developed and implemented microfluidic technologies for disease diagnostics and pathogen detection applications. Rezai is currently an Associate Professor at the Department of Mechanical Engineering at York University, Canada and the director of the Advanced Center for Microfluidics Technology and Engineering. Rezai's research interest is to expand fundamental understanding of interactions between fluids and nano- to micro-scale biological substances in their microenvironment habitats using biomimetic microfluidic devices and to employ this knowledge to devise efficient microsystems for facilitating research and development in human health-related applications.

Supplementary Information

Semi-Mobile *C. elegans* Electrotaxis Assay for Movement Screening and Neural Monitoring of Parkinson's Disease Models

Khaled Youssef[1], Daphne Archonta[1], Terrance J. Kubiseski[2], Anurag Tandon[3,4,] and Pouya Rezai*[,1]

[1]Department of Mechanical Engineering, York University, Toronto, ON, Canada
[2] Department of Biology, York University, Toronto, ON, Canada
[3]Tanz Centre for Research in Neurodegenerative Diseases, Toronto, Ontario, Canada
[4]Department of Medicine, University of Toronto, Toronto, Ontario, Canada

* Corresponding Author: BRG 433B, 4700 Keele St, Toronto, ON, M3J 1P3, Canada; Tel: 416-736-2100 ext. 44703; Email: prezai@yorku.ca

1. Microfluidic Chip Design and Fabrication

At first, the design was sketched by the computer-aided design (CAD) software SOLIDWORKS® (USA). The pattern was printed as a photomask on a 25,000 DPI transparency (CAD/Art Services Inc., USA). A 4 in Si wafer was cleaned using acetone for 30 s, isopropyl alcohol (IPA) for 30 s and deionized water for two minutes, followed by heating the wafer at 110 ˚C for 5 minutes to evaporate the molecular water layer. Then, Si wafer surface cleaning was performed for enhancing the photoresist adhesion by exposing it to Oxygen plasma (PDC-001-HP Harrick Plasma, USA) for 30 seconds. Four milliliters of SU-8 2075 was deposited on the Si substrate and pre-spun at 500 rpm for 5 s, then ramped to 3500 rpm for 30 s to achieve a 60µm-thick layer. Soft baking was performed at 65˚C for 3 minutes and 95 ˚C for 6 minutes prior to UV exposure at 365 nm with 11.1 mW/cm^2 (UV-KUB 2, KLOE, France) for 14s. Post bake was performed at 65 ˚C for 1 minute and 95 ˚C for 6 minutes, followed by rinsing the baked wafer in SU-8 developer for 5 minutes, then drying with an air gun. Finally, the mold was hard-baked for 25 minutes at 150 ˚C to obtain the final master mold. Features thicknesses were measured by a Bruker optical profiler (Bruker Optics, USA).

The negative replica of the master mold was fabricated using the standard soft lithography process [1]. Masterflex tubes (L/S 14 size, Gelsenkirchen, Germany) were placed over the inlet and outlet reservoirs on the master mold. Then, PDMS mixture in the ratio of 10 grams of elastomer base to 1 gram of curing agent was poured over the master mold and cured for 2 hours at 80˚C. Then, the peeled PDMS layer was irreversibly bonded to a glass substrate using oxygen plasma at 870 mTorr pressure and 30W for 30s. The bonded device was kept for 10 minutes at 65˚C to enhance bonding. For electric field stimulation, two copper electrodes were inserted into the inlet and outlet reservoirs of the electrotaxis screening channel by punching through the PDMS, and then the surrounding area was sealed by pouring liquid pre-polymer PDMS. Finally, the device was cured using a hotplate at 120 ˚C.

2. Numerical Simulation of Electric Field in the Microfluidic Device

Electric field distribution in the proposed microfluidic device was obtained using two-dimensional (2D) numerical simulation. In order to simulate the system, the steady-state direct-current electric module of the commercial software COMSOL Multiphysics® was used to solve the electric field within a conductive media using *Ohm's* law. The 2D geometry of the computational domain was generated using the computer-aided design (CAD) software SOLIDWORKS® and imported into COMSOL for grid generation and application of boundary conditions. The model consisted of the 300µm-wide and 2cm-long electrotaxis screening channel with two end reservoirs and a perpendicular tapering channel for worm trapping as shown in Figure 1 of the paper. Electric conductivity of M9 media was determined experimentally using a 300µm-wide straight microchannel and found to be approximately 1.6 siemens/meter. This value was manually inserted into our model. Electric insulation boundary condition was set at all boundaries except the two end-reservoirs of the main channel; one was defined with an electric potential of 8V, and the other was defined as ground. For grid generation, the built-in mesh module of COMSOL Multiphysics was used to generate triangular mesh elements. A grid independence study was conducted, and the number of elements obtained was 2e6. Moreover, the number of elements was increased at the trapping region. Figure S1 presents the computed electric field distribution across the device (Figure S1A) and in the tapered channel (Figure S1B). Figures S1C and S1D show the electric field distributions across lines A-A and B-B, confirming that the electric field in the main channel is uniformly 4V/cm and the trap has no effect on the electric field at the T-junction region in the main channel.

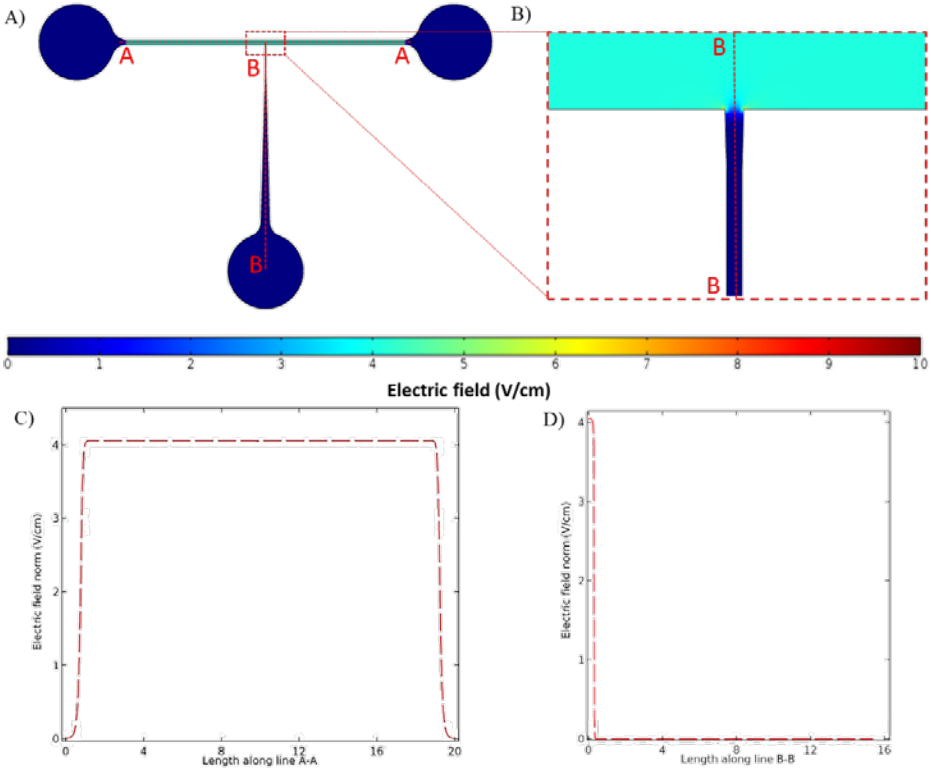

Figure S1: COMSOL simulation of electric field distribution in the microfluidic device when an 8V stimulus was applied along the electrotaxis channel (line A-A). (A) Electric field distribution in the chip. (B) Electric field distribution at the T-junction. (C) Electric field along line A-A, showing that the tapered channel has no effect on the electric field at the T-junction. (D) Electric field along line B-B, showing that the application of voltage in the electrotaxis channel does not result in an electric field inside the tapered channel.

3. Comparison of semi-mobile and freely moving *C. elegans* electrotaxis

In conventional electrotaxis, the worm can swim towards the cathode, and the behavioural test parameters (e.g., speed, ETI, and ETT) are quantified. Our technique can provide information regarding the ETI and ETT of the worm as well as imaging the worm fluorescently after immobilization (not achieved in conventional electrotaxis). In order to verify our technique, we compared the results obtained in our device for 12 worms with the results obtained by Salam et al. [2] using the same number of worms. As shown in Figure S2, we obtained an ETI of 95% in comparison to the conventional electrotaxis ETI of 85%. Our average ETI was 10% higher and the error associated with our ETI result was less than the freely moving assay. Moreover, our ETT value was significantly smaller than the one obtained by the conventional test. The average turning time in our experiment was ETT=0.5s compared with ETT=10.3s from the literature, which shows that the worms in our device respond faster and turn quicker towards the cathode. These characteristics in our proposed assay can lead to increasing the assay speed, throughput, sensitivity and simplicity.

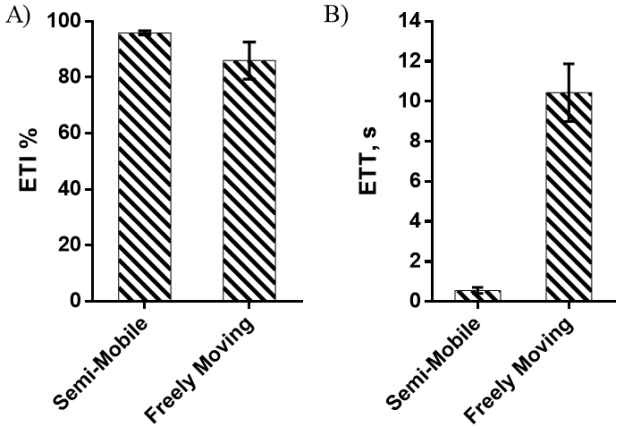

Figure S2: Comparison between the results obtained using our technique (N=12 tail-trapped semi-mobile worms) and the conventional freely-moving electrotaxis assays using N=12 wild-type worms obtained from Salam et al. [2]. *(A) Electrotaxis Time Index (ETI). (B) Electrotaxis Turning Time (ETT).*

4. Towards increasing the test throughput - A proof of concept multi-worm screening device

Increasing the assay throughput is the most reliable route towards the exploration of pharmacological therapeutics for uncured diseases [3]. Therefore, here, we attempted to provide a proof of concept microfluidic chip based on our developed assay to increase the test throughput by replicating the worm trap along the electrotaxis channel. The modifications do not meet the demands for high throughput screening yet, but this is the first step towards increasing the throughput of our technique in the future.

Figure S3A and S3B show the developed 60μm-thick single layer chip, which consists of an electrotaxis screening channel and eight perpendicular trapping channels separated by 1.2 mm. All trapping channels were connected via tree-like branches to a single reservoir for applying vacuum pressure. The electrotaxis channel length was increased from 2 cm to 3 cm to accommodate for the increased number of worms, and therefore, the applied voltage was increased from 8V to 12V to obtain a suitable range of electric field.

The same modeling approach reported in Section 1 was applied to determine the electric field distribution in the microfluidic device with multiple trapping channels (Figure S3C). Electric field

along the centerline A-A of the channel was plotted in Figure S3D where it is shown that the electric field varies symmetrically from 3.5 V/cm at the two center traps to 4.2 V/cm in the two outer traps and the main channel. The reason behind this variation is the electric paths provided by the U-shape channels connecting the traps to each other. The effect of this electric field variation on the electrotaxis response of young adult worms was neglected because the worms respond similarly to a range of 2-4 V/cm electric fields as reported earlier by Rezai et. al. [4]

Upon testing the device, most of the channels were filled with worms within 30s of activating the suction pressure (Figure S3B). From the 8 traps, N=6 were occupied with tail-trapped worms, N=1 with head-trapped worm and one trap was left open. The effect of DC electric field on the head-trapped worms is under investigation.

Although our proof of concept tests provided a promising perspective for increasing the test throughput, more experiments are needed to control the loading process and the trapped length of the worms, and to ensure that most of the worms are loaded with tail-first. Next, we aim at parallelization and automation of our microfluidic chip to improve on the exiting electrotaxis screening throughput of 20 worms per hour by Liu et al. [5].

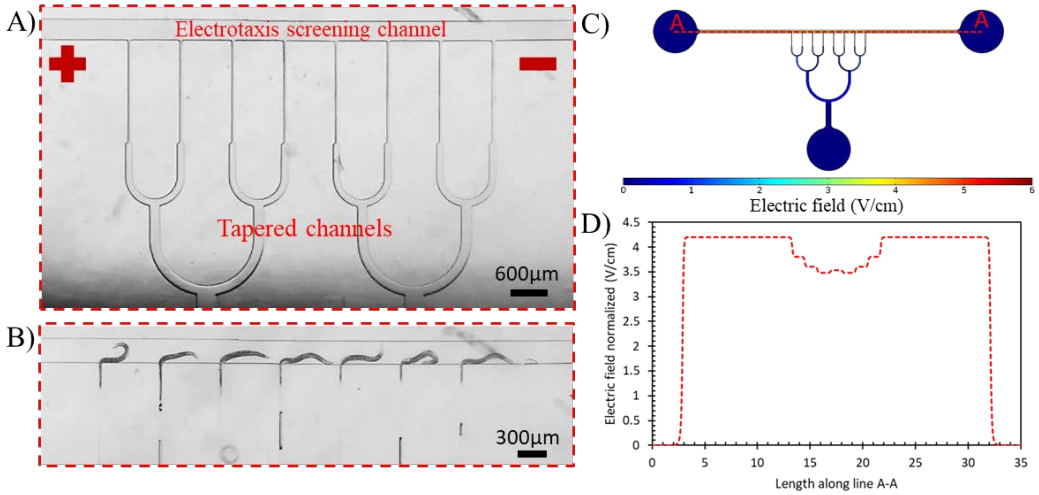

Figure S3: Proof of concept HTS microfluidic chip design and COMSOL simulation of electric field distribution in the multi-trap microfluidic device when a 12V stimulus was applied along the electrotaxis channel(A) A microscopic view of the chip showing the electrotaxis screening channel with end electrodes and branches of tapered channels, (B) Eight worms trapped in the chip for testing, (C) Electric field distribution in the chip, (D) Electric field along line A-A, showing that the electric field along the electrotaxis channel is in the optimal range for young adult worms according to Rezai et al. [4]

5. Supplementary Videos

Video S1: Full worm loading, electrotaxis monitoring and neuron screening procedure in the microfluidic device.
Video S2: A wild type worm response in the absence of the electric field.
Video S3: A wild type worm captured from its tail and responding to the electric field.
Video S4: A wild type worm captured from its head and responding to the electric field.
Video S5: A wild type animal showing complete paralysis in response to the electric field.
Video S6: A wild type animal showing sluggishness in response to the electric field.
Video S7: A wild type animal showing distracted response to the electric field.
Video S8: A wild type animal showing complete paralysis at 5mM 6-OHDA.

6. References

[1] Y. Xia, G.M. Whitesides, Soft lithography, Annual Review of Materials Science. 28 (1998) , pp.153–184, https://doi.org/10.1146/annurev.matsci.28.1.153.

[2] S. Salam, A. Ansari, S. Amon, P. Rezai, P.R. Selvaganapathy, R.K. Mishra, B.P. Gupta, A microfluidic phenotype analysis system reveals function of sensory and dopaminergic neuron signaling in C. elegans electrotactic swimming behavior , in: Worm, Taylor & Francis, 2013: p. e24558, https://doi.org/10.4161/worm.24558.

[3] H.E. Kinser, Z. Pincus, High-throughput screening in the C. elegans nervous system, Molecular and Cellular Neuroscience. 80 (2017) , pp.192–197, https://doi.org/10.1016/j.mcn.2016.06.001.

[4] P. Rezai, A. Siddiqui, P.R. Selvaganapathy, B.P. Gupta, Electrotaxis of Caenorhabditis elegans in a microfluidic environment, Lab on a Chip. 10 (2010) , pp.220–226, https://doi.org/10.1039/b917486a.

[5] D. Liu, B. Gupta, P.R. Selvaganapathy, An automated microfluidic system for screening Caenorhabditis elegans behaviors using electrotaxis, Biomicrofluidics. 10 (2016) , pp.14117, https://doi.org/10.1063/1.4941709.

EGG LAYING NEURON MEDIATES ELECTROSENSATION IN *CAENORHABDITIS ELEGANS*

Khaled Youssef[1], Daphne Archonta[1], Terrance J Kubiseski[2], Anurag Tandon[3], Pouya Rezai[1]

[1] *Department of Mechanical Engineering, York University, Toronto, ON, Canada*

[2] *Department of Biology, York University, Toronto, ON, Canada*

[3] *Tanz Centre for Research in Neurodegenerative Diseases, Toronto, ON, Canada*

ABSTRACT

C. elegans possess robust electrosensation behaviours which were thought to be predominantly mediated by a set of neurons located in the head region. However, in this paper, we show, for the first time, that neurons located at the mid-body are also contributing to electrosensing by precisely exposing specific body regions to electric field using our semi-mobile electrotaxis assay.

KEYWORDS: Microfluidics, *C. elegans*, Electrosensation, Egg-laying

INTRODUCTION

C. elegans is a small-size (~1mm) model organism for neurobehavioral studies with various experimental advantages of fast growth, short lifecycle, body transparency, simple neuronal system, and fully sequenced genome [1]. *C. elegans* exhibit sensory-evoked behaviors in response to various environmental cues [2]. For instance, it has been shown for *C. elegans* to innately swim towards the cathode in the presence of direct current (DC) electric field (EF), a behaviour termed electrotaxis [3,4]. Advances in genetic tools have aided in exploring some of the sensory neurons that mediate *C. elegans* electrosensation, which was found to be located predominantly at the worms' head [3]. Moreover, previous studies have been conducted by subjecting the whole worm to EF, hindering the capability of exposing certain parts of the worm to spatially investigate the neurons responsible for electrosensation. Here, we have exploited our recently developed semi-mobile worm electrotaxis assay [5] to explore whether stimulating the worm's head or tail will induce a directional electrotaxis behaviour. Our assay has aided in determining that neurons in the midbody region are contributing to the pathway of electrosensation.

EXPERIMENTAL METHODS

Spatial exposure was achieved by applying DC EF to partially immobilized worms (head- or tail-trapped) on-chip using the experimental setup in Fig. 1A. Our monolayer 60µm-thick microfluidic device (Fig. 1B-C) consisted of two perpendicular channels for electrotaxis assessment and partial trapping of the worm. EF was applied through two copper electrodes connected to the electrotaxis screening channel (2cm long and 300µm wide). A tapered perpendicular channel, narrowing from 30µm to 25µm, was used to load and pneumatically capture the worm either by the tail or head, also resulting in spatial EF isolation within the trap (tail or head in Fig. 1D).

N2 (wild-type control) and MT1082 *(egl-1(n487)) C. elegans* strains were used. Young adult worms (46-52µm long) were loaded individually into the device via the loading channel (Fig. 1B), and captured either by tail or head, leaving approximately 70-80% of their free-end to be exposed to EF in the electrotaxis screening channel. The trapped length was maintained constant during the experiments by incorporating an on-chip length scale within the chip and manipulating the pneumatic suction pressure. A sourcemeter was used to apply DC EF of 4 V/cm, and the electrotactic response was assessed using *Electrotaxis Time Index* (*ETI*) and *Electrotaxis Turning Time* (*ETT*) in Equations (1) and (2), respectively.

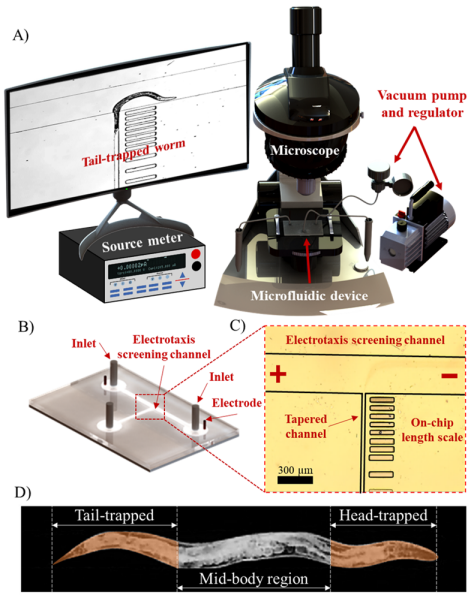

Figure 1: (A) Experimental setup. (B) A microfluidic device consisting of the electrotaxis screening channel (used for loading) and a suction channel for trapping the worms, shown in (C). (D) A worm schematic showing the parts isolated from EF stimulation using our proposed assay, leaving the mid-body exposed to EF in both cases.

$$\text{ETI (\%)} = \frac{\text{Time facing the cathode}}{\text{Total time exposed to current}} \quad (1)$$

$$\text{ETT (S)} = \text{Time needed to turn towards the cathode} \quad (2)$$

RESULTS AND DISCUSSION

With numerical modeling (Fig. 2A), full EF isolation of the trapped body region was confirmed by showing that there is no EF generated inside the trap (Line A-A in Fig. 2B). Moreover, we previously confirmed [5] that the semi-mobile tail-trapped *C. elegans* (tail isolated from EF) demonstrated a robust directional electrotaxis towards the cathode, which implies that the tail neurons are not heavily involved in electrosensation. Interestingly, the head-trapped worms (head isolated from EF) also showed a directional electrotaxis with their tail towards the cathode (Fig. 3), but with significantly lower ETI and slower ETT compared to the tail-trapped worms. This indicated that the head neurons are contributing to electrotaxis but are not exclusively responsible for it. So, we concluded that the mid-body neurons (e.g., ventral cord, vulva neurons) may be involved in electrotaxis. As proof of concept, MT1082 strain (lacking hermaphrodite-specific neurons (HSN) in mid-body, responsible for initiating egg-laying in *C. elegans*) was tested by trapping their tail in the device. The results showed that MT1082 worms were able to sense the EF and orient towards the cathode but again with significantly lower ETI and slower ETT (Fig. 4). Accordingly, we concluded that the loss of HSN motor neuron significantly decreases the electrosensory behaviour, which supports its involvement in electrotaxis.

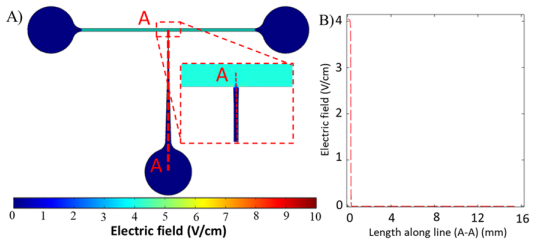

Figure 2: (A) EF distribution in the microfluidic due to an 8V stimulus. (B) Electric field along line A-A, ensuring that EF in the screening channel is 4V/cm and there is no EF generated in the suction channel.

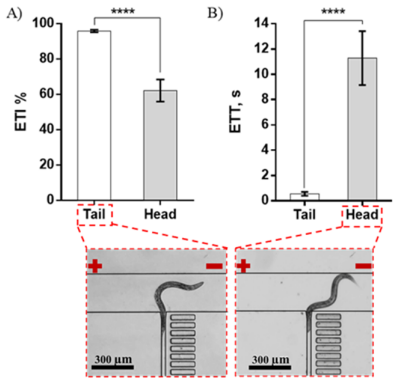

*Figure 3: (A) Electrotaxis time index (ETI) and (B) Electrotaxis Turning Time (ETT) of worms trapped by the head (N=7) or the tail (N =10), as shown by insets. Error bars are SEM; ****: $p < 0.0001$.*

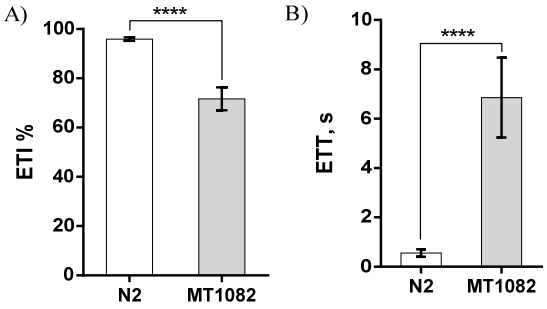

*Figure 4: (A) Electrotaxis time index (ETI) and (B) Electrotaxis Turning Time (ETT) of N2 control and MT 1082 worms trapped by the tail (N=12). Error bars are SEM; ****: $p < 0.0001$.*

CONCLUSION

In this paper, we have shown a technique to expose certain body parts of *C. elegans* to EF selectively and demonstrated the potential of our assay to understand the electrotaxis neural pathway. Most importantly, we validated our hypothesis that *C. elegans* electrosensation is not solely executed by the head neurons via testing a strain lacking a mid-body specific neuron. In the future, we will use our method to study the effect of knocking out different ventral cord neurons on electrotaxis.

REFERENCES

[1] Youssef K., Bayat P., Peimani A.R., Dibaji S., Rezai P., 2018. In Environmental, Chemical, & Medical Sensors, 199-225. Springer, Singapore.

[2] Youssef, K., Tandon, A., Rezai, P., 2019. Integrative Biology, 11(5), 186-207.

[3] Gabel C.V., Gabel H., Pavlichin D., Kao A., Clark D.A., Samuel A.D.,2007. J of Neuroscience,27(28),7586-96.

[4] Rezai, P., Siddiqui, A., Selvaganapathy, P.R. Gupta, B.P., 2010. Lab on a Chip, 10(2), 220-26.

[5] Youssef, K., Archonta, D., Kubiseski, T., Tandon, A., Rezai, P., 2020. Sensors and Actuators B: Chemical, 316, 128064.

B.3 Paper III: Electric Egg-laying: a New Approach for Regulating *C. elegans* Egg-laying Behaviour in a Microchannel Using Electric Field.

Youssef, K., Archonta, D., Kubiseski, T. J., Tandon, A., & Rezai, P. (2021) Electric Egg-laying: a New Approach for Regulating *C. elegans* Egg-laying Behaviour in a Microchannel Using Electric Field. Lab on a Chip, In press, DOI: 10.1039/D0LC00964D.

Lab on a Chip

PAPER

View Article Online
View Journal

Cite this: DOI: 10.1039/d0lc00964d

Electric egg-laying: a new approach for regulating *C. elegans* egg-laying behaviour in a microchannel using electric field†

Khaled Youssef,[a] Daphne Archonta,[a] Terrance J. Kubiseski,[b] Anurag Tandon[cd] and Pouya Rezai *[a]

Received 23rd September 2020,
Accepted 23rd January 2021

DOI: 10.1039/d0lc00964d

rsc.li/loc

In this paper, the novel effect of electric field (EF) on adult *C. elegans* egg-laying in a microchannel is discovered and correlated with neural and muscular activities. The quantitative effects of worm aging and EF strength, direction, and exposure duration on egg-laying are studied phenotypically using egg-count, body length, head movement, and transient neuronal activity readouts. Electric egg-laying rate increases significantly when worms face the anode and the response is EF-dependent, *i.e.* stronger (6 V cm^{-1}) and longer EF (40 s) exposure result in a shorter egg laying response duration. Worm aging significantly deteriorates the electric egg-laying behaviour with an 88% decrease in the egg-count from day-1 to day-4 post young-adult stage. Fluorescent imaging of intracellular calcium dynamics in the main parts of the egg-laying neural circuit demonstrates the involvement and sensitivity of the serotonergic hermaphrodite specific neurons (HSNs), vulva muscles, and ventral cord neurons to the EF. HSN mutation also results in a reduced rate of electric egg-laying allowing the use of this technique for cellular screening and mapping of the neural basis of electrosensation in *C. elegans*. This novel assay can be parallelized and performed in a high-throughput manner for drug and gene screening applications.

Introduction

A core question in neuroscience is to interrogate how sensory neurons are involved in eliciting a particular behavior. Perceiving a sensory stimulus by the central nervous system induces a flow of electric signals through the motor neurons to stimulate muscle contraction and behavior generation. Due to the complexity of the human brain, model organisms with a less complicated nervous system are used to unravel the functions of sensory-motor processes.[1]

The nematode *Caenorhabditis elegans* (*C. elegans*) is a free-living organism that has a simple and well-defined nervous system with a fully sequenced genome which makes it appealing for neuroscience research.[2,3] Although a hermaphrodite worm only possesses 302 neurons, it can perceive and respond to a wide range of stimuli such as chemicals, light, temperature, electric field (EF), and touch through the developed sensory amphid, phasmid, labial, and mechanosensory neurons.[4–9] *C. elegans* behaviors, including movement, egg-laying, and food intake are regulated by these sensory modalities and behavioral screening provides a great means to study neuronal functions and processes in *C. elegans*.

Electrotaxis is one of several behaviors preserved across many species, which is the ability of the organism to sense and move towards a desired direction in the presence of EF.[10,11] Gabel *et al.*[12] investigated the neuronal basis of electrotaxis using laser ablation of specific neurons in various transgenic *C. elegans* lines. ASJ and ASH neurons were highlighted as the primary electrotaxis sensory neurons, whereas RIM and AVA were reported to participate in reorientation maneuvers. *C. elegans* electrotaxis was found to be dependent on multiple genes such as *che-2*, *che-13*, *eat-4*, *osm-3*, *osm-5*, *osm-6*, *osm-10*, and *tax-6*. Recently, Chrisman *et al.*[13] elucidated the role of the AWC neuron pairs (AWC^{OFF} and AWC^{ON}) on electrotaxis and showed that genetic ablation of the neurons is less disruptive than the loss of function asymmetry.

C. elegans electrotaxis has also been studied in more controlled microenvironments using microfluidic devices.[14–19] Rezai *et al.*[15,16] were the first to exploit microfluidics for the investigation of electrotaxis under direct current (DC)[15] and alternating current (AC)[16] EF by measuring the worms' speed at different larval stages. Since

[a] Department of Mechanical Engineering, York University, Toronto, ON, Canada. E-mail: prezai@yorku.ca
[b] Department of Biology, York University, Toronto, ON, Canada
[c] Tanz Centre for Research in Neurodegenerative Diseases, Toronto, Ontario, Canada
[d] Department of Medicine, University of Toronto, Toronto, Ontario, Canada

† Electronic supplementary information (ESI) available. See DOI: 10.1039/d0lc00964d

then, electrotaxis has been used in various sorting applications[18–20] and as a tool for drug screening.[14,17] Most studies focused on the larval and young adult stages, giving less attention to the response at later adult ages. Moreover, investigations were limited to gait behavior in terms of speed, body bend frequency, and reorientation. Herein, we discovered that at later developmental stages, *C. elegans* exhibited unusual and less robust electrotaxis behavior and were interestingly stimulated to lay eggs in a microchannel, a phenomenon that has not been shown to date.

C. elegans egg-laying is an established rhythmic behavior of interest to the neuroscience community. It is controlled by a simple neural circuit that can be excited to produce a consistent behavioral output.[1,21] *C. elegans* egg-laying involves interactions between vulva muscles (vms), two hermaphrodite specific neurons (HSN), and six ventral cord (VC) neurons.[1] Worms lay eggs in a temporal stochastic manner that fluctuates between active state, during which the worm lay eggs, and inactive state, during which no egg-laying occurs. Several environmental factors can stimulate or halt egg-laying.[22] For instance, Sawin *et al.*[23] reported that mechanical stimulation using vibration inhibits egg-laying. Worms also halt egg-laying in hypertonic salt solutions such as M9 and in the absence of food. Fenk *et al.*[24] showed that egg-laying is inhibited by CO_2 exposure through modulation of the AWC olfactory neurons. Recently, Collins *et al.*[1] attempted to understand the egg-laying behavior and the function of each part of the circuit during the active and inactive states. During the active state, the overall behavior was phased with locomotion, while vms were activated by HSN and VC neurons to contract and expel fertilized eggs. Optogenetics is the primary method used to stimulate neurons to study the sensorimotor pathways involved in egg-laying.[1] However, it is restricted to genetically modified worms with light-sensitive ion channels, calling for a simple, on-demand, and inclusive egg-laying stimulation technique applicable to wild-type worms. In this endeavor, we propose the use of DC EF in a microchannel as a stimulus to evoke the egg-laying circuit and induce egg-laying on-demand.

In this paper, we demonstrate for the first time that DC EF evokes the *C. elegans* egg-laying neural circuit. In this context, a simple mono-layer microfluidic device was developed with end-electrodes for electric stimulation and an electrical trap to confine the worm in the field of view while allowing regular egg release. Moreover, the effects of adult worms age and EF direction, strength, and exposure duration on the number of eggs released were investigated. The worms' muscle activity was quantified through the rate of contraction and relaxation under the influence of EF, and we showed that it was independent of the EF direction. Transgenic lines expressing the fluorescent Ca^{2+} reporter GCaMP5 in HSNs, vms, and VCs neurons and an HSN mutant line were used to investigate the electric egg-laying behavior. Our technique can be used potentially for egg collection and synchronization as well as chemical and mutant screening. Moreover, it will aid in the investigation and mapping of the neural basis of electrosensation in *C. elegans*.

Materials and methods

C. elegans strains and growth

Nematodes were grown at 20 °C on standard nematode-growth medium (NGM) plates seeded with *Escherichia coli* (*E. coli*) strain OP50 as a food source.[25] OP50 *E. coli* bacteria were cultured in freshly prepared Luria Broth (LB) media (10 g bacto-tryptone, 5 g bacto-yeast, and 5 g NaCl in 1 L distilled water) overnight in a thermal shaker incubator at 37 °C. On the following day, 100 μL of the bacterial culture were used to seed the NGM plates. The strains used in this study are showing in Table 1, and they were obtained from the *Caenorhabditis Genetics Center* (University of Minnesota, USA). All experiments were performed under Biosafety Number 02-19 issued by York University's Biosafety Committee to PR.

In all experiments, age-synchronized, well-fed young adult worms were obtained using the alkaline hypochlorite treatment.[26] Briefly, gravid hermaphrodite worms were collected in a 15 mL Eppendorf tube and treated for 10 minutes with a solution of 3.875 mL double-distilled water, 125 μL NaOH, and 1 mL commercial bleach. Following the treatment, the eggs were obtained by centrifuging the sample at 1500 rpm and incubated at 20 °C overnight in 1 mL M9 buffer (3 g KH_2PO_4, 6 g Na_2HPO_4, 5 g NaCl, and 1 ml 1 M $MgSO_4$ in 1 L distilled water) using a RotoFlex™ tube rotator (RK-04397-40, Cole-Parmer, Canada). On the following day, the hatched larvae were plated on freshly prepared NGM plates to allow for standard growth. All experiments were conducted using worms at day one post young adult stage (~64 h or D1), except for age effect experiments in which the worms were transferred to a new NGM plate for consecutive day studies in D2 to D4.

Microfluidic chip design and fabrication

The proposed microfluidic device shown in Fig. 1A was designed to study the effect of DC EF on the egg-laying behaviour of *C. elegans* and to provide the ability to image the worms fluorescently. The mono-layer microfluidic device consisted of a 3 cm long straight microfluidic channel (300 μm wide) with a 1.3 mm long mid-section electrical trap (100 μm wide) to provide a symmetrical condition for the EF. All channels were 65 μm thick. The two end reservoirs were connected to two copper-wire electrodes. The electric trap enlarged in Fig. 1A was used as the test area to confine the worm's movement for studying the effect of EF direction, magnitude and duration, as well as worm age on EF induced egg-laying. The confinement was required to lessen the worm movement for easy monitoring of egg laying and fluorescent imaging. Moreover, numerical modeling was conducted to confirm the uniformity in the EF distribution along the channel when EF was applied (ESI† Section 1).

Table 1 *C. elegans* strains used in this study

Strain	Genotype	Description	Ref
N2	WT bristol	Wild type	
LX1918	*lite-1(ce314) vsIs164 lin-15(n765ts)* X	vms GCaMP5, mCherry	1
LX1960	*vsIs172; lite-1(ce314) lin-15(n765ts)* X	VC GCaMP5, mCherry	
LX2004	*lite-1(ce314), vsIs183 lin-15(n765ts)* X	HSN GCaMP5, mCherry	
LX1986	*vsIs177 lite-1(ce314) lin-15B&lin-15A(n765)* X	uv GCaMP5, mCherry	
MT1082	*egl-1 (n487)*	Egg-laying defective. Retains late stage eggs	21

The microfluidic device was fabricated using standard photo- and soft-lithography techniques.[27] To fabricate a negative replica, a 65 μm thick layer of SU-82075 photoresist (MicroChem Corporation, USA) was photolithographically patterned on a 4 inch diameter and 500 μm thick silicon wafer (Wafer World Inc., USA) using UV exposure at 365 nm with 11.1 mW cm^{-2} (UV-KUB 2, KLOE, France) for 14 s. Inlet and outlet Masterflex tubes (L/S 14 size, Gelsenkirchen, Germany) were placed over the master mold. Then, polydimethylsiloxane (PDMS, Dow Corning, USA) elastomer and curing agent were mixed at 10 : 1 ratio and poured over the master mold followed by curing for 2 hours at 80 °C. Then, the cured PDMS layer was peeled off the master mold, bonded to a pre-cleaned glass substrate (75 × 25 mm^2) by oxygen plasma (PDC-001-HP Harrick Plasma, USA) at 870 mTorr pressure and 30 W power for 30 s, and kept for 30 min at 65 °C to enhance bonding. EF stimulation was attained by punching two 3 cm long copper electrodes through the PDMS into the inlet and outlet tubes. Liquid PDMS mixture was used to seal the surrounding areas of the copper insertions to prevent leakage.

Experimental setup and procedures

The microfluidic device was installed on an inverted microscope (DMIL LED Inverted Routine Fluorescence Microscope, Leica, Germany), equipped with a color camera (MC170 HD, Leica, Germany), as shown in Fig. 1B. The two copper electrodes from the device were connected to a DC sourcemeter (Model 2410, Keithley Instruments Inc., USA) for EF stimulation. The sourcemeter was controlled using a custom-developed MATLAB code to regulate the applied voltage, stimulation time, and EF direction. The EF in the trap was varied from 2 to 8 V cm^{-1}, and the stimulation time was varied from 1 to 40 s. This range of EF in the trap was determined by a simple COMSOL Multiphysics model, after applying a voltage of 2.25 to 9 V across the channel, as described in ESI† Section 1. EF direction was decided based on the worm's head orientation in the channel after loading, *i.e.* anode or cathode stated when the worm head was towards the positive or negative electrodes, respectively.

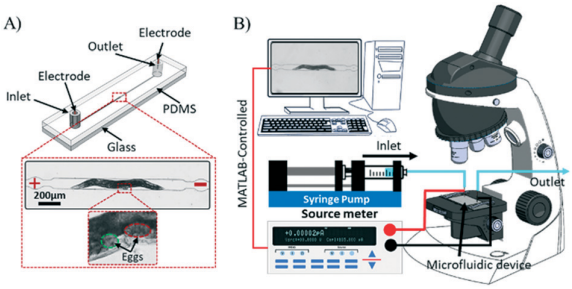

Fig. 1 (A) Microfluidic device (2.5 cm × 1 cm) consisting of an inlet, an outlet, and a symmetrical microchannel with a mid-trap for worm testing and two end electrodes for EF stimulation. (B) Experimental setup consisting of our microfluidic device, a microscope, a syringe pump, and an electrical sourcemeter.

Prior to the experiments, the device was filled with M9 buffer using a manual syringe connected to the inlet. The outlet was connected using a valve to two 15 mL centrifuge tubes, one for device washing and the other for egg-collection when needed. A single worm from a synchronized population (D1 to D4 post young adult) was manually picked (Wormstuff, USA) and loaded into the inlet tube of the device. Then, a 10 mL syringe filled with M9 was used to guide the worm to the middle electric trap manually and, once the worm reached the trap, the flow was stopped, and the worm was left for 60 s to acclimate to the environment before exposure to the EF. Next, the MATLAB code was run, and a series of step voltage pulses were initiated based on the desired EF and exposure duration. The EF pulse had an ON state of 1 to 40 s and an OFF state of 25 s for a fixed total exposure time of 10 min for each worm. Results were recorded in terms of the number of eggs and the time of egg-laying for behavioral assay. Video recording under fluorescent setting was done during neuron and muscle transient response assays. Then, the worm was flushed out of the chip to allow for the next worm to be tested.

Video processing and phenotypic analysis

The camera mounted on the microscope was used for acquiring movie clips of the experiments at 5× magnification with 30 frames per second (FPS) speed and 5-megapixel resolution. Our custom-written MATLAB code was used to process the recorded videos and detect the worms' centerline. For this, the user was asked whether to perform worm length measurement or fluorescent intensity analysis. If length analysis was selected, the user was asked to import a video and the first frame of the imported video was shown on the screen (Fig. 2Ai). The user was then asked to import the background image (Fig. 2Aii) which was taken from the chip

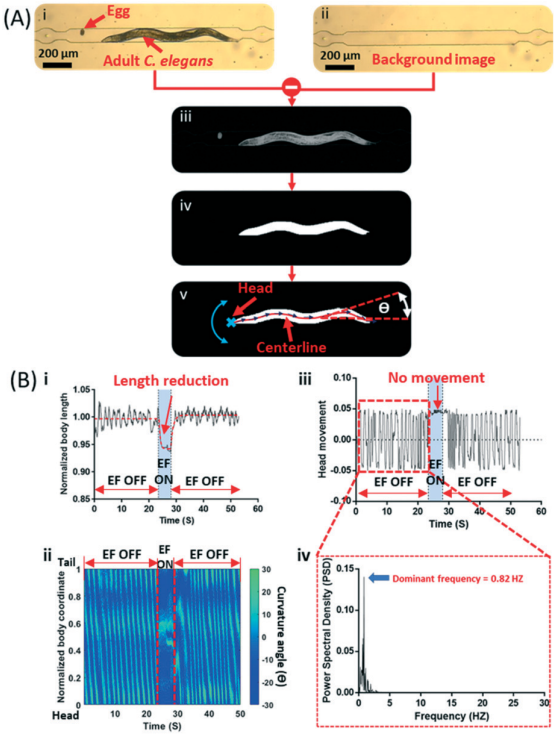

Fig. 2 Details of the MATLAB-based image processing code for frame by frame analysis of the recorded videos. (A) (i) A D1 adult worm captured inside the electric trap. (ii) The background image after pushing the worm out of the trap. (iii) Difference between (i) and (ii) to obtain an image with only the worm and the eggs. (iv) Binarized image and the largest connected object (the worm) retained. (v) The worm's centerline, head location and body segment curvature angle used for analysis. (B) (i) Normalized body length, (ii) body curvature plot, and (iii) head movement tracking of the worm inside the microfluidic device. Head tracking data was used to determine the dominant frequency in (iv) by taking the power spectrum density.

after unloading the worm. The background image was subtracted from each video frame (Fig. 2Aiii) and binarized (Fig. 2Aiv), achieving high-quality binarization of the worm image with all the other objects excluded from the image. For instance, Fig. 2Aiii shows an egg that was removed from the binary image in Fig. 2Aiv. Then, the white pixels in Fig. 2Aiv were used to obtain the centerline of the worm. The centerline was determined by rearranging the white pixels into vertical lines and getting the middle pixel of each vertical line in the *X*-direction. By connecting these pixels, the centerline (Fig. 2Av) was determined and used to measure the worms' length.

The worm's length was normalized by its length before EF exposure and plotted over time (Fig. 2Bi), then used as a readout for the electrically-induced body muscle contraction and relaxation. For these experiments, six worms were analyzed for three consecutive cycles of anode or cathode stimulation, giving a total of 18 measurements. Each cycle involved an excitation period of 5 s preceded and followed by 25 s acclimation periods. As shown in Fig. 2Bi, during the first 25 s, the worm length was not significantly changing; however, when the EF was turned on, the worm's length contracted for 5 s with an exponential-like decay. Then, when the EF was turned off, the worm started to relax, and the length returned to its original value rapidly (ESI† Video S1).

The worms' body movement was determined by tracking the body sinusoidal wave with time to derive the body curvature plots in Fig. 2Bii. These plots characterized how the bending waves propagated in time along the worm body, which were used to determine the swimming frequency during the on- and off-EF periods (ESI† Video S1). Worm body curvature was represented in terms of the tangent angle made by each body segment (θ in Fig. 2Av). Accordingly, Fig. 2Bii depicts the curvature angle θ of different worm body segments (0 for the head and 1 for the tail) as a function of time. A vertical line across the graph in Fig. 2Bii represents the sinusoidal shape of the worm at a specific time frame, whereas the observer can track the movement of specific body segments as a function of time by sketching a horizontal line. Moreover, the worm's head, symbolized by a cross sign in Fig. 2Av, was monitored to quantify the movement frequency by tracking the lateral head movement with time (Fig. 2Biii and iv). For instance, Fig. 2Biii shows a pattern of continuous sinusoidal waves during the EF-off period, followed by a pause period when the EF was applied and a resumed sinusoidal head movement pattern in the post-exposure period. Fig. 2Biv shows the power spectral destiny analysis to determine the dominant frequency for the sinusoidal head movement which was obtained by our MATLAB code.

Fluorescent intensity analysis was also done in our MATLAB code for the GCAMP strains reported in Table 1. Before applying the EF, it was necessary to ensure that the neurons or muscles reached the baseline activity before recording the video. Once the video was imported, the user was asked to select a region of interest (ROI), for instance around the vulva. In each video frame, the mean green fluorescent intensity of the ROI was determined (I_{ROI}), subtracted from the background intensity ($F = I_{ROI} - I_{background}$), normalized to the mean baseline activity $\left(\frac{\Delta F}{F_0} = \frac{F - F_0}{F_0}\right)$, and plotted *versus* time. The baseline activity (F_0) was quantified as the mean green fluorescent intensity of the ROI prior to the stimulus. The background intensity was obtained through selecting another ROI, similar in size to the target ROI, within the sides of the frame.

Off-chip locomotion assays

For off-chip locomotion analysis, the electrically exposed worms were collected after the experiment and transferred into 3 cm diameter Petri dishes containing 1 ml of M9 buffer. An upright Leica stereomicroscope (Leica MZ10 F fluorescence microscope, Leica, Germany) was used to video-record the worms swimming behaviour in M9. Then, the videos were post-processed using the worm tracker plugin in

Fiji software[28] to subtract the background and determine the average speed and swimming frequency. For comparison purposes, worms from the same population and age were transferred into M9, without exposure to EF, and their speed and swimming frequency were recorded as the control group (ESI† Section 2).

Statistical analysis

A pilot experiment was conducted to provide a base for determining the sample size using GPower software.[29] At least two replicates of 10 worms were used in the egg-laying experiments, and at least five worms were used for the length reduction, body bend, and fluorescent intensity analysis. The exact sample size used for each experiment is presented in the figure captions. The data were presented in two formats, either as the mean ± standard error of the mean (SEM) or using box plots with medians, 25% and 75% percentiles, and maximum and minimum data points. We used the Mann–Whitney test to determine the statistical significance between two groups, while the statistical differences among multiple data points were determined using one-way ANOVA analysis. The significance levels were identified by stars, *i.e.* * for p-value < 0.05, ** for p-value < 0.01, *** for p-value < 0.001, and **** for p-value < 0.0001.

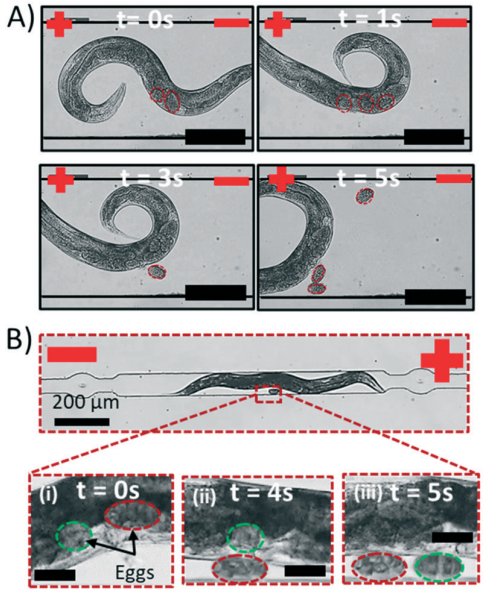

Fig. 3 (A) Electrotaxis re-orientation attempt of a D1 *C. elegans* in response to an EF of 6 V cm^{-1} which was accompanied by egg-laying inside a 300 µm wide microchannel. (B) Electric egg-laying behaviour of a D1 *C. elegans* in response to an EF of 6 V cm^{-1} inside the 100 µm wide electric trap of the proposed microchannel.

Results and discussion

Electric egg-laying of *C. elegans*

In a DC EF, *C. elegans* sense the strength and direction of the EF with amphid neurons and swim towards the negative pole on open agarose surfaces[12] and inside microchannels.[15] Aging has been shown to decrease the electrotactic response by 70% from young adult to day-8 adult stage.[30] Here, we asked for the first time whether EF induces any behavior other than electrotaxis in *C. elegans*, especially at gravid adult stages that electrotaxis weakens significantly. To answer this question, two microfluidic devices, one with a 300 µm-wide channel and one with a 100 µm-wide trap in the middle as shown in Fig. 1A, were used. The experimental setup demonstrated in Fig. 1B was used for electric stimulation of the worms as elaborately discussed in the Materials and Methods section. Video processing and analysis was done to assess various movement phenotypes that are shown in Fig. 2 and discussed in the Materials and methods section.

We fabricated a 4 cm-long and 300 µm-wide microfluidic electrotaxis channel[15] and tested the effect of EF on gravid adult worms. In these preliminary assays, worms were first facing towards the cathode, however when the EF was reversed, they showed a tendency to turn slowly towards the cathode and while doing so, they also deposited eggs ((ESI† Video S2)). For example, Fig. 3A shows sequential images of a D1 adult worm exposed to a 6 V cm^{-1} EF, showing egg-laying behaviour instead of electrotaxis over a period of 5 s. Counting the number of eggs and neuronal imaging of the worm in this wide-channel device imposed some challenges mainly due to the continuous and wide-range movement of the worm during egg deposition.

To address the limitations above, the microfluidic device shown in Fig. 1 was developed to restrain the worms' orientation while allowing egg release and fluorescent imaging during EF exposure. Fig. 3B shows sequential images of a D1 adult *C. elegans* in the electric trap of our device while being exposed to an EF of 6 V cm^{-1} with the cathode positioned at the tail of the worm. By applying the EF, we observed that although the worm could not rotate towards the cathode, it still deposited eggs over a period of 5 s. We also noticed that the egg-laying phenomena was accompanied by various movement kinematics in this device, including body shortening and immobilization which aided in on-chip neuron imaging of GCaMP strains as discussed later in this paper.

The discovery of *C. elegans* EF induced egg-laying in a close-fitting microchannel led us towards in-depth investigation of the effect of electric pulse direction, strength, and duration as well as worm age on the egg-laying behaviour in the following sections. We have also examined the involvement of neurons and muscles in electric egg laying.

Effect of EF direction on the egg-laying behaviour

D1 adult worms ($N = 70$) were positioned in the electrical trap of the microfluidic device and exposed to EF with cathode at their heads or tails. In the absence of EF, the worms moved in the trap with an average head movement frequency of 0.89 ± 0.18 Hz and no significant change in their swimming

kinematics (ESI† Video S1). Moreover, they showed no egg-laying behaviour during a maximum waiting time of 10 min. Then, a series of 6 V cm^{-1} EF pulses (5 s on and 25 s off) was applied for 10 minutes while the worms were facing either the cathode or the anode. ESI† Video S3 demonstrates the behaviour of one of these worms before, during and after exposure to EF with cathode at its tail. As shown in Fig. 4A, anode-facing worms deposited significantly more eggs in response to the EF (9 eggs/worm in average) compared to the cathode-facing worms (1 egg/worm) (ESI† Video S3). It is worth mentioning that from the 70 worms tested in each group, the egg-laying response rate was 92.8% *versus* 14.3% for the anode- and cathode-facing worms, respectively. Interestingly, this robustness in egg-laying response for the anode-facing worms is similar to *C. elegans* electrotaxis response rate when cathode is positioned at the posterior side of the worms.

To investigate the causes and effects behind the EF-induced egg-deposition, various locomotion kinematics such as changes in the worms' body length (Fig. 4B) and the head movement frequency were studied parametrically before, during and after EF exposure. Fig. 4C depicts the instantaneous length reduction due to EF exposure for anode- and cathode-facing worms. A significant shortening in the worms' length was observed in both cases, implying involvement of the body wall muscles in egg-deposition during EF exposure. However, the anode-facing worms had an average length contraction of 7.75%, which was significantly ($p < 0.01$) larger than the 5.8% contraction of the cathode-facing worms, as shown in Fig. 4Di. This corresponds well with the larger number of eggs released in the worms initially facing the anode as shown in Fig. 4A. Further discussions related to the dependency of muscles and neurons excitation on EF direction during contraction

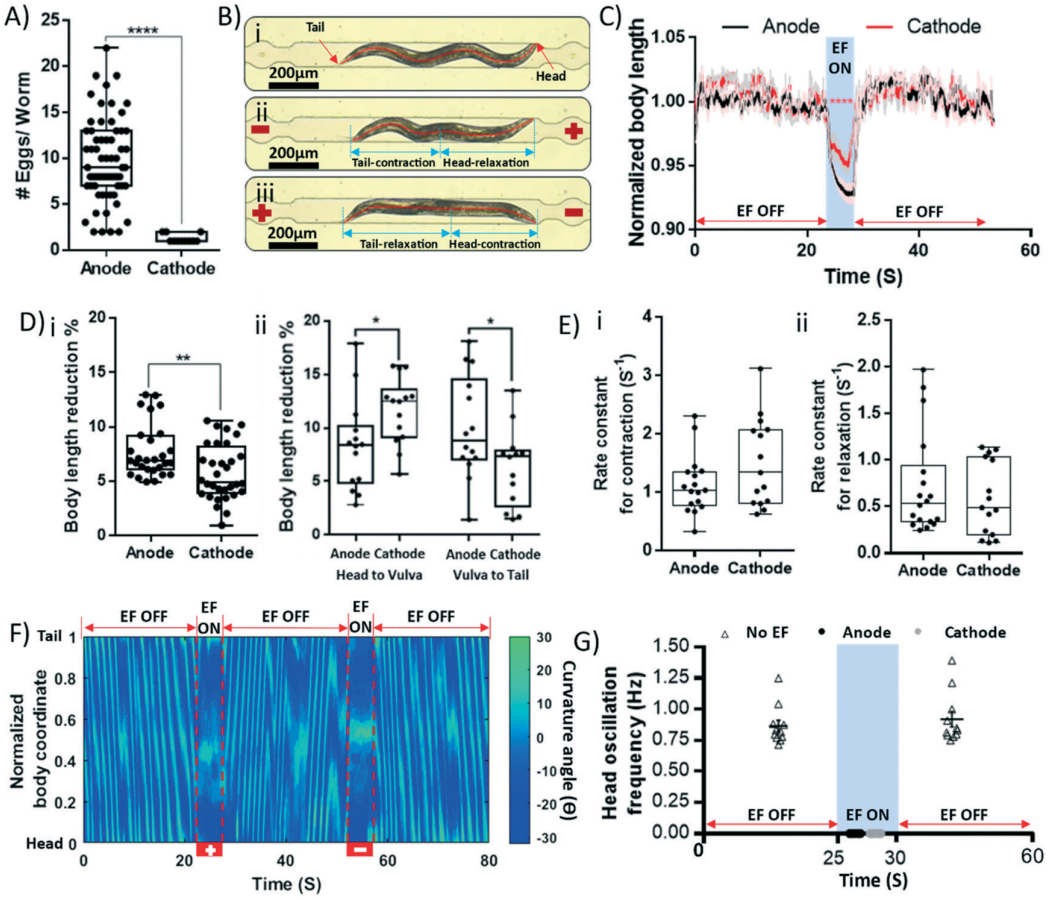

Fig. 4 The effect of EF direction on C. elegans egg-laying behaviour. EF of 6 V cm^{-1} was applied for up to 10 min in pulses with 5 s on and 25 s off cycles. (A) Number of eggs per worm for N = 70 worms that were facing towards the anode or cathode in the trap. (B) Optical microscopic images showing the worm in the electric trap during (i) no EF, (ii) anode-facing EF, (iii) cathode-facing EF. (C) Instantaneous normalized body length of anode-and cathode-facing worms (N = 18), showing contraction and relaxation periods fitted with one-phase decay and association models, respectively, to quantify the contraction-relaxation kinematics. (D) (i) Maximum total body length reduction and (ii) head-to-vulva and vulva-to-tail length reduction of worms facing either the anode or the cathode. (E) Rate constants for (i) contraction and (ii) relaxation. (F) Time-lapse normalized body curvature angle of a worm exposed to two EF pulses with anode and then cathode at head. (G) Worms head oscillation frequency during the on- and off-periods of the EF, showing a complete movement inhibition during EF stimulation for both anode-and cathode-facing worms.

and egg-laying, supporting the outcomes of this study, are provided later.

During the experiments, we also noticed that the muscle contraction-relaxation behaviour was not consistent between the anode and cathode-facing cases. For instance, in the anode-oriented worms, we observed a dominant contraction in the mid-region body muscles (Fig. 4Bii) while for the cathode-oriented worms, the contraction was significant in the headwall muscles as shown in Fig. 4Biii. To depict this quantitatively, body length reduction was analyzed separately on the head-to-vulva and vulva-to-tail sections of the worms, before and during EF exposure in anode- and cathode-facing worms (Fig. 4Dii). The results confirmed that contraction was associated with the head region in the cathode-facing worms while the anode-facing worms experienced dominant contraction in the mid-body or the tail region. In other words, regardless of orientation, the side of the worm facing the cathode experienced a more dominant contraction of the body. Moreover, contraction in the mid-body region where the vulva is located may be a reason for the worms expelling more eggs when facing the anode, *i.e.* exerting more force on the vulva muscles to twitch and lay eggs.

Muscle excitation-contraction coupling is an interesting process by which *C. elegans* crawl on an agar surface or swim in liquids. Having seen the effect of EF on muscles in our experiments, we became interested in examining the contraction-relaxation characteristics of the muscles. The data in Fig. 4C were further analyzed and fitted using an exponential decay or growth equation to determine how fast muscles contract or relax during and after EF activation. We aimed to figure out whether there is a difference in the contraction/relaxation kinetics under the two directional EF stimulations. Fig. 4E shows the rate constant of relaxation and contraction for anode- and cathode excitations. The results indicated no significant difference in the contraction and relaxation rates of both experimental conditions. Moreover, our data matched the contraction and relaxation rates reported by optogenetics for unexposed worms[31] (ESI† Fig. S3). This showed the potential use of our technique in studying the overall muscle kinetics of wild-type and potentially other worm strains.

Another interesting parameter observed in both anode- and cathode-facing worms was the loss of the swimming kinematics during the EF exposure, determined by the worms' body movement angle and head movement frequency. The body curvature of the worm in Fig. 4F fluctuated between ±30 degrees during the off-EF period, whereas it became constant during EF exposure due to the worm ceasing its movement as shown in Fig. 4G. The calculated swimming frequency during the off-EF period was 0.87 ± 0.046 Hz and 0.92 ± 0.06 Hz before and after the stimulus, respectively, whereas, during the on-EF period, the frequency reduced to zero. This further confirmed that during EF exposure, the worms ceased movement, contracted their bodies, and deposited eggs in the device.

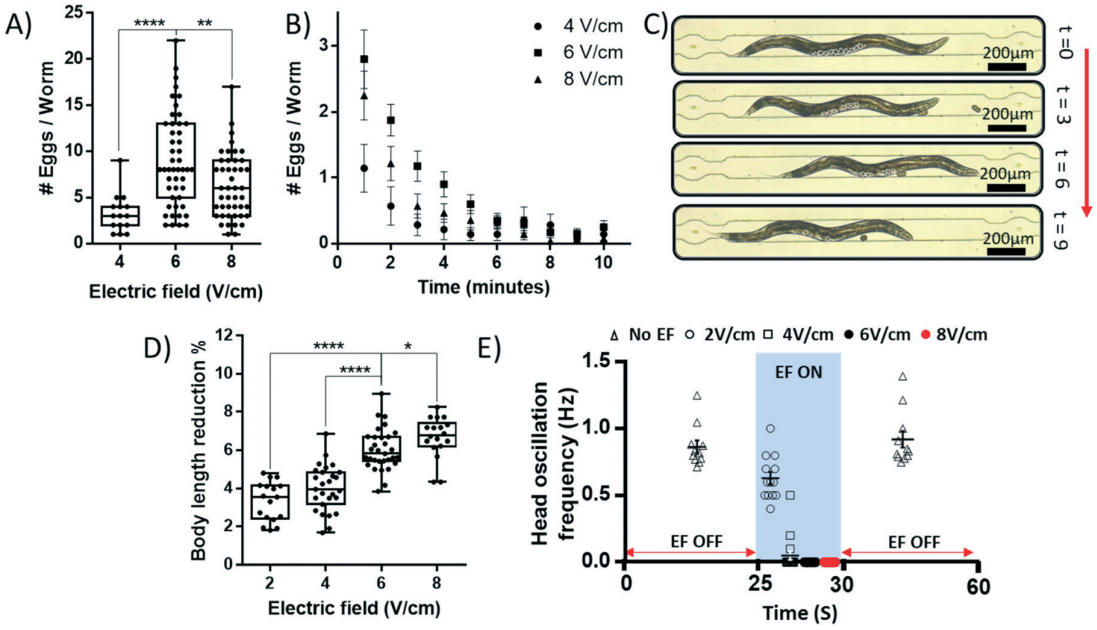

Fig. 5 The effect of EF strength on egg-laying behaviour of D1 anode-facing wildtype worms using 5 s on and 25 s off pulses for 10 min. Number of eggs per worm for at least N = 20 worms at different EF strengths is shown (A) for the whole 10 min period and (B) at the end of each minute. (C) Time lapse images showing egg-laying and emptying the uterus without reproducing new eggs (time is represented in minutes). (D) Relative body length reduction percentages during EF stimulation at different EFs. (E) Worm head movement frequency during on- and off-periods of EF at different EF strengths.

Effect of EF strength on the egg-laying behaviour

Having established the importance of worms orientation towards the anode for electric egg-laying, here, we asked if EF strength has a dominant effect on this novel behaviour. Fig. 5A shows the effect of 5 s-long EF pulses with 2–8 V cm^{-1} strengths on the egg-laying, body length and oscillation frequency of D1 wildtype worms facing the anode. The results showed a robust and peaking egg-laying activity at EF = 6 V cm^{-1} while a 2 V cm^{-1} EF did not induce any egg-laying (therefore omitted from Fig. 5). At low EF of 4 V cm^{-1}, a significant decrease in egg-laying was observed compared to 6 and 8 V cm^{-1}. Although an EF of 8 V cm^{-1} stimulated the worms to expel eggs, the number of extracted eggs significantly decreased compared to 6 V cm^{-1}.

To better understand the effect of EF strength, we analyzed the rate of egg-laying per minute over the 10 min stimulation period (Fig. 5B). At all times during the experiment, the number of eggs expelled at 6 V cm^{-1} was more than 4 and 8 V cm^{-1} EFs. Egg-release rate decreased with time for all EFs and reached a minimum value at approximately 6 min post EF exposure, after which the rate plateaued. This was because *C. elegans* hermaphrodites usually store around 10–15 fertilized eggs in their uterus. Naturally, the worms give birth to 2–3 eggs every 20–25 min,[21] which means that their capability to sustain a constant number of eggs in the uterus is limited under normal conditions. In our microfluidic chip, most eggs were expelled in the first 4 min, and the worms were not able to produce new eggs during the 10 min experimental period. This was confirmed by time-lapse optical images of worms during the 10 min period in Fig. 5C, illustrating that the number of eggs in the uterus decreases over time with no new eggs produced.

The effect of EF strength on egg laying may be understood further by performing body length analysis as shown in Fig. 5D. Increasing the EF strength consistently resulted in more significant body length shortening, which might be a reason behind expelling more eggs. The shortening effect was most significant when increasing the EF from 4 to 6 V cm^{-1} which corresponded well with the significant increase in the rate of egg-laying at this condition. Moreover, it is well understood that *C. elegans* electrotaxis increases with EF in the range of 2–6 V cm^{-1},[15] which is the reason behind the worms' increased tendency to turn towards the cathode in our device, while the channel's low width was preventing this reaction. Thus, the worms shrank instead of turning and, in response to the shrinkage, they expelled more eggs. The shortening phenotype has also been correlated with the activation of the VC neurons or the body wall muscles[1] which will be discussed later in this paper. Moreover, the increase in body shortening resulted in a significant decrease in the head movement frequency when increasing the EF from 2 to 8 V cm^{-1} as shown in Fig. 5E. Lastly, the slight reduction in egg laying at 8 V cm^{-1} may be attributed to the EF-induced paralysis which was also reported for freely moving worms by Rezai *et al.*[15] in wide electrotaxis channels.

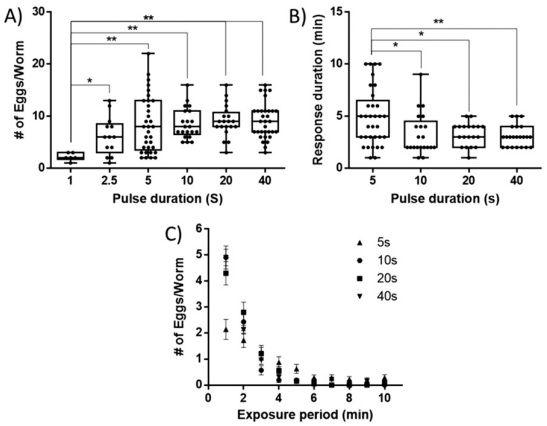

Fig. 6 The effect of EF pulse duration on the egg-laying behaviour of D1 anode-facing wildtype worms at 6 V cm^{-1} EF. (A) Number of eggs per worm for at least N = 20 worms at different pulse durations. (B) Overall egg-laying response duration at different pulse durations. (C) Time-lapse rate of egg-laying at different pulse durations (legend).

Effect of EF pulse duration on the egg-laying behaviour

The research hypothesis investigated in this section was the effect of pulse duration on electric egg laying of adult *C. elegans*. Moreover, extracting more eggs in a short period is of interest to many *C. elegans* laboratories for age-synchronizing the worms. Thus, the exposure time to the electric pulse was varied from 1 to 40 s to investigate its effect on the egg-laying process. Fig. 6A shows the total number of eggs released over 10 min by D1 wildtype worms which gradually increased with pulse duration until it reached a constant rate beyond the 5 s stimulation period. Fig. 6B shows that increasing the pulse duration from 5 s to 40s stimulated the worms to expel their eggs significantly faster (ESI† Video S4), as interpreted by shorter egg-laying durations. The egg-laying response duration was recorded based on when the worm stopped to give an egg for three consecutive pulses at each pulse duration. To better understand the EF pulse effect, we also plotted the time-lapse egg-laying rate for all pulse durations, as shown in Fig. 6C. This presentation confirmed that at longer pulses, the worms give more eggs in a shorter overall duration, perhaps due to contractions and vulva muscle openings lingering for longer periods of times during each pulse.

Effect of worm age on the egg-laying behaviour

C. elegans has been proposed as a promising model for aging studies.[32] It is well understood that aging causes a progressive decrease in the egg-production rate[33] and electrotaxis of *C. elegans*.[30] However, the effect of aging on electric egg-laying of *C. elegans* has not been studied. Here, we studied the electric egg-laying of worms aged from D1 to D4 past young adult stage using 5 s long EF pulses of 6 V cm^{-1} for 10 min. Fig. 7A shows that worms of all ages were responsive to EF, with a continuous significant decrease in their egg laying from D1 to D4. To compare our data with the

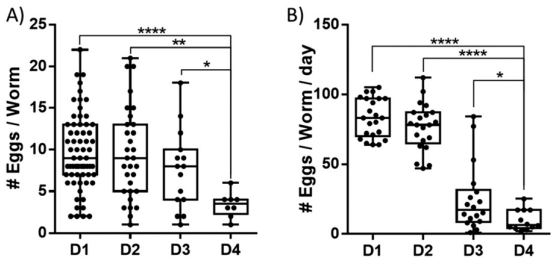

Fig. 7 Aging effect on the egg-laying behaviour of (A) anode-facing adult worms at 6 V cm^{-1} EF and 5 s pulse duration in the microfluidic device, compared with (B) worms natural (uninduced) egg-laying off-chip on NGM plates.

typical egg-release results for natural egg-laying (uninduced), we performed an off-chip egg-counting assay for 20 worms at ages D1 to D4, raised on NGM plates. The results in Fig. 7B showed a slight decrease in the egg-laying rate from D1 to D2, followed by a significant decline from D2 to D3 and D4. The electric egg-laying results follow the same trend of natural egg-laying, noting that the difference between the number of eggs obtained in Fig. 7A (electric) and 7B (natural) is due to differences between the assay times (10 min for electrical and full day for natural). Moreover, the decrease in D4 worm's response in both cases can be attributed to the age-related deficiency of egg-laying reproductive system, *i.e.* most of the expelled eggs were lysed or broken once ejected by the vulva.

Neuron and muscle activities during electric egg-laying behaviour

According to *C. elegans* egg-laying wiring diagram in Fig. 8A,[1] direct synaptic connections between HSN and VC neurons are required to command vms to enter the active state and stimulate egg-laying. Previous studies showed the level of coordination between the activation of the egg-laying neural circuit and egg production.[1] Here, we aimed at investigating the level of coordination between the EF stimulation and the egg-laying neural circuit using the genetically encoded calcium indicator, GCaMP.[34] We chose the transgenic strains LX1918, LX2004, LX1960, and LX1986 (Table 1) because they express the fluorescent Ca^{2+} reporter GCaMP in vms, HSN, VCs neurons, and uv1 cells, respectively. Primarily, we investigated the electric egg-laying of all the strains and observed that they deposit significantly more eggs while

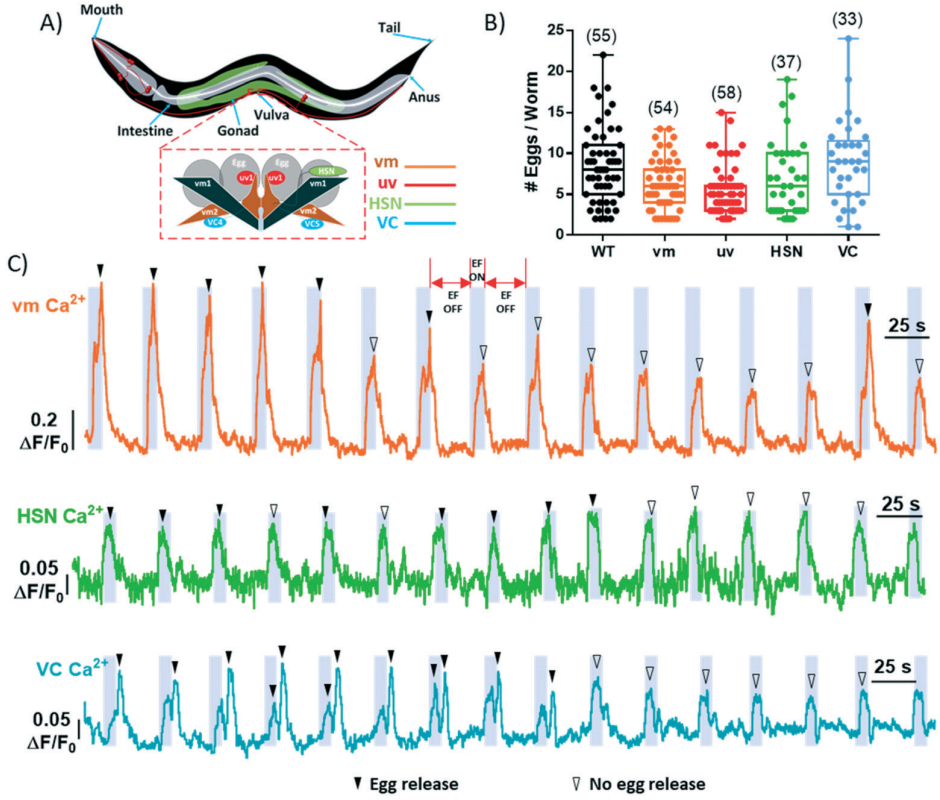

Fig. 8 Effect of EF pulses (6 V cm^{-1}, 5 s on, 25 s off) on egg laying neurons and muscles of *C. elegans*. (A) Schematic of the egg-laying neuromuscular circuit, showing the vms (orange), HSN (green), VC neurons (blue), and uv1 cells (red). (B) Number of eggs per worm for worms facing towards the anode and exposed to EF pulses of 10 minutes. Sample sizes are mentioned between brackets in the graph. (C) Eight-minutes recordings of fluorescent activity in vms, HSN and VC neurons, during the ON (gray-shaded) and OFF (white-shaded) EF periods. Filled arrow heads represent egg-laying events and empty arrow heads represent no-egg laying event.

facing the anode in response to EF pulses of 6 V cm^{-1}, which was statistically similar in counts to that of the wildtype worms (Fig. 8B).

Using long-term fluorescent imaging of calcium transients, we investigated the activation of the vms, HSNs and VC neurons during electric egg laying in our microfluidic device (ESI† Video S5–S10). An EF of 6 V cm^{-1} was applied as a series of pulses of 5 s on and 25 s off, while the worms were facing the anode, resulting in 16 consecutive cycles as shown in Fig. 8C for representative worms. In all strains, we observed a striking increase in the activity of cells (Fig. 8C) due to cell depolarization during the anodal stimulation that was mostly associated with egg-laying events (black filled triangles). No egg release (black empty triangles) happened mostly at the second half of the experiments during pulses 8–16, expectedly due to the depletion of uterus and lack of

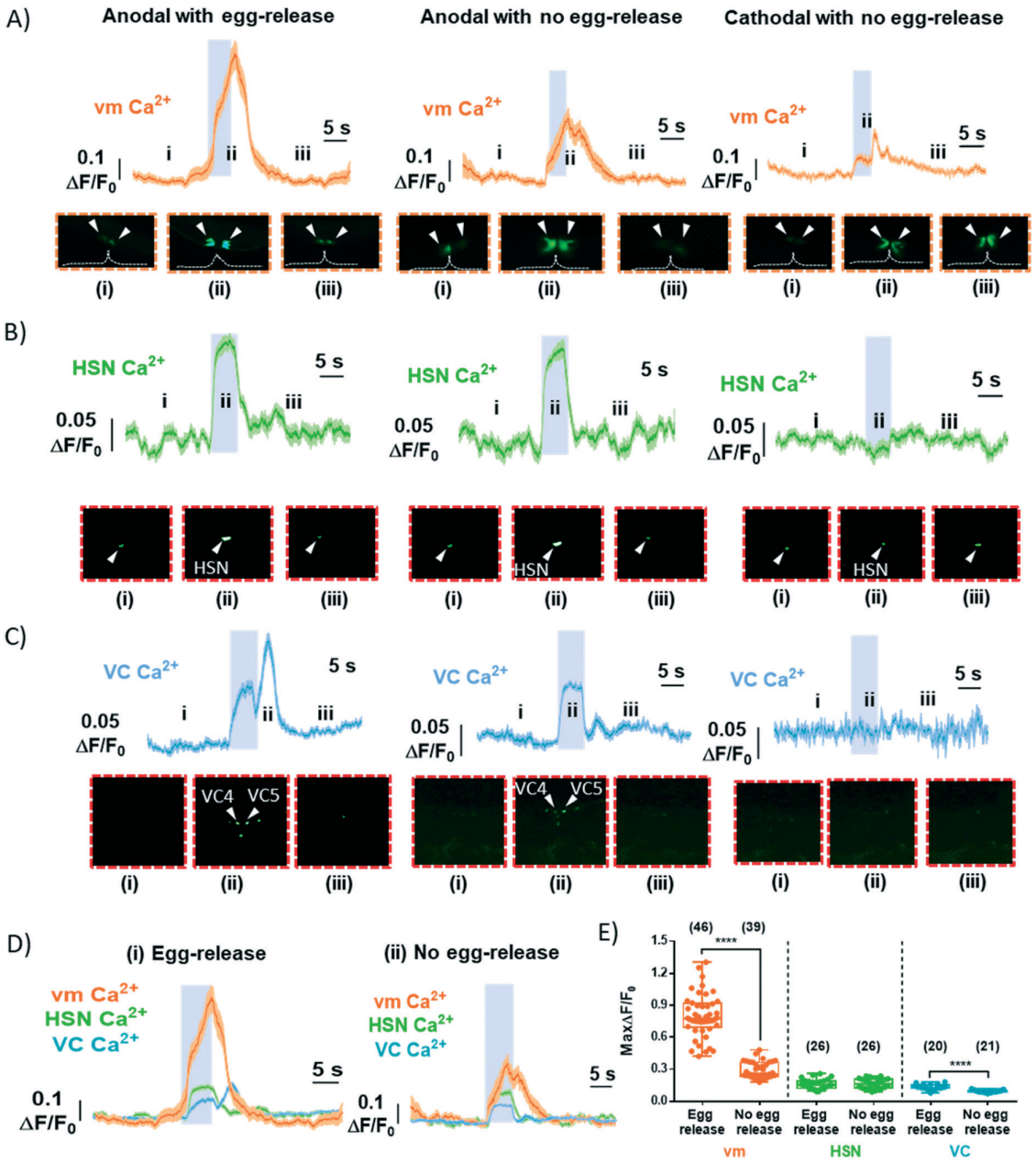

Fig. 9 Ca^{2+} transients and individual fluorescence imaging frames recorded during anodal stimulation (left with egg-release and middle with no egg-release) and cathodal stimulation (right with no egg-release) for (A) vms, (B) HSNs, and (C) VC neurons. (D) Overlapped Ca^{2+} transients of the vms, HSN, and VC neurons during (i) egg-release and (ii) no egg-release states. (E) Peak normalized fluorescent activities of vms, HSNs and VC neurons during egg release and no egg release states under anodal stimulation. In all conditions, 6 V cm^{-1} EF pulses with 5 s on and 25 s off were used.

eggs in the vicinity of the vulva to be released upon pulsation.

In Fig. 8C, we were able to distinguish between the strong depolarizations associated with strong twitches of the vms during egg-laying events (black filled triangles) and the weak contractions with no egg-laying events (black empty triangle) (ESI† Video S5). The same trend was observed for the VC neurons with higher Ca^{2+} transients during egg-laying (ESI† Video S7). The magnitudes of HSNs activities were not correlated as strongly with egg-release, but all egg-laying events were accompanied by HSN firing (ESI† Video S9). uv1 Ca^{2+} transients were weak to be recorded using our microscopy thus it has been excluded from the analysis. It is also worth mentioning that we rarely observed fluorescent activities in the vms, HSNs, and VCs in the absence of the EF stimulus, which shows the sensitivity of these cells to EF (ESI† Video S6, S8, and S10). That was also expected due to the use of M9 buffer, a hypertonic solution, which inhibits the worm from egg-deposition,[22] proving that the proposed electric egg extraction technique is solely stimulated through the application of DC EF. According to these results, we anticipate that our system will be of interest to further investigate the electrosensation in *C. elegans*.

For population investigations, we overlapped the cycles associated with anodal exposures with and without egg-deposition, as well as cathodal exposures (all without egg deposition) for the vms, HSNs, and VC neurons (Fig. 9A–C). Fluorescent images of representative worms are also provided prior, during, and after an EF pulse stimulation for all cases. The overlapped cycles showed robust Ca^{2+} transients in vms, HSNs, and VC neurons when worms were facing the anode regardless of the egg-laying event. In contrast and when the worms were facing the cathode, a slight increase in the Ca^{2+} transients during the EF with a small peak right after the EF pulse was observed in vms, while no response was given by HSNs and VC neurons in this condition. These findings show that the cell activities are associated with the EF direction, and contraction and egg-laying happen only when the HSNs, VC neurons and vms are strongly stimulated in the anodal mode. Our findings also suggest that the egg-laying circuit is involved in *C. elegans* electrosensation, and perhaps electrotaxis, which has not been reported previously.

Fig. 9D shows the overlapped transient activities of vms, HSNs and VC neurons during anodal exposure, separately illustrated for egg-release or no egg-release states. We noticed that egg-laying usually happened after HSN activation during the EF pulse, which was not different between the egg-release and no egg-release states. This suggests that HSNs activation is necessary for the worm to enter the egg-laying active state which matches with the results obtained by Collins *et al.*[1] VC neurons and vms were also activated but with different patterns based on egg release. Mechanical deformation of the vulva happening due to egg-deposition was correlated with a significant increase in the Ca^{2+} transients of both the vms during the pulse and the VC neurons after the pulse.

In order to quantitatively determine the cell excitation levels for each strain, we plotted the peak intensities at anodal stimulation during the egg-release and no egg-release states (Fig. 9E). vms twitches were observed strongly during the egg-laying events with a wide opening of the vulva to allow for egg-deposition (Fig. 9A), whereas the no-egg laying events were associated with significantly weaker twitches ($p < 0.0001$) (Fig. 9A and E). The peak anodal responses of HSNs were statistically similar in amplitude during egg release or no egg release events (Fig. 9E). VC peak transients were similar in amplitude to the HSNs and were mostly related to the VC4 and VC5 that are in proximity to the vulva (Fig. 8A). We noticed an increase in the VCs Ca^{2+} transients during the egg-release compared to no egg release state which were statistically dissimilar ($p < 0.0001$, Fig. 9E). We attributed the increase in the activities of vms and VC neurons, during the egg-laying states, to the actual deformation caused by the egg while passing through the vulva, which has also been suggested by Collins *et al.*[1] This study has provided exciting insights about the egg-laying pathway due to exposure to EF, but the reason behind cell excitability towards the anode, not the cathode, needs further investigation.

Electric egg-laying behaviour of HSN mutant *C. elegans*

HSNs, located in the vulva area, play a vital role in the egg-laying process.[21] Vulva muscles are directly connected to the HSNs through neuromuscular junctions. A substantial reduction in the egg-laying rate has been associated with the ablation or abnormal development of the HSNs.[1,21,22] HSNs mutations have contributed to the understanding of the rhythmic behaviour of egg-laying and it has been shown that exogenous serotonin can directly stimulate the vms to lay eggs in the absence of HSNs.[1] In the previous section, we showed that HSNs are activated during the anodal EF excitation period to stimulate the vms for egg release. Here, we aimed at investigating whether the loss of HSNs will reduce the electric egg-laying rate to show the application of our technique in mutant screening.

Age synchronized MT1082 worms (*egl-1*) were tested at the same age as the wildtype N2 worms (D1 past young adult stage). Normally, the MT1082 strain is strongly defective in egg-laying with a bag of ~50 eggs accumulated in their uterus compared to ~15 eggs in the wildtype (Fig. 10A) and a resultant larger size (Fig. 10B) (ESI† Video S11). The egg-laying rate and swimming kinematics of the MT1082 in response to 6 V cm^{-1} EF pulses (5 s on and 25 s off) were investigated in comparison to the N2 strain with the results shown in Fig. 10C.

Our results in Fig. 10C showed that, out of a total of 100 worms tested, $N = 31$ of MT1082 responded to the EF and expelled a significantly less number of eggs per worm compared to the N2 ($N = 65$ responders). It is worth emphasizing that the number of non-responders to EF in the MT1082 was significant which reflects the fact that MT1082 is strongly defective in egg-laying even in the presence of EF.

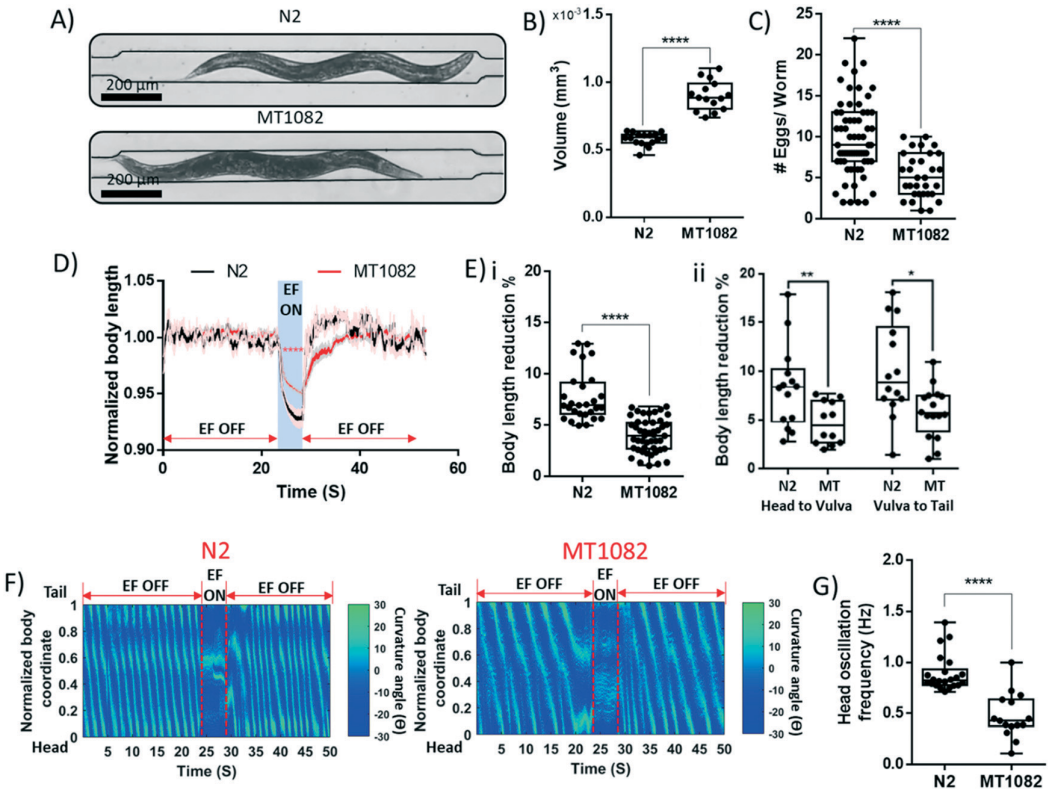

Fig. 10 The effect of EF on the worms egg-laying behaviour for wildtype N2 and MT1082, supported by quantitative analysis of the worm kinematics. EF of 6 V cm^{-1} was applied for up to 10 minutes in pulses with 5 s on and 25 s off cycles. (A) Bright-field images of both strains in the microfluidic device, showing that MT1082 contains more eggs (bloating behaviour) at the age of D1. (B) Approximated volume comparison between the two strains. (C) Number of eggs per worm for N = 65 worms for N2 and N = 31 worms for MT1082. (D) Instantaneous normalized body length of both strains (N = 18). (E) (i) Maximum total body length reduction and (ii) head-to-vulva and vulva-to-tail length reduction of both strains. (F) Time-lapse normalized body curvature angle of N2 and MT1082. (G) Worms head oscillation frequency during the off-EF periods.

As anticipated from our previous results, the decrease in egg-laying was accompanied by a decrease in the body length shortening of MT1082 compared to the N2, as shown in Fig. 10D. Moreover, the reduction in length was more towards the tail than the head, like the wildtype behaviour (Fig. 10E). Fig. 10F shows the curvature contours of both strains for a one-pulse stimulation cycle. The swimming frequency of MT1082 was significantly lower than the N2 during the off-EF period, quantified in Fig. 10G, whereas both strains completely stopped movement during the on-EF period. Altogether, our microfluidic chip has aided, for the first time, in studying the role of HSNs in electrosensation and egg laying, and we showed that loss of HSNs does not fully stop the electrical egg deposition, but it decreases the egg-laying rate significantly.

Conclusions

Like many model organisms, *C. elegans* respond to the electric field (EF) in a robust, concise, and persistent manner, by crawling towards the negative electrode of a polarized system, a behaviour termed electrotaxis. Previous studies have solely focused on the electrotactic-induced *C. elegans'* movement and its use for chemical and genetic screening within microfluidic devices. In this paper, we further investigated *C. elegans* electrosensation and introduced, for the first time, a novel EF-evoked behaviour, termed electric egg-laying in a simple to use microfluidic device that enabled trapping and exposure of individual worms to controlled EF conditions. We investigated the effect of worm aging and EF strength, direction, and pulse duration on the egg-laying behaviour, and showed that on-demand egg-deposition could be electrically stimulated in our microfluidic device.

Briefly, we characterized the electric egg-laying behaviour in a worm-fitting microchannel and determined the limiting worm age and EF strength, direction, and pulse duration within which maximum egg-deposition is observed. Egg-count was quantified along with several other phenotypes, including body length, head movement, and transient neuronal activities as measures of electrosensation at a single animal resolution. Interestingly and similar to stimulation of electrotaxis behaviour, electric egg-laying was maximized for the anode-facing worms with a significant increase in the egg-count and reduction in the body length and head

motion. The EF stimulation was found to be associated with shortening in the body length and a decrease in the head movement frequency. Moreover, the worms appeared significantly more sensitive at the EF strength of 6 V cm^{-1}, while all worms exhibited significantly lower response at low EF strengths. The egg-count was found to be independent of pulse duration, whereas the egg-laying response rate and duration were indirectly proportional to pulse duration. Due to the reduction in response duration at longer pulses, our technique has the potential to provide the pathway for developing a high-throughput egg synchronization method without involvement of chemicals (*e.g.* bleach) or harming the organism.

Our findings also implied that electric egg-laying decreases with worm aging, following the natural off-chip behaviour. Previous studies have shown that egg-laying can be used as a quantitative and user-independent indicator for drug screening and physiological aging. However, aging and life-span studies utilize fluorodeoxyuridine (FUdR), an inhibitor of DNA synthesis, in a *C. elegans* population to block progeny production and assist the maintenance of synchronous nematode populations for longer times.[35] FUdR has shown complex effects on aging in *C. elegans*, which opposes its use in aging studies. This gap in experimental procedures could be breached through the use of EF induced egg-release to deplete the uterus allowing for an extended period without progeny production. Moreover, egg-laying has been reported as a quick technique for antidiabetic drug screening.[35] Therefore, our technique can be an asset to shortening the egg-laying rate assay time and provide a fast quantification technique for drug screening. We anticipate that an appealing follow-up would be to validate the technique using established off-chip protocols for disease-specific compounds.

This is the first time a connection between the egg-laying circuit and electrosensation is reported, unraveling a pathway for further investigation and mapping of the neural basis governing this phenomenon in *C. elegans*. Various strains, expressing intracellular calcium ion dynamics among the egg-laying neural circuit, including HSNs, VC neurons, and vms were imaged during the EF stimulation. The results exhibited EF directional-dependency of the HSNs, VCs, and vms, which might elucidate the innate cathode-driven orientation of *C. elegans* as a safety mechanism to lower the excitation of its cells. We further tested a mutated strain lacking the HSNs and demonstrated that EF still induces egg-laying but with a defective phenotype, which shows the applicability of our technique for mutant screening. We envision that with small modifications to the existing design, several nematodes can be tested simultaneously under identical conditions, accommodating the needs to develop higher throughput electric egg-laying screening devices.

Altogether, our paper discusses novel electrically induced physiological and behavioural phenotypes discovered in *C. elegans* aiming to drive new hypotheses on the biological mechanisms governing electrosensation. Additionally, we established that EF stimulation of *C. elegans* within our microfluidic device has no adverse effects on the physiology of the nematodes.

Conflicts of interest

The author(s) declared no conflict of interest.

Acknowledgements

This work was supported by Natural Sciences and Engineering Research Council (NSERC) of Canada and the Early Researcher Award to PR and the Ontario Trillium Scholarship to KY.

References

1 K. M. Collins, A. Bode, R. W. Fernandez, J. E. Tanis, J. C. Brewer, M. S. Creamer and M. R. Koelle, *eLife*, 2016, **5**, e21126.
2 A. C. Hart, *Behavior*, ed. The C. elegans Research Community, 2006, url: http://www.wormbook.org.
3 B. P. Gupta and P. Rezai, *Micromachines*, 2016, **7**, 123.
4 H. E. Kinser and Z. Pincus, *Mol. Cell. Neurosci.*, 2017, **80**, 192–197.
5 A. J. Harrington, S. Hamamichi, G. A. Caldwell and K. A. Caldwell, *Dev. Dyn.*, 2010, **239**, 1282–1295.
6 C. D. Link, *Exp. Gerontol.*, 2006, **41**, 1007–1013.
7 M. Artal-Sanz, L. de Jong and N. Tavernarakis, *Biotechnol. J.*, 2006, **1**, 1405–1418.
8 K. Youssef, A. Tandon and P. Rezai, *Integr. Biol.*, 2019, **11**, 186–207.
9 K. Youssef, P. Bayat, A. R. Peimani, S. Dibaji and P. Rezai, in *Environmental, Chemical and Medical Sensors*, Springer, 2018, pp. 199–225.
10 M. M. Shanmugam, *Biology, Engineering and Medicine*, 2017, **2**, 1–5.
11 N. C. Sukul and N. A. Croll, *J. Nematol.*, 1978, **10**, 314–317.
12 C. V. Gabel, H. Gabel, D. Pavlichin, A. Kao, D. A. Clark and A. D. T. Samuel, *J. Neurosci.*, 2007, **27**, 7586–7596.
13 S. D. Chrisman, C. B. Waite, A. G. Scoville and L. Carnell, *PLoS One*, 2016, **11**(3), e0151320.
14 H. S. Chuang, W. J. Kuo, C. L. Lee, I. H. Chu and C. S. Chen, *Sci. Rep.*, 2016, **6**, 1–11.
15 P. Rezai, A. Siddiqui, P. R. Selvaganapathy and B. P. Gupta, *Lab Chip*, 2010, **10**, 220–226.
16 P. Rezai, A. Siddiqui, P. R. Selvaganapathy and B. P. Gupta, *Appl. Phys. Lett.*, 2010, **96**, 153702.
17 S. Salam, A. Ansari, S. Amon, P. Rezai, P. R. Selvaganapathy, R. K. Mishra and B. P. Gupta, in *Worm*, Taylor & Francis, 2013, vol. 2, p. e24558.
18 P. Rezai, S. Salam, B. P. Gupta and P. R. Selvaganapathy, *15th International Conference on Miniaturized Systems for Chemistry and Life Sciences 2011, MicroTAS 2011*, 2011, 2, 723–725.
19 X. Wang, R. Hu, A. Ge, L. Hu, S. Wang, X. Feng, W. Du and B. F. Liu, *Lab Chip*, 2015, **15**, 2513–2521.

20 B. Han, D. Kim, U. H. Ko and J. H. Shin, *Lab Chip*, 2012, **12**, 4128–4134.
21 W. R. Schafer, *Annu. Rev. Genet.*, 2006, **40**, 487–509.
22 W. R. Schafer, in WormBook: The Online Review of *C. elegans* Biology [Internet], *WormBook*, 2005.
23 E. R. Sawin, *Thesis dissertation*, Massachusetts Institute of Technology, Cambridge, USA, 1996.
24 L. A. Fenk and M. de Bono, *Proc. Natl. Acad. Sci. U. S. A.*, 2015, **112**, E3525–E3534.
25 T. Stiernagle, *C. elegans*, 1999, **2**, 51–67.
26 M. Porta-de-la-Riva, L. Fontrodona, A. Villanueva and J. Cerón, *J. Visualized Exp.*, 2012, e4019.
27 Y. Xia and G. M. Whitesides, *Annu. Rev. Mater. Sci.*, 1998, **28**, 153–184.
28 J. Schindelin, I. Arganda-Carreras, E. Frise, V. Kaynig, M. Longair, T. Pietzsch, S. Preibisch, C. Rueden, S. Saalfeld, B. Schmid, J. Y. Tinevez, D. J. White, V. Hartenstein, K. Eliceiri, P. Tomancak and A. Cardona, *Nat. Methods*, 2012, **9**, 676–682.
29 F. Faul, E. Erdfelder, A. G. Lang and A. Buchner, *Behav. Res. Methods*, 2007, **39**, 175–191.
30 X. Manière, F. Lebois, I. Matic, B. Ladoux, J.-M. Di Meglio and P. Hersen, *PLoS One*, 2011, **6**(2), e16637.
31 H. Hwang, D. E. Barnes, Y. Matsunaga, G. M. Benian, S. Ono and H. Lu, *Sci. Rep.*, 2016, **6**, 19900.
32 X. Chen, J. W. Barclay, R. D. Burgoyne and A. Morgan, *Chem. Cent. J.*, 2015, **9**, 65.
33 C. L. Pickett and K. Kornfeld, *Aging Cell*, 2013, **12**, 544–553.
34 N. Chronis, M. Zimmer and C. I. Bargmann, *Nat. Methods*, 2007, **4**, 727–731.
35 H. Wang, Y. Zhao and Z. Zhang, *Biochem. Biophys. Res. Commun.*, 2019, **509**, 694–699.

Electronic Supplementary Material (ESI) for Lab on a Chip.

Supplementary materials

Electric Egg-Laying: A New Approach for Regulating *C. elegans* Egg-Laying Behaviour in a Microchannel using Electric Field

Khaled Youssef[1], Daphne Archonta[1], Terrance J. Kubiseski[2], Anurag Tandon[3,4], and Pouya Rezai[1,*]

[1] Department of Mechanical Engineering, York University, Toronto, ON, Canada
[2] Department of Biology, York University, Toronto, ON, Canada
[3] Tanz Centre for Research in Neurodegenerative Diseases, Toronto, Ontario, Canada
[4] Department of Medicine, University of Toronto, Toronto, Ontario, Canada

* Corresponding Author: BRG 433B, 4700 Keele St, Toronto, ON, M3J 1P3, Canada; Tel: 416-736-2100 ext. 44703; Email: prezai@yorku.ca

1. Numerical Simulation of Electric Field in the Microfluidic Device

The analysis of the electric field (EF) distribution and uniformity in our microfluidic device was conducted through a two dimensional (2D) numerical simulation. Using the steady-state direct-current (DC) electric module of the COMSOL Multiphysics® software, Ohm's law was solved to determine the EF distribution through the conductive media within the microchannel. The design of the microfluidic features was done in SOLIDWORKS® and consequently analyzed by COMSOL after determination of the boundary conditions and the grid formation on the 2D model. The device comprised of a 3 cm-long and 300 μm-wide channel containing a 100 μm-wide trap in the middle of the design, acting as an on-chip trap for the worm (Figure 1A in the main paper). M9 conductivity was determined experimentally in a similar 300μm-wide channel and measured to be 1.6 siemens/m, a parameter that was added to the numerical model. An electrical insulation boundary condition was applied to all the boundaries of the device. The two end reservoirs were set as an 8V electric potential and the ground, respectively. Grid formation was achieved by using the built-in mesh generation module of COMSOL Multiphysics software, applying a triangular mesh to the features. Figure S1A depicts the EF distribution within the device and the on-chip trap. Figure S1B is showing the EF distribution along line A-A, confirming that the EF is uniform at 2, 4, 6, and 8 V/cm for on-trap exposure. Electric potential of 2.25, 4.5, 6.9 and 9 V were found to be respectively applied at the end-reservoir to achieve the 2, 4, 6, and 8 V/cm EFs required in the trap,

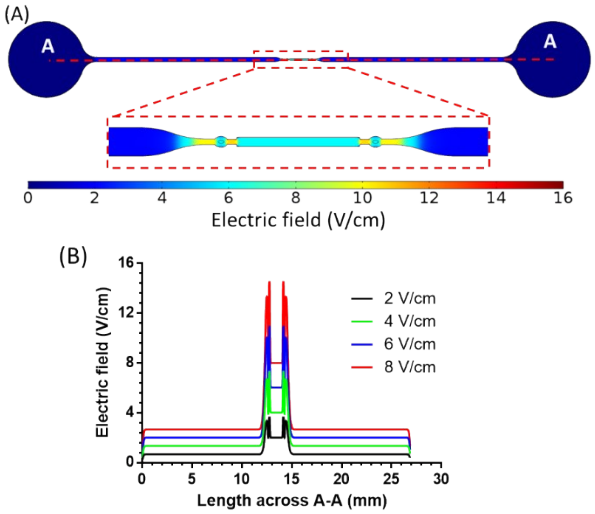

Figure S1: COMSOL simulation of electric field distribution in the microfluidic device when a 7V stimulus was applied along the channel. (A) Electric field distribution in the chip with an inset showing the electric field distribution in the trap region. (B) Electric fields along line A-A in various conditions achieved by applying an electric potential across the reservoirs.

2. Effect of EF exposure on *C. elegans physiology*

Ten worms were randomly collected out of the chip after being exposed to 6V/cm for 10 min (5s on, 25s off pulses) to compare their locomotion behaviours to a group of worms not exposed to EF. At the first glance, the worms were normally swimming in M9 buffer with no apparent morphological defects or abnormal movements. Quantitative analysis in Figure S2 also shows that there is no significant difference in the average speed and body bend frequency of the EF exposed worms compared with the control group. Although these results suggest that the effect of EF in a short time after experiments may be benign on *C. elegans*, but further viability and lifespan experiments are needed if the exposed worms are to be used for extended experiments or off-spring studies.

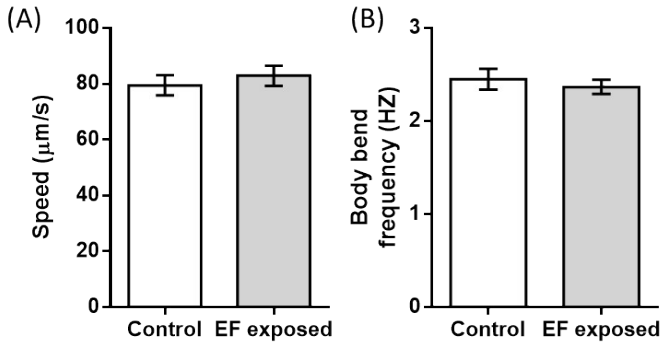

Figure S2: Effect of EF pulses on C. elegans movement behaviour. EF pulses of 6V/cm for 5s on and 25s off were applied for 10 minutes and the (A) speed and (B) body bend frequency of the worms post exposure were compared to the controls with no EF exposure.

3. Comparison of Contraction and Relaxation Rate Constants of Electrical and Optogenetic Methods

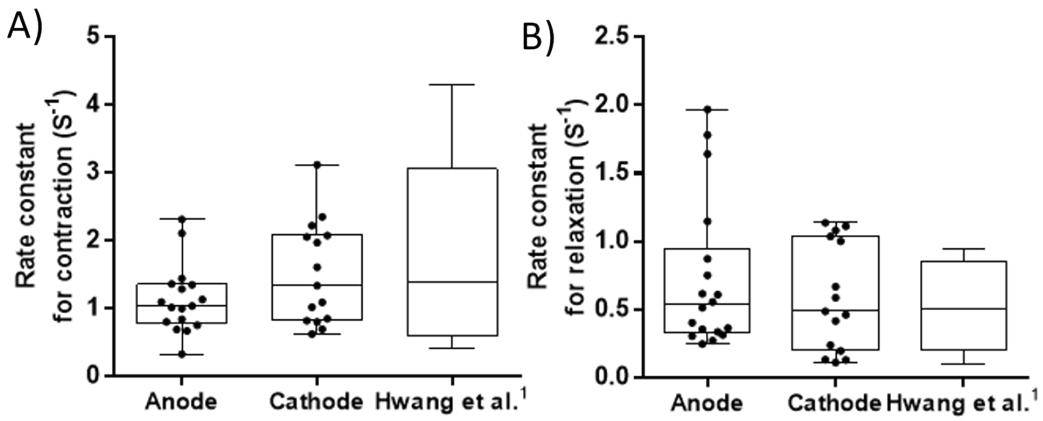

Figure S3: Rate constant for (A) contraction and (B) relaxation of C. elegans muscles using electrical stimulation (our technique) and optogenetics[1]

4. Supplementary Videos

Video S1: Image processing for determination of worm centerline, head and tail movement in pulses of 5s on and 25s off at EF of 6 V/cm

Video S2: EF effect on D1 worm inside a 300µm-wide channel at EF of 6V/cm for 5s pulse duration.

Video S3: The effect of EF direction on *C. elegans* egg-laying behaviour inside our microfludic device at EF of 6V/cm for 5s pulses of anodal and cathodal head stimulation.

Video S4: The effect of EF pulse duration on the egg-laying behaviour at EF of 6V/cm for 40s pulse duration.

Video S5: Vulva muscles Ca^{2+} transients during anodal stimulation at EF of 6V/cm in pulses with 5s on and 25s off cycles.

Video S6: Vulva muscles Ca^{2+} transients during cathodal stimulation at EF of 6V/cm in 5s pulses.

Video S7: HSNs Ca^{2+} transients during anodal stimulation at EF of 6V/cm in 5s pulses.

Video S8: HSNs Ca^{2+} transients during cathodal stimulation at EF of 6V/cm in 5s pulses.

Video S9: VCs Ca^{2+} transients during anodal stimulation at EF of 6V/cm in 5s pulses.

Video S10: VCs Ca^{2+} transients during cathodal stimulation at EF of 6V/cm in 5s pulses.

Video S11: The effect of EF on the worms' egg-laying behaviour for MT1082 strain.

5. References

1 H. Hwang, D. E. Barnes, Y. Matsunaga, G. M. Benian, S. Ono and H. Lu, *Scientific reports*, 2016, **6**, 19900.

B.4 Paper IV: Microplastic Toxicity at the Neuronal, Behavioural and Physiological Levels Investigated on *C. elegans* in a Multi-Nematode Lab-on-a-Chip Device with Population and Single-Worm Screening Capability

Youssef, K., Archonta, D., Kubiseski, T. J., Tandon, A., & Rezai, P. (2021) Microplastic Toxicity at the Neuronal, Behavioural and Physiological Levels Investigated on *C. elegans* in a Multi-Nematode Lab-on-a-Chip Device with Population and Single-Worm Screening Capability. Science of the Total Environment "Under review".

Microplastic Toxicity at the Neuronal, Behavioural and Physiological Levels Investigated on *C. elegans* in a Multi-Nematode Lab-on-a-Chip Device with Population and Single-Worm Screening Capability

Khaled Youssef[a], Daphne Archonta[a], Terrance J. Kubiseseki[b], Anurag Tandon[c,d], and Pouya Rezai*[a]

[a] Department of Mechanical Engineering, York University, Toronto, ON, Canada

[b] Department of Biology, York University, Toronto, ON, Canada

[c] Tanz Centre for Research in Neurodegenerative Diseases, Toronto, Ontario, Canada

[d] Department of Medicine, University of Toronto, Toronto, Ontario, Canada

* Corresponding Author: BRG 433B, 4700 Keele St, Toronto, ON, M3J 1P3, Canada; Tel: 416-736-2100 ext. 44703; Email: prezai@yorku.ca

Abstract

Environmental pollutants like microplastics are posing health concerns on aquatic animals and the ecosystem. Microplastic toxicity studies using *C. elegans* as a model are evolving but methodologically hindered from obtaining statistically strong data sets, detecting toxicity effects based on microplastics uptake, and correlating physiological and behavioural effects at an individual-worm level. In this paper, we report a novel microfluidic electric egg-laying assay for phenotypical assessment of multiple worms in parallel. The effects of glucose and polystyrene microplastics at various concentrations on the worms' electric egg-laying, length, diameter, and length contraction during exposure to electric signal were studied. The device contained eight parallel worm-dwelling microchannels called electric traps, with equivalent electrical fields, in which the worms were electrically stimulated for egg deposition and fluorescently imaged for assessment of neuronal and microplastic uptake expression. A new bidirectional stimulation technique was developed, and the device design was optimized to achieve a testing efficiency of 91.25%. Exposure of worms to 100mM glucose resulted in a significant reduction in their egg-laying and size. The effects of 1µm polystyrene microparticles at concentrations of 100 and 1000 mg/L on the electric egg-laying behaviour, size, and neurodegeneration of N2 and NW1229 (expressing GFP pan-neuronally) worms were also studied. Of the two concentrations, 1000 mg/L caused severe egg-laying deficiency and growth retardation as well as neurodegeneration. Additionally, using single-worm level phenotyping, we noticed intra-population variability in microplastics uptake and correlation with the above physiological and behavioural phenotypes, which was hidden in the population-averaged results. Taken together, these results suggest the appropriateness of our microfluidic assay for toxicological studies and for assessing the phenotypical heterogeneity in response to microplastics.

Keywords: Microplastics Toxicity, *C. elegans*, Microfluidics, Egg-laying, Neurodegeneration, Ecotoxicology.

INTRODUCTION

The discharge of environmental toxicants such as plastics, pesticides, carcinogens, antimicrobial products, and neurotoxins to the environment is escalating, which poses a significant burden on society, and the ecosystem's health and safety.[1–3] Some of these toxicants have been linked to neurodegeneration effects and reproductive complications.[4,5] A total of 359 million metric tons of plastics were manufactured from 1950 to 2018[6], leading to a severe accumulation of plastic waste in the environment. Plastic debris of less than 5 mm in size, termed microplastics[1], has become a major concern because it can travel over long distances in the air and aquatic environments while being easily ingested by organisms and animals.[3,5,7,8]

The effects of microplastics and their characteristics of shape, size, and concentration on marine life and the ecosystem have been studied and shown to result in various dose-dependent toxicities, including neural, behavioural, and reproductive toxicity.[9–12] The use of mammalian animal models limits the sample size in these studies and weakens their statistical strength. Such assays are also laborious, expensive, and time-consuming.[13,14] Rapid and high-throughput *in-vivo* screening assays for microplastic toxicity studies are urgently needed. In this front, simple model organisms such as *Caenorhabditis elegans*, *Drosophila melanogaster*, and *Danio rerio* have been used for toxicological studies to rapidly examine the effects of different pollutants at throughputs higher than animal-based assays.[15–18]

C. elegans has been used as a model organism for studying microplastics toxicity, offering versatile experimental advantages including small size, short life cycle, ease of maintenance, biological simplicity, and body transparency, leading to its suitability for genetic modification and high-throughput cell-to-behaviour toxicity screening.[19–21] Ingestion and intestinal accumulation of microplastics smaller than 5μm have been shown in *C. elegans*.[10,22,23] Microplastics negatively affected *C. elegans* phenotypical behaviours such as locomotion and body bend frequency as well as its growth and reproduction.[9–12,22–24]

Lei et al.[11] studied the effects of exposing *C. elegans* to 1 mg/L of 0.1-5μm polystyrene microparticles, using locomotory behaviours, growth, and lifespan as toxicity indicators. Their investigations demonstrated that 1μm particles significantly deteriorated the survival and growth rate and caused oxidative damage to cholinergic and GABAnergic neurons, which was ameliorated by natural antioxidants such as curcumin. The same group

investigated the toxic effects of different microplastics, including polyamides, polyethylene, polypropylene, polyvinyl chloride, and polystyrene at various concentrations of 0.5-10 mg/m^2.[12] All microplastics showed similar toxic effects on the survival rate of *C. elegans*, indicating no apparent dose- or material-dependent relationship. However, different sizes of 0.1-5μm microparticles showed a size-dependent lethality with a significant decrease in the reproduction rate and brood size at 1μm microparticles. Yu et al.[22] investigated the toxicity mechanisms of 1 μm polystyrene microplastics on *C. elegans* at different concentrations of 0-100 μg/L. Exposure to concentrations higher than 10μg/L induced a significant reduction in worms' head thrash, body bend, body length, and brood size. The toxicity was attributed to the increased reactive oxygen species expression and intestinal damage. The above-mentioned studies showed the effects of microplastics at relatively low concentrations. Therefore, Kim et al.[25] exposed *C. elegans* to 42 and 530 nm polystyrene particles at higher concentrations up to 100 mg/L and showed a significant reduction in the brood size. The effect of microplastics on other behaviours of *C. elegans*, such as reproduction, remains largely unknown. Another gap is the heterogeneity of microplastics uptake by the worms and a lack of understanding of correlating phenotypic toxicities, which requires the use of single-worm assays.

C. elegans reproduction is a rhythmic activity that has been established as a robust readout for investigating the toxic effects of different materials.[22,26] The egg-laying rate is measured by performing progeny counting over several hours. The entire process takes up to 8 hours and requires worm picking expertise without affecting its health, followed by counting the eggs. This conventional technique is cumbersome and limited in throughput to a few worms per hour. To address this limitation, we recently reported a novel technique to stimulate egg-laying of adult *C. elegans* on-demand using electric pulses in a microchannel (termed electric egg-laying).[27,28] The throughput of our device was limited to 5 worms/hr, hindering the feasibility of using it in toxicological studies on 100s of worms/assay.

In this paper, we report a new microfluidic device for electric egg-laying analysis and on-chip fluorescent imaging of multiple worms in parallel and apply it for the first time to toxicity screening of microplastics. The established effect of glucose on natural reproduction[29] was used as a proof-of-principle experiment to test the suitability of our assay. Then, we demonstrated the novel application of our method for microplastic toxicity studies, showing the adverse effects of microplastics on the electric egg-laying behaviour of *C. elegans* and its

correlation with microplastic accumulation in the worms. We achieved an assay time of 10 min and a throughput of up to 40 worms/hr, which was mainly limited by our microscopic field of view. Our method is significantly faster than conventional egg-laying assays with 4 hr assay time and 5 worms/hr throughput. Moreover, we showed another interesting advantage of our device for investigating the effect of microplastics uptake in correlation with multiple physiological and behavioural phenotypes of *C. elegans*, all at a single-worm resolution, which is not readily achievable by conventional methods.

MATERIALS AND METHODS

C. elegans culturing

Wild type *C. elegans* strain was obtained from the *Caenorhabditis* Genetics Center (University of Minnesota, USA) and maintained at approximately 22°C on freshly prepared standard nematode growth media (NGM) plates with *Escherichia coli* (*E. coli*) strain *OP50* as a food source.[30] All assays were performed with well-fed gravid hermaphrodite worms (day one post young adult stage (~64hrs)) obtained using the conventional alkaline hypochlorite (bleach) treatment.[31] Briefly, one week prior to the experiments, a chunked NGM plate was prepared and left for three days until a majority of the worms reached the gravid adult stage. All worms were washed off the plate in a 15 mL Eppendorf tube and exposed for 10 min to a solution of 3.875 mL double-distilled water, 125 µL NaOH, and 1 mL commercial bleach. The eggs were then collected by washing off the bleach solution using double-distilled water and centrifuging at 1500 rpm. The collected eggs were allowed to hatch into L1 larvae overnight in 1 mL of M9 buffer (3 g KH_2PO_4, 6 g Na_2HPO_4, 5 g NaCl, and 1 mL 1 M $MgSO_4$ in 1 L distilled water) using a RotoFlex™ tube rotator (RK-04397-40, Cole-Parmer, Canada). L1 larvae were collected by centrifuging and seeded on top of NGM plates, containing glucose or microplastics when needed.

C. elegans exposure to glucose and microplastics

Glucose was used as an established toxicant to natural egg-laying[29] to test the performance of our multi-worm device before using microplastics. NGM plates were prepared 5 days before the experiment, either with or without 100mM of glucose, and left for three days before bacterial seeding.[29] Luria Broth (LB) media (10 g

Bacto-tryptone, 5 g Bacto-yeast, and 5 g NaCl in 1 L distilled water) was inoculated with a single colony of OP50 and cultured overnight at 37°C in a thermal shaker-incubator.[30] Then, the NGM plates with or without glucose were seeded with 100 μL of the freshly prepared bacteria culture and left for two days before being used. L1 larvae were seeded on top of NGM plates with or without glucose for $\sim 64\ hr$ at 22°C until they become gravid adults and ready for our experiments.

Some studies[11,12] have shown that the toxicity of microparticles *on C. elegans* is size-dependent rather than material- or dose-dependent, and 1μm particles have been shown to be an effective size. Our microplastic exposure protocol was based on the method introduced by Schöpfer et al.[24]. One percent (w/v) stock solutions of 1-1.4μm high-intensity polystyrene Nile red fluorescent microparticles were procured from Spherotech Inc (FH-1056-2, Lake Forest, USA). Microplastic feed suspensions were prepared at concentrations of 100 and 1000 mg/L in a mixture of M9 buffer and *E. coli OP50*. Aliquots of 100 μL of the prepared solutions were seeded on top of bacterial lawns on NGM plates. Then, the microplastic-seeded plates were left to dry for two days before being used to expose the worms. The microplastics distribution was confirmed to be uniform on top of the bacterial lawn with a fluorescent microscope (Leica MZ10F fluorescence microscope, Leica, Wetzlar, Germany). For control experiments, plates were seeded only with 100 μL of the *E. coli* in M9 buffer. The prepared plates were then used for *C. elegans* growth from the L1 stage to the gravid adult stage (~64 hr) at 22°C for our experiments.

Off-chip egg-laying assay

The off-chip egg-laying assay was conducted for the glucose experiments as a validation step to prove that glucose was affecting the worms.[29] On the day of the experiment, 25 worms per group (control and glucose exposed) were randomly picked and seeded on new NGM plates with and without glucose, respectively. After three hours, the worms were picked off the plates, and the number of laid eggs was counted using an inverted microscope (BIM-500FLD, Bio-imager Inc., Canada) equipped with a camera (SN 14120187, Point Grey Research Inc. Canada). Counting the eggs on a plate took 60 min on average. The obtained number of eggs was compared to the control egg-count.

Microfluidic chip design and fabrication

The microfluidic device shown in Figure 1A was developed to enhance the throughput of our recently reported electric egg-laying method[27,28], then used for glucose and microplastic toxicity studies.

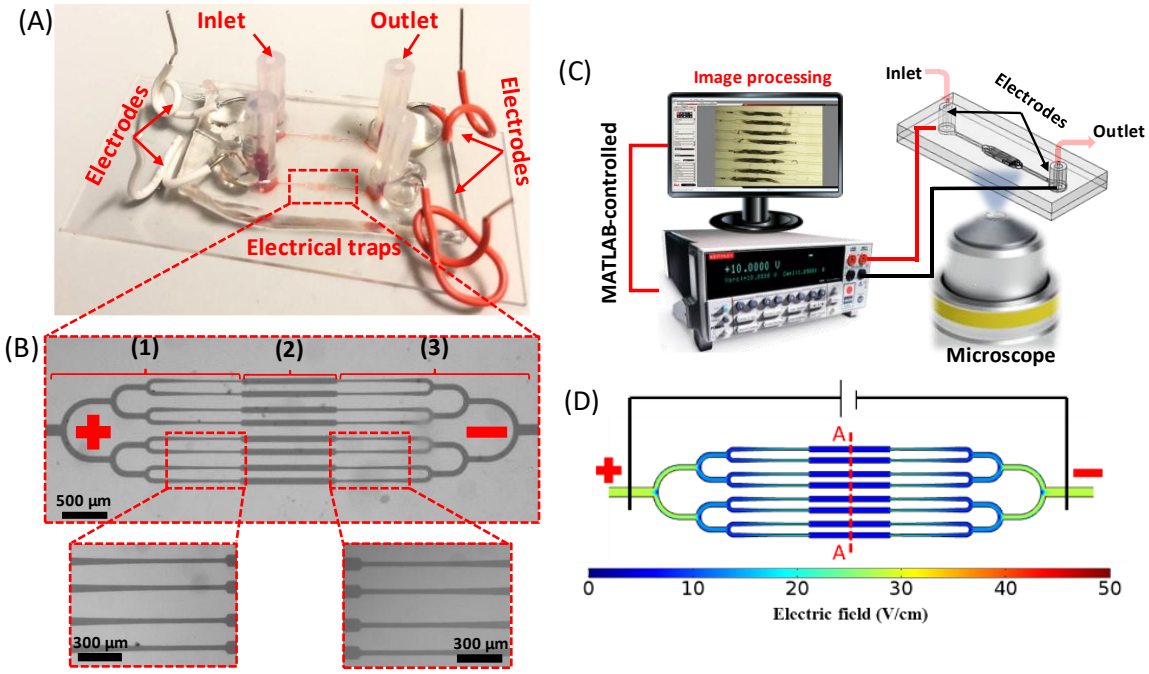

Figure 1: Microfluidic device and experimental setup for studying the electric egg-laying of 8 worms in parallel. (A) An image of the actual chip, housing two devices in parallel, each consisting of one inlet and one outlet interconnected with three-channel sections shown in (B): (1) Tree-like worm loading and distribution channels with end-tapered channels (left inset), (2) 8 parallel electrical traps for worm housing and imaging during the experiment, and (3) worm unloading channels with tapered connections to the electric traps (right inset). (C) Schematic of the experimental setup composing of the microfluidic device mounted on an inverted microscope and connected to a sourcemeter controlled by MATLAB. (D) COMSOL Multiphysics simulation of the electric field distribution throughout the chip to obtain a constant electric field of 6 V/cm in the electric traps using V= 34 V at the inlet-outlet electrodes.

The 75 µm thick polydimethylsiloxane (PDMS) channel network in Figure 1B consisted of three-channel segments, i.e., (1) branching channels for worm loading and distribution with tapered endings (left inset of Figure 1B); (2) eight parallel 85 µm-wide and 1.3 mm long electric traps for worms' egg-laying and imaging;

and (3) branching channels for worm unloading and collection. The tapered ends of the loading channels started from a width of 60 µm and narrowed down to different widths of 30, 35, or 40 µm in three different device designs. The electrical traps were located at the mid-section of the device to provide a symmetrical electric field (EF) distribution delivered through the application of a DC voltage between the two metal wires in the inlet and outlet reservoirs.

The tree-like loading and unloading channels were inspired by Hulme et al.[32] to ensure smooth loading and equal distribution of the worms across the 8 channels and maintain equal EF distribution. The loading and EF stimulation techniques benefit from the concept of maintaining constant channel dimensions at each bifurcation to preserve the same pressure and voltage drop up to the electrical traps. The pressure and voltage drops, as well as the hydrodynamic and electrical resistances, can be estimated using Hagen-Poiseuille's (Eq. 1) and Ohm's law (Eq. 2), respectively.

$$\Delta P = R_f Q, \qquad R_f = \frac{128 \mu l}{\pi D^4} \tag{1}$$

$$\Delta V = R_e I, \qquad R_e = \frac{\rho l}{A} \tag{2}$$

where Q is the flow rate, R_f is the fluid flow resistance, D is the channel hydraulic diameter, l is the channel length, μ is the fluid dynamic viscosity, A is the cross-sectional area, R_e is the electrical resistance, I is the electric current, and ρ is the electric resistivity.

Standard photo[33]- and soft-lithography[34] techniques were used to fabricate the microfluidic device. At first, a SU-8 master mold was fabricated on a 4 in diameter and 500 µm thick silicon wafer (Wafer World Inc., USA) by UV (365nm with 11.1mW/cm^2) exposure (UV-KUB 2, KLOE, France) of a 75 µm thick layer of SU-8 2075 photoresist (MicroChem Corporation, USA) for 20s. Then, to fabricate the negative replica of the master mold, a 10:1 mixture of PDMS elastomer and curing agent (Dow Corning, USA) was degasified, poured over the SU-8 mold, after placing two Masterflex tubes (L/S 14 size, Gelsenkirchen, Germany) over the inlet and outlet reservoirs, and cured for 2 hours at 80°C. An oxygen plasma machine (PDC-001-HP Harrick Plasma, USA) was used to bond the cured PDMS layer to a glass substrate at 870 mTorr pressure and 30 W power for 30s. Once the device was bonded, the two electrodes were punched through the inlet and outlet tubing for voltage

application. Finally, to prevent leakage, the electrode punched areas were sealed with PDMS prepolymer and left to cure at 150°C for 5 minutes.

Microfluidic egg-laying assay

Figure 1C depicts the experimental setup used to investigate the electric egg-laying of multiple worms in parallel and simultaneously image them at a single animal resolution. The experimental setup consisted of (1) our microfluidic device installed on a Leica inverted microscope (DMIL LED Inverted Routine Fluorescence Microscope, Leica, Germany) and imaged using a colour camera (MC170 HD, Leica, Germany), and (2) a direct current sourcemeter (Model 2410, Keithley Instruments Inc., USA) connected to the two electrodes at the inlet and outlet of the microfluidic device. The camera was used for recording movie clips and fluorescent images which were analysed using a custom-made MATLAB code. The code was also used to control the sourcemeter and apply the desired EF pulses while changing the EF polarity when needed. According to our single channel-based egg-laying experiments, an EF of 6 V/cm was needed to maximize egg-laying in *C. elegans*.[27,35] The required voltage to obtain this EF in the new microfluidic device was estimated to be 34 V using a simple COMSOL Multiphysics simulation (Figure 1D), as described in the Supplementary file Section S1.

To make our device accessible by the end-users, we eliminated the use of any fluidic control units such as syringe pumps, and the worms were manually manipulated using syringes. Briefly, a syringe filled with M9 buffer was connected to the inlet and used to fill in the device. Eight one day old worms were picked up manually from a NGM plate and loaded into the inlet. The worms were pressure-pulsed towards the electrical traps (Figure 2A) (Supplementary Video S1), and the loading efficiency (Eq. 3) was quantified and compared between the three devices with various loading tapered channel sizes.

$$Loading\ efficieny\ = \frac{Number\ of\ occupied\ traps}{Total\ number\ of\ traps} \times 100 \quad (3)$$

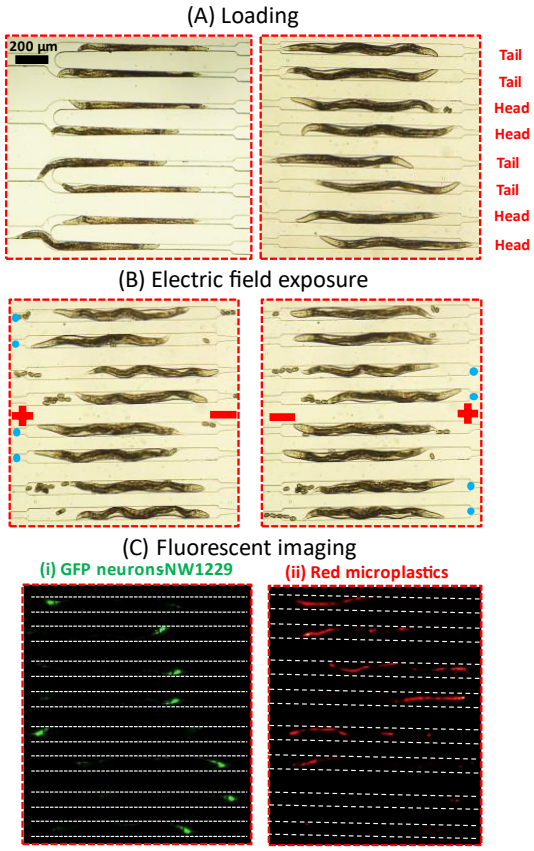

Figure 2: Capturing and investigating the electric egg-laying behaviour and microplastic accumulation in 8 worms in parallel. (A) Loading procedure through the branching channels resulting in a 50% tail vs. head orientation in the electric traps. (B) Egg-laying response of worms when the anode was at their head or tail. The eggs observed in the traps were deposited mostly when the worms were exposed to anode at their head, as donated by a blue circle beside them. (C) fluorescent images at the traps showing (i) GFP neurons of NW1229 worms and (ii) red fluorescent microplastics ingested by the same worms in (i). Channel walls are highlighted with white dashed lines for better observation.

Prior to EF stimulation, a 60 s acclimation period was used during which the flow was stopped by maintaining the inlet and outlet tubes at the same height level. Our previous experiments showed that the anode-facing worms could deposit significantly more eggs[27,35], highlighting that the worm loading orientation with respect to the EF direction could affect our results. To maintain an equal exposure condition among randomly oriented worms in our device (as shown in Figure 2A), we adopted a new EF stimulation technique in which a series of

5s anodal and 5s cathodal pulses, separated by 25s acclimation periods, was applied for 10 min (Figure 2B). This ensured that each worm was stimulated with 10 anodal and 10 cathodal pulses during an experiment. Next, fluorescent imaging was conducted at 5x magnification for determining the accumulation of microplastics in each worm that was tested in the device (Figure 2C) (Supplementary Video S1). Then, the worms were flushed out of the chip for the next round of worms to be loaded.

Data acquisition and analysis

The results, including the electric egg-count, the worms' length, diameter, and length reduction during EF exposure, as well as mean fluorescent intensity expression of neurons (GFP) and microplastics (RFP), were extracted from the recorded videos using our custom-written MATLAB code.[27] A step was added at the beginning of the code to select the 8 regions of interest around the worms in the electric traps. These regions were cropped, and the worms were individually analyzed, as shown in Figure S1.

We used two techniques for presenting our population-based data, i.e., bar plots with the mean ± standard error of the mean (SEM) and box plots with medians, 25% and 75% percentiles, and maximum and minimum data points. The population-based results were reported only for the worms responding to EF. The statistical significance between any two groups was determined using the Mann-Whitney test, while the following representation was used for identifying the significance level, i.e., * for p-value<0.05, ** for p-value<0.01, *** for p-value<0.001, and **** for p-value<0.0001.

Hierarchical Cluster Analysis (HCA) was performed to understand the toxicity effects of microplastics at single worm resolution. This technique helped identify the worm sub-groups, called clusters, that shared common phenotypes and quantified the differences between individual worms and the sub-groups. The built-in algorithm in MATLAB was used to perform the clustering analysis. The readout parameters mentioned above were standardized using Eq. 4 with their respective averages from the control worms. Each data point was assigned to a cluster by calculating the minimum Euclidean distance between the data point and the cluster centroid.

$$X_{std} = \frac{(X_i - \bar{X})}{\sigma} \qquad (4)$$

where X_{std} is the standardized value of the data point, X_i is the data point of interest (i.e., egg-count, length, diameter, length reduction, and fluorescent intensity), $\bar{X}$ is the control sample mean, and σ is the control sample standard deviation.

Principal Component Analysis (PCA) was performed to reduce the dimensionality and obtain the parameters with the highest level of information in our datasets. Briefly, in PCA, a new set of variables called the principal components are derived by using linear combinations of the original parameters. The principal components in our studies were calculated using the Minitab software and ranked based on their decreasing eigen-values. Eigen-value represents the amount of variance in the principal component. Therefore, the first two to three principal components can explain 80% of the total variance, making them suitable for representing the entire dataset, hence reducing the dimensionality. Contributions of each original parameter towards the top principal components were calculated by normalizing the coefficients of the principal components to their L^1 norms. The L^1 norm is the summation of all absolute values of the coefficient of each parameter in the principal component. Using this technique, we isolated and reported the original parameters with the highest level of information.

RESULTS AND DISCUSSIONS

In this paper, we first investigated three different designs of the microfluidic device (Figure 1) with various tapering channel sizes and quantified the worm loading and orientation efficiencies. Using the best design, we tested a new bidirectional EF stimulation protocol to ensure that the egg-laying results in the multi-worm device were comparable with the results from our single-channel device. As a proof of concept for toxicity analysis, worms were exposed to 100 mM glucose, and their electric egg count was quantified for the first time. Finally, we showed another novel application of our assay for investigating the toxicity effects of polystyrene microplastics and possible correlations between microplastic ingestion level and other on-chip phenotypes at a single-worm resolution.

Loading efficiency of the microfluidic chip

The response of freely moving gravid adult worms to EF in a close-fitting microchannel was studied by us previously at a single worm throughput, and worms were shown to deposit eggs in a controlled manner.[27,28] The

effects of EF direction, strength, and exposure duration as well as the worms' age and involvement of neurons and muscles in electric egg-laying were demonstrated, highlighting the potential of this method for toxicological studies at the cell to behaviour level. Here, we improved our technology by performing electric egg-laying and on-chip imaging on 8 worms in parallel, which was restricted by our microscope field of view of 2.2×1.7 mm^2. We were also able to keep the worms' identity known during the experiments for correlating the microplastic accumulation levels with the electric egg-laying response and some physiological parameters at a single animal resolution.

Our microfluidic device in Figure 1 was designed to (1) distribute 8 worms across the electrical traps, (2) restrain them within traps during EF stimulation, and (3) allow egg release and fluorescent imaging of the worms (Supplementary Video S1). The loading performance of our microfluidic device strongly depended on the tapered channels connecting the inlet channel network to the electrical traps (Figure 1B). They helped impeding the worms from slipping into the electric traps uncontrollably. Three microfluidic devices with tapered loading channels narrowing from a width of 60 µm into 30, 35, or 40 µm were tested for loading efficiency (Figure S2).

A total of 80 worms (in 10 trials) were tested in each device, and the tapered channel with a 30 µm wide outlet aided in smooth worm loading into the electrical traps with the highest loading efficiency of 91.25% (73/80 worms). The 35 and 40 µm-wide tapered channels showed significantly lower loading efficiencies of 56.25% (45/80 worms) and 47.5% (38/80 worms), respectively. They were large for maintaining the worms during loading while sometimes accepting more than one worm per channel. The same loading technique was used previously by Banse et al.[36] with a similar tapered loading channel dimension of 28 µm. Thus, the rest of the experiments were conducted using the 30 µm-wide tapered channel device.

Assay time and EF pulsation effects

In our single-worm electric egg-laying experiments[27,28], we observed a significantly higher egg-count for worms when the anode was positioned at their anterior sides (i.e., anodal exposure). We call this method a unidirectional pulsation since we could choose the anode position with respect to the single worm orientation in this device. In a new set of experiments with our single-worm device in Figure 3A, 20 unidirectional anodal pulses (6 V/cm, 5s on, 25s off) were applied within a 10-minute experimental duration to study the egg-laying of N=32 wildtype

worms. The number of eggs laid by a worm per minute dropped rapidly in the first 5 minutes and plateaued at almost no eggs per worm from minute 5 to minute 10. Figure 3B shows the total number of eggs laid per worm after 5 or 10 minutes in the single-worm device, with no statistically significant difference between the two groups (p-value>0.05). Within the first 5 minutes, the worms were exposed to 10 unidirectional anodal pulses which were selected for the rest of the experiments.

In our preliminary experiments with the multi-worm device, we noticed that the worms were oriented randomly with approximately 50% head or tail towards the trap (Figure 2A). This prevented the use of unidirectional pulses because approximately half of the worms would have been exposed to cathodal pulses, leading to no egg-laying response and waste of animals. Similar longitudinal orientation in the multi-worm device may have been achieved by preconditioning the worms with a longitudinal stimulus (e.g., controlled EF[37] or flow[38]), but this would have added complexity to our procedures.

We tested a new bidirectional pulsation method in order to use all the head and tail loaded worms in the multi-worm device. Accordingly, a series of 10 bidirectional EF pulses (+6V/cm for 5s, 25s off, -6V/cm for 5s, 25s off) were applied, aiming to stimulate each worm with an equal number of anodal and cathodal pulses. While this method ensured exposing each worm to 10 anodal pulses as determined in Figure 3A-3B, it also stretched the experimental duration from 5 to 10 minutes.

The effect of bidirectional pulsation with 10 anodal and 10 cathodal pulses (within 10 min) was first investigated in the single-worm device (Figure 3C, middle column). For the sake of comparison, the worms' response to 10 unidirectional anodal pulses within 5 min in the single-worm device was also provided in Figure 3C, left column. As shown, the responses with both methods were statistically similar, proving that the cathodal exposures did not contribute significantly towards the egg-laying response in the bidirectional exposure method.

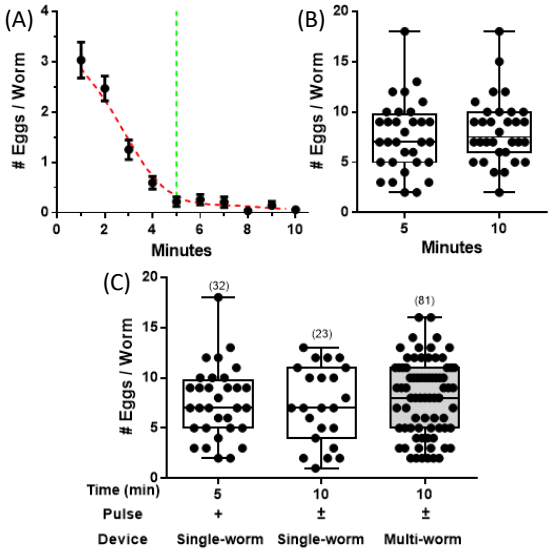

Figure 3: The effects of stimulation time and pulsation method on the electric egg-laying behaviour of adult C. elegans. (A) The number of eggs per worm for N=32 worms at 6V/cm using unidirectional pulsation (5s on, 25s off) inside our single-worm device[28]. (B) The total number of eggs deposited at the end of minutes 5 and 10 in (A). (C) Effects of unidirectional (+) pulsation for N=32 in the single-worm device and bidirectional (±) pulsation for N=23 and N=81 worms in the single- and multi-worm devices, respectively, studied on the number of eggs per worm during 5 and 10 minutes.

The above results ensured us that the bidirectional pulsation technique could be used in the multi-worm device to increase the throughput of the assay. The result of this experiment is also shown in Figure 3C (right grey column), depicting no statistical difference between the single-worm and multi-worm device responses while enabling us to increase the sample size from 23 to 81 worms and reduce the assay time from 4 to 2 hr, respectively.

With the multi-worm device and the bidirectional pulsation method, we were able to reach an egg-laying assay throughput of up to 40 worms/hr, which could be increased in the future with a larger microscope field of view. Compared to our electrical single-worm chip and the natural on-plate egg-laying technique, which can reach a throughput of approximately 5 worms/hr, our multi-worm assay can provide opportunities for testing more

chemicals in a faster way. Next, we show the novel applications of our technique for glucose and microplastics toxicity testing.

Effect of glucose on the electric egg-laying of *C. elegans*

C. elegans egg-laying circuit consists of a simple neuronal system that is serotonin-controlled. It has been used as an effective readout for identifying the effects of drugs and neurotransmitters. The egg-laying rate is affected by the culture conditions and the availability of food. For instance, different studies have shown the adverse effects of glucose on the natural egg-laying rate and life span of *C. elegans* as an application for antidiabetic drug screening.[29,39–43] Moreover, two recent studies illustrated the associated neurotoxicity effects of glucose on protein aggregation in *C. elegans* models of Parkinson's and Huntington's diseases.[44,45] Given the laboriousness and time-consuming nature of these experiments, we asked whether glucose affects the electrical egg-laying response of *C. elegans* and if this method can be used to speed up such chemical screening studies.

In each experiment, synchronized one day old adult worms were randomly picked from 100 mM glucose-dosed and un-dosed control NGM plates and loaded into the multi-worm device for testing using bidirectional pulsation at EF=6 V/cm. Their electric egg-laying count, length, diameter, and body length reduction during EF exposure were quantified, as shown in Figure 4. We also monitored the natural egg-laying behaviour of 25 worms off-chip for comparison purposes. Our egg-laying results in Figures 4A and 4B for on- and off-chip worms, respectively, showed that the control worms exhibited a strong egg-laying behaviour as illustrated by their high egg-counts in both experiments. The number of eggs/worm deposited off-chip was higher because eggs were allowed to be laid naturally over 3 hr in this experiment, which was significantly longer than the 10 min period used to electrically induce eggs on-chip. In other words, the off-chip worms had more time to reproduce new eggs, while the on-chip worms were egg-depleted rapidly and removed from the device. More importantly, the worms grown on the glucose plates showed noticeable natural and electrical egg-laying deficiencies, determined by their significantly lower egg-counts. Both on- and off-chip egg-laying experiments followed the same trends, indicating the suitability of our microfluidic technique for rapid glucose screening.

The off-chip experiment was not only time consuming (5 worms/hr) but also prone to the possibility of damaging the worms during the transfer process and miscounting the eggs while searching the plates.

Conversely, we performed the on-chip experiments on 90-120 worms in less than three hours (30-40 worms/hr throughput) using our multi-worm device with the ability to wash the worms off the plate and into the device without having to pick and potentially damage them. Egg-laying was done on animals spatially restricted in one place, which made the assay less prone to errors in egg counting. Moreover, our technique provided not only the egg-count but also other quantitative readouts, as shown in Figure 4C-4E.

It has been shown that glucose affects the worm growth with a discrepancy in the literature, i.e., papers showing an increase[43,45] or decrease[41,46] in the worms' size. Here, we investigated whether exposure to 100 mM glucose results in changes in the worms' growth by measuring their lengths and diameters on the multi-worm device after the egg-laying assay. As shown in Figure 4C-4D, the glucose-fed worms were significantly shorter (20%) with no change in their diameter compared to the control worms. Therefore, the electric egg-laying deficiency in Figure 4B may be attributed to retardation in the growth rate.

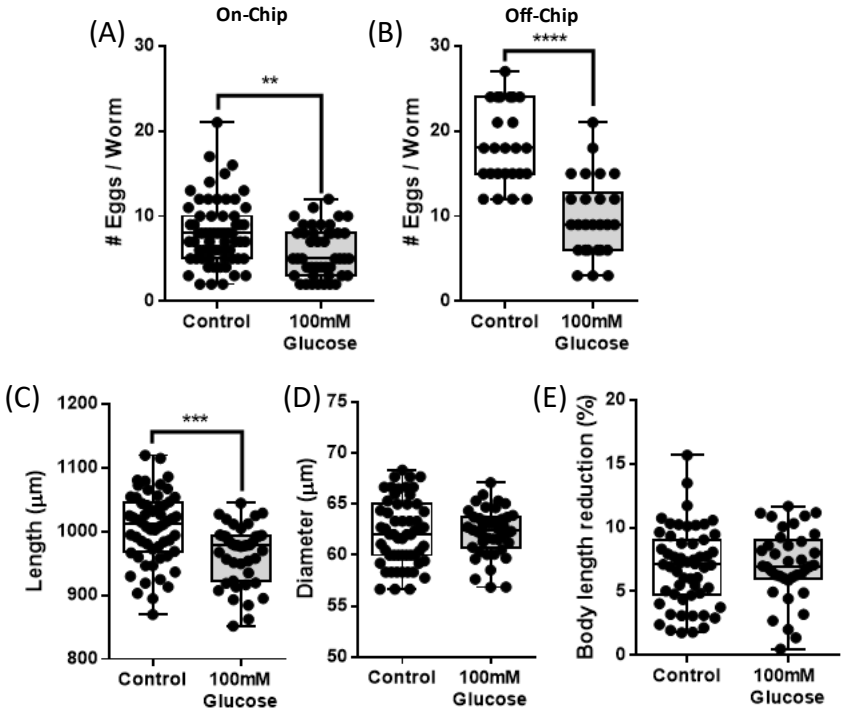

Figure 4: The effect of 100 mM glucose on the (A) natural off-chip (N=25) and (B) electric on-chip (N=65 and 44 for control and glucose treated worms respectively) egg-laying of adult C. elegans. EF of 6V/cm was

applied for 10 min in pulses with ±5s on and 25s off periods. Worms (C) length, (D) diameter, and (E) body length reduction during anodal stimulation were also quantified.

The decrease in worms' length might also be accompanied by possible changes in the worms' muscle integrity. In our single-worm egg-laying experiments[28], we showed that, during EF stimulations, worms contract their bodies in a consistent manner to release eggs. Body shortening was quantified in Figure 4E during the anodal pulses in the multi-worm device for the control and 100mM glucose-fed worms. No significant change was observed in the body length reduction during EF exposure, indicating no detectable effect of glucose on the body wall muscle activities of *C. elegans*. Yet, a deeper analysis of the contraction-relaxation mechanisms might reveal subtle phenotypes that need to be investigated in the future.

Altogether, using glucose, we provided a proof of concept for the use of our technique in determining the toxic effects of chemicals. We also showed that glucose induces abnormal electric egg-laying behaviour in *C. elegans*, which was on par with natural egg-laying behaviour reported earlier by Teshiba et al.[29]. In the future, we aim to use the technique for antidiabetic drug screening and other relevant diseases.

Effect of microplastics on the electric egg-laying of *C. elegans*

Recently, exposure to microplastics has been shown to cause significant changes in nematodes locomotory behaviours, life span, and growth rate.[23] Microfluidics has not been used to study the microplastics toxicity on *C. elegans*. Our device not only provides the possibility to obtain various phenotypic behaviours but also allows imaging the worms individually and keeping their identity known during an experiment. In this study, we exposed N2 worms to 100 and 1000 mg/L concentrations of 1µm red fluorescent polystyrene microparticles and investigated the accumulation of microplastics in the worms using fluorescent microscopy. The subsequent effects of microplastics on the worms' electric egg-laying, length, diameter, and body contraction during EF exposure were also investigated.

Figure 5A shows that increasing the microplastics concentration increased the red fluorescent intensity expression in N2 *C. elegans* with microplastics accumulation in the intestine and the pharynx. The quantitative data in Figure 5B, normalized based on the signal at 1000 mg/L, demonstrates that the microplastic uptake at

100 mg/L was not significant, compared to the control worms, but increased drastically at 1000 mg/L microplastics.

Figure 5C shows that as the microplastics concentration in the culture plate increases, the number of eggs laid electrically by a worm in our device decreases. For instance, at 100 mg/L, the microplastics uptake was relatively low (Figure 5B), resulting in a low toxic effect on egg-laying, confirmed with a slightly lower but statistically insignificant egg deposition of these worms compared to the controls, and a low number of non-responding worms (N=2/39). However, worms exposed to 1000 mg/L microplastics ingested more microplastics (Figure 5B), and their electric egg-laying was significantly lower than controls ($P<0.0001$, Figure 5C). It is also worth emphasizing that the number of non-responders (N = 11/51) to EF in the 1000 mg/L sample was significant which confirms the toxicity of microplastics on egg-laying.

In terms of body size, Figure 5D-5E show that the worms exposed to 1000 mg/L microplastics were significantly smaller than the control worms in length ($P<0.0001$) and diameter ($P<0.01$). However, the worms exposed to 100 mg/L microplastics were larger than controls in both length and diameter ($P<0.0001$). The reason behind this observation is still unknown to us and needs further investigation. Although some researchers have reported a negative effect of microplastics on *C. elegans* length[10,11,22], others have shown similar results in terms of the non-correlating effect of microplastics on the worms' length.[24]

Lastly, Figure 5F shows the length reduction of worms under various microplastic exposure conditions during anodal stimulations (electrical egg-laying) in our device. Length reduction did not change significantly for the treated worms compared to controls ($P>0.5$), indicating that microplastics did not affect the muscle contractions. We concluded that the lower egg depositions at higher microplastic concentrations, observed in Figure 5C, were potentially attributed to egg production deficiency and not the muscle activities.

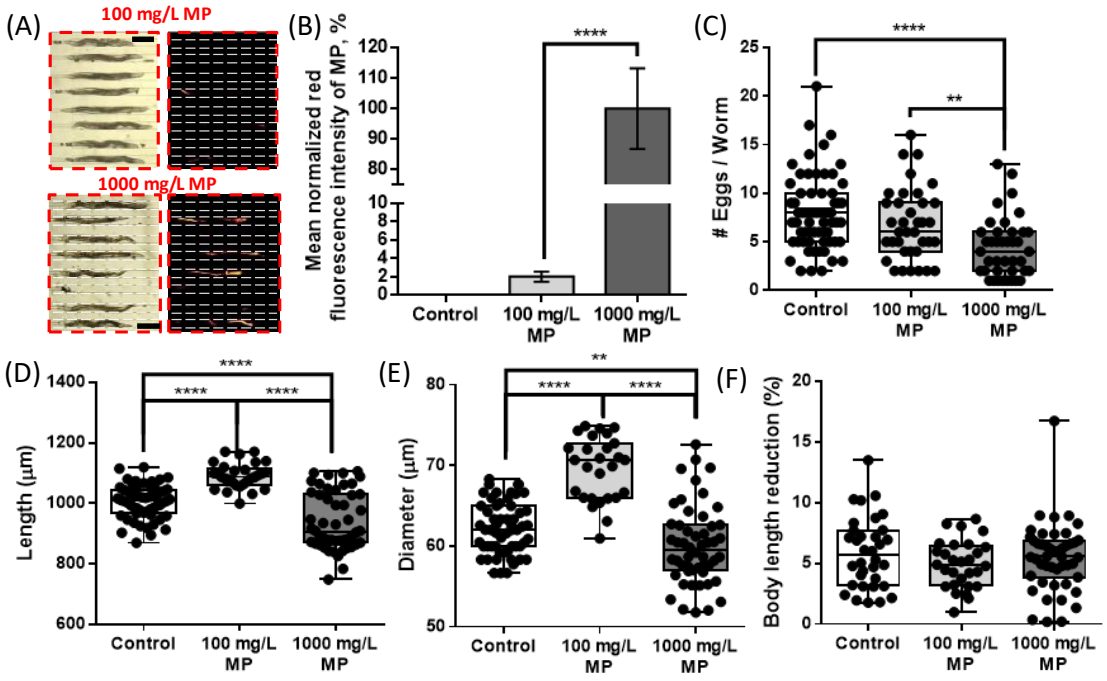

Figure 5: The effect of microplastics (MP) at 100 and 1000 mg/L concentrations on adult N2 C. elegans. EF=6V/cm was applied for 10 min in pulses with ±5s on and 25s off cycles. (A) Bright field and fluorescent images for the worms exposed to 100 (N= 37/39) and 1000 mg/L (N= 40/51) microplastics, indicating red fluorescent microplastic uptake (Scale bar = 200 µm). (B) Microplastic intake rate determined by calculating the mean red fluorescent intensity of the ingested microplastics and normalizing with the signal at 1000 mg/L. (C) Number of electrically deposited eggs per worm counted over 10 min. (D) Length and (E) diameter of the worms at each microplastic concentration compared to control worms (N=44). (F) Maximum total body length reduction during anodal stimulation (electrical egg-laying) in the device.

Effect of microplastics on the neuronal system of *C. elegans*

Two recent studies[11,47] have reported neuronal damages associated with nano- and micro-plastics exposure in *C. elegans* GABAergic, cholinergic, and dopaminergic neurons, suggesting that the locomotory deficiencies may be due to neurotoxicity. Our goal was to investigate the relationship between the microplastics induced neurotoxicity, growth deficiency, and electric egg-laying using NW1229, a transgenic strain expressing GFP pan-neuronally. NW1229 worms were exposed to 100 and 1000 mg/L of 1 µm red fluorescent polystyrene

particles. They were then loaded into the device, and their microplastics intake (red fluorescence), electric egg count, length, diameter, length reduction during anodal stimulation, and GFP expression of the neurons were investigated. The results are shown in Figures 6 and 7.

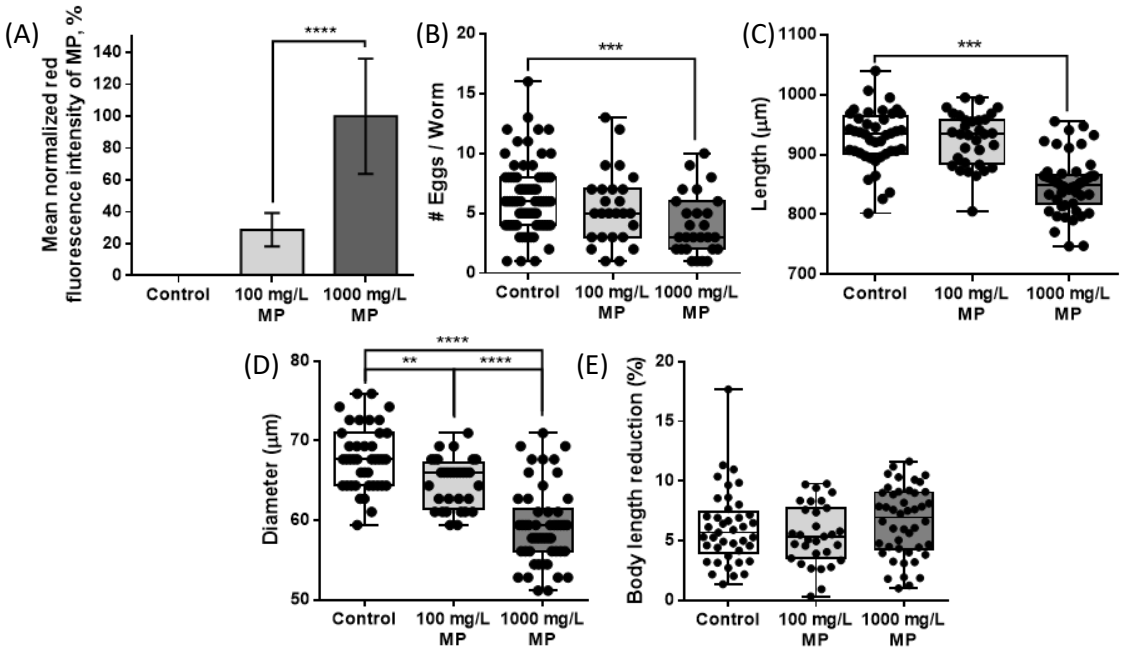

Figure 6: The effect of microplastics (MP) at 100 mg/L (N =26/30) and 1000 mg/L (N= 27/45) concentrations on adult NW1229 C. elegans expressing GFP pan-neuronally. EF=6V/cm was applied for 10 min in pulses with ±5s on and 25s off cycles. (A) Microplastic intake rate determined by calculating the mean red fluorescent intensity of the ingested microplastics and normalizing with the signal at 1000 mg/L. (B) Number of electrically deposited eggs per worm counted over 10 min. (C) Length and (D) diameter of the worms at each microplastic concentration compared to control worms (N = 41). (E) Maximum total body length reduction during anodal stimulation (electric egg-laying) in the device.

Results in Figure 6A showed similar trends to the microplastics uptake by N2 worms (Figure 5B). Control worms not exposed to microplastics did not express any red fluorescent while microplastics ingested at 1000 mg/L concentration was significantly higher than 100 mg/L ($P<0.0001$). Our egg-laying results in Figure 6B showed that the untreated worms exhibited a strong electric egg-deposition, as demonstrated by their high egg count. However, the worms treated with microplastics exhibited noticeable egg-laying deficiency at 1000 mg/L

concentration (P<0.001). At 100 mg/L, microplastics had a slight effect on egg deposition, which was not significantly different from controls, just like what we observed for N2 worms. Also, the number of non-responders (N = 18/45) to EF in the 1000 mg/L sample was higher than the 100 mg/L (N =4/30). In terms of body size, Figures 6C-6D show that the worms exposed to 100 mg/L microplastics were similar in length (P> 0.5) but significantly thinner in diameter (P<0.01) compared to the control worms. This was contrary to what we observed for the N2 strain, which requires further investigation in the future. The worms treated with 1000 mg/L microplastics were significantly shorter (P<0.0001) and thinner (P<0.0001) than the control worms and the 100 mg/L treated worms. Finally, we confirmed that the anodal length reductions for all conditions were consistent and similar to our observation for the N2 worms, indicating that the length reduction was not significantly (P>0.2) altered due to exposure to microplastics (Figure 6E).

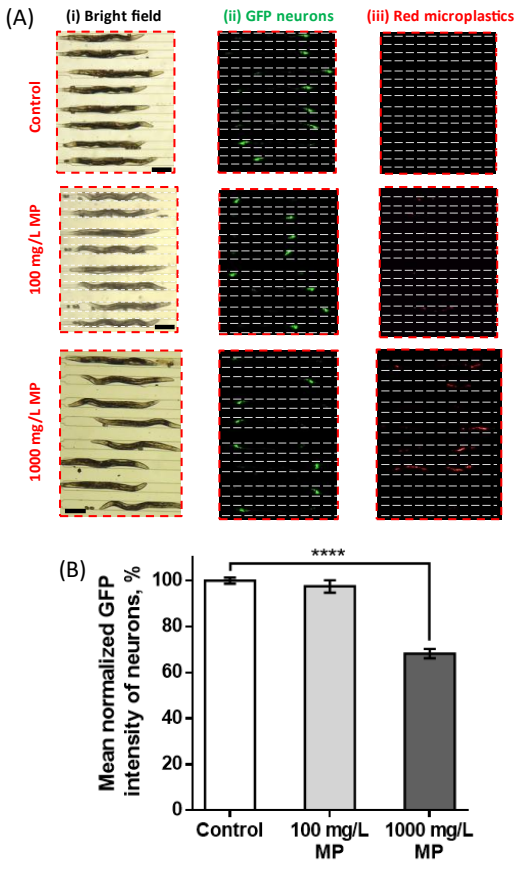

Figure 7: GFP expression of NW1229 C. elegans fed with 100 and 1000 mg/L. (A) Normalized mean fluorescent intensities. (B) Bright field (Scale bar = 200 µm) (i) and fluorescent images for neuronal system (ii) and microplastics (iii) at 0 (control), 100, and 1000 mg/L microplastics.

To investigate neurotoxicity, following the 10 min egg-laying experiment, GFP expressing neurons and red fluorescent microparticles in the worms were separately imaged in the electric traps (Figure 7A). The mean GFP intensities of neurons at both microplastic concentrations were normalized by the average GFP value obtained for the control worms grown without microplastics (Figure 7B). Similar to the electric egg-laying results, exposure to 100 mg/L microplastics resulted in insignificant ($P>0.6$) GFP decay compared to the control worms. However, a significant decrease ($P <0.0001$) of approximately 35% in GFP expression was obtained at 1000 mg/L microplastic exposure (Figure 7B), similar to the egg-count reduction in the same condition (Figure 6B). The decreasing trend in GFP expression at both concentrations is in line with the increasing trend in microplastics uptake, shown in Figure 6A for the NW1229 worms. The above results show the appropriateness of our technique for toxicity assessment from neuron to behaviour level. Moreover, our results confirmed that microplastics toxicity is not specific towards certain neurons, whereas GFP expression decayed over the entire body of the worm. This was also confirmed previously using off-chip assays that showed neurodegeneration for specific neurons as well as defective locomotory behaviour.[23]

Altogether, our results showed the suitability of our microfluidic technique to study glucose and microplastics toxicity in *C. elegans* and detect the associated behavioural and neuronal abnormalities, quantitively and at a population resolution. The following section will show the potential of our device for use in single-worm level neurobehavioural toxicity studies.

Single-worm analysis reveals heterogeneity in microplastics uptake and correlating egg-laying and physiological phenotypes

In recent years, physicians have found that drug-patient interactions are highly important, demonstrating the need for developing individualized diagnoses and treatments that take patient variabilities into account[48]. In the case of *C. elegans*, multiple microfluidic devices have recently shown that analysing the data in an individual-based manner would reveal subtle phenotypes that were hidden in population measurements[49,50]. Here, we

questioned the heterogeneity of microplastics uptake and toxicity, and show that our microfluidic device can be used to perform phenotypical and neuronal analyses at single-animal resolution and at a throughput higher than conventional assays for microplastics toxicity assessment.

As described in the Materials and Methods section, HCA and PCA were performed on individual N2 and NW1229 worms treated with microplastics at 100 and 1000 mg/L, and the results were compared with their counterpart control worms. The egg-count, worm length, worm diameter, length reduction during anodal stimulation, and normalized mean GFP and RFP fluorescent intensities, representing neurons and microplastics, respectively, were quantified for individual worms.

Figure 8Ai shows the heatmap representing the clustering generated by the HCA algorithm for N2 worms. Columns and rows represent individual worms and their phenotypes, respectively. The data were standardized using Eq.4 based on the control worm parameters. Thus, in Figure 8Ai, the color gradients depict whether a parameter of interest is quantitatively similar (white), lower (dark blue), or higher (dark red) than the average of the control group. The only exemption was the microplastic uptake RFP parameter for which the 100 mg/L data was selected as standardization reference since the control worms were not exposed to microplastics, expressing zero RFP intensity.

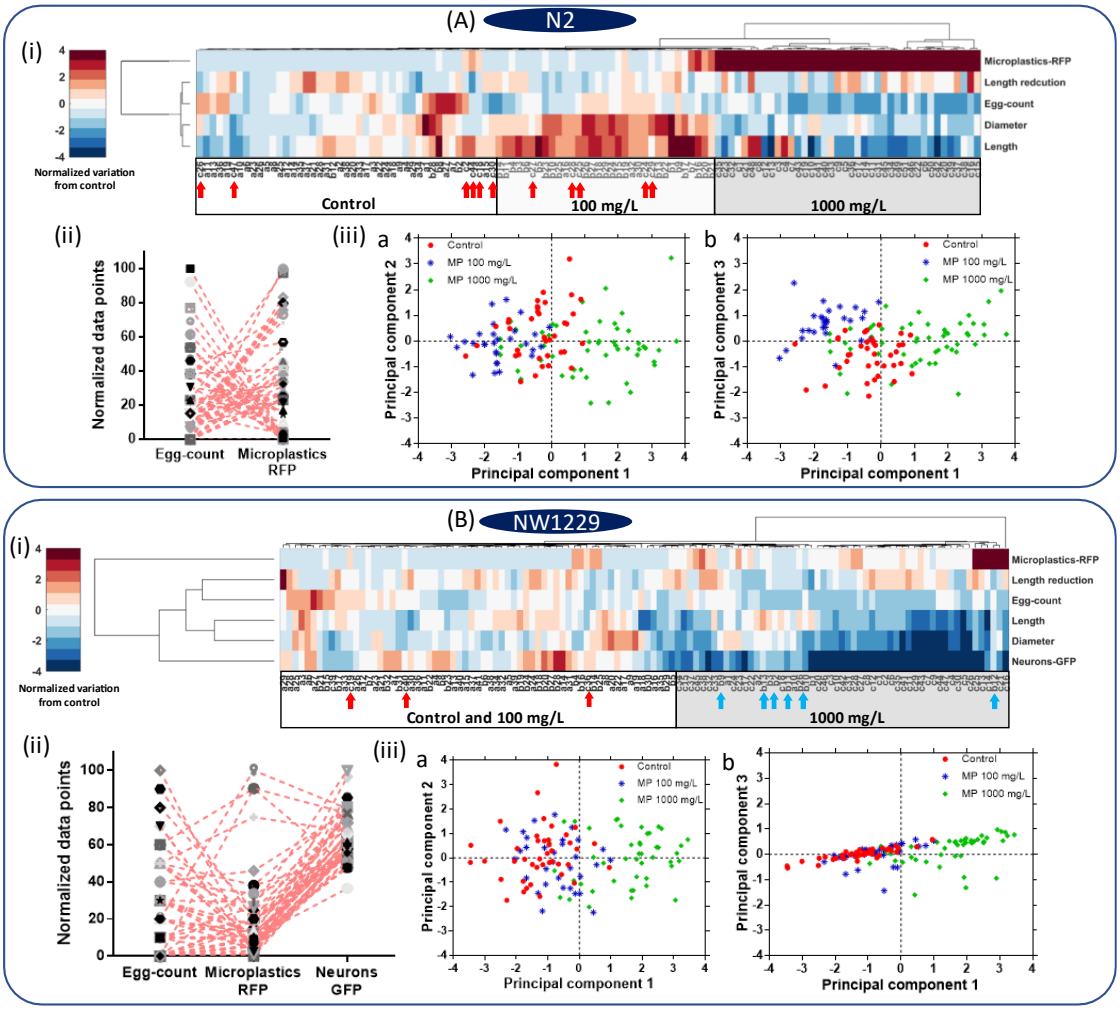

Figure 8: Phenotypic analysis of individual worms, (A) N2 and (B) NW1229, including control worms and ones treated with 100 and 1000 mg/L microplastics. (i) Hierarchical Cluster Analysis (HCA) of different phenotypes of the control and microplastic-exposed worms. (ii) Normalized individual responses of egg-count, microplastic uptake and GFP expression (NW1229 strain only) at 1000 mg/L. (iii) Principal Component Analysis (PCA) of control, 100 and 1000 mg/L microplastic-exposed worms.

Figure 8Ai shows that the control worms were mostly clustered at the left-hand side of the graph, followed by the worms exposed to 100 and 1000 mg/L microplastics. Generally, the graph confirms the population trends discussed earlier in the paper, but at an individual worm level. It shows that the microplastics uptake at 1000 mg/L was much higher than the 100 mg/L, for most of the worms, and the worms' diameter and length at 1000 mg/L were lower than the control and 100 mg/L worms. Moreover, the electric egg-laying rate for the worms

that took more microplastics was always lowered. Interestingly, using the clustering technique, we were able to isolate individual worms treated with 1000 mg/L microplastics that were behaving like untreated worms, with high egg count and low microplastics accumulation. These worms were clustered within the control or 100 mg/L populations as depicted with red arrows in Figure 8Ai. This showed the heterogeneity of microplastic uptake in the worms treated in the same way, which necessitates single-animal resolution assays like the one offered here to isolate such worms and understand their correlating phenotypes correctly. Such data points were hidden in our population-based averaging results offered in the previous sections, and this is the case in conventional worm screening assays, especially when they involve behavioral phenotyping.

HCA and PCA revealed some hidden correlations between the independent parameters. For instance, using PCA, the contribution of each parameter to the first, second, and third principal components, computed in Table S1, showed that the egg-count and the microplastics uptake level are inversely proportional. In other words, worms with higher microplastics expression were defective in egg-laying. To better visualize this correlation, we focused on the 1000 mg/L treated worms and normalized the egg-count and microplastics fluorescent expression parameters to obtain similar scales for comparison purposes. Then we plotted both parameters while preserving the identity of individual worms by connecting dash-lines, as shown in Figure 8Aii. Moreover, our results were further confirmed by plotting the calculated scores from the PCA using the first, second, and third principal components (Figure 8Aiii). This figure also confirms that the 1000 mg/L treated worms were clustered together with some individuals behaving like control and existing within the control cluster as discussed above.

Similar results were obtained for the NW1229 strain as shown in Figure 8B. Briefly, HCA analysis in Figure 8Bi created two main clusters for the 1000 mg/L worms at the right-hand side and the control and 100 mg/L worms mixed at the left-hand side, explaining their population trends described earlier. The heatmap illustrates increase in the microplastic uptake at 1000 mg/L exposure, and corresponding decreases in the egg-count, length, diameter, and neurons GFP expression of the worms. The graph also shows that there was a large variation in microplastics uptake within the 1000 mg/L population with some worms showing a significantly higher uptake than the others. Moreover, some NW1229 worms, exposed to 100 mg/L (blue arrows) and 1000 mg/L (red arrows) microplastics, were not placed in their respective clusters in Figure 8Bi. For these worms, the level of microplastics uptake (or GFP expression) was on par with the same phenotypes in their clusters.

The PCA analysis in Table S2 for NW1229 worms showed similar trends to the N2 strain, demonstrating that the microplastics uptake and egg-count were inversely proportional. However, there was no obvious pattern between the microplastics uptake and neurodegeneration. This was observed in Figure 8Bii by plotting the individual responses of 1000 mg/L worms for the egg-count, microplastics uptake, and neurons fluorescent expression while preserving the worms' identity. Lastly, Figure 8Biii shows that only using the first and second principal components, our results were further confirmed, and the 1000 mg/L treated worms were clustered together, whereas the control and 100 mg/L treated worms were mixed.

All in all, we envision that our microfluidic device, coupled with the clustering techniques above, would be of benefit to develop individualized drug and pollutant screening assays for *C. elegans*.

Conclusion

As an emerging toxicant, microplastics have been recently spotted in abundance throughout the environment. *C. elegans* is a simple and easy to use model organism for toxicological studies. Previous studies showed the negative effects of microplastics on *C. elegans* phenotypical behaviours using conventional assays, which are time-consuming and laborious, limiting the possibility of developing high throughput toxicity screening methods. Moreover, previous studies have solely focused on the natural behaviours of *C. elegans* while paying less attention to the sensory-motor evoked phenotypes to assess the neuronal system integrity. Therefore, in this paper, we developed a microfluidic device to exploit the newly introduced *C. elegans* electric egg-laying behaviour for toxicity studies.

Our device enabled trapping and exposing up to 8 individual worms in parallel to EF while allowing on-chip fluorescent imaging. We optimized our microfluidic device and adopted a new bidirectional stimulation technique to achieve a throughput of 40 worms/hr, which can be further enhanced in the future with a larger microscope field of view. Large datasets of multiple parameters such as electric egg-count, worm length, worm diameter, length reduction, and neuronal and microplastics mean fluorescent intensities were obtained and analyzed in population-averaged and individual-worm approaches.

The effect of glucose was investigated as a proof of concept for toxicity assays. Our findings implied that 100 mM of glucose induced abnormal electric egg-laying behaviour and resulted in a smaller body size. Thus, in the future, we aim to use the technique for antidiabetic drug screening. Moreover, we employed our device with two *C. elegans* strains (N2 and NW1229) to investigate the toxicity effects of 1 µm polystyrene microparticles at concentrations of 100 and 1000 mg/L on electric egg-laying and worm size as well as neurodegeneration in a faster manner using single-worm phenotyping. Our results showed that exposing the worms to 1000 mg/L caused severe egg-laying deficiency and neurodegeneration, and reduction in body size. Lastly, using HCA and PCA, we showed that single-worm phenotyping could reveal heterogeneity in microplastics uptake, which was correlated with the deficiency in egg-laying.

In the future, we aim to develop a microfluidic device for life-long phenotyping of microplastics toxicity while allowing for sensory-motor behavioural studies. Our technique can also be used as an ecotoxicity screening technique for determining the sublethal effects of other materials such as heavy metals on *C. elegans.*

Author Contributions

Khaled Youssef: Methodology, Investigation, Formal analysis, Validation, Data curation, Visualization, Writing - original draft. **Daphne Archonta**: Data curation and analysis. **Terrance J. Kubiseski**: Conceptualization, Writing - review & editing. **Anurag Tandon**: Supervision, Validation, Writing - review & editing. **Pouya Rezai**: Conceptualization, Methodology, Validation, Resources, Writing - review & editing, Supervision, Funding acquisition.

Conflicts of interest

The author(s) declared no conflict of interest.

Acknowledgements

This work was supported by Natural Sciences and Engineering Research Council (NSERC) of Canada and the Early Researcher Award to PR and the Ontario Trillium Scholarship to KY.

References

1. Wright SL, Kelly FJ. Plastic and Human Health: A Micro Issue? *Environmental Science and Technology*. 2017;51(12):6634-6647. doi:10.1021/acs.est.7b00423
2. Geyer R, Jambeck JR, Law KL. Production, use, and fate of all plastics ever made. *Science Advances*. 2017;3(7):e1700782. doi:10.1126/sciadv.1700782
3. Sharma S, Chatterjee S. Microplastic pollution, a threat to marine ecosystem and human health: a short review. *Environmental Science and Pollution Research*. 2017;24(27):21530-21547. doi:10.1007/s11356-017-9910-8
4. Sussarellu R, Suquet M, Thomas Y, et al. Oyster reproduction is affected by exposure to polystyrene microplastics. *Proceedings of the National Academy of Sciences*. 2016;113(9):2430 LP - 2435. doi:10.1073/pnas.1519019113
5. Prüst M, Meijer J, Westerink RHS. The plastic brain: neurotoxicity of micro- and nanoplastics. *Particle and Fibre Toxicology*. 2020;17(1):24. doi:10.1186/s12989-020-00358-y
6. PlasticsEurope (PEMRG). (September 25, 2019). Production of plastics worldwide from 1950 to 2018 (in million metric tons)* [Graph]. In Statista. Retrieved December 09, 2020, from https://www.statista.com/statistics/282732/global-production-of-plastics-sin.
7. de Sá LC, Oliveira M, Ribeiro F, Rocha TL, Futter MN. Studies of the effects of microplastics on aquatic organisms: What do we know and where should we focus our efforts in the future? *Science of the Total Environment*. 2018;645:1029-1039. doi:10.1016/j.scitotenv.2018.07.207
8. Pennino MG, Bachiller E, Lloret-Lloret E, et al. Ingestion of microplastics and occurrence of parasite association in Mediterranean anchovy and sardine. *Marine Pollution Bulletin*. 2020;158:111399. doi:10.1016/j.marpolbul.2020.111399
9. Kim SW, Kim D, Jeong SW, An YJ. Size-dependent effects of polystyrene plastic particles on the nematode Caenorhabditis elegans as related to soil physicochemical properties. *Environmental Pollution*. 2020;258:113740. doi:10.1016/j.envpol.2019.113740
10. Shang X, Lu J, Feng C, et al. Microplastic (1 and 5 μm) exposure disturbs lifespan and intestine function in the nematode Caenorhabditis elegans. *Science of the Total Environment*. 2020;705:135837.

doi:10.1016/j.scitotenv.2019.135837

11. Lei L, Liu M, Song Y, et al. Polystyrene (nano)microplastics cause size-dependent neurotoxicity, oxidative damage and other adverse effects in Caenorhabditis elegans. *Environmental Science: Nano*. 2018;5(8):2009-2020. doi:10.1039/c8en00412a
12. Lei L, Wu S, Lu S, et al. Microplastic particles cause intestinal damage and other adverse effects in zebrafish Danio rerio and nematode Caenorhabditis elegans. *Science of the Total Environment*. 2018;619-620:1-8. doi:10.1016/j.scitotenv.2017.11.103
13. Olivier K, Karanth S. Toxicology testing: in vivo mammalian models. In: *An Introduction to Interdisciplinary Toxicology*. Elsevier; 2020:487-506. doi:10.1016/b978-0-12-813602-7.00035-1
14. Yong CQY, Valiyaveetill S, Tang BL. Toxicity of Microplastics and Nanoplastics in Mammalian Systems. *International Journal of Environmental Research and Public Health*. 2020;17(5):1509. doi:10.3390/ijerph17051509
15. Hunt PR. The C. elegans model in toxicity testing. *Journal of Applied Toxicology*. 2017;37(1):50-59. doi:10.1002/jat.3357
16. Rand MD, Montgomery SL, Prince L, Vorojeikina D. Developmental Toxicity Assays Using the *Drosophila* Model. *Current Protocols in Toxicology*. 2014;59(1):1.12.1-1.12.20. doi:10.1002/0471140856.tx0112s59
17. Rubinstein AL. Zebrafish assays for drug toxicity screening. *Expert Opinion on Drug Metabolism and Toxicology*. 2006;2(2):231-240. doi:10.1517/17425255.2.2.231
18. Caballero MV, Candiracci M. Zebrafish as screening model for detecting toxicity and drugs efficacy. *Journal of Unexplored Medical Data*. 2018;3(2):4. doi:10.20517/2572-8180.2017.15
19. Youssef K, Bayat P, Peimani AR, Dibaji S, Rezai P. Miniaturized Sensors and Actuators for Biological Studies on Small Model Organisms of Disease. In: *Environmental, Chemical and Medical Sensors*. Springer; 2018:199-225. doi:10.1007/978-981-10-7751-7_9
20. Youssef K, Tandon A, Rezai P. Studying Parkinson's disease using Caenorhabditis elegans models in microfluidic devices. *Integrative biology : quantitative biosciences from nano to macro*. 2019;11(5):186-207. doi:10.1093/intbio/zyz017

21. Gupta BP, Rezai P. Microfluidic approaches for manipulating, imaging, and screening C. elegans. *Micromachines*. 2016;7(7):123. doi:10.3390/mi7070123

22. Yu Y, Chen H, Hua X, et al. Polystyrene microplastics (PS-MPs) toxicity induced oxidative stress and intestinal injury in nematode Caenorhabditis elegans. *Science of the Total Environment*. 2020;726:138679. doi:10.1016/j.scitotenv.2020.138679

23. Hu J, Li X, Lei L, Cao C, Wang D, He D. The Toxicity of (Nano)Microplastics on C. elegans and Its Mechanisms. In: He D, Luo Y, eds. *Microplastics in Terrestrial Environments: Emerging Contaminants and Major Challenges*. Cham: Springer International Publishing; 2020:259-278. doi:10.1007/698_2020_452

24. Schöpfer L, Menzel R, Schnepf U, et al. Microplastics Effects on Reproduction and Body Length of the Soil-Dwelling Nematode Caenorhabditis elegans. *Frontiers in Environmental Science*. 2020;8:41. doi:10.3389/fenvs.2020.00041

25. Kim Y, Jeong J, Lee S, Choi I, Choi J. Identification of adverse outcome pathway related to high-density polyethylene microplastics exposure: Caenorhabditis elegans transcription factor RNAi screening and zebrafish study. *Journal of Hazardous Materials*. 2020;388:121725. doi:10.1016/j.jhazmat.2019.121725

26. Maulik M, Mitra S, Bult-Ito A, Taylor BE, Vayndorf EM. Behavioral phenotyping and pathological indicators of Parkinson's disease in C. elegans models. *Frontiers in Genetics*. 2017;8(JUN):77. doi:10.3389/fgene.2017.00077

27. Youssef K, Archonta D, Kubiseski TJ, Tandon A, Rezai P. Electric Egg-Laying: Effect of Electric Field in a Microchannel on C. elegans Egg-Laying Behavior. *bioRxiv*. 2020.

28. Youssef K, Archonta D, Kubiseski TJ, Tandon A, Rezai P. Electric Egg-Laying: Effect of Electric Field in a Microchannel on C. elegans Egg-Laying Behavior. *Lab on a Chip*. 2021:Under review.

29. Teshiba E, Miyahara K, Takeya H. Glucose-induced abnormal egg-laying rate in Caenorhabditis elegans. *Bioscience, Biotechnology, and Biochemistry*. 2016;80(7):1436-1439. doi:10.1080/09168451.2016.1158634

30. Stiernagle T. Maintenance of C. elegans. *C elegans*. 1999;2:51-67.

31. Porta-de-la-Riva M, Fontrodona L, Villanueva A, Cerón J. Basic Caenorhabditis elegans methods: Synchronization and observation. *Journal of Visualized Experiments*. 2012;(64):e4019. doi:10.3791/4019

32. Hulme SE, Shevkoplyas SS, Apfeld J, Fontana W, Whitesides GM. A microfabricated array of clamps for immobilizing and imaging C. elegans. *Lab on a Chip*. 2007;7(11):1515-1523. doi:10.1039/b707861g

33. Aryasomayajula A, Bayat P, Rezai P, Selvaganapathy PR. Microfluidic Devices and Their Applications. In: *Springer Handbook of Nanotechnology*. Springer; 2017:487-536.

34. Xia Y, Whitesides GM. Soft lithography. *Annual Review of Materials Science*. 1998;28(1):153-184. doi:10.1146/annurev.matsci.28.1.153

35. Youssef K, Archonta D, Kubiseski T, Tandon A, Rezai P. On-Demand Electric Field Induced Egg Laying of CAENORHABDITIS ELEGANS. In: *Mtas 2019*. Basel, Switzerland; 2019:392-393.

36. Banse SA, Blue BW, Robinson KJ, Jarrett CM, Phillips PC. The Stress-Chip: A microfluidic platform for stress analysis in Caenorhabditis elegans. Kim H, ed. *PLOS ONE*. 2019;14(5):e0216283. doi:10.1371/journal.pone.0216283

37. Youssef K, Archonta D, Kubiseski T, Tandon A, Rezai P. Parallel-Channel Electrotaxis and Neuron Screening of Caenorhabditis elegans. *Micromachines*. 2020;11(8):756.

38. Ge A, Wang X, Ge M, et al. Profile analysis of: C. elegans rheotaxis behavior using a microfluidic device. *Lab on a Chip*. 2019;19(3):475-483. doi:10.1039/c8lc01087k

39. Schulz TJ, Zarse K, Voigt A, Urban N, Birringer M, Ristow M. Glucose Restriction Extends Caenorhabditis elegans Life Span by Inducing Mitochondrial Respiration and Increasing Oxidative Stress. *Cell Metabolism*. 2007;6(4):280-293. doi:10.1016/j.cmet.2007.08.011

40. Schlotterer A, Kukudov G, Bozorgmehr F, et al. C. elegans as model for the study of high glucose-mediated life span reduction. *Diabetes*. 2009;58(11):2450-2456. doi:10.2337/db09-0567

41. Wang X, Zhang L, Zhang L, et al. Effects of excess sugars and lipids on the growth and development of Caenorhabditis elegans. *Genes and Nutrition*. 2020;15(1):1. doi:10.1186/s12263-020-0659-1

42. Lee SJ, Murphy CT, Kenyon C. Glucose Shortens the Life Span of C. elegans by Downregulating

DAF-16/FOXO Activity and Aquaporin Gene Expression. *Cell Metabolism*. 2009;10(5):379-391. doi:10.1016/j.cmet.2009.10.003

43. Alcántar-Fernández J, Navarro RE, Salazar-Martínez AM, Pérez-Andrade ME, Miranda-Ríos J. Caenorhabditis elegans respond to high-glucose diets through a network of stress-responsive transcription factors. Dupuy D, ed. *PLOS ONE*. 2018;13(7):e0199888. doi:10.1371/journal.pone.0199888

44. Landon G, Whitney W, Priya R, Mindy F. Glucose effects on polyglutamine-induced proteotoxic stress in Caenorhabditis elegans. *Biochemical and Biophysical Research Communications*. 2020;522(3):709-715. doi:10.1016/j.bbrc.2019.11.159

45. GUZMAN AC DE, Kim EJ, Cho JH, Kim JH, Choi SS. High Glucose Diet Attenuates Dopaminergic Neuronal Function in C. elegans Leading to Acceleration of Aging Process. May 2020. doi:10.21203/rs.3.rs-29098/v1

46. Lei W, Beaudoin-Chabot C, Thibault G. Glucose increases the lifespan of post-reproductive C. elegans independently of FOXO. *bioRxiv*. June 2018:347435. doi:10.1101/347435

47. Qu M, Kong Y, Yuan Y, Wang D. Neuronal damage induced by nanopolystyrene particles in nematode Caenorhabditis elegans. *Environmental Science: Nano*. 2019;6(8):2591-2601. doi:10.1039/C9EN00473D

48. Schork NJ. Personalized medicine: time for one-person trials. *Nature*. 2015;520(7549):609-611.

49. Letizia MC, Cornaglia M, Trouillon R, et al. Microfluidics-enabled phenotyping of a whole population of C. elegans worms over their embryonic and post-embryonic development at single-organism resolution. *Microsystems & Nanoengineering*. 2018;4(1):6. doi:10.1038/s41378-018-0003-8

50. Kopito RB, Levine E. Durable spatiotemporal surveillance of Caenorhabditis elegans response to environmental cues. *Lab on a Chip*. 2014;14(4):764-770. doi:10.1039/c3lc51061a

Microplastic Toxicity at the Neuronal, Behavioural and Physiological Levels Investigated on *C. elegans* in a Multi-Nematode Lab-on-a-Chip Device with Population and Single-Worm Screening Capability

Khaled Youssef[a], Daphne Archonta[a], Terrance J. Kubiseski[b], Anurag Tandon[c,d], and Pouya Rezai[a,*]

[a] Department of Mechanical Engineering, York University, Toronto, ON, Canada
[b] Department of Biology, York University, Toronto, ON, Canada
[c] Tanz Centre for Research in Neurodegenerative Diseases, Toronto, Ontario, Canada
[d] Department of Medicine, University of Toronto, Toronto, Ontario, Canada

* Corresponding Author: BRG 433B, 4700 Keele St, Toronto, ON, M3J 1P3, Canada; Tel: 416-736-2100 ext. 44703; Email: prezai@yorku.ca

S1. Numerical Simulation of Electric Field in the Microfluidic Device

A two dimensional (2D) numerical simulation was conducted to obtain the electric field (EF) distribution in the microfluidic device. The steady-state direct-current (DC) module of the COMSOL Multiphysics® software was used to determine the EF using Ohm's law. The computer-aided design (CAD) software SOLIDWORKS® was used to generate the computational domain that was imported into COMSOL for mesh generation. The microfluidic device contained 8 parallel worm-dwelling microchannels called electric traps in which the worms were electrically stimulated for egg deposition (Figure 1 of the paper). Each electric trap was 85 µm-wide and 1.3 mm long. The electric traps had tapering channels at their anterior-posterior sides which were connected to the inlet and outlet channels via tree-like branching channels. The boundary conditions included an electric insulation applied to all boundaries, and electric potentials of 34V and ground applied at the two end reservoirs. For mesh generation, the triangular automatic mesh generation module of COMSOL was utilized. The EF distribution within the microfluidic device determined through the simulation is depicted in Figure 1 of the paper.

S2. Supplementary Figures

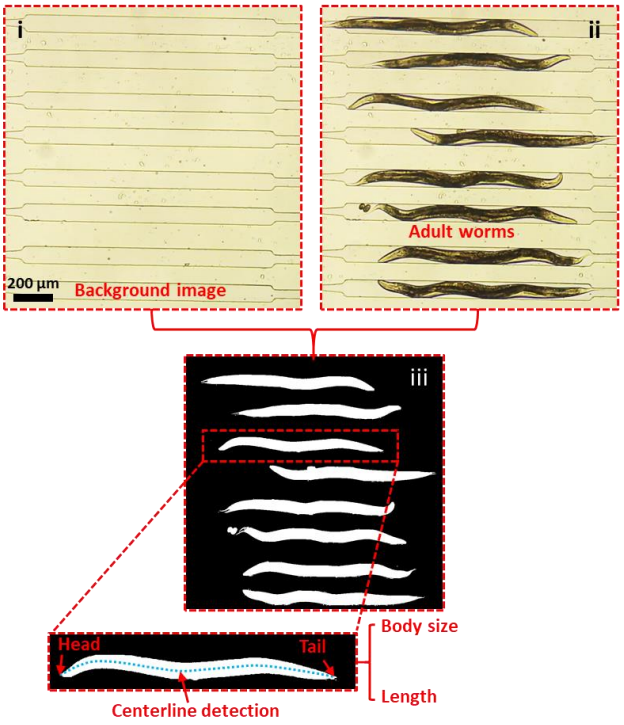

Figure S1: Data analysis by MATLAB image processing. Background subtraction was done using images (i) and (ii) to obtain the binary image (iii). (iii) Binarized image showing all worms with an inset of a single worm that was used for centerline detection and analysis of body length and length reduction.

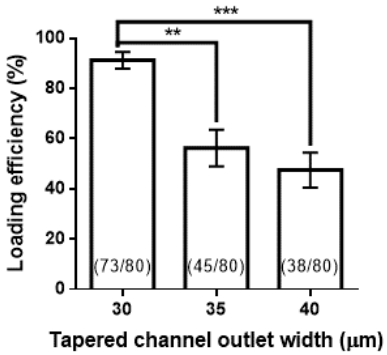

Figure S2: Worm loading efficiency of the 8 electric traps in three microfluidic devices tested with different tapered channel end-widths of 30, 35, and 40 µm. A total of 80 worms in 10 trials were tested in each device.

S3. Supplementary Videos

Video S1: Worm loading, egg-laying, and neuronal and microplastics imaging in the microfluidic device.